TABLE OF CONTENTS

LIST OF FIGURES

LIST OF TABLES

NOMENCLATURES

A	Area, m^2
$\boldsymbol{A}$	Hessian matrix of the objective function
A_c	Cross sectional area of the channel, m^2
A_s	Cross sectional area of the structure, m^2
Be	Bejan number
$\boldsymbol{B}_i$	Hessian matrix of the inequality function
CF – 2	Counter-flow row
CF – 3	Counter-flow channel
$\boldsymbol{C}_j$	Hessian matrix of the equality function
C_P	Specific heat at constant pressure, J/kg K
Cyl	Cylindrical configuration
a, b, c	Diagonals of Hessian matrices ***A, B, C***
d_h	Hydraulic diameter, m
D	Substantial derivative
E-T	Equilateral triangle
$f(\boldsymbol{x})$	Objective function
$\tilde{f}(\boldsymbol{x})$	Objective approximate function
g	Gravity
$g_i(\boldsymbol{x})$	*i*-th inequality constraint function
$\tilde{g}_i(\boldsymbol{x})$	*i*-th inequality constraint approximate function

G	Computational domain width
h	Elemental height , m
h	Enthalpy, J.kg^{-1}
h	Heat transfer coefficient, W.m^{-2}K^{-1}
h_c	Channel height , m
$h_j(\boldsymbol{x})$	j-th equality constraint function
$\tilde{h}_j(\boldsymbol{x})$	j-th equality constraint approximate function
H	Structure height, m
i	Mesh iteration index
$\boldsymbol{I}$	Identity matrix
$I–T$	Isosceles right triangle
k	Thermal conductivity, W/mK
k_r	Conductivity ratio
L	Axial length, m
N	Number of channels
n	Normal
P	Pressure, kPa
P_c	Perimeter of the channel
P_o	Poiseuille number
$PF-1$	Parallel – flow
Pr	Prandtl number
$P[k]$	Successive sub-problem

$p(\boldsymbol{x})$	Penalty function
$\dot{q}''$	heat flux, W/m^2
q_s'''	Internal heat generation density, W/m^3
$\dot{q}$	Heat transfer rate, W
$\tilde{Q}$	Heat transfer, W
$\mathbb{R}^n$	*n*-dimensional real space
R	Dimensionless thermal resistance
Re	Reynolds number
R^2	Coefficient of correlation
s	Channel spacing, m
Sqr	Square configuration
T	Temperature, $^{\circ}$C
$\tilde{T}_{\max}$	Dimensionless maximum temperature, $\left(\tilde{T}_{\max} = \frac{T - T_{in}}{q''' v^{2/3} / k_f}\right)$
$\vec{u}$	Velocity vector, m/s
V	Global structure volume, m^3
v_c	Channel volume, m^3
v_{el}	Elemental volume, m^3
W	Structure width, m
w	Elemental width, m
x, y, z	Cartesian coordinates, m
$\boldsymbol{x}^*$	Design variables

$\boldsymbol{x}^k$	Design points
m,n,l,k,r	Positive integer

Greek symbols

α	Thermal diffusivity, m^2/s
β	Penalty function parameter for equality constraint
μ	Viscosity, kg/m.s
ν	Kinematics viscosity, m^2/s
ρ	Density, kg/m^3
∂	Differential or Derivative
∞	Far extreme end, free stream
ϕ	Porosity
Δ	Difference
∇	Differential operator or gradient function
τ	Shear stress, Pa
γ	Convergence criterion
γ	Penalty function parameter for objective constraint
δ	Kronecker delta function
δ	Move limit
ε	Value tolerance
λ	Vexing coefficient
ξ	Characteristic length scale

Φ	Dissipation function
ρ	Penalty function parameter
μ	Large positive value
Ω	Dimensionless temperature difference

Subscripts

$\sqcup$	Dimensionless
in	Inlet
l	Large
opt	Optimum
s	Solid
sm	Small
r	Ratio
0	Initial
1	Phase 1
1,2,3,4	Design variable number
ave	Average
best	Best
c	Channel
f	Fluid
f	Function
h	Hydraulic

inlet	Inlet
L	Length
max	Maximum
min	Minimum
norm	Normalised
i,j,k,l,n	Positive integers
opt	Optimum
solid	Solid
s	Surface
w	Wall
x	Step size
∞	Free stream

Superscripts

T	Transpose
k	Positive integer

PUBLICATIONS IN JOURNALS, BOOKS AND CONFERENCE PROCEEDINGS

The following articles, book chapter and conference papers were produced during this research.

1. **O.T. Olakoyejo**, T. Bello-Ochende and J.P Meyer, "Mathematical optimisation of laminar forced convection heat transfer through a vascularised solid with square channels", *International Journal of Heat and Mass Transfer*, Vol. 55, pp. 2402-2411, 2012. **(Published)**

2. **O.T. Olakoyejo**, T. Bello-Ochende and J.P Meyer; "Constructal conjugate cooling channels with internal heat generation", *International Journal of Heat and Mass Transfer*, Vol. 55, pp. 4385-4396, 2012. **(Published)**

3. T. Bello-Ochende, **O.T. Olakoyejo** and J.P Meyer, Chapter 11, "Constructal Design of Rectangular Conjugate Channels" **Published in the book, "*Constructal Law and the Unifying Principle of Design",*** L.A.O Rocha, S. Lorente and A. Bejan, eds., pp. 177-194, Springer Publishers, New York, 2012. **(Published)**

4. J.P Meyer**, O.T. Olakoyejo**, and T. Bello-Ochende; "Constructal optimisation of conjugate triangular cooling channels with internal heat generation",

International communication of Heat and Mass Transfer, Vol. 39, pp. 1093 - 1100, 2012. **(Published)**.

5. T. Bello-Ochende, **O.T. Olakoyejo**, and J.P Meyer; "Constructal flow orientation in conjugate cooling channels with internal heat generation", *International Journal of Heat and Mass Transfer*, Vol. 57, pp. 241 - 249, 2013. **(Published)**.

6. **O.T. Olakoyejo**, T. Bello-Ochende and J.P Meyer, "Optimisation of circular cooling channels with internal heat generation", *Proceedings of the 7th International Conference on Heat Transfer, Fluid Mechanics and Thermodynamics*, Antalya, Turkey, pp. 1345-1350, 19-21 July 2010. **(Presented)**

7. **O.T. Olakoyejo**, T. Bello-Ochende and J.P Meyer, "Geometric Optimisation of Forced Convection In Cooling Channels With Internal Heat Generation *Proceedings of the 14th International Heat Transfer Conference*, Washington D.C, USA, pp. 1345-1350, 8 -13 August 2010. **(Presented)**

8. **O.T. Olakoyejo**, T. Bello-Ochende and J.P Meyer, "Geometric optimisation of forced convection in a vascularised material", *Proceedings of the 8th International Conference on Heat Transfer, Fluid Mechacs and Thermodynamics*, Pointe Aux Piments, Mauritius, pp. 38 - 43, 11-13 July, 2011 (**Presented and awarded best paper of the session**).

9. **O.T. Olakoyejo**, T. Bello-Ochende and J.P. Meyer, "Constructal optimisation of rectangular conjugate cooling channels for minimum thermal resistance*"*, *Proceedings of the Constructal Law Conference*, 01-02 December, 2011, Porto Alegre, Universidade Federal do Rio Grande do Sul, Brazil. **(Presented)**

10. **O.T. Olakoyejo**, T. Bello-Ochende and J.P Meyer, "Optimisation of conjugate triangular cooling channels with internal heat generation", *9th International Conference on Heat Transfer, Fluid Mechanics and Thermodynamics, Malta,* 16 -18 July, 2012. **(Presented)**

11. **O.T. Olakoyejo**, T. Bello-Ochende and J.P Meyer, "Flow orientation in conjugate cooling channels with internal heat generation", *9th International Conference on Heat Transfer, Fluid Mechanics and Thermodynamics, Malta,* July 16 – 18, 2012. **(Presented).**

1

CHAPTER 1: INTRODUCTION

1.1. BACKGROUND

Heat generating devices, such as high power electronic equipments and heat exchangers are widely applicable in engineering fields such as the automobile industry, power system, heating and air conditioning, chemical engineering, electronic chip cooling, and in the aerospace and nuclear energy sectors. Heat generation can cause overheating problems and thermal stresses and may leads to system failure. The removal of heat from these devices has been a critical challenge to thermal design engineers and researchers. Heat generating devices are designed in such a way as to optimise the structural geometry by packing and arranging array of cooling channels into given and available volume constraint without exceeding the allowable temperature limit specified by the manufacturers. For example, in the design of an electronic package, it is desirable to pack as many of the electronic chips as possible into in a fixed volume. This translates into the maximisation of heat transfer density or the minimisation of overall global thermal resistance, which is a measure of the thermal performance of the cooling devices.

Heat transfer in heat generating devices occurs by conjugate heat conduction and forced convection. Heat conduction is the transfer of thermal energy from more energetic particles to less energetic counterparts. This is largely influenced by the thermal conductivity of the material. Heat transfer by convection is made possible by

the movement of fluid molecules. When this movement is facilitated by external forces such as fans and pumps, the term, 'forced convection' is used. The convective heat transfer is influenced by the heat transfer coefficient. The performance of cooling system is measured by its thermal resistance *R*, which can be expressed for conductive and convective heat transfer as shown in Equations (1.1) and (1.2) respectively:

$$R_{\text{cond}} = \frac{1}{kA} \tag{1.1}$$

$$R_{\text{conv}} = \frac{1}{hA} \tag{1.2}$$

where h and k are the convective heat transfer coefficient and thermal conductivity respectively. These factors greatly influence the overall performance of the system as also expressed in equation (1.3):

$$Nu = \frac{h\xi}{k} \tag{1.3}$$

where ξ is a characteristic length scale which could be external or internal length scale

However, in modern heat transfer, the new trend for thermal performance is shape and geometric optimisation. Constructal theory and design [1, 2] have emerged as an evolutionary design philosophy for developing flow architectures that offer greater flow access and system performance. The constructal method - constructal design - is based on the principle of objective and constraints. The approach is summarised by the constructal law [1, 2]: *For a finite-size system to persist in time (to live), it must*

evolve in such a way that it provides easier access to the imposed (global) currents that flow through it.

In all problems of Constructal design, especially, engineering analyses, the characteristic dimension ξ or A of the configuration (shape, size) is unknown prior to optimisation process and this must be determined optimally for the overall thermal performance of the system. But, from equation (1.1) – (1.3) to minimise thermal resistance or maximise thermal conductance, ξ needs to be increased subject to the global volume constraint. However, we cannot keep increasing this characteristic dimension indefinitely because the global volume constraint is fixed. Constructal theory [2] suggests that we must find the correct optimal values of ξ or cross-section area that provide the direction of greater flow access or less global flow resistances in order to minimise global thermal resistance. That is, the number of the lengths necessary to draw the domain minus number of constraints gives the number of degrees of freedom.

The application of this evolutionary design approach to the discovery of internal heat exchanger started with Bejan and Sciubba [3]. These researchers obtained the design rule for spacing an array of parallel plates to channels so that the heat transfer density of a volume filled with heat generating components was maximum. The spacing was determined by using the intersection of asymptotes method.

Bejan and his co-researchers later applied the theory to the conductive cooling of electronics with internal heat generation and other convective heat transfer optimisations [4-11]. These studies played a significant and important role in the extension and application of Constructal theory and design to problems in engineering, other branches of science and even in the humanities [12, 13]. In addition, Constructal theory has been employed to describe deterministically the generation of shapes in nature [1].

From Equations (1.1) to (1.3), it is obvious that the geometry (size and shape) of the cooling structure plays a crucial role in the performance of its cooling channels. Other factors that influence the cooling performance of a heat-generating device include materials selected. In case constructal law (in relation to thermal design and management), geometry in terms of size and shape is the most important factor that the designers and engineers can control. In general, for optimum thermal performance, multivariable optimisations of the various geometric parameters of the cooling structures must be considered. The fact is that the impact of a single geometric parameter cannot be generalised without considering its consequence on the other parameters. For example, increasing the channel aspect ratio will generally improve the overall thermal performance of the system for a fixed-flow rate, [14, 15].

Analytical solutions for the optimisation of cooling channels always prove to excel in the search for solutions to specific design problems [16-18]. Although the analytical

optimisation may be limited and not perfect due to the various assumptions made when using this procedure, it remains a powerful method.

The advent of computational fluid dynamics (CFD) simulations has made numerical optimisation more interesting and robust in designing near-optimal solutions for various applications of cooling devices [19-21]. Coupled with the advent of supercomputers over the last few decades, CFD has proven to give more accurate predictions for flow velocity, temperature and various thermodynamic properties.

Furthermore, optimisations by experimentation [22-29] are performed in heat transfer analyses to investigate the effects of various geometric parameters on the thermal performance of heat exchangers and cooling devices. However, experimental optimisation is very expensive and time consuming compared to analytical and numerical optimisations. Unlike numerical studies, many design variables cannot be varied simultaneously to produce the global optimisation that gives the desired objective function in experimental studies. Another unique advantage of numerical analysis over experimental analysis is that it provides more quantitative insight into the flow and heat transfer process, especially at the micro-scale level. It is often difficult to use conventional measurement techniques with the micro-scale channels to extract data despite the validity of the conventional governing differential equations for fluid flow and heat transfer analyses and continuum flow assumption in the micro-scale devices.

Coupling CFD with the mathematical algorithm for optimisation has proved to be capable of producing optimal designs within reasonable computational times. Modern high-speed computers have made it possible to automate the optimisation process by integrating and coupling the CFD software package with the optimisation algorithm for the optimal modification of various design parameters. Hence, numerical optimisation is a systematic way of searching for an optimal design based on certain specified criteria. The optimisation algorithm could be integrated into numerical modelling, which would enable optimal design to be achieved for the overall thermal performance of the system.

1.2. MOTIVATION

The Constructal theory by Bejan [1, 2, 30] which is aimed at the optimisation of shapes and structure has been the major inspiration for this research. This is because the advent of compact high density components required the investigation of novel and modern techniques for removing heat from heat generating devices for an optimal performance at minimised cost. The constructal theory provided the ideas on how to optimise all the constraints.

1.3. JUSTIFICATION (THE NEED FOR THIS STUDY)

From the literature, the optimisation of the global performance of heat-exchanging devices is still a difficult task because of different design parameters involved. There is a need for further and extensive research into improving cooling channel materials so as to ensure high performance, more efficient, more accurate, long lasting and low cost heat exchanging. Since the design variables are mutually interdependent parameters, they cannot be optimised individually to achieve the near-optimal solution of the global performance.

Bejan *et al*. [31] argue that "when a system consists of several components, the overall system should be optimised, since optimisation of components individually does not guarantee an optimum overall system". This argument is supported by Ordonez and Bejan [32] who suggested that an entire system can be conceived from the beginning as a system designed to perform certain global objectives optimally, rather than as an assembly of already existing parts. Therefore, we believe that there is a need to introduce a mathematical algorithm that can be coupled with CFD in the optimisation process in order to achieve a near-optimal solution of the global performance.

Most of the currently applied methods are time-consuming, expensive and do not achieve a near-optimal solution. The advance in technology improvement and especially the advent of CFD has brought about great improvement, which has made it possible to analyse of difficult design variables with a satisfactory design. However,

the approach is to assume that there must be optimal design variables at which the system will perform best. Thus, a multidimensional and robust gradient-based optimisation algorithm that does not require an explicit line search is introduced and incorporated into the finite volume solver and grid (geometry and mesh) generation package. Its aim is to search and identify the optimal design variables at which the system will perform optimally. The combination of CFD and mathematical optimisation algorithms can produce unexpected improvement in the design optimisation process.

The advantage of our mathematical optimisation algorithm – which will be discussed in detail later – is that it can be coupled with the CFD simulation and grid generation packages in a MATLAB environment. This is done in such a way that it captures the numerical objective function in the simulation that is not available analytically, and searches for and identifies the optimal design variables that correspond to the objectives function.

1.4. AIM OF THE PRESENT RESEARCH

The aim of the current research is to carry out theoretical and numerical optimisation studies on conjugate heat transfer in cooling channels with variable cross-sections based on constructal theory and design. Also, we propose, develop and implement a design optimisation methodology that is founded on mathematical gradient-based techniques that will allow the optimisation of a peak temperature profile for the entire

system. This will be achieved by coupling computational fluid dynamics and a mathematical algorithm. The design parameters become design variables and the optimisation process with respect with these design variables is automatically taken into account by the optimisation algorithm. The approximated peak temperature profile obtained from the computational fluid dynamics simulation is used in the optimisation process for the computation of an objective function.

1.5. OBJECTIVES OF THE PRESENT RESEARCH

The objective of this study is to geometrically optimise the cooling structure in such a way that the global thermal resistance or peak temperature between the volume and the cooling fluid is minimised.

1.6. SCOPE OF THE STUDY

In this thesis, an optimal design approach is employed to computationally and efficiently optimise the heat transfer capabilities of cooling channels of different cross-sectional shapes by means of theoretical analysis, computational fluid dynamics and numerical optimisation algorithm. Five different cross-sectional shapes of cooling channels are introduced, namely cylindrical, square, isosceles, equilateral triangular and rectangular cooling channels.

Our models can be used for the entire laminar flow range, materials of different thermal conductivities and any fluid having Prandtl numbers ≥ 0.71. However, water

is used throughout the research as cooling fluid. Also, the fluid flow and heat transfer are steady-state, three-dimensional, conjugate and constant thermo-physical properties.

The models are designed for micro-scale devices because of recent developments in large-scale Micro-Electro Mechanical Systems (MEMS) with low-cost and small-space advantages, as well as high heat dissipation ability (e.g compact heat exchangers and micro-channel heat sinks). However, the models are also applicable to all the heat exchange devices at that mini- and macro-scale level, because convectional governing equations are used (also valid for micro, mini and macro-scale devices)

This research takes a comprehensive look at the optimisation of heat transfer such as peak temperature (global thermal resistance) at the hotspot of heat-generating devices that experience heating and need to be cooled and the cooling channels. All the design variables are subjected to various constraints which are numerically approximated by the automated optimisation algorithm.

1.7. RESEARCH METHODOLOGY

The objectives of this research were accomplished by both numerical and theoretical analysis. The analytical solution was based on the intersection of asymptotes method and scale analysis. The numerical simulations that were guided by the analytical solutions give a comprehensive explanation of the global thermal behaviour of the

problem. The numerical method involves the modelling and discretisation of the computational domain, the solving of conjugate heat transfer by using necessary governing equations, and the processing of results. An automated mathematical optimisation algorithm that uses numerically approximated functions is employed by coupling it to the commercial Computational fluid dynamic software – FLUENT – to search the optimal design variables that minimised thermal resistance. The detailed procedures of both numerical and theoretical analysis are discussed in the subsequent chapters.

1.8. MATERIAL SELECTION

Material selection is a very important part of the optimised design of cooling devices design as it provides a good balance between thermal properties, weight and material cost. For example, diamonds prove to be best suited for any cooling devices design but their use in heat-exchanging devices design is highly impractical from an economic point of view. Materials such as aluminium and copper dominate the materials commonly used in heat exchangers (recently silicon was introduced for use in micro-channel heat sinks), as they provide a good balance of the thermal conductivity-to-density ratio. The effect of material properties on the minimum thermal resistance will be shown in the later part of the thesis.

1.9. ORGANISATION OF THE THESIS

This thesis consists of ten chapters and each chapter is divided into sections and subsections. These provide a detailed description of the subject matter and make for easy reading and referencing. The chapters of the thesis are itemised below:

- Chapter One introduces the constructal theory and presents the motivation, justification and background of the study.

- Chapter Two provides literature reviews on the subject of Constructal theory with the focus on engineering applications especially heat transfer analysis.

- Chapter Three contains a review of the numerical model employed for the analysis, which is explained with the computational domain used for the simulations of cooling channels and vascularised material. The mass, momentum and energy conservation equations governing the transport of mass and heat are discussed. The iterative method of coupling these governing differential equations is also shown.

- Chapter Four deals with the subject of numerical optimisation and focuses on the operation of the DYNAMIC-Q algorithm. The underlying principles and governing equations of the optimisation algorithm are discussed.

- Chapter Five presents and develops a theoretical solution to the optimal channel geometry of parallel channels of different cross-sectional shapes that penetrate and cool a volume with uniformly distributed internal heat generation. This is based on an application of the intersection of asymptotes method and scale analysis to provide proof of the existence of an optimal geometry that minimises the peak temperature and global thermal resistance in a heat generation volume with an array of channels of different shapes. The geometric configurations of the cooling channels optimised are cylindrical, square, rectangular and triangular (isosceles right and equilateral).

- Chapter Six investigates further analytical solutions by implementing the numerical modelling and mathematical optimisation methodology developed in Chapters Three and Four. These are aimed at simulating and optimising the geometric configurations of conjugate heat transfer in cooling channels with different cross-sectional shapes and uniformly distributed internal heat generation. The steps involved in coupling the optimisation algorithm with FLUENT (a commercial computational fluid dynamic software) are also shown.

- Chapter Seven develops (numerically and analytically) the geometric optimisation of parallel cooling channels in the forced convection of a vascularised material with the localised self-cooling property subjected to a

heat flux on one side in such a way that the peak temperature is minimised at every point in the solid body. The analytical solution is also based on the application of the intersection of asymptotes method and scale analysis to provide an optimal geometry that minimises the peak temperature and global thermal resistance. The effect of material properties on the minimum thermal resistance and optimised internal configuration is also shown.

- Chapter Eight presents a three-dimensional geometric optimisation of conjugate cooling channels in forced convection and internal heat generation within the solid, for an array of circular cooling channels and different flow orientations based on constructal theory. Three flow orientations were studied: the study started with an array of channels with parallel flow; followed by an array of channels in which the flow of every second row is in counter direction, and lastly an array of channels in which the flow in every channel is opposite to the previous channel. The configuration and flow orientation were optimised in such a way that the peak temperature and global thermal resistance were minimised, subject to the constraint of fixed global volume of solid material.

- Chapter Nine provides a general summary of the findings of the study. It also presents the conclusions and contributions, as well as recommendations for future work.

CHAPTER 2: LITERATURE REVIEW

2.1. INTRODUCTION

This chapter deals with the literature review relevant to this thesis and gives an insight into the constructal theory and design and the effect of geometry on the heat transfer capabilities of cooling channels of heat-generating devices. Continuous literature studies and reviews were carried out during the research work.

2.2. CONSTRUCTAL THEORY

The application of this evolutionary design approach to the discovery of internal heat exchanger started with Bejan and Sciubba [3], who proposed the design rule for the spacing of an array of parallel plates to channels in such a way that the heat transfer density of a volume filled with heat-generating components was maximal. The spacing was determined by using intersection of asymptotes method. This philosophy was applied to all the facets of flow system design, from biology and physics, to engineering and social organisation [33-45].

In nature, water always takes the path of least flow resistance when of navigating in the river basin [33]. Thermodynamically, every system exhibits a level of imperfection due to entropy generation which leads to the degradation of performance

of the system [34]. However, a system must adjust itself to operate maximally by optimising the process and geometric configuration of the system to reduce the entropy.

In medicine [35], this physical law can also be applied to the treatment of cancer. The spreading of cancer can be controlled by maintaining the temperature field of the unaffected tissues in the neighbourhood of the turmoil below the temperature at which the cancer virus can survive. In the business world [36,37], constructal theory shows that transportation costs can be minimised by optimising the transportation routes of goods and products from one area to another in a dendritic form so as to travel shortest and easiest distance.

In heat transfer [38], the peak temperature must be minimised at every hot spot of a system. This promotes better thermal performance and avoids thermal stress by optimising shape and geometry.

In fluid mechanics [39], Bejan proposed that the flows pressure drop can be minimised by optimising the internal flow architecture of different ducts with variable cross-sections and by using constructal theory.

In academia [40-41], the constructal law was used to optimise the hierarchal rankings of universities in the global flow of knowledge. Also in military defence, the

constructal law was used to provide insight into and information on the optimisation of warfare tactics and strategy [42].

In sport industry [43- 45], constructal law has been used to optimised and predict the fastest men/women in athletics and swimming.

Other area of the applications of constructal law in the humanities, natural sciences and social sciences can also be found in [46-50].

The recent comment by Meyer [51] on Bejan and Lorente's work [52] on constructal theory and those of other researchers [53-59] shows that the application of constructal law in human life, nature and all fields of educational design is a wide road to future progress.

In this thesis our focus is on the first engineering application of constructal theory, which is the optimisation shape and structure for heat transfer and fluid flow [60-71]. The advantage of constructal law in the engineering field is that the flow architecture is not assumed in advance, but it is the consequence of allowing the structure to morph [72]. The applications of this theory have been reviewed recently by Bejan and Lorente [12], They argue that under certain global constraints, the best architecture of a flow system can be archived as the one that gives little global flow resistances, or allows high global flow access. In other words, the shapes of the channels and unit structure that is subject to global constraint are allowed to morph. The development of

heat exchangers and multi-scale architecture by constructal theory was also, reviewed by Reis [73] and Fan and Luo [74].

2.3. HEAT TRANSFER IN COOLING CHANNELS

2.3.1. Theoretical analysis

Bau [75], provided an analytical model solution that minimises thermal resistance by reducing maximum heat surface temperature and temperature gradient. He did this by optimising the cross-sectional dimension of the rectangular conduit of micro heat exchangers in terms of uniform and non-uniform width as a function of the axial coordinate of the conduit. The analytical model for a non-uniform conduit proved to be more effective in reducing the maximum surface temperature compared to the model with a uniform cross section of the conduits.

Yilmaz *et al.* [76] analytically studied the optimum shape and dimensions for convective heat transfer of laminar flow at constant wall temperatures for ducts with parallel plate, circular, square and equilateral triangle geometries. Approximate equations were derived in the form of maximum dimensionless heat flux and optimum dimensionless hydraulic diameter in terms of the duct shape factors and the Prandlt number (*Pr*).

Yang *et al* [77] presented a thermal optimization of a stack of printed circuit board using an entropy generation minimisation (EGM) method. They provided a dimensionless optimal channel spacing correlation in terms of the Reynolds number (Re) and height-to-width ratio.

Bejan and Fautrelle [78] maximised the heat transfer density in a multiscale structure filled by multiple length scale plates that generate heat. They inserted additional parallel plates and optimised the spacing in the flow structure.

Knight *et al*. [79-81] presented the governing equations for fluid dynamic and heat transfer in a generalised, dimensionless form, along with a geometrical relationship that can be used to determine the dimensions of a rectangular micro-channel heat sink that result in the minimisation of thermal resistance and they later performed an experiment to verify and validate their analytical optimisation scheme.

Muzychka [17] used this theory and Bejan's intersection of asymptotes method to present an analytical optimisation of circular and non-circular cooling channel geometries. He also studied and analysed the optimisation of microtube heat sinks and heat exchangers for maximum thermal heat transfer by using a multiscale design approach based on Constructal theory [18]. In his analysis, he was able to show that through the use of interstitial microtubes, the maximum heat transfer rate density for an array of circular tubes could be increased.

Bejan and Fautrelle [68] maximised the heat transfer density in a multiscale structure filled by multiple length scale plates that generate heat. They inserted additional parallel plates and optimised the spacing in the flow structure.

Knupp et al. [82] presented an analytical approach towards conjugated conduction-convection heat transfer problems by proposing a single domain formulation for modeling both the fluid stream and the channel wall regions. This made use of coefficients represented as space variable functions with abrupt transitions occurring at the fluid-wall interface region.

2.3.2. Numerical analysis

Kim and Anand [83] performed a two-dimensional numerical simulation of laminar developing flow and heat transfer between a series of parallel plates with surface-mounted discrete heat sources.

Ryu *et al.* [84] conducted a three-dimensional numerical analysis and presented an optimisation techniques called random search techniques to investigate the effect of thermal entrance on the thermal performance of a micro-channel heat sink and to predict the optimal design variables that minimise the thermal resistance of microchannel. They noted that thermal entrance effects could not be ignored especially when the working fluid was water, due to the thin thermal boundary layer in the developing region.

Fedorov and Viskanta [85] as well as Qu and Mudawar [86] used conventional Navier – Stokes and energy equations to analyse (numerically) a three-dimensional fluid flow and conjugate heat transfer characteristic in a rectangular silicon micro-channel heat sink, using water as coolant. The effect of the Reynolds number and thermal conductivity of the solid substrate were also considered. Their results in terms of frictional coefficient and thermal resistant as a function of the Reynolds number were compared and found to be in good agreement the with analytical solution of Shah and London [87] and the experimental solution of Kawano *et al*. [88]. Their models showed that the forced convective water-cooled micro-channnel heat sink has superior potential for application in the thermal management of the electronics package.

Ambatipudi and Rahman [89] performed numerical simulations for conjugate heat transfer in micro-channel heat sinks. The channel depth, channel width, number of channels and flow rate were used as design variables. They found that the performance of a heat sink can be improved by increasing the number of channels in the heat sink and the flow rate through the heat sink.

Chen [90] further investigated this influence mainly by studying the aspect ratio and effective thermal conductivity in forced convection heat transfer within a micro-channel. As the aspect ratio increased, fluid temperature and the overall Nusselt number increased. However, the influence of the channel aspect ratio on the temperature of the solid was minimal.

Da Silva *et al.* [91, 92] optimised the space allocation on a surface and wall occupied by discrete heat sources with a given heat generation rate by natural and forced convection. They used the constructal theory to minimise the temperature of the hot spot on the wall.

Bello-Ochende and Bejan [93] studied and numerically extended the initial work of Bejan and Fautrelle [68], based on the concept of constructal theory. Also, Bello-Ochende *et al.* [94-97] conducted a three-dimensional optimisation of heat sinks and cooling channels with heat flux. They used scale analysis and the intersection of asymptotes method (based on constructal theory) to investigate and predict the design and optimisation of the geometric configurations of the cooling channels.

Furthermore, Bello-Ochende *et al*. [98] numerically reported a new design concept to improve the constructal design for increasing the heat transfer rate density by using wrinkled entrance regions in square ducts with laminar-forced convection. The numerical simulations results showed the effects of the dimensionless pressure drop on the optimised configurations, as well as an enhanced heat transfer rate density. Bello-Ochende *et al.* [99] optimised the internal configurations of rectangular micro-channels heat sink subjected to high heat flux. Other works of Bello-Ochende and his co-researchers using Constructal theory in engineering application can be found in [100-103].

Rajkumar, *et al.* [104] presented a numerical solution of laminar conjugate natural convection in a vertical channel containing a short planar heat generating element by using a hybrid finite element/finite volume method together with a restricted domain approach. They also provided a correlation for dimensionless temperature as a function of dimensionless volumetric heat generation.

Mohammed *et al.* [105] conducted numerical simulations to solve the three-dimensional steady and conjugate heat transfer governing equations by using the Finite-Volume Method (FVM) to evaluate the effect of studies for different channel shapes on the performance of MCHS with the same cross-section.

Rocha *et al.* [106] and Biserni *et al.* [107] applied the constructal theory to optimise the geometry of C- and H-shaped cavities respectively that intrude into a solid conducting wall in order to minimise the thermal resistance between the solid and the cavities. Also, Biserni *et al.* [108] minimised the thermal resistance between the solid and the cavities by optimising the geometry of inverted fin shapes that also intrude into a solid conducting wall.

Lorenzini and Rocha [109] and, as well as Lorenzini *et al.* [110] used the constructal theory to minimise the thermal resistance between the solid and the cavities by optimising the geometry of isothermal cavities that evolve from T- and Y-shape of a solid conducting wall. Also, Lorenzini et al. [111- 113] optimised the complex assemblies of fins and cavity spaces. They used constructal theory and design to

minimise the thermal resistance between the solid conducting wall and the cavities by increasing the degrees of freedom that can lead to improvements in the performance of flow systems.

Salimpour *et al.* [114] studied numerically the optimal scale channels of circular and non-circular configurations to achieve maximum heat transfer density.

Matos *et al.* [115, 116] performed a numerical and experimental analysis of laminar-forced convective heat transfer. Air was used as an external cooling fluid. They conducted a two-dimensional numerical analysis for the geometric optimisation of staggered circular and elliptic tubes [115]. Here, they provided an optimum spacing between rows of tubes in such a way that a maximum rate of heat transfer between the constraint volume and the cooling fluid (free stream) was obtained. As stated, they conducted a three-dimensional numerical and experimental analysis [116] and presented geometric optimisation for staggered arrangements as well as for finned circular and elliptic tubes heat exchangers that were subjected to a fixed-volume constraint so as to maximise the volumetric heat transfer density. In their analysis, they considered three degrees of freedom – (the spacing between rows of tubes, the eccentricity of the tubes, and the fin-to-fin spacing) – as design constraints. The global optimal results with respect to these three degrees of freedom were established and expressed in a dimensionless form. Their result showed that the elliptical tubes have higher global performance.

Ordonez [117] conducted a two-dimensional heat transfer analysis in a heat-generated volume with cylindrical cooling channels and air as the working fluid. In their, Dirker and Meyer [118] investigated a three-dimensional numerical simulation. They considered the optimal thermal behaviour and performance of embedded internal cooling layers in a rectangular heat-generating volume of an electronic structure under two thermal boundary conditions by the use of externally mounted heat sinks. Their results showed that the thermal performance of an embedded layered technique strongly depends on the fraction of the volume occupied by cooling layers and the ratio of the thermal conductivities of the cooling layers and the heat-generating layers. Their technique – when compared with a traditional planar conduction approach – was found to better peak temperatures, because the traditional approach neglected layer thickness

Reis *et al*. [119] optimised the internal configurations of parallel plate and cylindrical channels using Constructal theory to understand the morphology of particle agglomeration and the design of air-cleaning devices.

In fuel cell [120 - 122], Constructal law was used to optimise the internal architecture and external structure of a Proton exchange membrane (PEM) and a single solid oxide (SO) fuel cell so that the power density was maximised.

Obayopo *et al*. [123] studied a three-dimensional numerical optimisation of the effect of operating and internal design parameters of PEM fuel cell performance that would

maximise the current density of the fuel cell. They showed that the maximised current density increases as the mass flow rate of the reactant gas increases at an optimal channel depth. Obayopo *et al*. [124] also investigated the effect of pin fins of small hydraulic diameter transversely arranged along the internal flow channel on the reactant gas distribution and pressure drop characteristics of the fuel cell performance. There existed an optimal pin fin clearance ratio, which offered minimum pumping power requirements and that maximum fuel cell performance.

2.4. VASCULARISED SOLID WITH COOLING CHANNELS

Recent advancements in the constructal theory have led to another cooling concept – vascularised material – getting a relative amount of attention. Material with the property of self-healing and self-cooling is becoming increasingly promising in heat transfer analysis [125-130]. The development of vascularisation of materials indicates flow architectures that conduct and circulate fluids at every point within the solid body. This solid body (slab) may be performing or experiencing mechanical functions such as mechanical loading, sensing and morphing. The self-cooling ability of vascularised material to bathe volumetrically at every point of a solid body gave rise to the concept of – ‘smart materials’.

In smart materials, constructal theory and design [1,2] helps with the vascularisation of the smart material structure by morphing the flow architecture configuration to provide easier and greater access of flow through it.

Kim *et al.* [130] theoretically and numerically analysed vascularised materials with heating from one side and coolant forced from the other side for parallel plates and cylindrical channel configurations. They attempted to find the channel configurations that minimised the non-uniform temperature distribution of a vascularised solid body.

Cho *et al.* [131] numerically investigated the flow and thermal behaviour of vascular cooling plate for the volumetric bathing of the smart structures.

Constructal theory applications on the vascularisation revolution of smart materials can also be found in open literature [132-137].

Wang *et al*. [133] investigated systematically optimised channel diameters, the shapes of the loops formed by the closest channels, the shapes of the vascularised slabs of two-dimensional bodies (by employing multi-scale grids) and tree-shaped flow structures that will justify the designs for smart materials with self-healing and self-cooling functionality. Also, Kim *et al.* [134] numerically proposed the use of tree-shaped flow architectures to vascularise a solid body and prevent the overheating that would be caused by intense side heating.

Kim *et al*. [135] also showed the emergence of vascular design in three dimensions of smart material. They focused on a mass flow network to understand how to define and refine vascular designs for a particular application by minimising the total system pressure loss as a measure of the overall goodness of a network design.

Wang *et al.* [136] numerically considered the use of vasculatures to evaluate the volumetric cooling performance of slabs with embedded flow architectures consisting of grids and radial channels. The results showed that grids have lower global flow resistance than radial designs while local junction losses are important.

The constructal theory for optimisation of several components and systems, as well as of components in many engineering applications (such as in the area of energy and power sectors, civil engineering, industrial air-conditioning system, chemical engineering nano-fluid designs) has been extensively discussed and documented in the literature [138-181].

2.5. BEJAN NUMBER

Prior to 1992, a lot of dimensionless numbers named after researchers based on their finding and discovering , such as the Reynolds number (*Re*), which has to do with viscous flow in forced convection, the Rayleigh number (*Ra*) applies to natural convection, and the Prandlt number (*Pr*), – that deals with convective heat transfer.

However, Bejan and Sciubba [3] came up with a new dimensionless number called the dimensionless pressure difference number in an attempt to optimise the spacing of an array of parallel plate to channels so that the heat transfer density of a volume filled with heat generating components is maximised by using the method of intersection of asymptotes method. Bhattacharjee and Grosshandler [182], and Petrescu[183] later called this dimensionless pressure difference number as Bejan number (*Be*).

The Bejan number (*Be*) plays the same role in forced convection that the Rayleigh number (*Ra*) plays in natural convection [184-185]. *Be* is used by many authors [17-19, 64-70] to describe the driving force in forced convective heat transfer.

2.6. FLOW ORIENTATION IN CONJUGATE COOLING CHANNELS

The growing constructal theory literature focuses on convective heat transfer analysis, but does consider the effects of flow orientation. However, Ma *et al.* [186] experimentally investigated the flow resistance and forced convective heat transfer influence for flow orientation in a packed channel that experience heating at the bottom. Wang *et al*. [187] carried out a numerical investigation to study the effect of the orientation of a heat sink on the thermal performance of a PCM-based cooling system.

Other research on the effect of orientation can be seen in [188-191]. Huang *et al*. [188] carried out experimental analysis on natural convection heat transfer for square pin fin heat sinks subject to the influence of orientation. They found out that the downward facing orientation yields the lowest heat transfer coefficient compare to upward and sideward facing orientations. However, the heat transfer coefficients for upward and sideward facing orientations are of comparable magnitude. Zhang *et al*.[189] performed experimental and theoretical studies of the effects of orientation on flow boiling critical heat flux (CHF). The results showed that the interfacial lift-off model is very effective at capturing the overall dependence of CHF on orientation. P. Dutta, and S. Dutta [190] experimentally investigated the heat transfer and frictional loss behavior of turbulent flow in a rectangular channel with isoflux heating from the upper surface for different sizes, positions, and orientations of inclined baffles attached to the heated surface. It was found that both average and local Nusselt numbers are significantly dependent on the baffle plate orientation and the Nusselt number ratio decreases as the plate is placed at a more streamlined position.

2.7. MATHEMATICAL OPTIMISATION ALGORITHM

The history of mathematical optimisation dates back to the 1940s when it was first used as steepest descent for solving very simple problems where functions of many variables are considered [192]. Different types of algorithms have been developed to

solve the optimisation problem. These include the genetic algorithm, multiplier methods, surrogate, annealing simulation, Powel algorithm and sequential quadratic programming [192 - 198].

Foli *et al*. [196] analytically and numerically studied geometric optimisation of micro-heat exchangers by using a multi-objective genetic algorithm to maximize the heat transfer rate and minimizing the pressure drop. Husain and Kim [197] numerically performed a multi-objective performance optimisation of microchannel heat sinks by applying surrogate analysis and an evolutionary algorithm to obtain global Pareto-optimal solutions that gave minimum thermal resistance.

Baodong *et al*. [198] numerically presented a multi-objective optimisation design of a micro-channel heat sink by using an adaptive genetic algorithm to simultaneously minimise thermal resistance and pressure drop.

2.8. CONCLUSION

This chapter referred to some of the available literature on constructal theory and design. It also, provide information on the geometric optimisation of cooling channels and various optimisation techniques used in the past to optimally design heat generating devices . The bulk of the published work includes theoretical analysis, and

numerical modelling, which are used to generate optimal correlations with regard to the thermal performance of different heat generating devices.

This research provides novel method of optimising the thermal structure and cooling channel flow architecture by theoretical and numerical analyses coupled with optimisation algorithm with the aim of at further improving and enhancing the performance of thermal system.

The self-healing and self-cooling ability of vascularised material to bathe volumetrically at every point of a solid body is becoming increasingly promising in heat transfer analysis. Constructal theory ideally helps in the vascularisation of the smart material structure by morphing the flow architecture configuration to provide easier and greater access of flow through it. The works on vascularisation of the smart material structure found in literature have only been done on flat plates and cylindrical channel configurations. This work extended the knowledge by considering square configuration with the use of a mathematical optimisation algorithm.

Again, the growing constructal theory in literature does not consider the effects of flow orientation on convective heat transfer analysis. Our research on effects of flow orientation is new and novel, especially in cases where an array of channels which in

flow of the every second row is in counter flow with its neighbours; and an array of channels in which flow in all the channels are counter flow to one another.

Also, based on the literature, most of the algorithms used in the past did not handled the effect of a numerical noise function during simulation or its effect on the gradient-based optimisation algorithms due to the influence of changes of grid and convergence problem during iterations. This could lead to inaccurate solutions. The ability of our mathematical optimisation algorithm to be coupled with simulation software and to capture data directly from the simulation and its ability to overcome the numerical noise made our solution unique optimal design.

3

CHAPTER 3: NUMERICAL MODELLING

3.1. INTRODUCTION

This chapter deals with the processes that are involved in the numerical modelling of heat transfer and flow, discretisation of the computational domain, solving of the heat and mass transport governing equations and processing of the results. The commercial CFD software FLUENT [199] is used for the numerical analysis, which will be discussed in detail in the subsequent sections.

3.2. MODELLING PROCEDURE

Recently time, the modelling of fluid flow and heat transfer problems have been made easy by the development of CFD codes structured around numerical algorithms. The numerical analysis consists of three stages, namely:

1. Pre-processing: This involves defining and developing the computational domain, geometry, mesh generation and discretisations, as well as the selection domain boundaries for the purposes of simulation.
2. Solver execution: This involves the integration and solving of the governing equations at various nodal points across the computational domain.
3. Post-processing: This involves the analysis of results and provision of visualisation tools such as grid displays, the generation of contour plots of various parameters of interest and particle tracking [200].

3.3. GEOMETRY AND GRID GENERATION

Geometry and grid generation constitute a major part of the pre-processing stage in a CFD analysis. The process involves dividing the computational domain into a finite number of discretised control volumes on which the governing equations can be solved.

The Geometry and Mesh Building Intelligent Toolkit (GAMBIT) [201] is a commercial automated grid generator. With the help of a graphical user interface (GUI), it is used to construct finite volume models and create the geometry for generating meshes. The model and meshes are exported to FLUENT software for simulation and analysis. GAMBIT [201] and FLUENT 6.3 [199] can be automated by means of journal input files during optimisation process by setting up a computational model and mesh generation.

The governing non-linear partial differential equations used for the fluid flow and heat transfer analysis include the conservation of mass (continuity), conservation of momentum and conservation of energy - coupled through density-pressure relationship.

3.4. CONSERVATION OF MASS

In an Eulerian reference frame, the equation of continuity in its most general form for fluids is given by [202]

$$\frac{D\rho}{Dt} + \rho \text{ div } u = 0 \tag{3.1}$$

where ρ is the density of the fluid, t is the time and $\boldsymbol{V}$ is the velocity vector of the fluid. For incompressible flow (constant density), Equation 3.1 reduces to:

$$\rho \text{ div } u = 0 \tag{3.2}$$

3.5. CONSERVATION OF MOMENTUM

The momentum conservation equation is formally derived from Newton's second law, which relates the applied force to the resulting acceleration of a particle with mass. For Newtonian viscous fluids, Navier and Stokes fundamentally derived the following equation using the indicial notation:

$$\rho \frac{DU}{Dt} = \rho \boldsymbol{g} - \nabla P + \frac{\partial}{\partial x_j}\left[\mu \left(\frac{\partial u_i}{\partial x_j} + \frac{\partial u_j}{\partial x_i} \right) \right] + \delta_{ij} \lambda \text{ div U} \tag{3.3}$$

where $\boldsymbol{g}$ is the vector acceleration of gravity, P is the pressure, x is the spatial coordinate, μ is the coefficient of viscosity, u is the velocity component, δ_{ij} is the Kronecker delta function and λ is the vexing coefficient associated with volume expansion [202]. Using Stokes' hypothesis, $\lambda = -\frac{2}{3}\mu$.

For incompressible flow, the vexing coefficient λ and div U (due to the continuity relationship) vanish, simplifying Equation 3.3 to:

$$\rho\left(\vec{u}\cdot\nabla\vec{u}\right)=-\nabla P+\mu\nabla^2\vec{u} \tag{3.4}$$

3.6. CONSERVATION OF ENERGY

The conservation equation is derived from the first law of thermodynamics, which states that an increase in energy is a result of work and heat added to the system. Neglecting radiative effects, the energy equation in its standard form can be written as:

$$\rho\frac{Dh}{Dt}=\frac{DP}{Dt}+\text{div}(k\ \nabla T)+\Phi \tag{3.5}$$

where h is the enthalpy of the fluid, k is its thermal conductivity, T is the temperature of the fluid and Φ represents the dissipation function expressed as:

$$\Phi=\mu\left[2\left(\frac{\partial u}{\partial x}\right)^2+2\left(\frac{\partial v}{\partial y}\right)^2+2\left(\frac{\partial w}{\partial z}\right)^2+\left(\frac{\partial v}{\partial x}+\frac{\partial u}{\partial y}\right)^2+\left(\frac{\partial w}{\partial y}+\frac{\partial v}{\partial z}\right)^2+\left(\frac{\partial u}{\partial z}+\frac{\partial w}{\partial x}\right)^2\right]+\lambda\left(\frac{\partial u}{\partial x}+\frac{\partial v}{\partial y}+\frac{\partial w}{\partial z}\right)^2 \tag{3.6}$$

For incompressible flow with constant thermal conductivity and low velocities, the viscous dissipation becomes negligible. Thus, Equation 3.5 can be simplified to:

$$\rho_f C_{Pf}\left(\vec{u}\cdot\nabla T\right)=k_f\nabla^2T \tag{3.7}$$

while the energy equation for a solid with internal heat generation is given as:

$$k_s\nabla^2T+q_s'''\ =\ 0 \tag{3.8}$$

where, k_f and k_s represent the thermal conductivity of the fluid and solid respectively. The simplified equations are in steady state.

3.7. BOUNDARY CONDITIONS

When a meshed geometry with grid is imported into FLUENT [199], boundary conditions for various surfaces and parameters need to be specified to run the simulations. The boundary conditions are guided by the types of engineering problems we want to solve.

3.8. NUMERICAL SOLUTION TECHNIQUE

This section deals with the numerical techniques implemented by using a three-dimensional coupled density-based commercial package FLUENT™ [199] in solving the mass, momentum and energy conserving equations that employs a finite volume method (FVM). The details of the method were explained by Patankar [203].

The computational domain is discretised into a finite number of discrete elements and control volumes. The combined convection and diffusion terms in the momentum and energy equations are integrated on each discrete element and control volume thereby constructing algebraic equations for the discrete dependent variables to be solved. The discretised equations are linearised and the resulting system of linear equations is solved to yield updated values of the dependent variables.

Furthermore, the governing equations which are non-linear and coupled are solved by segregating them from one another. Hence, several iteration processes of the solution loop must be performed [199] before a converged solution is obtained. A flow chart representing an overview of numerical steps of the iterative process is shown in Figure 3.1.

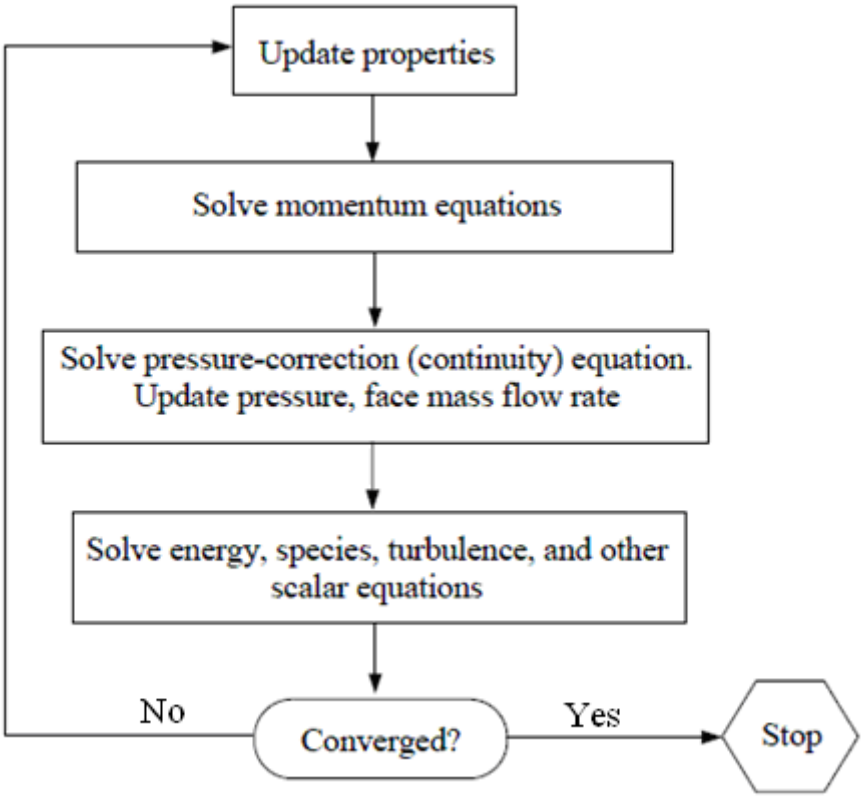

Figure 3. 1 : Overview of the segregated solution method [199]

3.9. CONCLUSIONS

This chapter focused on the processes involved in solving fluid flow and heat transfer problems by using a three-dimensional coupled density-based commercial package FLUENT™. A set of non-linear partial differential equations governing the transport of mass and heat is discussed. The numerical scheme implemented in solving the flow and heat transfer is also examined.

4

CHAPTER 4: NUMERICAL OPTIMISATION

4.1. INTRODUCTION

This section examines the theory governing the mathematical optimisation algorithms used in this thesis, together with the numerical modelling technique described in Chapter 3. We also examine an overview of the optimisation technique, which is described in detail in the subsequent sections.

4.2. NUMERICAL OPTIMISATION

The mathematical or numerical optimisation often known as non-linear programming is described as a systematic method to find the minimum or maximum of a specific function for a given set of constraints. This helps in finding the best design under certain design constraints by changing the appropriate design variables. It can also be defined as the solving of a problem or task in the best way that can be expressed mathematically or numerically. Optimisation models arise in almost every area of human endeavours. In economics, optimisation is the maximisation of profit, maximisation of efficiency and minimisation of loss or risk. In engineering, optimisation is the design of a building or machinery to minimise the weight or maximise strength in order to avoid failure. The history of mathematical optimisation date back to the 1940s when it was first used as steepest descent for solving very simple problems in cases where functions of many variables are considered[192].

4.3. NON-LINEAR CONSTRAINED OPTIMISATION

In mathematical optimisation, an optimal solution is obtained by changing some parameters known as the design variables while the function to be optimised (minimised or maximised) is called the objective or cost function $f(\boldsymbol{x})$. The design variables are generally represented by a vector $\boldsymbol{x}^*$. The optimisation problem becomes a constrained optimisation problem when some constraints in the form of inequalities $g_i(\boldsymbol{x})$ or equalities $h_j(\boldsymbol{x})$ are introduced into the process; else the problem is an unconstrained optimisation problem. The unconstrained optimisation problem is solved more easily, compared to a constrained optimisation problem. This is because the former is reduced to the search of finding the minimum or maximum values of the objective function $f(\boldsymbol{x})$. For the constrained optimisation problem, the optimisation becomes very complex. The constraints will have to be treated in a special way by introduction of a penalty function.

In general, the non-linear constrained optimisation problem can be expressed in mathematical form as

$$\min_{x} f(x); \left[x_1, \ldots x_2, \ldots . x_i \ldots X_n, \right]^T, \; x_i \in \square^n, \tag{4.1}$$

subject to

$$g_j(x) \leq 0, \; j = 1, 2, \ldots . p, \tag{4.2}$$

$$h_k(x) = 0, k = 1, 2, \ldots . q, \tag{4.3}$$

where $f(x)$, $g_j(x)$, $h_k(x)$ are scalar functions of the vector x and they are defined as objective or merit functions, inequality constraint functions and equality constraint functions, respectively. The components of vector x are called design variables. The solution of the problem in Equations (4.1) to (4.3) is given as vector x^*:

$$x^* = \left[x_1^*, x_2^*, \ldots ., x_n^*, \right]^T \tag{4.4.}$$

This gives the lowest value of the objective function $f(\boldsymbol{x})$ subject to specified inequality and equality constraints. In a situation where the objective function $f(\boldsymbol{x})$ is to be maximised, the minimisation algorithm is still applicable. However, the setting will be $f_{max}(\boldsymbol{x}) = -f(\boldsymbol{x})$. Figure 4.1 represents the transformation of the maximisation problem to a minimisation problem [192].

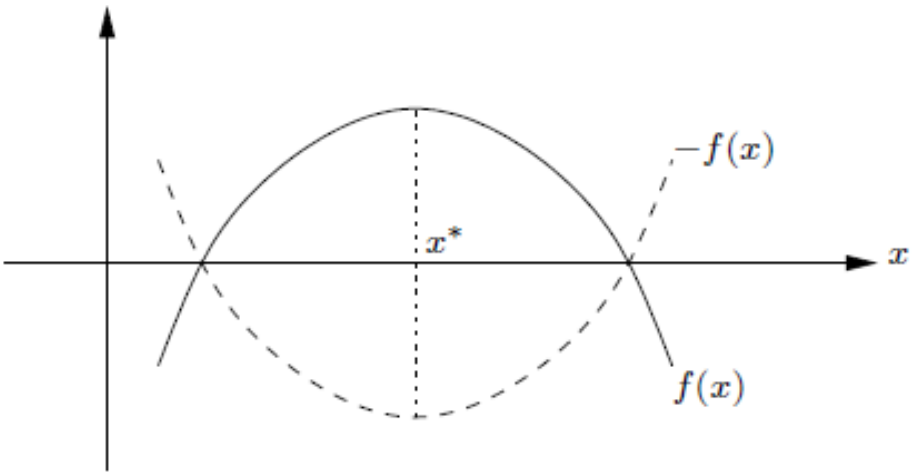

Figure 4. 1 : Graphical representation of a maximisation problem [192]

As stated in Chapter 2 different types of algorithms have been developed to solve the optimisation problem of Equations (4.1) to (4.3). These include the generic algorithm, multiplier methods, surrogate, annealing simulation, Powel algorithm and sequential quadratic programming [192]. Some mathematical algorithms are commercially available. However, new algorithms are being developed to solve the inhibiting complications experienced with the available methods. Only the optimisation algorithms used in this study are discussed next.

4.4. OPTIMISATION ALGORITHMS

The Leapfrog Optimisation Program for Constrained Problems (LFOPC) and DYNAMIC-Q algorithms [204, 205] were used as optimisation processes in this study to optimise an approximation solution to the original problem. The LFOPC algorithm

is applied to the penalty function parameter in three phases, which increases the rate of searching for an optimal design solution in limited time. DYNAMIC-Q is a gradient-based algorithm and is good at handling optimisation problems with a large number of variables with minimal storage requirements of the computer RAM. Also, unlike genetic algorithm methods, the DYNAMIC-Q is not computationally expensive, as complex functions that are expensive to compute numerically are approximated using spherical quadratic approximate functions. Both LFOPC and DYNAMIC-Q algorithms are discussed in detail in the subsequent sections.

4.4.1. Leapfrog optimisation program for constrained problems (LFOPC)

Snyman's original LFOP [204, 205] was adapted to handle constrained problems of equality and inequality constraints by introducing a penalty function formulation of the original problem in three phases [206 - 208]. The penalty function formulated as

$$p(\boldsymbol{x}) = \gamma f(\boldsymbol{x}) + \sum_{i=1}^{m} \alpha_i g_i(\boldsymbol{x})^2 + \sum_{j=1}^{n} \beta_j h_j(\boldsymbol{x})^2 \tag{4.5}$$

where

$$\alpha_i = \begin{cases} 0 \text{ if } g_i(\boldsymbol{x}) \le 0 \\ \rho_i \text{ if } g_i(\boldsymbol{x}) > 0 \end{cases} \tag{4.6}$$

To simplify the algorithm, the penalty parameters ρ_i and β_j take on the same positive value μ, that is $\rho_i = \beta_j = \mu$. As the value of μ increases, say $\mu = \propto$, the unconstrained minimum of $p(\boldsymbol{x})$ solves the constrained problem of Equations (4.1 – 4.3); hence the solution to the constrained problem becomes more accurate at a very high value of μ. The unconstrained optimisation problem on the other becomes ill-conditioned at a very high value of μ.Therefore, the penalty parameter should be increased gradually until it reaches the limit value of μ. The later is then kept constant until convergence is reached with minimum violation of the inequality constraints in the initial design steps [206]. The penalty function formulation of the constrained problem in Equation (4.2) occurs in three phases and will be next discussed as executed in the optimisation process.

4.4.1.1. Penalty formulation: Phase 0

In this phase, for a given initial guess of the design variable $\boldsymbol{x}_0$*, the penalty parameter introduced is given a value of μ_0. The penalty function is subsequently minimised using the Leapfrog optimisation program (LFOP) and with $\gamma = 1$ resulting in an optimum design variable vector $\boldsymbol{x}(\mu_o)$* after convergence. The LFOP automatically scales the constraints to make sure that the violation of a constraint on the gradient of penalty function is approximately the same for all the constraints. At this optimal point, the active inequality constraints are checked and identified for

spatial violation. If no active inequality constraints are found (constraints that are violated), and no equality constraints either, this optimal point must certainly be the optimal minimum value of the optimisation problem and the algorithm is then completed.

4.4.1.2. Penalty formulation: Phase 1

This phase is initialised by increasing the value of the penalty parameter μ when active inequality constraints are obtained from the solution of Phase 0. The penalty function parameter for objective constraints is again set to $\gamma = 1$. Also the approximate design point, $\boldsymbol{x}(\mu_o)^*$ obtained from Phase 0 is used as the starting guess, after which the penalty parameter is minimised by LFOP. Following convergence, a more accurate solution of the original problem is found and active inequality constraints that may be different from that of phase 0 are again identified. If there are no active constraints, and the solution $\boldsymbol{x}(\mu_1)^*$ becomes the optimal solution of the optimisation problem then the algorithm is terminated

4.4.1.3. Penalty formulation: Phase 2

In this last phase, the penalty function parameter for objective constraint is again set to $\gamma = 0$. The optimal solution from phase 1 is used as the initial guess and the penalty parameter is then minimised by LFOP. The optimisation algorithm will search for an optimal solution of the optimisation problem, which corresponds to the intersection of

the active constraints. However, if the active constraints do not intersect, the optimisation algorithm will find the best likely solution, which is usually closer to the real solution with little active constraint violation.

4.4.2. DYNAMIC-Q optimisation algorithm

The DYNAMIC-Q optimisation algorithm was developed by Snyman *et al.* [204, 208 -210] at the University of Pretoria. The Dynamic-Q is a multidimensional and robust gradient-based optimisation algorithm that does not require an explicit line search of the objective functions. The technique involves the application of a dynamic trajectory LFOPC optimisation algorithm to successive approximate quadratic sub-problem of the original problem [207], hence the name "DYNAMIC-Q". The DYNAMIC-Q can handle numerical analyses obtained from CFD and FEM simulations efficiently by dealing with all noise functions due to grid changes, convergence and the numerical accuracy of the computer.

In this method, the successive sub-problems $P[l]$, $l = 0,1,2,...$ are generated at successive design points $\boldsymbol{x}^l$, starting with an initial arbitrary design x^0 to a solution x^*. They develop the spherical quadratic approximations to approximate the objective functions or constraints, or both of the objective functions and constraints, provided that they are not analytically given or very numerically expensive to compute [208,210]. The spherical quadratic approximations are given by:

$$\tilde{f}(x) = f\left(x^{(l)}\right) + \nabla^T f\left(x^{(l)}\right)\left(x - x^{(l)}\right) + \frac{1}{2}\left(x - x^{(l)}\right)^T A\left(x - x^{(l)}\right) \tag{4.7}$$

$$\tilde{g}_i(x) = g_i\left(x^{(l)}\right) + \nabla^T g_i\left(x^{(l)}\right)\left(x - x^{(l)}\right) + \frac{1}{2}\left(x - x^{(l)}\right)^T B_i^{(l)}\left(x - x^{(l)}\right), \qquad i = 1,....p \tag{4.8}$$

$$\tilde{h}_j(x) = h_j\left(x^{(l)}\right) + \nabla^T h_j\left(x^{(l)}\right)\left(x - x^{(l)}\right) + \frac{1}{2}\left(x - x^{(l)}\right)^T C_j^{(l)}\left(x - x^{(l)}\right), \qquad j = 1,....q \tag{4.9}$$

where $\nabla^T f$, $\nabla^T g_i$ and $\nabla^T h_j$ denote the gradient vector, and can be approximated by a forward finite-difference scheme if these vectors are not known analytically. A, $B_i^{(l)}$ and $C_j^{(l)}$ are approximate Hessian matrices of the objective function, inequality constraint and equality constraint functions respectively. The approximations are defined by the diagonal matrix as

$$A = diag(a, a, ..., a) = aI \tag{4.10}$$

$$B_i = b_i I \tag{4.11}$$

$$C_j = c_j I \tag{4.12}$$

where ***I*** represents the identity matrix.

The convergence of the solution is achieved in a stable manner and controlled by imposing move limits on the design variables during the optimisation process. The move limit δ_l takes on the form of the constraint by limiting the movement of each

design variables $\boldsymbol{x}_l^k$ and not allowing the new design point to move too far away from the current design point. The move limit of single inequality constraints is described as

$$g_\delta\left(x_i\right)\left\|x_i - x_i^{l-1}\right\|^2 - \delta_i^2 \le 0, \qquad i = 1,2,...n \tag{4.13}$$

where δ_i is the approximately chosen step limit for each design variable.

The Dynamic-Q is terminated when either the normalised step size is:

$$\Delta x_{norm} = \frac{\left\|x_i - x_i^{l-1}\right\|}{1+\left\|x_i\right\|} \le \varepsilon_x \tag{4.14}$$

or the normalised change in the function value is:

$$\Delta f_{norm} = \frac{\left|f_i - f_{best}\right|}{1+\left|f_{best}\right|} \le \varepsilon_f \tag{4.15}$$

where ε_x and ε_f are the step size and function value tolerances respectively.

4.5. FORWARD DIFFERENCING SCHEME FOR GRADIENT APPROXIMATION

The gradient vector of the objective function (obtained from the numerical simulation) at a specified design point x with respect to each of the design variables x_i is approximated by the first- order forward differencing scheme given as

$$\frac{\partial f(x)}{\partial x_i} \approx \frac{f\left(x+\Delta x_i\right)-f(x)}{\Delta x_i} \qquad i=1,2....,n \tag{4.16}$$

where $\Delta x_i = \left[0,0,....,\Delta x_i,....0\right]^T$, is the suitable step size.

The inequality and equality constraints gradient vectors on the other hand are also approximated within the algorithm by the first- order forward differencing scheme in a similar way. They are represented (4.17) and (4.18) respectively as:

$$\frac{\partial g_j(x)}{\partial x_i} \approx \frac{g_j\left(x+\Delta x_i\right)-g_j(x)}{\Delta x_i} \qquad j=1,2...., p \tag{4.17}$$

$$\frac{\partial h_k(x)}{\partial x_i} \approx \frac{h_k\left(x+\Delta x_i\right)-h_k(x)}{\Delta x_i} \qquad k=1,2...., q \tag{4.18}$$

4.6. EFFECT OF THE NOISY FUNCTIONS OF THE FORWARD DIFFERENCING SCHEME ON THE OPTIMISATION ALGORITHM

Noisy functions could occur in objective functions in many engineering design problems. They comprise experimental and numerical simulation analyses as a result of the activities of a complex sequence of calculations involving measured or computed quantities. This may lead to inaccurate solutions. Experimental noise may cause error due to the influence of the environment, while numerical noise may be caused by changes of grid, convergence problems during iterations and numerical accuracy of the computer. The size of the step Δx used in the differencing scheme is very important when approximating the derivative functions. If the size of the step is not carefully chosen, it can pose a noise that result in incorrect solutions [211 - 215]. Therefore, it is essential to choose a step size Δx carefully so that it drastically minimises the noise and gives an accurate representation of the global gradient of the function.

Figure 4.2 shows the effect of noise on the selection of the step size Δx of a function obtained from a numerical simulation. Ideally, a very small step size Δx is expected to give an accurate approximation of the global gradient of a function. However, due to the existence of noise function in optimisation algorithms, the approximation of the global gradient of the function may be inaccurate when a small step size Δx is used as shown in Figure 4.2(a). Thus, using a large enough step size will reduce the

influence of the noise as shown in Figure 4.2(b), but this will also lead to a wrong or inaccurate approximation of the gradients.

To ensure that the step size chosen is ideal, the optimisation problem should be worked out several times with different starting guesses. If the solution converges to the same value, then it can be concluded that the step size is sufficient. If discrepancies are observed, however, the step size should be modified until discrepancies in the results are extremely reduced.

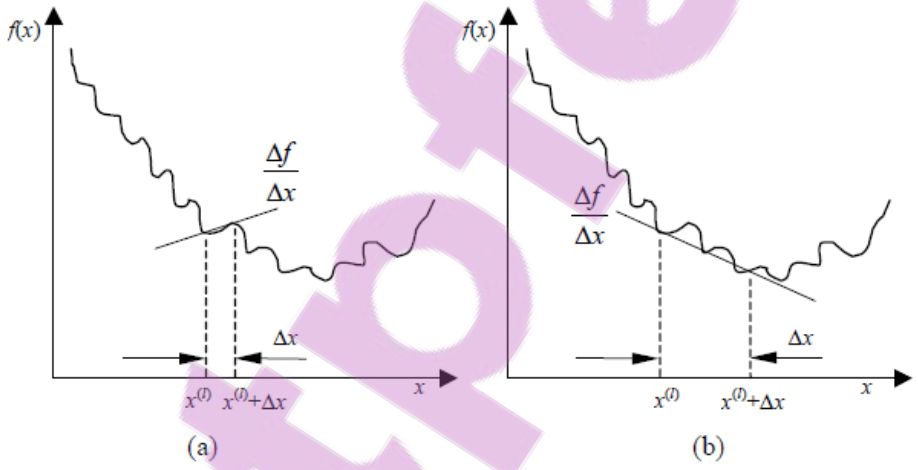

Figure 4. 2： Graph depicting the effect of step size on gradient approximation [192]

4.7. CONCLUSION

This chapter focused in details on the mathematical optimisation algorithms used in this study, namely the LFOPC and DYNAMIC-Q algorithms. The DYNAMIC-Q, which builds on the LFOPC algorithm, presented a multi-dimensional, accurate,

reliable and robust penalty method for solving practical constrained engineering design problems and helps in the optimal design of systems. The effect of numerical noise function during simulation and its effect on the gradient-based optimisation algorithms were also discussed and an efficient way of dealing with the associated problems was suggested.

5

CHAPTER 5: INTERSECTION OF ASYMPTOTES METHOD FOR CONJUGATE CHANNELS WITH INTERNAL HEAT GENERATION[1],[2]

5.1. INTRODUCTION

This chapter deals with the theoretical analysis of geometrical optimisation. It is presented for different configurations using the intersection of asymptotes method to provide the existence of an optimal geometry that minimises the global thermal resistance.

[1] This research chapter, together with Chapter 6, has been published in part: O.T. Olakoyejo, T. Bello-Ochende and J.P Meyer, "Constructal conjugate cooling channels with internal heat generation", *International Journal of Heat and Mass Transfer*. Vol. 55, pp. 4385 - 4396, 2012.

[2] This research chapter, together with Chapter 6, has been published in part: J.P Meyer; O.T. Olakoyejo and T. Bello-Ochende, "Constructal optimisation of conjugate triangular cooling channels with internal heat generation", *International communication of Heat and Mass Transfer*, Vol. 39, pp. 1093 - 1100, 2012.

5.2. OVERVIEW OF THE INTERSECTION OF ASYMPTOTES METHOD

This section presents and develops a theoretical solution to the optimal channel geometry of parallel channels with different cross-sectional shapes that penetrate and cool a volume with uniformly distributed internal heat generation, q_s'''.

The cooling fluid is water which is assumed to be in single-phase, steady and a Newtonian fluid with constant thermo-physical properties. The flow is laminar and is forced through the cooling channels by a specified pressure difference ΔP, across the axial length of the structure. Water is more effective than air because the air-cooling techniques are not likely to meet the challenge of high heat dissipation in electronic packages [216, 217].

The total volume and the volume porosity (ϕ) occupied by the channels are fixed. The objective is to achieve minimum global thermal resistance.

In this study, five different types of channel configurations namely cylindrical, square, equilateral and isosceles right triangular and rectangular channels are introduced as shown in Figure 5.1.

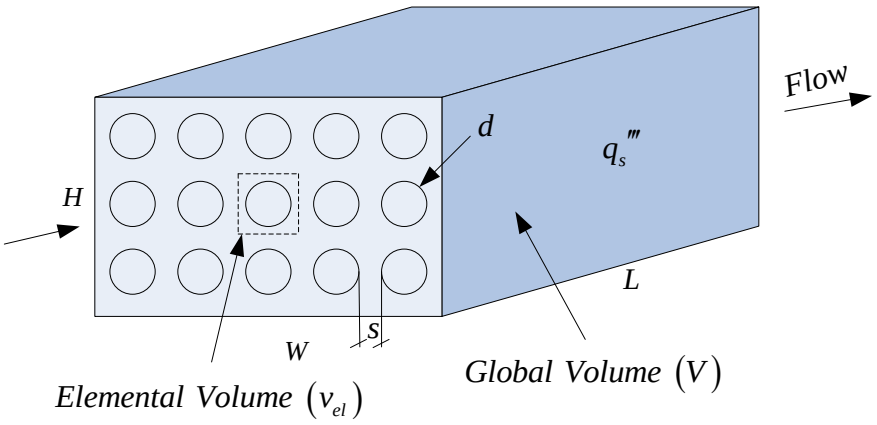
Flow
d
q_s'''
H
L
W
s
Elemental Volume (v_{el})
Global Volume (V)

(a)

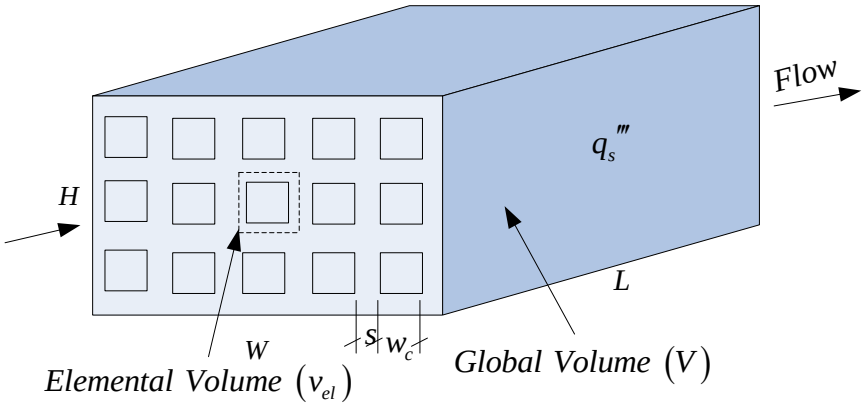
Flow
q_s'''
H
L
W
s
w_c
Elemental Volume (v_{el})
Global Volume (V)

(b)

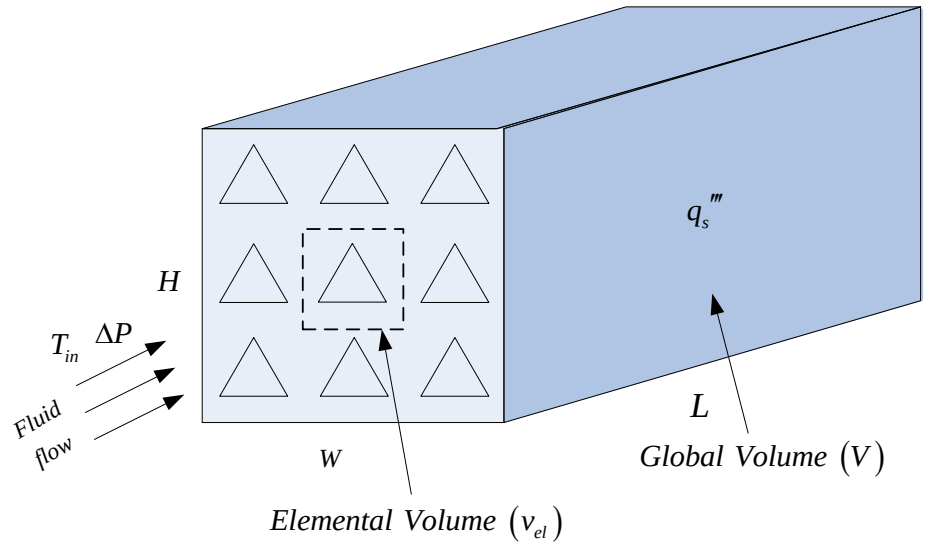

(c)

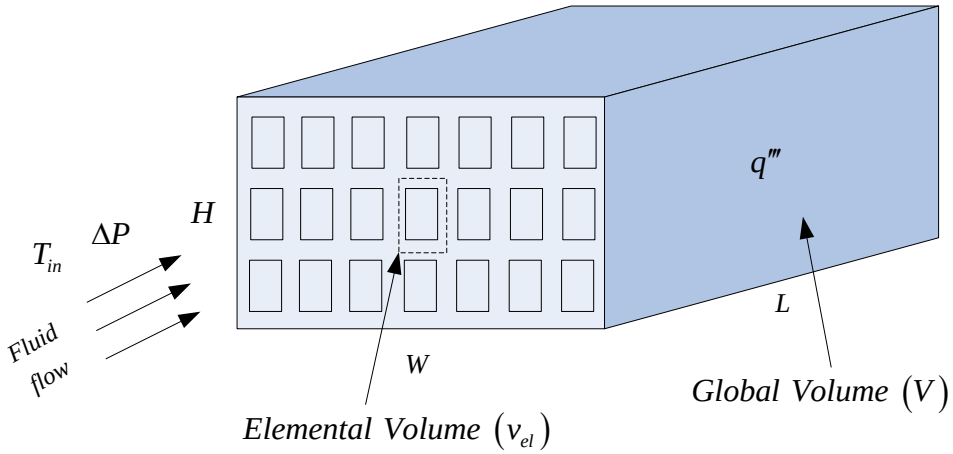

(d)

Figure 5. 1 : Ducts with (a) cylindrical (b) square (c) triangular (d) rectangular cooling channels

The optimisation is based on the intersection of asymptotes method and scale analysis. The optimal channel geometries and minimum global thermal resistance between volume and coolant are reported for all the configurations. The optimal

geometries are determined as trade-offs between the two operating extremes of each configuration channel in which the heat transfer mechanism operates – the extreme limit of a small channel with fully developed flow and the extreme limit of a large channel with the distinct boundary layer.

The following assumptions are also made throughout the analysis: the inlet temperature and the pressure difference ΔP are fixed with a uniform flow distribution in all the channels, laminar flow, constant cross-sectional area of the channels, negligible inlet and exit plenum losses, and negligible axial conduction. An elemental volume is considered because of the symmetry of the heat distribution.

The heat generated in the elemental volume [17, 19] is

$$\dot{q} = q'''\left(A_s - A_c\right)L \tag{5.1}$$

The heat is conducted and deposited as the heat flux, q'', through the solid wall to the fluid, therefore,

$$q'''\left(A_s - A_c\right)L = q''P_cL \tag{5.2}$$

The porosity is assumed to be fixed at $\phi = A_c/A_s$, therefore Equation (5.2) becomes

$$q'' = \frac{1}{4}q'''d_h\beta \tag{5.3}$$

where β is the numerical value determined from the porosity of the channel and is defined as:

$$\beta = \left(\frac{1-\phi}{\phi} \right) \tag{5.4}$$

and d_h is the channel hydraulic diameter defined as:

$$d_h = \frac{4A_c}{P_c} \tag{5.5}$$

The global thermal resistance or global thermal conductance will be determined in two extreme limits.

5.2.1. Extreme limit 1: small channel

When the channel's characteristic dimension is very small and very slender, that is $d_h \to 0$ and $d_h \ll L$, the flow is fully developed along the length, L. See Figure 5.2 for its cylindrical configuration

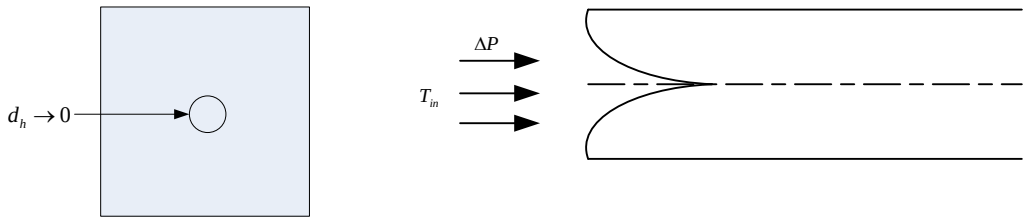

Figure 5. 2 : The extreme limit of the channel's characteristic dimension is very small and very slender, i.e. $d_h \to 0$ **and** $d_h \ll L$

According to the first law of thermodynamics, the rate of heat transfer in a unit volume to the working fluid is equal to enthalpy gained by the working fluid, and then for constant, C_p

$$\dot{q}_s = \rho A_c \bar{u} C_p \left(T_{out} - T_{in}\right) \tag{5.6}$$

In this extreme limit, the fluid in the channel quickly becomes a fully developed flow and the working fluid is overworked in such a way that the outlet temperature T_{out} approaches the peak temperature, $T_{\max}$, at the solid structure.

Therefore, Equation (5.6) becomes

$$\dot{q}_{sm} = \rho A_c \bar{u} C_p \left(T_{\max} - T_{in}\right) \tag{5.7}$$

This is equal to the heat deposited as heat flux, q'' through the wall to the fluid.

Therefore,

$$\rho A_c \bar{u} C_p \left(T_{\max} - T_{in}\right) = q'' P_c L \tag{5.8}$$

when the flow is fully developed, the average velocity $\bar{u}$, is given by Hagen-Poiseuille as:

$$\bar{u} = \frac{\Delta P \varsigma^2}{4 \mu P_{o_\varsigma} L} \tag{5.9}$$

where ς is the characteristic dimension used to define the Poiseuille number, P_o, and in this case the hydraulic diameter, d_h.

Combine Equations (5.8) and (5.9) and substitute ς for d_h, then rearrange to get

$$\left(T_{\max}-T_{in}\right)=q''\left(\frac{16\mu P_{o_{d_h}}L^2}{\rho {d_h}^3 C_p \Delta P}\right) \tag{5.10}$$

Substitute Equation (5.3) for Equation (5.10) and rearrange to get

$$\frac{\left(T_{\max}-T_{in}\right)}{q'''L^2}=\beta\left(\frac{4\mu P_{o_{d_h}}}{\rho {d_h}^2 C_p \Delta P}\right) \tag{5.11}$$

But

$$C_p=\frac{k_f \,\mathrm{Pr}}{\rho\nu} \tag{5.12}$$

Substitute Equation (5.12) for Equation (5.11) and rearrange the formula as

$$\frac{k_f\left(T_w-T_{in}\right)}{q'''L^2}=\beta\left(\frac{4\mu\nu P_{o_{d_h}}}{{d_h}^2\,\mathrm{Pr}\,\Delta P}\right) \tag{5.13}$$

The dimensionless global thermal resistance is defined in terms of dimensionless pressure difference as

$$R=\left[\frac{k_f\left(T_w-T_{in}\right)}{q'''L^2}\right]\cong 4P_{o_{d_h}}\beta\left(\frac{d_h}{L}\right)^{-2}Be^{-1} \tag{5.14}$$

where

$$Be=\frac{\Delta P L^2}{\mu\alpha} \tag{5.15}$$

From Equation (5.14) for a smaller channel $d_h \ll L$, the thermal resistance is inversely proportional to d_h^2. Keeping β (which is a function of porosity) constant, it shows that the global thermal resistance increases as the hydraulic diameter decreases.

5.2.2. Extreme limit 2: large channel

In this extreme limit, the channel's characteristic dimension is sufficiently large, that is, $d_h \to \infty$, the boundary layer of surface becomes distinct and the channel diameter is larger than the boundary layer thickness. The working fluid is not properly utilised and working fluid outside the boundary layers becomes useless and the body is not properly cooled in the downstream for cylindrical configuration (Figure 5.3).

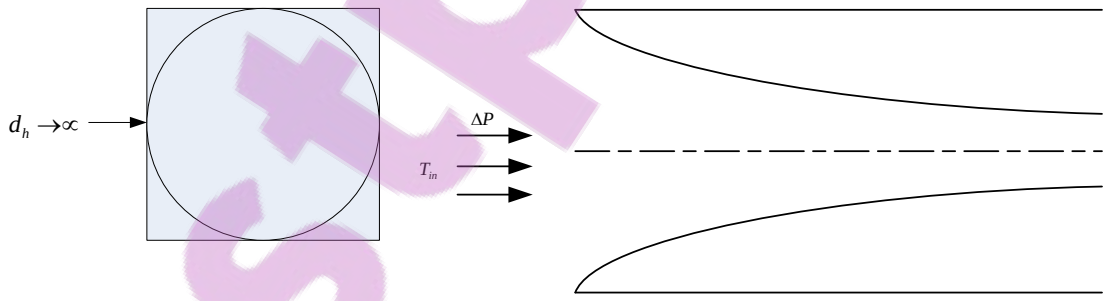

Figure 5. 3 : The extreme limit of the channel's characteristic dimension is sufficiently large, that is $d_h \to \infty$

The rate of heat transfer across the thermal boundary layer is

$$\dot{q}_l = hA_s\left(T_{\max} - T_{in}\right) \tag{5.16}$$

and the heat flux is

$$\dot{q}_l'' = h\left(T_{\max} - T_{in}\right) \tag{5.17}$$

The heat transfer rate can be related to the Nusselt number and heat transfer coefficient over the unit system. The heat transfer coefficient is defined for a laminar boundary layer as [31]

$$\frac{hL}{k_f} = 0.453 k_f \, \mathrm{Pr}^{1/3} \, \mathrm{Re}^{1/2}, \qquad \text{for,} \quad 0.5 < \mathrm{Pr} < 10 \tag{5.18}$$

Substitute Equation (5.18) for (5.17) to get

$$\dot{q}_l'' = \frac{0.453 k_f \, \mathrm{Pr}^{1/3} \, \mathrm{Re}^{1/2}}{L}\left(T_{\max} - T_{in}\right) \tag{5.19}$$

where

$$\mathrm{Re}_L = \frac{\bar{u}_\infty L}{\nu} \tag{5.20}$$

and u_∞ is the free-stream velocity that sweeps the boundary layers. The longitudinal pressure force balance on the control volume inscribed inside a unit volume channel is:

$$\Delta P A_c = P_c L \bar{\tau}_w \tag{5.21}$$

where $\bar{\tau}_w$ is the average wall shear stress across the length and can be obtained from the laminar boundary layer flow solution [218] as

$$\bar{\tau}_w = 0.664 \rho u_\infty^2 \, \mathrm{Re}_L^{-1/2} \tag{5.22}$$

Combine Equations (5.5) and (5.20) with Equation (5.22) to obtain

$$\mathrm{Re}_L = \left(\frac{\Delta P d_h L}{2.656 \rho \nu^2} \right)^{2/3} \tag{5.23}$$

Substitute Equation (5.23) for Equation (5.19) to obtain

$$\dot{q}_l'' = \frac{0.3271 k_f \, \mathrm{Pr}^{1/3}}{L} \left(\frac{\Delta P d_h L}{\rho \nu^2} \right)^{1/3} \left(T_{\max} - T_{in} \right) \tag{5.24}$$

Further substitution of Equation (5.3) for Equation (5.24) and rearrangement of the formula defines the dimensionless global thermal resistance as:

$$R = \left[\frac{k_f \left(T_{\max} - T_{in} \right)}{q''' L^2} \right] \cong 0.7643 \beta \left(\frac{d_h}{L} \right)^{2/3} Be^{-1/3} \tag{5.25}$$

From Equation (5.25), for a larger channel, the global thermal resistance is directly proportional to $d_h{}^{2/3}$. Keeping β (which is a function of porosity) constant, confirms that as the hydraulic diameter becomes larger, the global thermal resistance increases.

5.2.3. Optimal channel diameter and spacing

The optimal behaviour of asymptotes is shown in Figure 5.4 where the fluid is fully developed and utilised. The geometric optimisation in terms of channel could be achieved by combining Equations (5.14) and (5.25), and using the intersection of asymptotes method as shown in Figure 5.5.

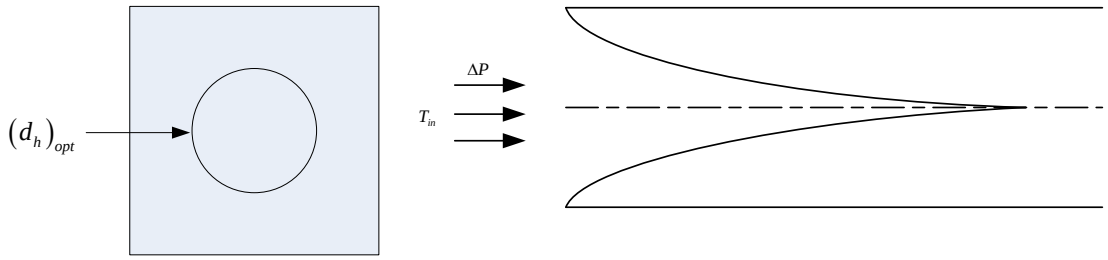

Figure 5. 4 : The optimal limit of the channel's characteristic dimension

The optimal dimension can generally be approximated for the two configurations as the hydraulic diameter where the two extreme curves intersect. The intersection result is

$$\left(\frac{d_h}{L}\right)_{opt} \approx 1.8602 P_{o_{d_h}}{}^{3/8} Be^{-1/4} \tag{5.26}$$

where $d_{h_{opt}}$ is the optimal hydraulic diameter and for circular channel $P_{o_{d_h}} = 8$. Hence Equation (5.26) reduces to

$$\left(\frac{d_h}{L}\right)_{opt} \approx 4.057 Be^{-1/4} \tag{5.27}$$

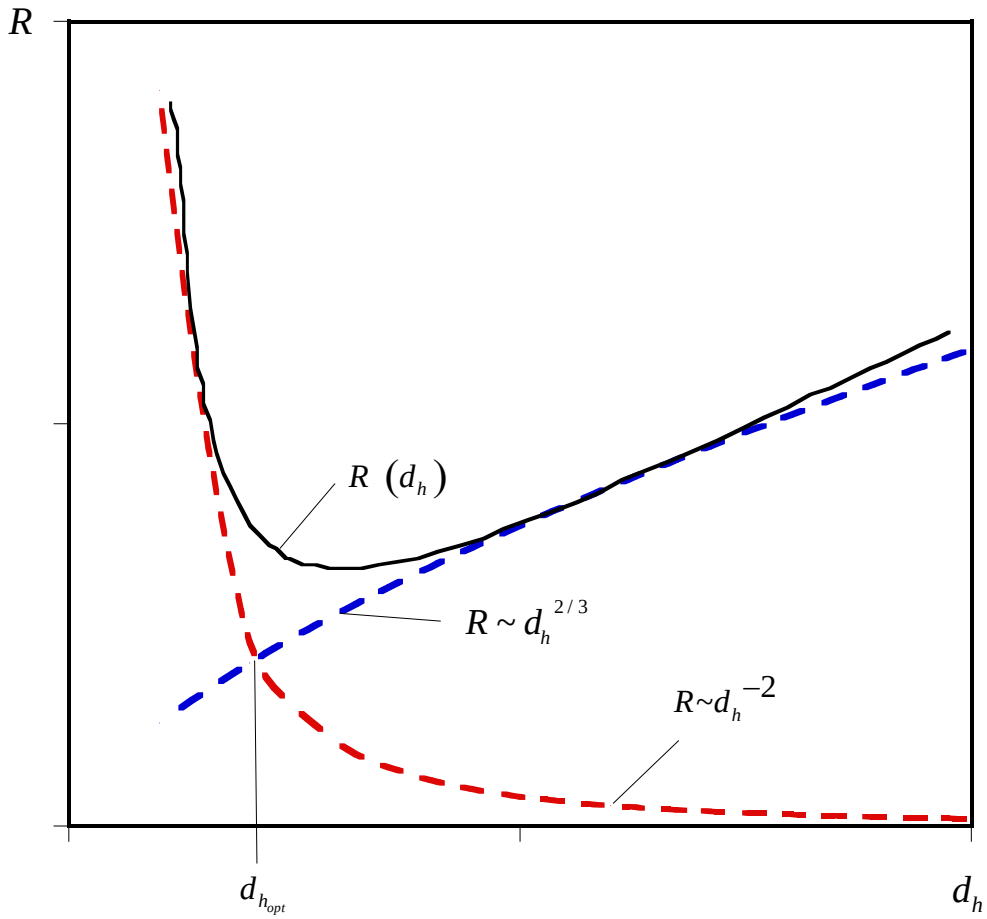

Figure 5. 5 : Intersection of asymptotes method: Global thermal resistance

For a square channel with hydraulic diameter d_h, $P_{o_{d_h}} = 7$

Hence Equation (5.26) reduces to:

$$\left(\frac{d_h}{L}\right)_{opt} \approx 3.859 Be^{-1/4} \tag{5.28}$$

for an isosceles right triangle channel with hydraulic diameter d_h, $P_{o_{d_h}} = 6.577$,

Equation (5.26) therefore reduces to

$$\left(\frac{d_h}{L}\right)_{opt} \approx 3.7698 Be^{-1/4} \tag{5.29}$$

For an equilateral triangle channel with hydraulic diameter d_h, $P_{o_{d_h}} = 6.625$ Hence Equation (5.26) reduces to:

$$\left(\frac{d_h}{L}\right)_{opt} \approx 3.7801 Be^{-1/4} \tag{5.30}$$

For a rectangular channel, the Poiseuille number can be approximated as

$$P_{o_{d_h}} = \frac{12}{\left(1+AR_c^{-1}\right)^2\left[1-\frac{192}{\pi^5}AR_c^{-1}\tanh\left(\frac{\pi}{2}AR_c\right)\right]} \tag{5.31}$$

hence Equation (5.26) combined with Equation (5.30) can be rewritten followed as:

$$\left(\frac{d_h}{L}\right)_{opt} \approx 4.7234\left[\left(1+AR_c^{-1}\right)^2\left[1-\frac{192}{\pi^5}AR_c^{-1}\tanh\left(\frac{\pi}{2}AR_c\right)\right]\right]^{-3/8} Be^{-1/4} \tag{5.32}$$

The optimal spacing s_{opt} follows from Equations (3), (5) and (5.26):

$$\left(\frac{s}{L}\right)_{opt} \approx 1.8602\left[\left(1+\beta\right)^{1/2}-1\right]P_{o_{d_h}}{}^{3/8} Be^{-1/4} \tag{5.33}$$

Equations (5.26) and (5.33) show that in the two extremes, the hydraulic diameter and channel spacing decreases as the pressure difference increases for fixed porosity.

The minimum dimensionless global thermal resistance can be obtained for an elemental volume for all the channels configurations that correspond to the optimal geometries. This can be by substituting Equation (5.26) into for Equation (5.14):

$$R_{\min} = 1.156\beta P_{o_{d_h}}{}^{1/4} Be^{-1/2} \tag{5.34}$$

Equation (5.34) shows that the thermal resistance decreases monotonically as Be increases for a fixed porosity.

The minimised dimensionless global thermal resistance of a circular channel with $P_{o_{d_h}} = 8$ is

$$R_{\min} = 1.9442\beta Be^{-1/2} \tag{5.35}$$

and the minimised dimensionless global thermal resistance of a square channel with $P_{o_{d_h}} = 7$ is:

$$R_{\min} = 1.8803\beta Be^{-1/2} \tag{5.36}$$

The minimised dimensionless global thermal resistance of a isosceles right triangle channel with $P_{o_{d_h}} = 6.577$ is

$$R_{\min} = 1.8513\beta Be^{-1/2} \tag{5.37}$$

and the minimised dimensionless global thermal resistance of a an equilateral triangular channel with $P_{o_{d_h}} = 6.625$ is

$$R_{\min} = 1.8546\beta Be^{-1/2} \tag{5.38}$$

The minimised dimensionless global thermal resistance of a rectangular channel with approximated $P_{o_{d_h}}$ of Equation. (5.31) is

$$R_{\min} = 2.1516\left[\left(1+AR_c^{-1}\right)^2\left[1-\frac{192}{\pi^5}AR_c^{-1}\tanh\left(\frac{\pi}{2}AR_c\right)\right]\right]^{-1/4}\beta Be^{-1/2} \tag{5.39}$$

5.3. SUMMARY OF THE THEORETICAL OPTIMISATION FOR ALL THE COOLING CHANNEL SHAPES

5.3.1. Effect of Applied dimensionless pressure difference on the minimised dimensionless global thermal resistance

Figure 5.6 shows the minimised dimensionless global thermal resistance as a function of dimensionless pressure difference at optimised design variables for the cylindrical, square, equilateral and isosceles triangular configurations. Minimised thermal resistance monotonically decreases as the applied dimensionless pressure difference number across the axial length increases for fixed porosity. The cylindrical channel has the highest thermal resistance while the triangular channels have the lowest thermal resistance for a given applied dimensionless pressure difference number. This is due to the fact that triangular configurations have high shear stress corners. Also, Figure 5.7 shows the minimised dimensionless global thermal resistance as a function of dimensionless pressure difference at optimised design variables for rectangular configurations. Minimised thermal resistance decreases as the applied dimensionless pressure difference number across the axial length at different aspect ratios increases.

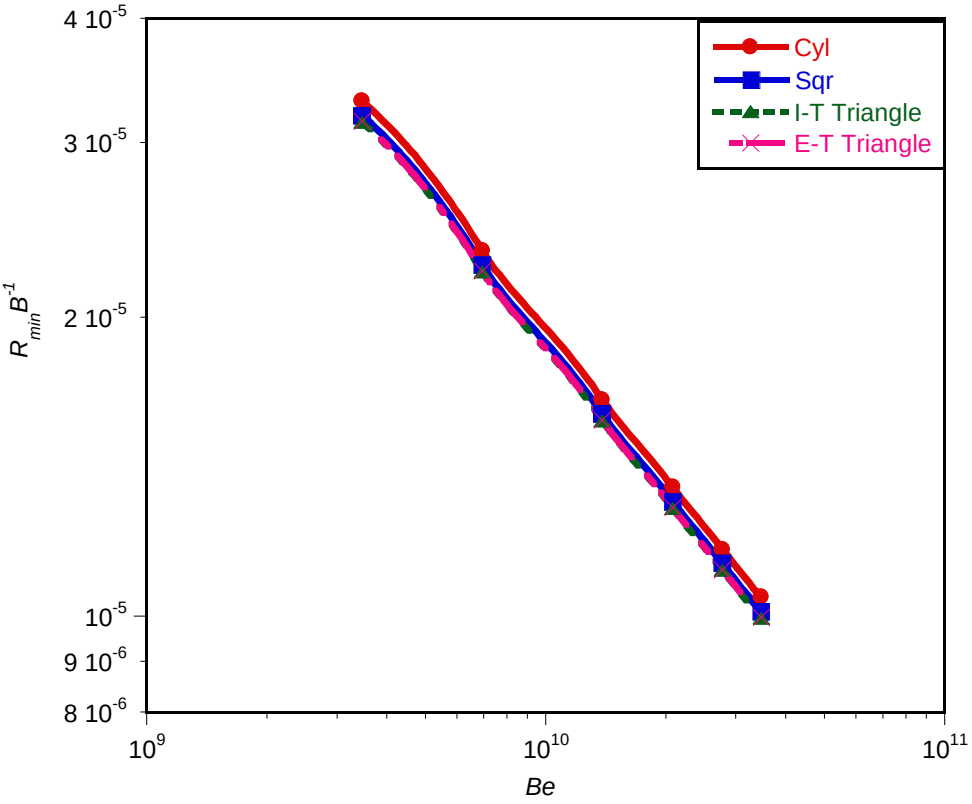

Figure 5. 6 : Effect of applied dimensionless pressure difference on the dimensionless global thermal resistance

5.3.2. Effect of applied dimensionless pressure difference on optimised design variables

Figure 5.8 shows the effect of the dimensionless pressure difference on the optimised hydraulic diameter for the cylindrical, square, equilateral and isosceles triangular configurations. The curve shows that design variables decrease as the applied dimensionless pressure difference for fixed porosity increases. The graph also shows

that unique optimal design geometries exist for each applied dimensionless pressure number and for each configuration.

Furthermore, Figure 5.9 shows the graph of dimensionless pressure difference as a function of the dimensionless hydraulic diameter for the rectangular configuration. The curve indicates that optimised the dimensionless hydraulic diameter decreases as the applied dimensionless pressure difference for fixed porosity increases. The graph also shows that unique optimal design geometries exist for each applied dimensionless pressure difference at different aspect ratios.

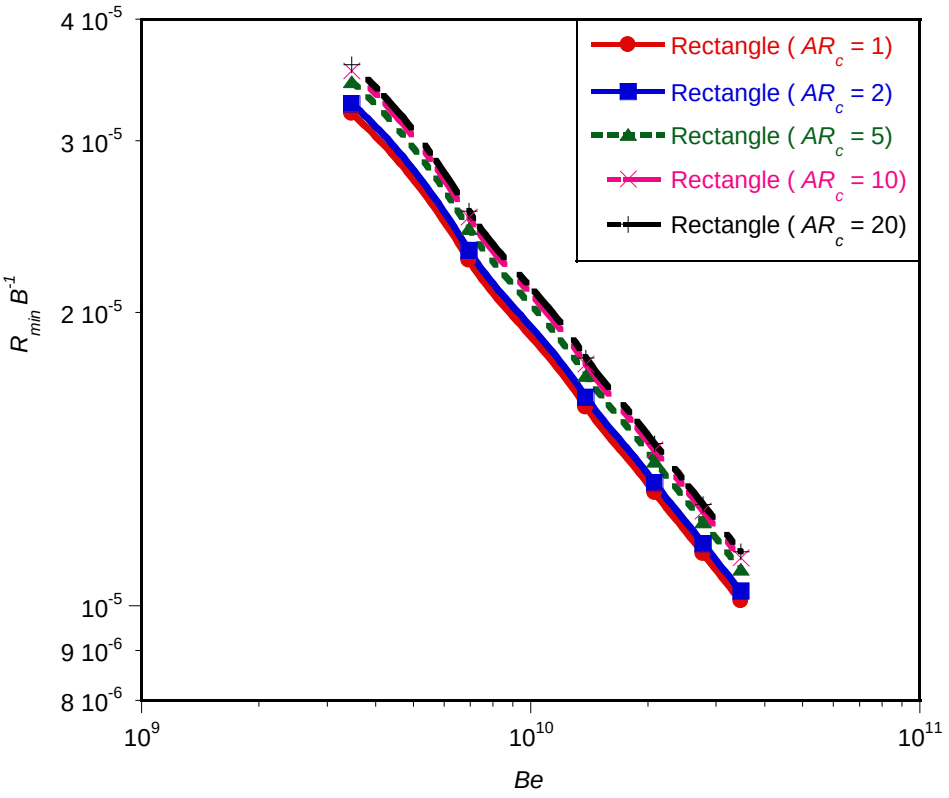

Figure 5. 7 : Effect of applied dimensionless pressure difference on the dimensionless global thermal resistance

In summary, the best parallel-channel structure for suppressing the hot spots of heat-generating devices should have the hydraulic diameter shown in Equation (5.26). The minimised global thermal resistance decreases further by increasing the applied pressure difference number (*Be*) and reducing the channel-to-channel spacing and hydraulic diameter smaller.

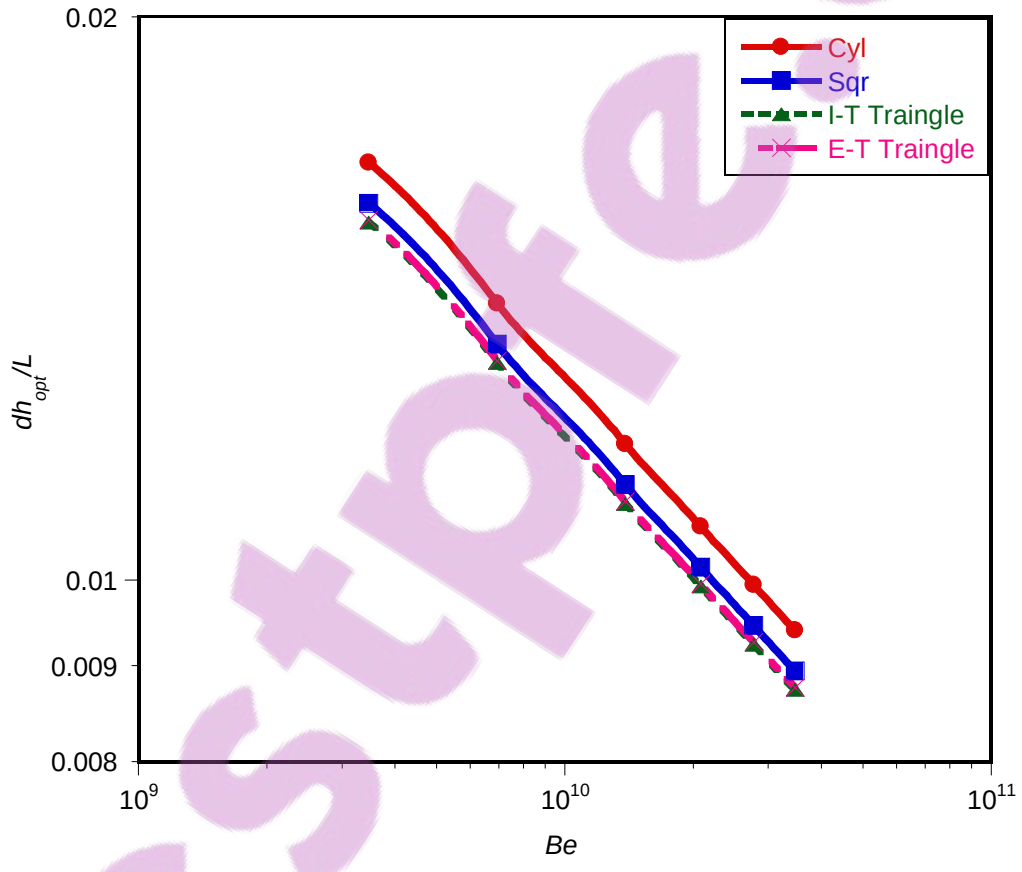

Figure 5. 8 : Effect of applied dimensionless pressure difference on the dimensionless global thermal resistance

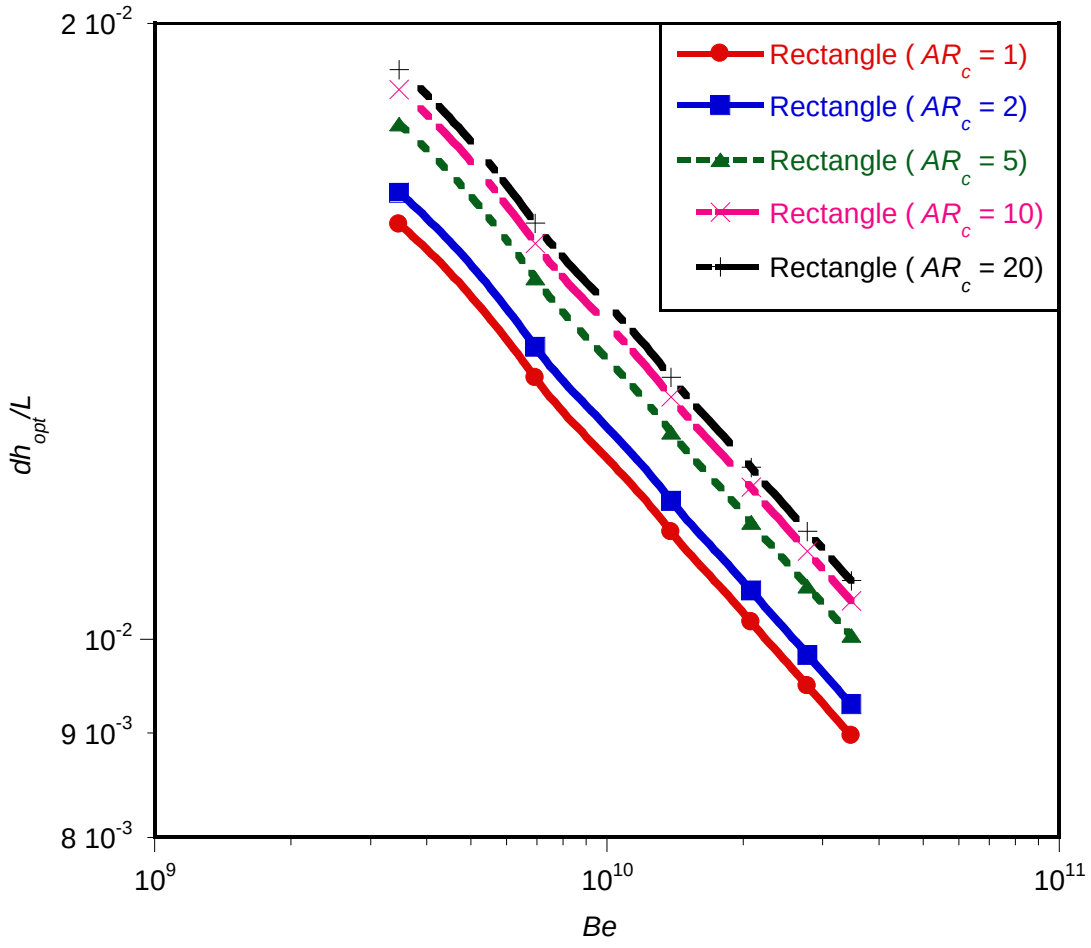

Figure 5. 9 : Effect of applied dimensionless pressure difference on the dimensionless global thermal resistance

5.4. CONCLUSION

This chapter presented and developed an overview of the analytical solution to the geometrical optimisation of the external structures and internal architectures of parallel channels of different cross-sectional shapes for cooling volumes that generate heat uniformly. The intersection of asymptotes method was used to provide the existence of an optimal geometry, which minimises the global thermal resistance.

The cooling fluid is driven by forced convection through the channels by the pressure difference across the channels. The optimal channel geometry was determined as a trade-off between the two extremes in which the heat transfer mechanism operates, in other words the extreme limit of the small channel and extreme limit of the large channel. The porosity of the volume penetrated by the array of channels was assumed given.

The optimal spacing between adjacent channels in the array can be derived from the optimal channel sizes already determined. The structure of channels and channel-to-channel spacing are optimal when each flow passage is just long enough to allow for its thermal boundary layers to merge at the exit as shown in Figure 5.4. This can be done by ensuring that the cooling volume is used to its fullest by packing the channels in such a way that every portion of flow passage is worked in a heat transfer form.

The next chapter will provide the numerical solutions for achieving optimal geometry, which minimises the global thermal resistance. The theoretical and the numerical solutions will also be compared.

6

CHAPTER 6: NUMERICAL OPTIMISATION OF CONJUGATE HEAT TRANSFER IN COOLING CHANNELS WITH DIFFERENT CROSS-SECTIONAL SHAPES[3],[4]

6.1. INTRODUCTION

This chapter focuses on the study of the numerical approximation of three-dimensional conjugate heat transfer in heat generated solid structures. It examines the geometric optimisation of a fixed and finite global volume of solid materials in an array of cooling channels with different cross-sectional configurations which experience a uniform internal heat generation, which will result in the minimal global thermal resistance. The objective is the building of a smaller construct to form a larger construct body that will minimise the global thermal resistance or, inversely, maximise the heat transfer rate density (the total heat transfer rate per unit volume).

[3] This research chapter, together with chapter 5 has been published in part: O.T. Olakoyejo, T. Bello-Ochende and J.P Meyer, "Constructal conjugate cooling channels with internal heat generation", *International Journal of Heat and Mass Transfer*. Vol. 55, pp. 4385 - 4396, 2012.

[4] This research chapter, together with chapter 5 has been published in part: J.P Meyer; O.T. Olakoyejo and T. Bello-Ochende, "Constructal optimisation of conjugate triangular cooling channels with internal heat generation", *International communication of Heat and Mass Transfer*, Vol. 39, pp. 1093 - 1100, 2012.

This is achieved by forcing a coolant to the heated spot in a fast and efficient way so as to drastically reduce the peak temperature at any point inside the volume that needs cooling. The optimisation process is carried out numerically under total fixed-volume and manufacturing constraints. As in all problems of constructal design, the configuration (shape, size) is unknown and must be determined. The mathematical optimisation algorithm described in Chapter 4 is introduced to search and identify the design variables at which the system will perform at an optimum. Thus the minimum thermal resistance between the fixed volume and the cooling fluid is obtained as the desired objective function for all the cases of geometrical shape studied. The present numerical results and the analytical solutions proposed in Chapter 5 are compared for each case study. The numerical solutions of all the case studies are also compared before the chapter is concluded.

6.2. CASE STUDY 1: CYLINDRICAL AND SQUARE COOLING CHANNEL EMBEDDED IN HIGH-CONDUCTING SOLID

This case study builds on the research previously carried out by Ordonez [117]. He conducted a two-dimensional heat transfer analysis in a heat-generated volume with an array of cylindrical cooling channels and air as the working fluid in which he minimised the global thermal resistance.

The present case study examines the three-dimensional numerical thermal resistance analysis in a heat-generated volume with separate cylindrical and square cooling channels and water as cooling fluid. A computational elemental volume cell will be modelled by using the symmetrical property of heat distribution. However, a mathematical optimisation algorithm (DYNAMIC-Q) will be used to find the optimal peak temperature hence (thermal resistance) by varying the geometric parameters of the geometries subject to various constraints. The various heat transfer and optimisation results obtained will then be compared with analytical solutions of Chapter 5 and those found in the literature.

6.2.1. Computational model

The physical circular and square configurations are shown schematically in Figure 5.1(a) and 5.1(b). The system consists of parallel cooling channels of length L and fixed global volume, V . The internal heat generation in the solid material is q_s''' . An elemental volume, v_{el} , consisting of a cooling channel and the surrounding solid, was used for analysis because it was assumed that heat distribution inside the structure was symmetrical. However, the elemental volume v_{el} is not fixed and is allowed to morph by varying the cross-sectional shape v_c of the cooling channel for fixed porosity. The heat transfer in the elemental volume is a conjugate problem, and it combines heat conduction in the solid and the convection in the working fluid. These

two modes of heat transfer are coupled together through the continuity of heat flux at the solid-fluid interface.

6.2.1.1. Design variables

In Figure 6.1, an elemental volume, v_{el}, constraint is considered to be composed of an elemental cooling channel of hydraulic diameter, d_h, and the surrounding solid of thickness s (spacing between channels). These variables are defined as follows:

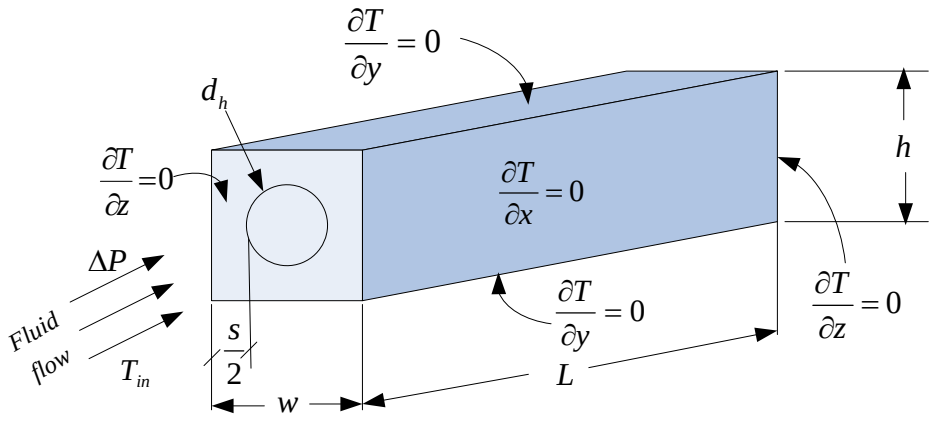

(a)

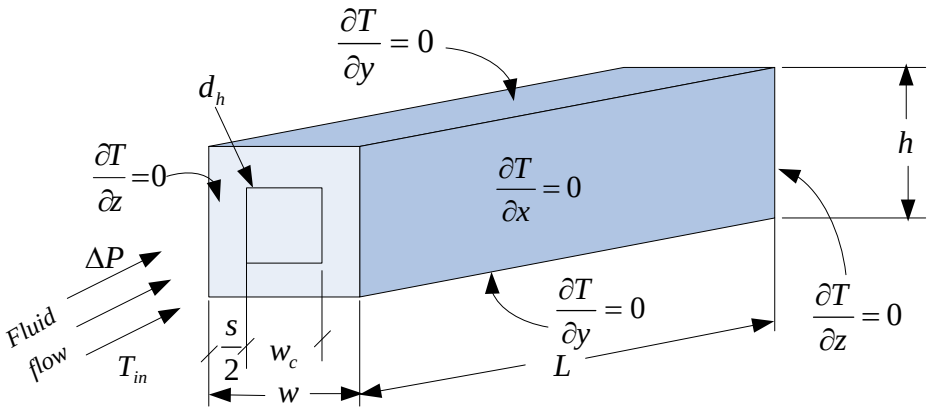

(b)

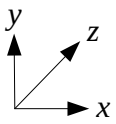

Figure 6. 1 : The boundary conditions of the three-dimensional computational domain of the cooling channel: (a) cylinder (b) square

$$w = h \tag{6.1}$$

$$v_{el} = w^2 L \tag{6.2}$$

$$w = d_h + s \tag{6.3}$$

Therefore, the total number of channels in the structure arrangement can be defined as

$$N = \frac{HW}{\left(d_h + s\right)^2} \tag{6.4}$$

However, the void fraction or porosity of the unit structure can be defined [117] as:

$$\phi = \frac{v_c}{v_{el}} \approx \left(\frac{d_h}{w}\right)^2 \tag{6.5}$$

The fundamental problem under consideration is the numerical optimisation of the hydraulic diameter, d_h, and spacing between channels, s, which corresponds to the minimum resistance of a fixed volume for a given pressure difference. The optimisation is evaluated from the analysis of the extreme limits of $\left(0 \le v_{el} \le \infty\right)$, $\left(0 \le d_h \le \infty\right)$ and the extreme limits of $\left(0 \le s \le \infty\right)$. The optimal values of the design variables within the prescribed interval of the extreme limits exhibit the minimum thermal resistance.

The temperature distribution in the model was determined by solving numerically for the conservation of mass, momentum and energy equations (Equations (3.31) to (3.38) of Chapter 3). The discretised three-dimensional computational domains of the circular and square configurations are shown in Figure 6.2. The cooling fluid was water, which is assumed to be in single-phase, steady, and a Newtonian fluid with constant thermo-physical properties. The water was forced through the cooling channels by a specified pressure difference, ΔP, across the axial length of the structure. Other assumptions imposed on the two configurations model are as follows:

The continuity of the heat flux at the interface between the solid and the liquid is given as:

$$k_s \frac{\partial T}{\partial n}\bigg| = k_f \frac{\partial T}{\partial n}\bigg| \tag{6.6}$$

A no-slip boundary condition is specified at the wall of the channel,

$$\vec{u} = 0 \tag{6.7}$$

and at the inlet ($x = 0$)

$$u_x = u_y = 0 \tag{6.8}$$

$$T = T_{in} \tag{6.9}$$

$$P = \frac{Be\alpha\mu}{L^2} + P_{out} \tag{6.10}$$

where, Be is the dimensionless pressure difference called the Bejan number [182, 183].

At the channel outlet $(x = L)$, a zero normal stress is prescribed, and

$$P_{out} = 1\ atm \tag{6.11}$$

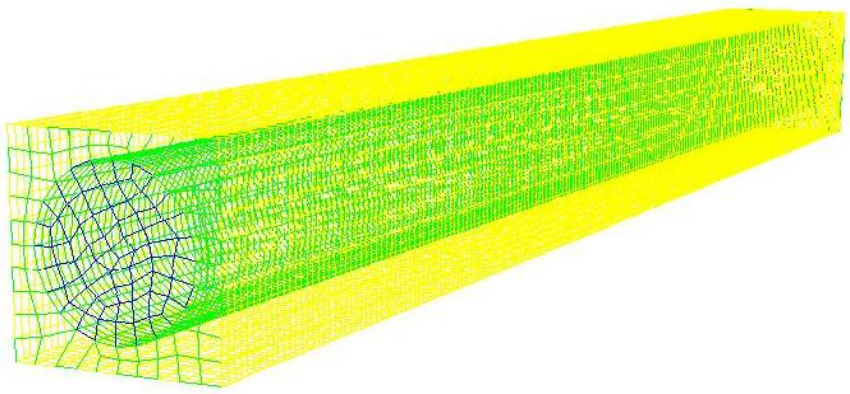

(a)

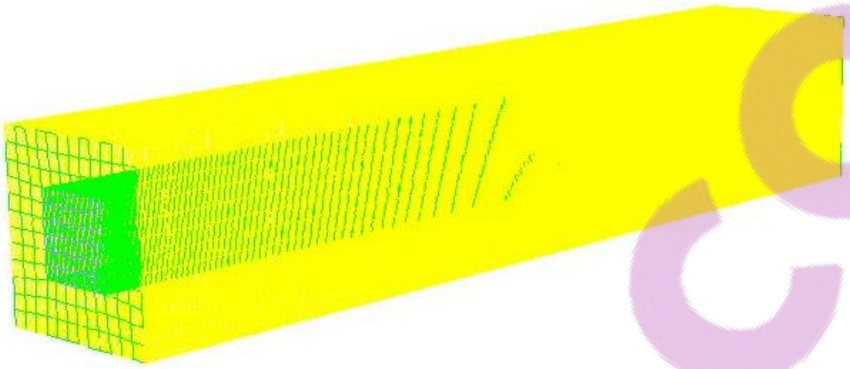

(b)

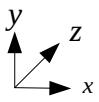

Figure 6. 2 : The discretised 3-D computational domain: (a) cylinder (b) square

At the solid boundaries, all the outside walls and plane of symmetry of the solid structure were modelled as adiabatic as shown in Figure 6.1. Hence

$$\nabla T = 0 \tag{6.12}$$

and an internal heat generation, q'''_s is assumed in the solid material.

The measure of performance is the minimum global thermal resistance, which could be expressed in a dimensionless form as:

$$R_{\min} = \frac{k_f \left(T_{\max} - T_{in}\right)_{\min}}{q'''_s L^2} \tag{6.13}$$

and it is a function of the optimised design variables and the peak temperature,

$$R_{\min} = f\left(d_{h_{opt}},\ s_{opt},\ v_{el_{opt}},\ T_{\max_{\min}}\right) \tag{6.14}$$

where R_{min} is the minimised dimensionless thermal resistance for the optimised design variables. The inverse of R_{min} is the maximised overall global thermal conductance.

6.2.2. Numerical procedure

The simulation procedure began by fixing the length of the channel, applied pressure difference, porosity, internal heat generation and material properties. We also kept varying the values of elemental volume and the hydraulic diameter of the channel in order to identify the best (optimal) internal and external geometries that minimised the peak temperature.

The numerical solution of continuity, momentum and energy equations (Equations (3.1) to (3.8) of Chapter 3) along with the boundary conditions (Equations (6.6) to (6.12)) was obtained by using a three-dimensional commercial package FLUENT™ [199], which employs a finite volume method. The details of the method are explained by Patankar [203]. The computational fluid dynamics package was coupled with the geometry and mesh generation package GAMBIT [201] using MATLAB [219] to allow the automation and running of the simulation process. After the simulation converged, an output file was obtained containing all the necessary simulation data and results for the post-processing and analysis. The computational

domain was discretised using hexahedral/wedge elements. A second-order upwind scheme was used to discretise the combined convection and diffusion terms in the momentum and energy equations. The SIMPLE algorithm was then employed to solve the coupled pressure-velocity fields of the transport equations. The solution is assumed to be converged when the normalised residuals of the mass and momentum equations fall below 10^{-6} and while the residual convergence of energy equation was set to less than 10^{-10}. The number of grid cells used for the simulations varied for different elemental volume and porosities. However, grid independence tests for several mesh refinements were carried out to ensure the accuracy of the numerical results. The convergence criterion for the overall thermal resistance as the quantity monitored is

$$\gamma = \frac{\left|\left(T_{\max}\right)_i - \left(T_{\max}\right)_{i-1}\right|}{\left|\left(T_{\max}\right)_i\right|} \leq 0.01 \tag{6.15}$$

where i is the mesh iteration index. The mesh becomes more refined as i increases. The $i-1$ mesh is selected as a converged mesh when the criterion Equation (6.15) is satisfied. The model and solution were implemented using an Intel Core(TM) 2Duo 1.6 GHz PC with 2 GB of DDRam. The average time of the simulation and convergence for each operating value of design variable and dimensionless pressure difference number was in the range of 1– 4 hours.

6.2.3. Grid analysis and code validation

To ensure accurate results, several grid independence test were conducted until a mesh size with negligible changes in peak temperature was obtained. Figures 6.3 and 6.4 show the grid independence test for cylindrical and square configurations respectively, for $v_{el} = 0.4\,\text{mm}^3$ and $\phi = 0.2$ and $\Delta P = 50\ kPa$.

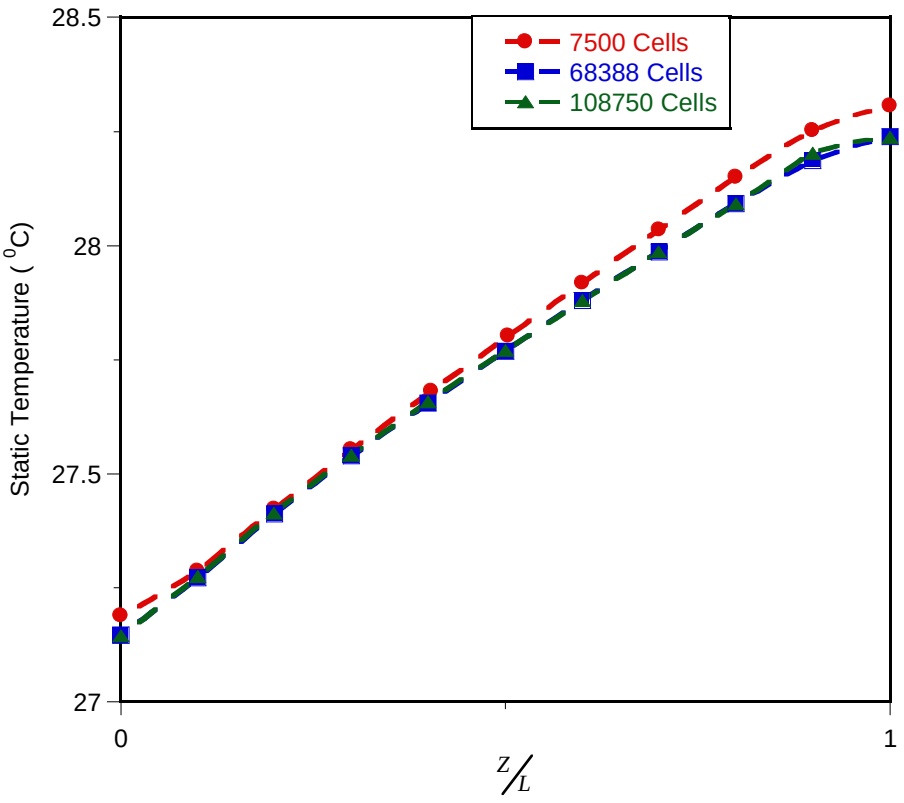

Figure 6. 3: Grid independent test for cylindrical configuration at fixed pressure difference and porosity

Computational cell densities of 7 500, 68 388 and 108 750 were used for the cylindrical configuration grid independence test. It was observed that almost identical results were predicted when 68 388 and 108 750 cells were used. Therefore, a further

increase in the cell density beyond 68 388 has a negligible effect on the numerical result. Again, computational cell densities of 16317, 26 688 and 50 000 were used for the square configuration grid independence test. It was observed that almost identical results were predicted when 26 688 and 50 000 cells were used. Therefore, any further increase in the cell density beyond 26 688 has a negligible effect on the numerical result.

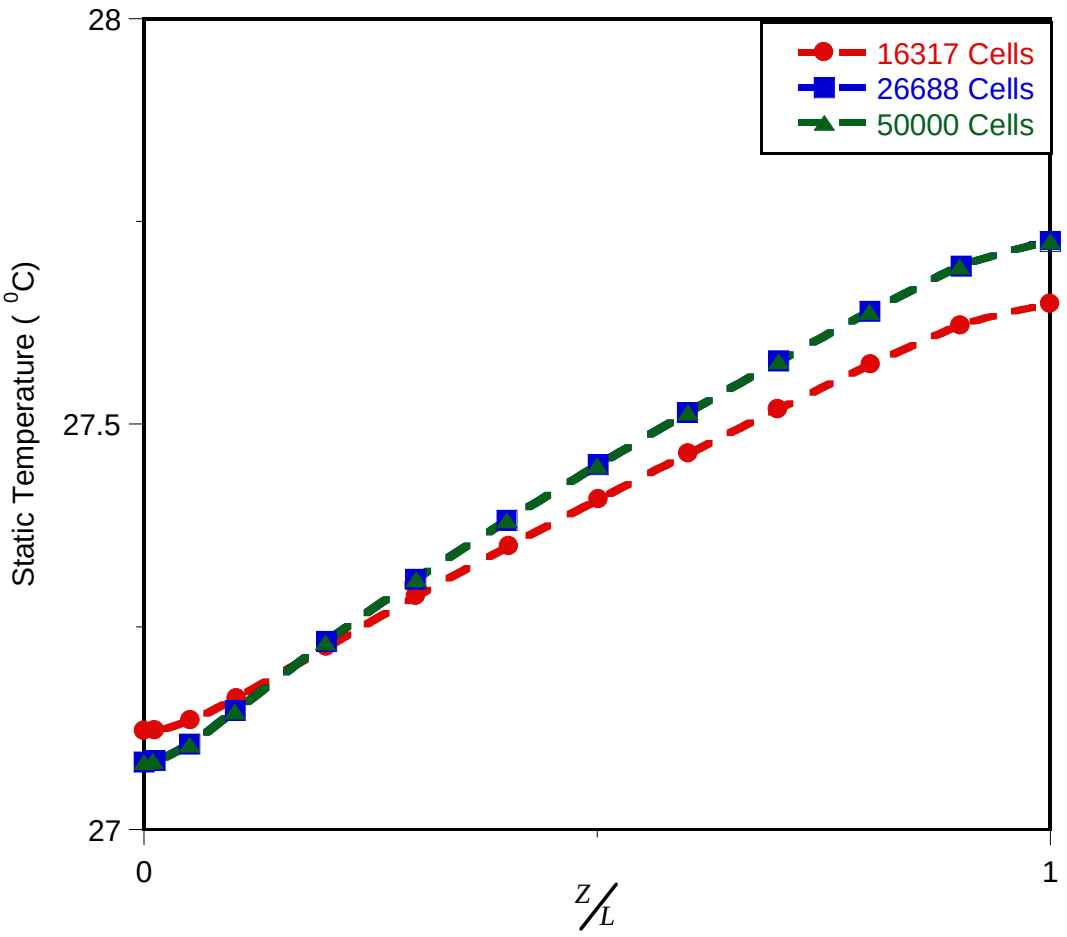

Figure 6. 4 : Grid independence test for a square configuration at fixed pressure difference and porosity

The validation of the numerical simulation was also carried out by comparing the present simulation for a circular configuration with the dimensionless temperature simulation of Ordonez [117] as shown in Figure 6.5. The curves were found to be similar in trend, while the optimised hydraulic diameters were also found to be in good agreement. However, the difference in the dimensionless maximum thermal temperature may be due to the kind of mesh refinement used. Our computation mesh is more refined than that of Ordonez [117].

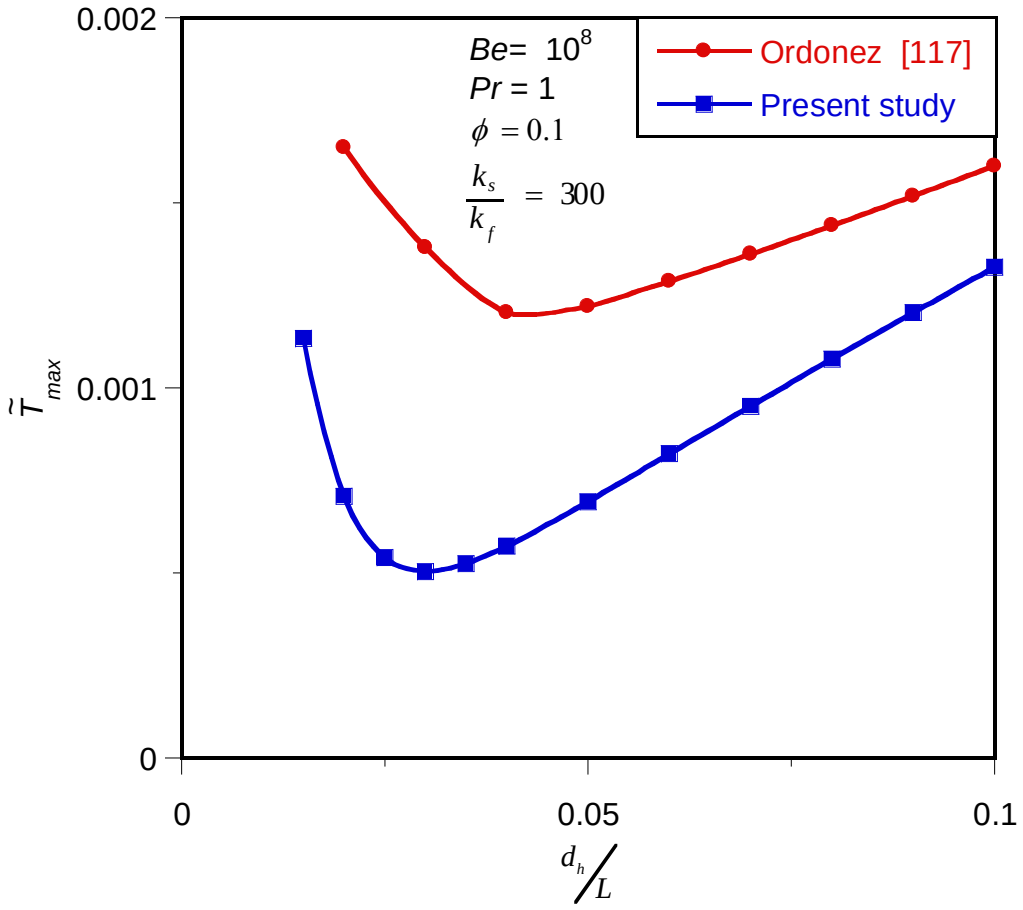

Figure 6. 5 : Thermal resistance curves: present study and that of Ordonez [117]

6.2.4. Numerical results using a traditional method

In this section, the numerical results are presented using a traditional method by post-processing the simulation data and results manually. We present the results for the case when the elemental volume of the structure was in the range of $0.025\ \text{mm}^3 \leq v_{el} \leq 5\ \text{mm}^3$; the porosities ranged between $0.1 \leq \phi \leq 0.2$; the fixed length of L was 10 mm and fixed applied pressure differences of $\Delta P = 50$ kPa. The thermal conductivity of the solid structure (silicon) was 148 W/m.K; and the internal heat generation within the solid was taken to be fixed at 100 kW/m^3. The thermo-physical properties of water [202] used in this study were based on water at 300 K and the inlet water temperature was therefore fixed at this temperature.

Figures 6.6 and 6.7 show the existence of an optimal hydraulic diameter and channel spacing in which the peak temperature is minimised at any point in the channel for the two configurations studied.

Figure 6.6 shows the peak temperature as a function of the hydraulic diameter of the channels. It shows that there exists an optimal channel hydraulic diameter, which lies in the range $0.005 \leq d_h/L \leq 0.022$ and minimises the peak temperature. The minimum peak temperature exist is in achieved when the optimal channel spacing exists in the range of $0.005 \leq s/L \leq 0.035$. These indicate that the peak temperature decreases as

global design variables increase and that maximal (optimal) values of the design variables are reached beyond which the peak temperature begins to increase.

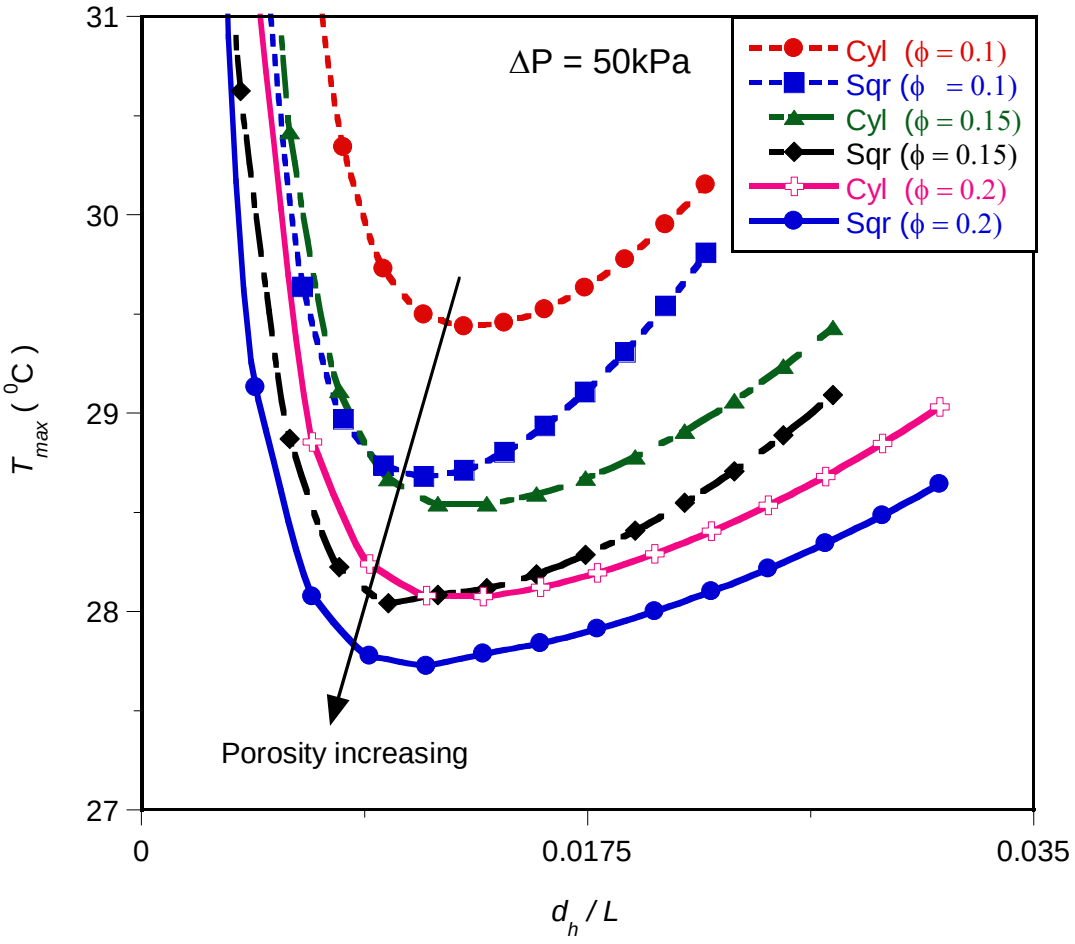

Figure 6. 6 : Effect of optimised hydraulic diameter d_h on the peak temperature

Thus, the global peak temperature decreases as the design variables decrease – until it gets to the optimal design values. Any increase or decrease in the design variable beyond the optimal values indicates that the working fluid is not properly engaged in the cooling process, which is detrimental to the global performance of the system.

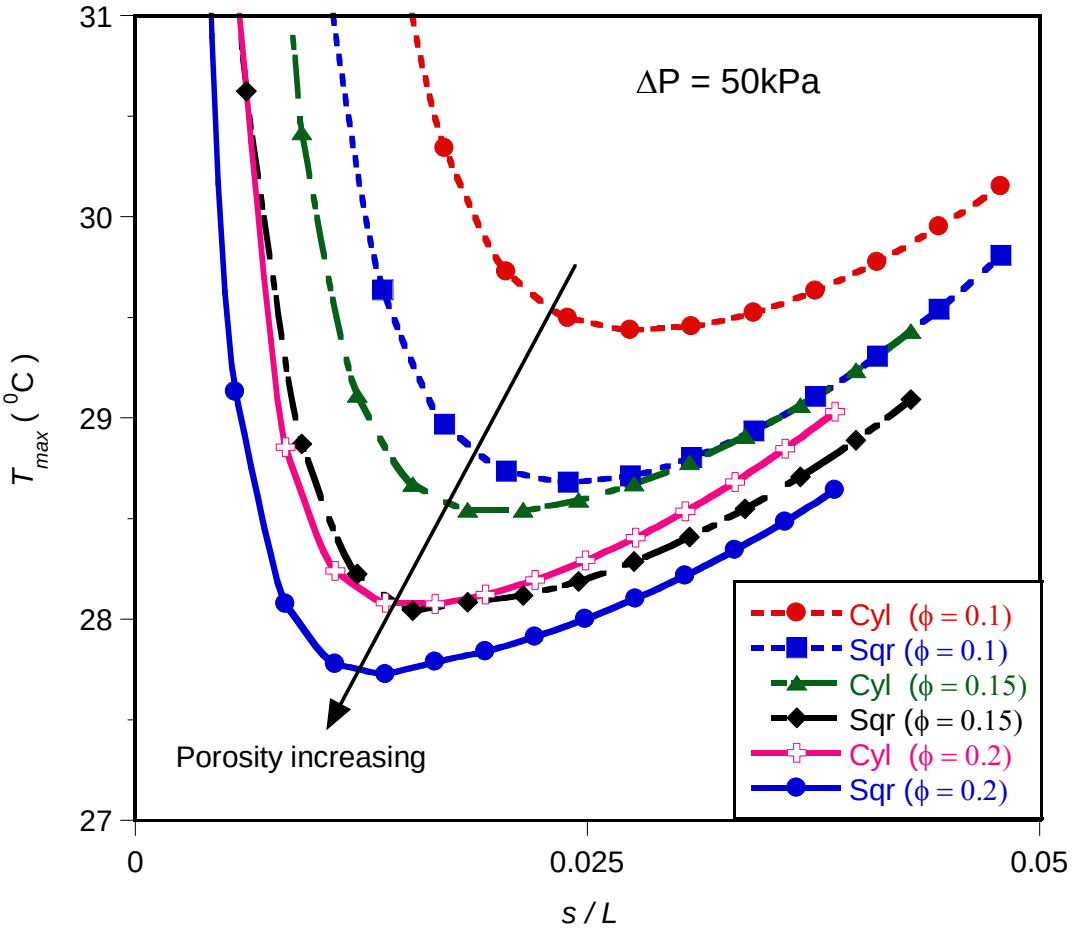

Figure 6. 7: Effect of optimised channel spacing on the peak temperature

Also, the elemental volume of the structure has a strong effect on the peak temperature as shown in Figure 6.8. It shows that there is an optimal elemental volume of the structure that minimises the peak temperature and this lies in the range of $0.2\ \text{mm}^3 \leq v_{el} \leq 2\ \text{mm}^3$.

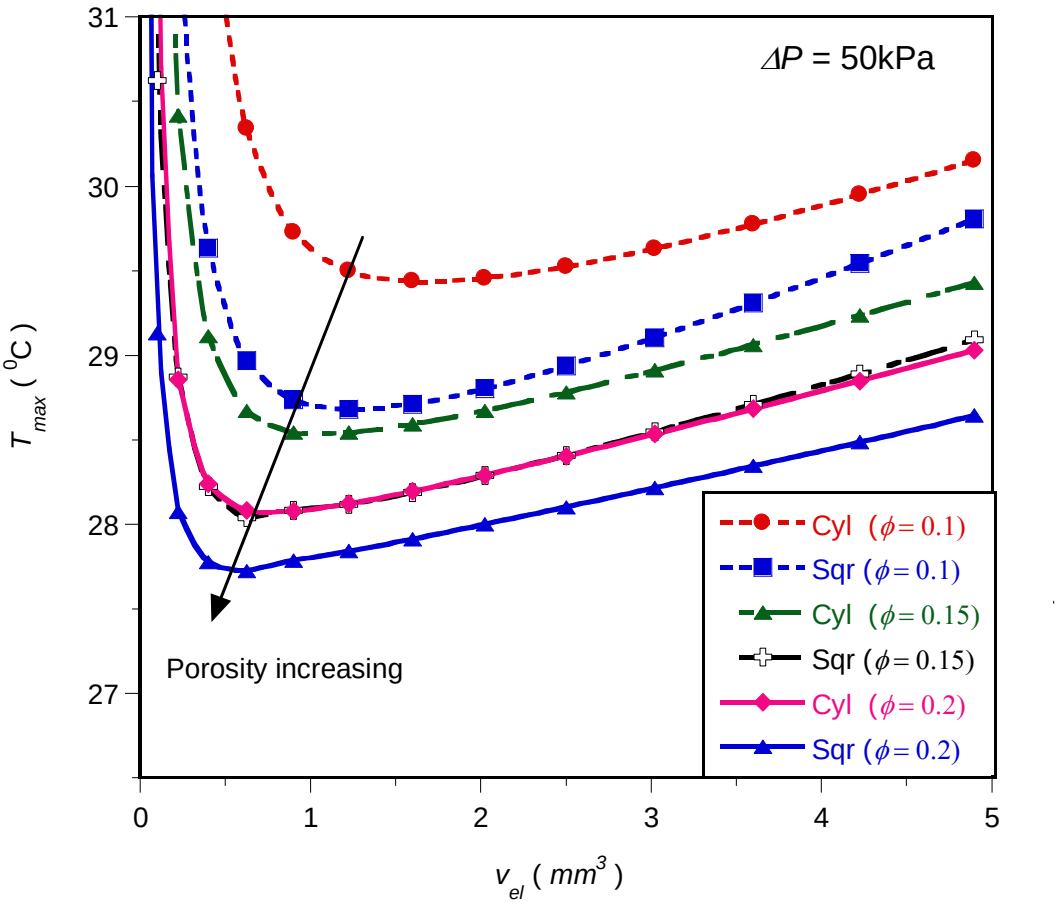

Figure 6. 8 : Effect of optimised elemental volume v_{el} on the peak temperature

The results show that the optimal arrangement of the elemental volume for the entire structure at this fixed pressure difference should be very small in order to achieve better cooling. Again, Figure 6.9 shows existence of an optimal total number of channels required in the structure. This minimised the peak temperature and also lies in the range of $10 \le N \le 120$.

It is clear from Figures 6.6 to 6.9 that porosity has a significant effect on the peak temperature and the overall thermal resistance. There is no optimum porosity. The

best performance occurs at the highest porosity, which means that as the porosity increases, the peak temperature decreases.

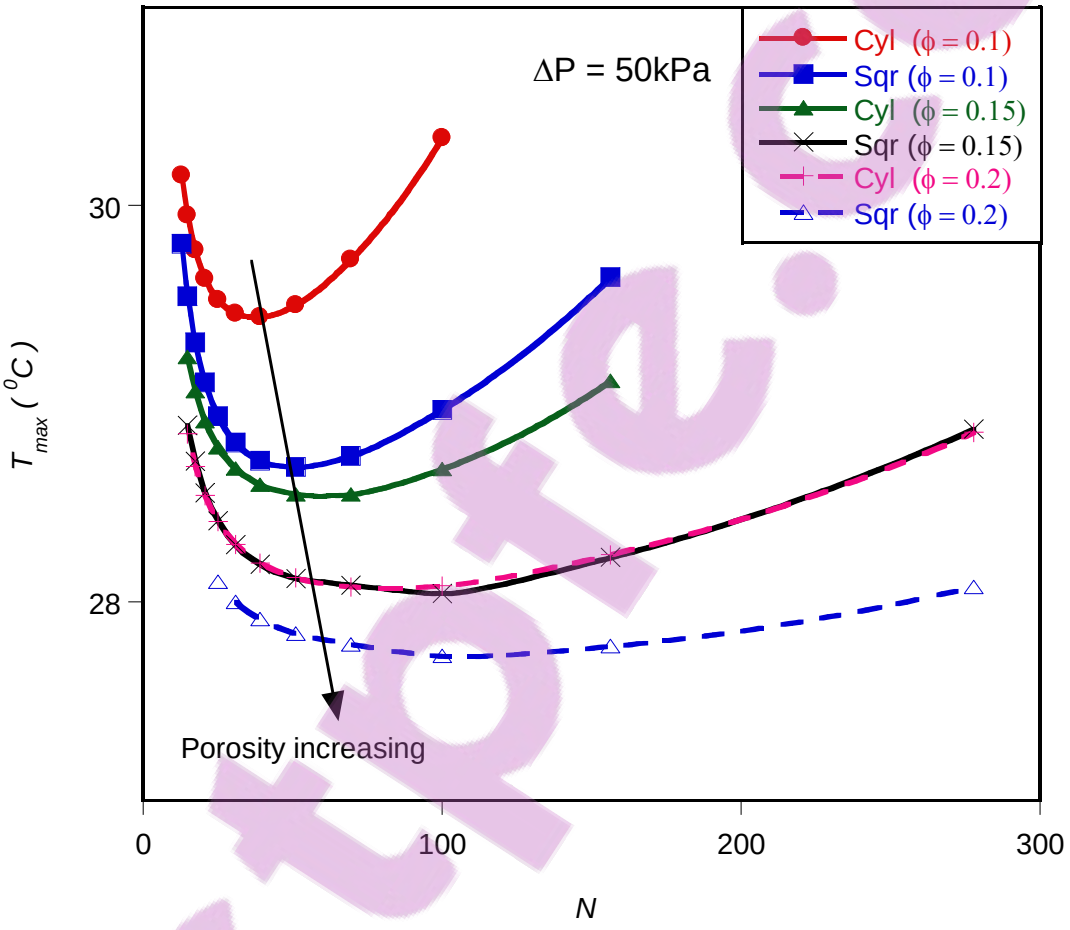

Figure 6. 9 : Effect of an optimised total number of channels *N* on the peak temperature

6.2.5. Mathematical formulation of the optimisation problem

The results shown in the preceding session were obtained using a traditional method to post-process the simulation data and results manually. In this section, the entire solution and results are obtained by using a mathematical optimisation algorithm that

searches and identifies the design variables at which the system will perform optimally, since the design variables are mutually interdependent. The approach is to assume that there must be optima design variables at which the system will perform best. A numerical algorithm, Dynamic-Q [208], is employed and incorporated and coupled with the finite volume solver and grid (geometry and mesh) generation package. Figure 6.10 contains a flow chart representing the numerical and optimisation procedure to search and identify the optimal design variables at which the system will perform optimally for greater efficiency and better accuracy. The algorithm is also specifically designed to handle constraint problems where the objective and constraint functions are expensive to evaluate.

The mathematical optimisation algorithm is a multidimensional and robust gradient-based optimisation algorithm that does not require an explicit line search. The details of the Dynamic-Q were discussed in Chapter 4 and it application can also be found in open literature [213-215].

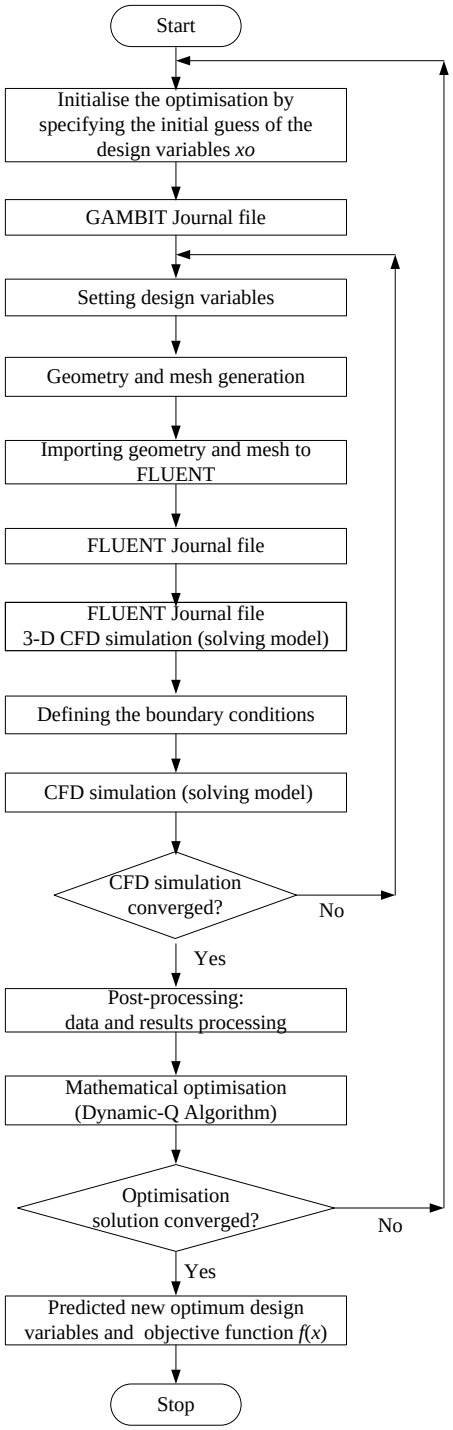

Figure 6. 10 : Flow chart of the numerical simulation process for cooling channels embedded in a high conducting solid

6.2.6. Optimisation problem and design variable constraints

The optimisation technique described above was applied to the models described in Section 6.2.1. The constraint ranges for the optimisation were

$$0.1 \leq \phi \leq 0.2 \tag{6.16}$$

$$0.025\text{mm}^3 \leq v_{el} \leq 5\text{mm}^3 \tag{6.17}$$

$$0 \leq w \leq L \tag{6.18}$$

$$0 \leq d_h \leq w \tag{6.19}$$

and

$$0 \leq s \leq w \tag{6.20}$$

The design and optimisation technique involve the search for and identification of the channel layout that minimises the peak temperature, $T_{\max}$, so that the minimum thermal resistance between the fixed volume and the cooling fluid is obtained with the desired objectives function. This function is not available analytically but it is obtained via a computational fluid dynamic simulation using FLUENT [60].

The hydraulic diameter, channel spacing and elemental volume were considered design variables for the two configurations in the study. A number of numerical optimisations and calculations were carried out within the design constraint ranges given in Equations (6.16) – (6.20), and the results are presented in the next section to show the optimal behaviour of the entire system. The elemental volume of the

structure was in the range of 0.025 mm^3 to 5 mm^3. The optimisation process was repeated for pressure differences across the axial length ranging from 5 kPa to 50 kPa.

6.2.7. Mathematical statement of the optimisation problem

The variables chosen for the mathematical statement are:

$$x_1 = d_h \tag{6.21}$$

$$x_2 = w \tag{6.22}$$

Substituting Equations (6.21) to (6.22) into Equations (6.16) to (6.20) results in the objective and constraints functions given in Equations (6.23) to (6.25). The inequality functions g_1(x) and g_2(x) are derived from the porosity constraint of Equation (6.5). The mathematical statement of the optimisation problem is then written as:

$$f(x) = T_{\max} \tag{6.23}$$

$$g_1(x) = 0.1{x_2}^2 - {x_1}^2 \leq 0 \tag{6.24}$$

$$g_2(x) = {x_1}^2 - 0.2{x_2}^2 \leq 0 \tag{6.25}$$

6.2.8. Parameterisation of geometry and automation of the optimisation process

In order to optimise the performance of the cooling channels, design variables of the geometry should be parameterised because geometric modelling mesh generations are

usually time consuming and labour intensive processes in the analysis computational fluid dynamic problems. The research work requires a large number of CFD simulations to be performed. Therefore, a MATLAB [219] code was developed to read a set of parameters of the geometry. The parameterised code automatically generates GAMBIT [201] and FLUENT script files; runs the scripts and performs post-processing to capture the results in terms of peak temperature as an objective function for different parametric values of each case of configuration studied.

This code starts by reading the parametric values of all the CFD cases and writing GAMBIT and FLUENT journal files for each case. GAMBIT [201] subsequently reads the Gambit journal, generates the mesh and import mesh created into FLUENT for each case. FLUENT [199] then runs the FLUENT journal that reads the corresponding created mesh and sets the model equations, boundary conditions, and solver settings. The FLUENT [199] finally writes maximum peak temperature, as well as mass weighted average and static pressure reports for the boundaries of interest to an output file for each case and process them all so as to calculate final global thermal resistance.

The optimisation problem was done automatically by coupling together the computational fluid dynamics package, FLUENT[199] and the geometry and mesh generation package, GAMBIT [201] with the mathematical optimisation algorithm. The MATLAB [219] code was used so as to allow the automation, mesh generation

and running of the simulation process. This was done by the creation of both GAMBIT [201] and FLUENT [199] journal files, where executed in MATLAB [219] by Windows executable files.

The optimisation algorithm was established by initiating a starting guess value of the design variables. A GAMBIT [58] journal file (*designvariable.jou*) was subsequently written and executed in MATLAB [219]. Another GAMBIT journal file (*CylinderDYNQNEW.jou*) was executed to generate the computational unit geometry mesh while using the geometrical parameters declared by the previous GAMBIT journal file (*designvariable.jou*) operation. The mesh created was imported into FLUENT where simulations and post-processing were carried out by the FLUENT journal file (*fluentDYNQNEW.jou*), Next a temperature data file (*CylinderTemp*.dat) was written stating all the temperatures at the various computational cells. This data file was then read into MATLAB [219], where the maximum temperature was found and equated to the objective function. The DYNAMIC-Q optimisation algorithm provided in Appendix A and written in MATLAB [219] was then used to find better (optimal) design variable vectors where the objective function is achieved. This cycle continued until convergence occurred with the step size and function value convergence tolerances set at 10^{-6} and 10^{-10} respectively. The average time of the simulation and convergence when coupling the FLUENT with mathematical optimisation algorithm for each operating value of dimensionless pressure difference number and configuration was in the range of 12 – 36 hours depending on the channel configuration.

Figure 6.10 provides a flow chart of the automated optimisation process. Appendix B.1 and B.2 show the parametric GAMBIT journal files for geometry with circular and square cooling channels respectively. Appendix C shows the FLUENT journal file according to which simulation was run.

6.2.9. Sensitivity analysis of the selection of forward differencing step size

As discussed in Chapter 4. 6, noise exists in any simulation. It is therefore essential to carefully choose a step size Δx to be used in the differencing scheme carefully so that it reduces the noise and gives an accurate representation of the global gradient of the function. A sensitivity analysis was performed by selecting different values of the step size of design variables that gave a smooth objective function that would later be used as a candidate step size. This candidate step size was then verified by running the optimisation program with various starting guesses and checking for any discrepancies in the final solution. Figure 6.11 shows a graph of peak temperature as a function of the hydraulic diameter of cylindrical cooling channels with step sizes of 10^{-6} and 10^{-4} . Although, different values of the step size of hydraulic diameter as design variable considered are 10^{-6}, 10^{-5}, 10^{-4} and 10^{-3}. A step size of 10^{-4} gives a smooth continuous function of maximum peak temperature and it indeed proved to be an ideal forward differencing scheme step size for other design variables. Figure 6.12 shows a graph of peak temperature as a function of channel spacing with the chosen candidate step size of 10^{-4}.

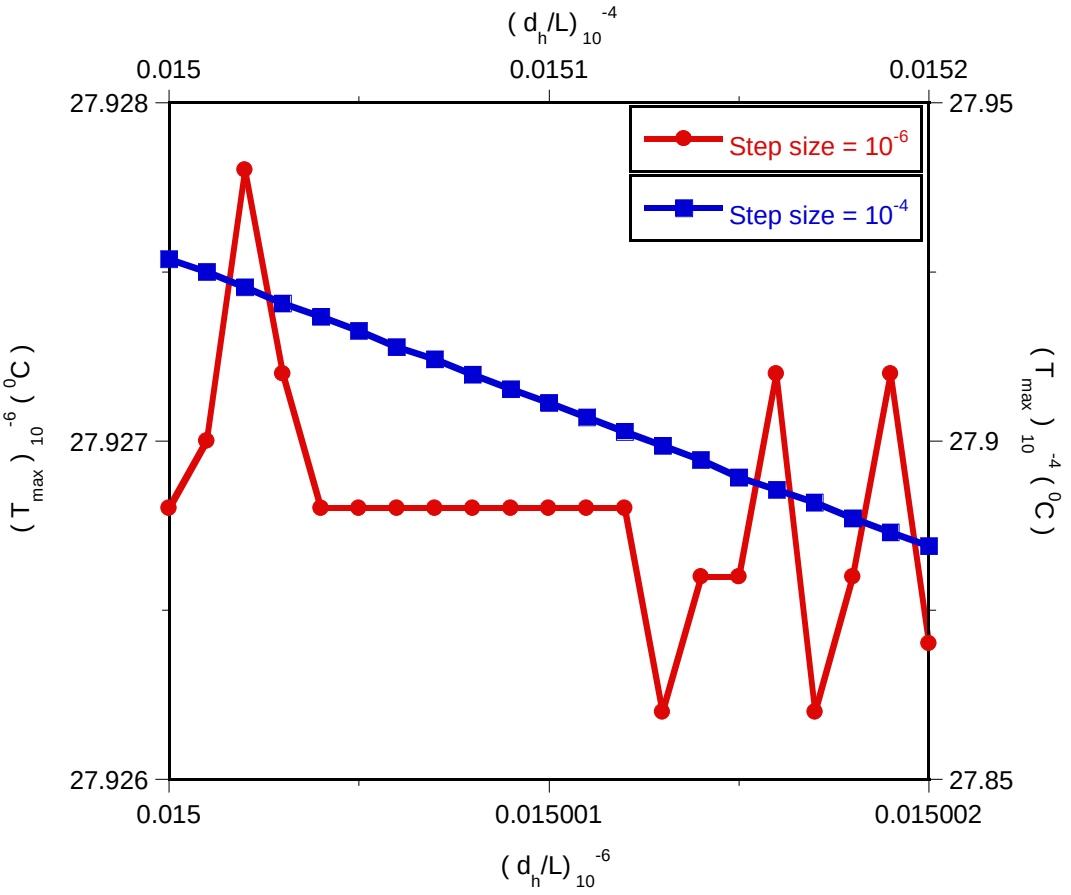

Figure 6. 11 : Plotting of peak temperature for different hydraulic diameter values with step sizes of 10^{-6} and 10^{-4}

Figure 6.13 also shows peak temperature as a function of the hydraulic diameter of square cooling channels with similar sensitivity analysis procedure as for the cylindrical cooling channels. In Figure 6.14 below peak temperature is shown as a function of channel spacing with a candidate step size of 10^{-4}.

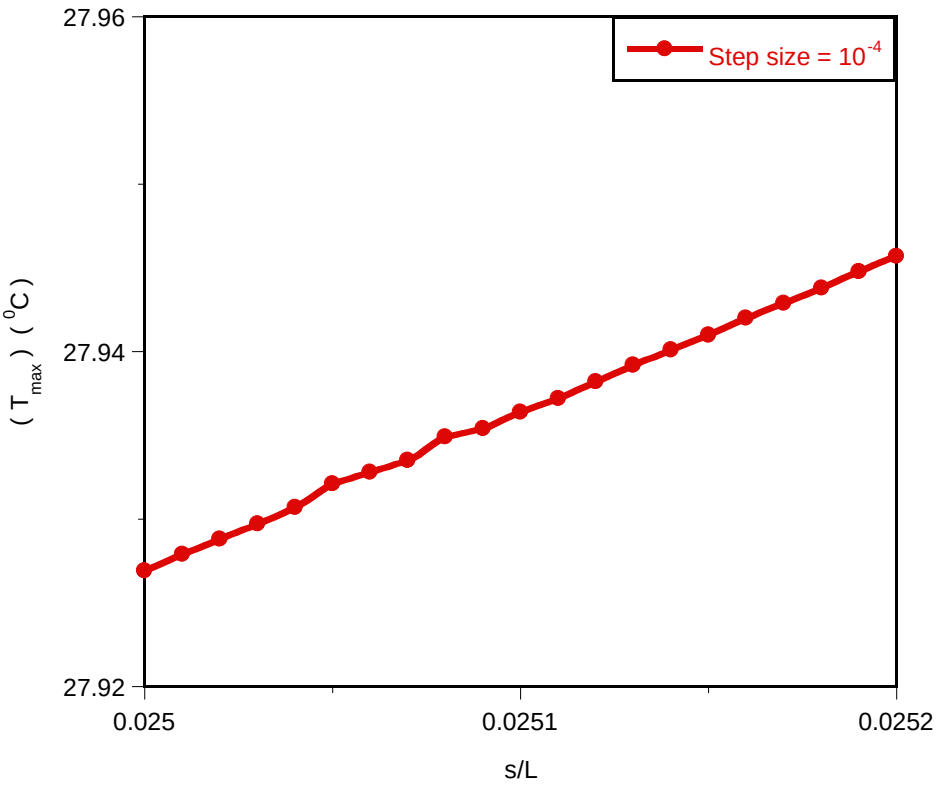

Figure 6. 12 : Plotting temperature for the different channels spacing values with a step size of 10^{-4}

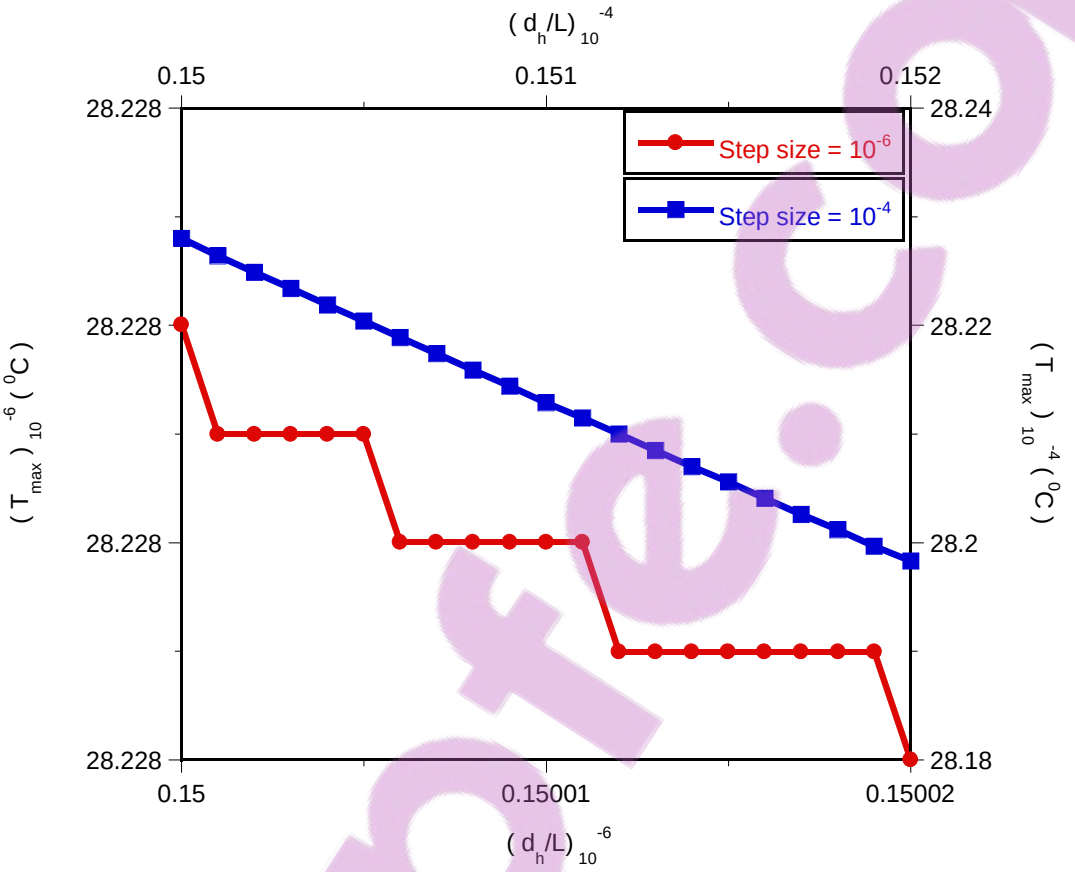

Figure 6. 13 : Plot of temperature for different hydraulic diameter values with step sizes of 10^{-6} and 10^{-4}

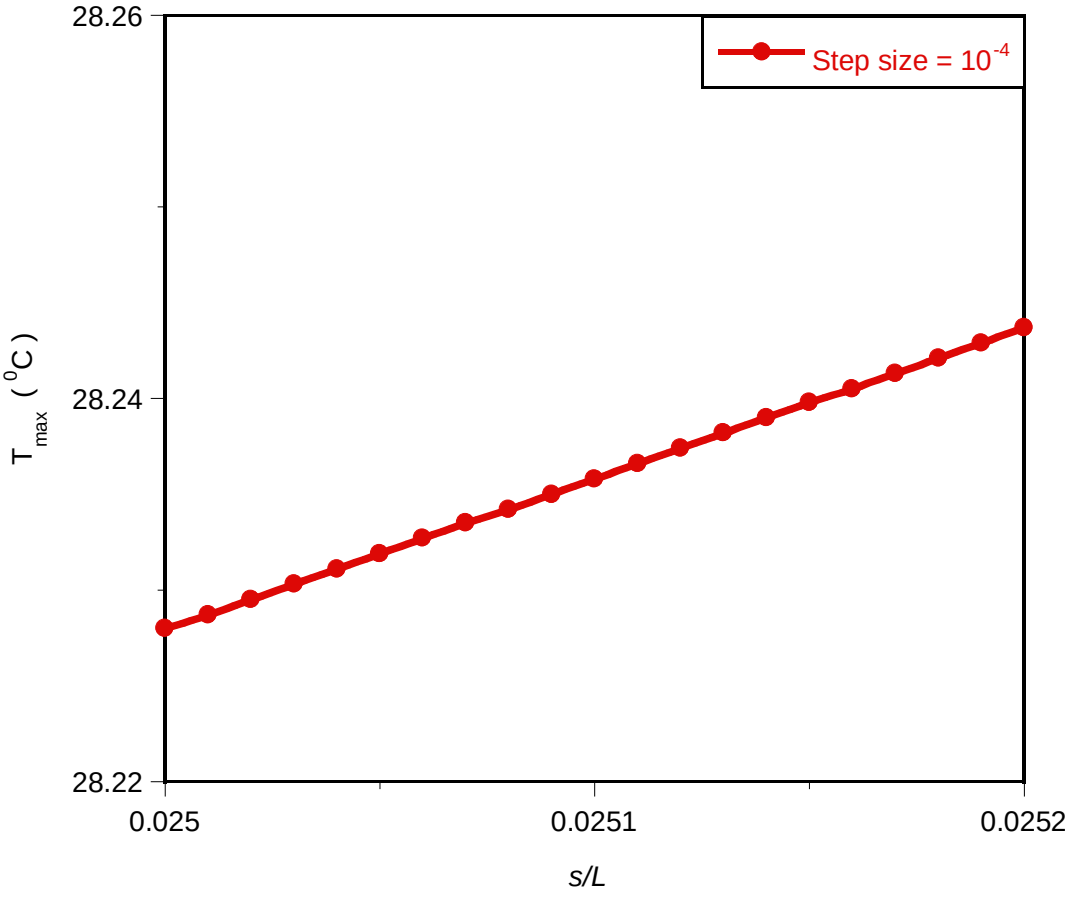

Figure 6. 14 : Plotting temperature for different channels spacing values with a step size of 10^{-4}

6.1.10 Optimisation results

Figure 6.15 shows the optimisation search history of the objective function with respect to iteration for cylindrical configuration in the optimisation searching process by the mathematical optimiser.

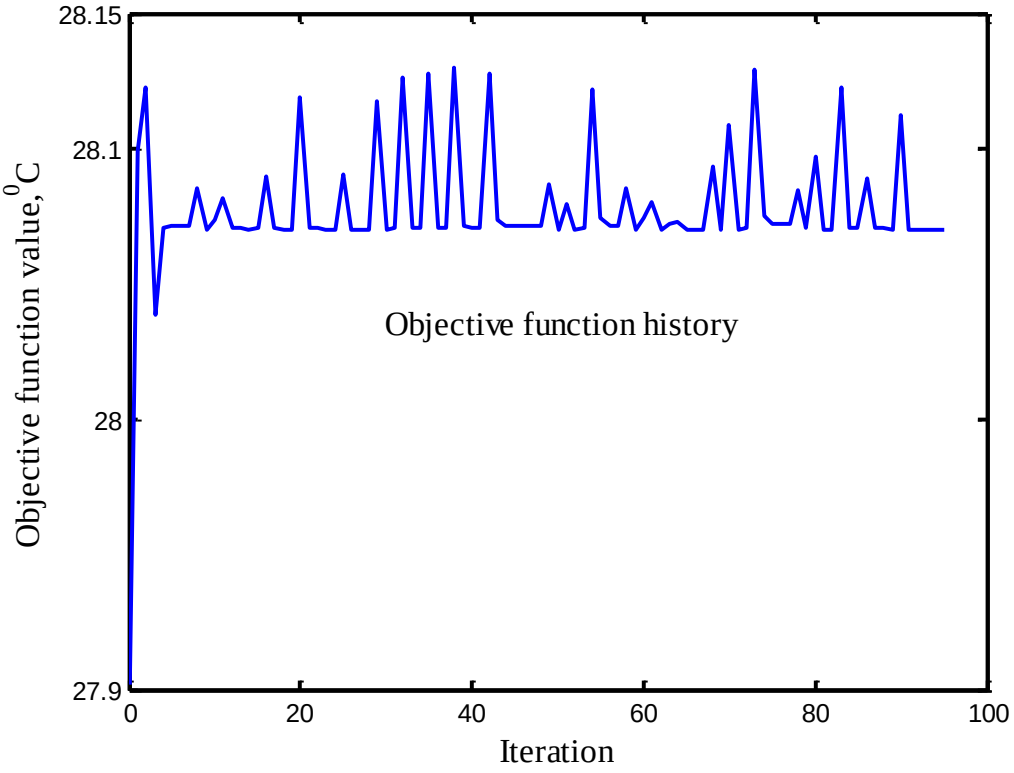

Figure 6. 15 : Objective function history for cylindrical configuration

Figures 6.16 and 6.17 compare the performance of the cooling channel between for the traditional method and mathematical optimiser respectively. Figure 6.16 shows minimised peak temperature curves as a function of pressure drop between the traditional method and the optimiser. The optimised result performs slightly better than the traditional method. The optimisation method relies on the gradients values, and that is why they are more efficient when compared to the traditional method. Figure 6.17 also shows the optimised hydraulic diameter curves. The optimised hydraulic diameter decreases as the pressure difference increases, and the optimised

hydraulic diameter is smaller in the optimisation process than in the traditional method. In the case of the traditional method, the graph shows that when the pressure difference is beyond 30 *kPa*, the pressure difference has no effect on the optimised hydraulic diameter. In contrast, pressure difference slightly influences the optimised shape.

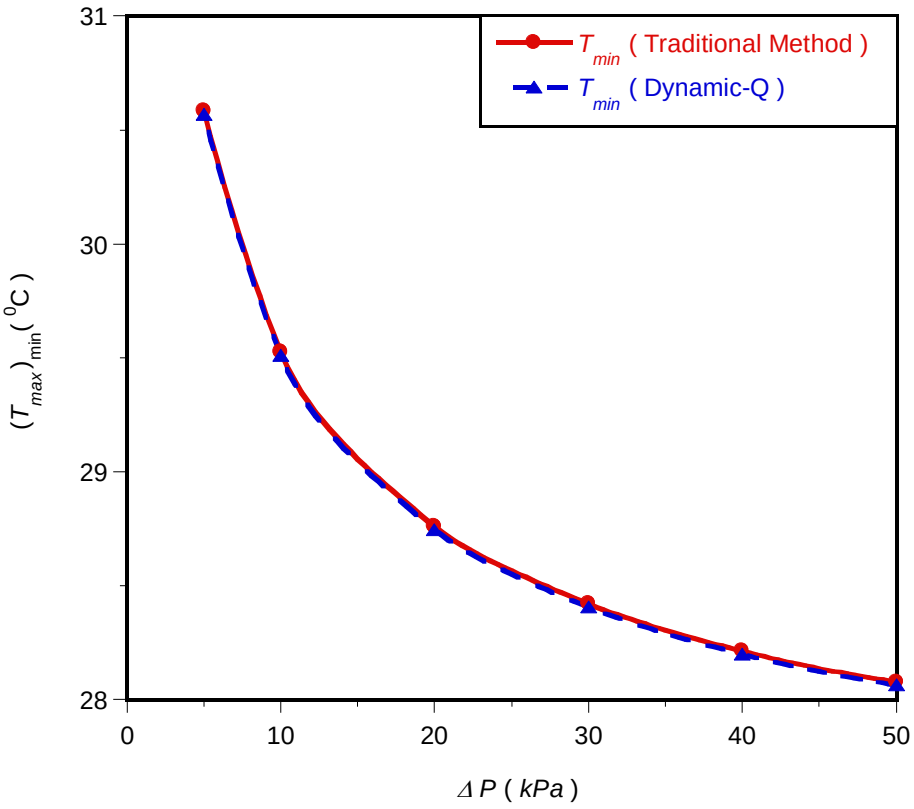

Figure 6. 16 : Comparison of the minimised temperature curves for the traditional method and the optimised cylindrical configuration

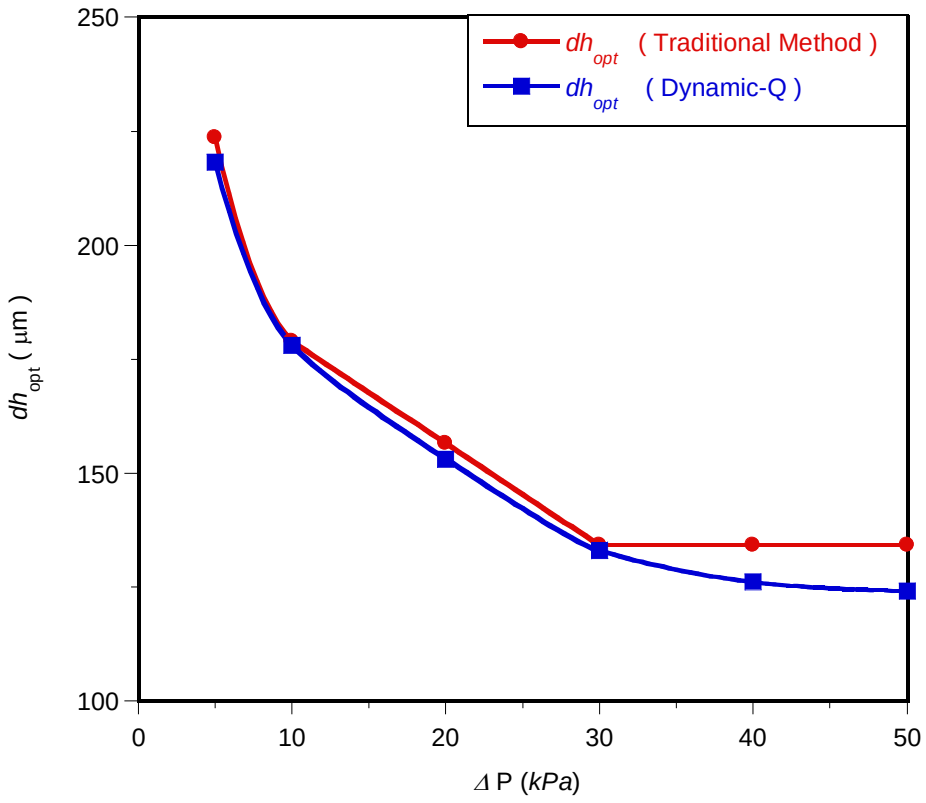

Figure 6. 17 : Comparison of the optimised design variable curves between the traditional method and optimised for cylindrical configuration

6.2.9.1. Effect of applied pressure difference on optimised geometry and minimised thermal resistance

Figure 6.18 shows the effect of the minimised thermal resistance as a function of applied dimensionless pressure difference. Minimised thermal resistance decreases as the applied dimensionless pressure difference number across the axial length and porosity increase. The trend is in agreement with previous work [30].

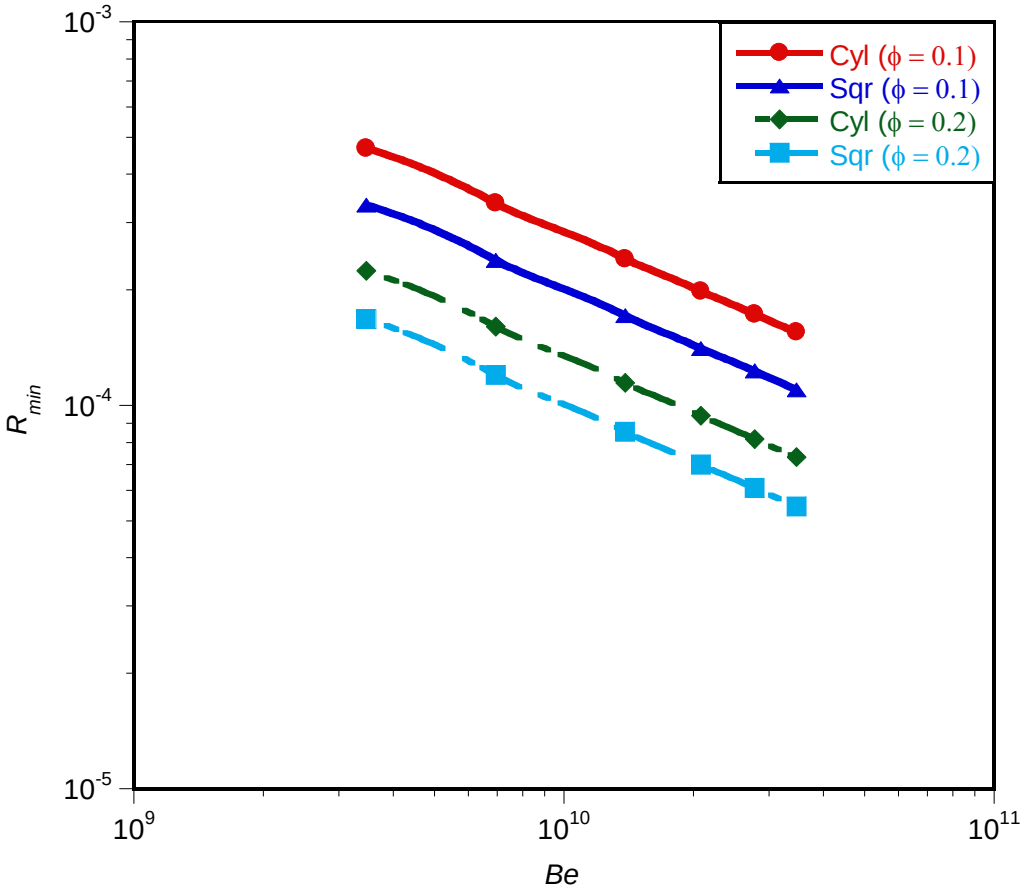

Figure 6. 18 : Effect of dimensionless pressure difference on the dimensionless global thermal resistance

Figure 6.19 shows that there is optima elemental volume for each of the two configurations. It also shows that the optimised global elemental volume decreases as the dimensionless pressure difference increases. Furthermore, there exists a unique optimal elemental volume of geometry for each of the applied pressure differences that minimise the global thermal resistance. This volume lies in the region of $0.5\ \text{mm}^3 \le v_{el} \le 2.4\ \text{mm}^3$. It confirms that the optimal arrangement of the

elemental volume for the entire structure should be very small to achieve better cooling.

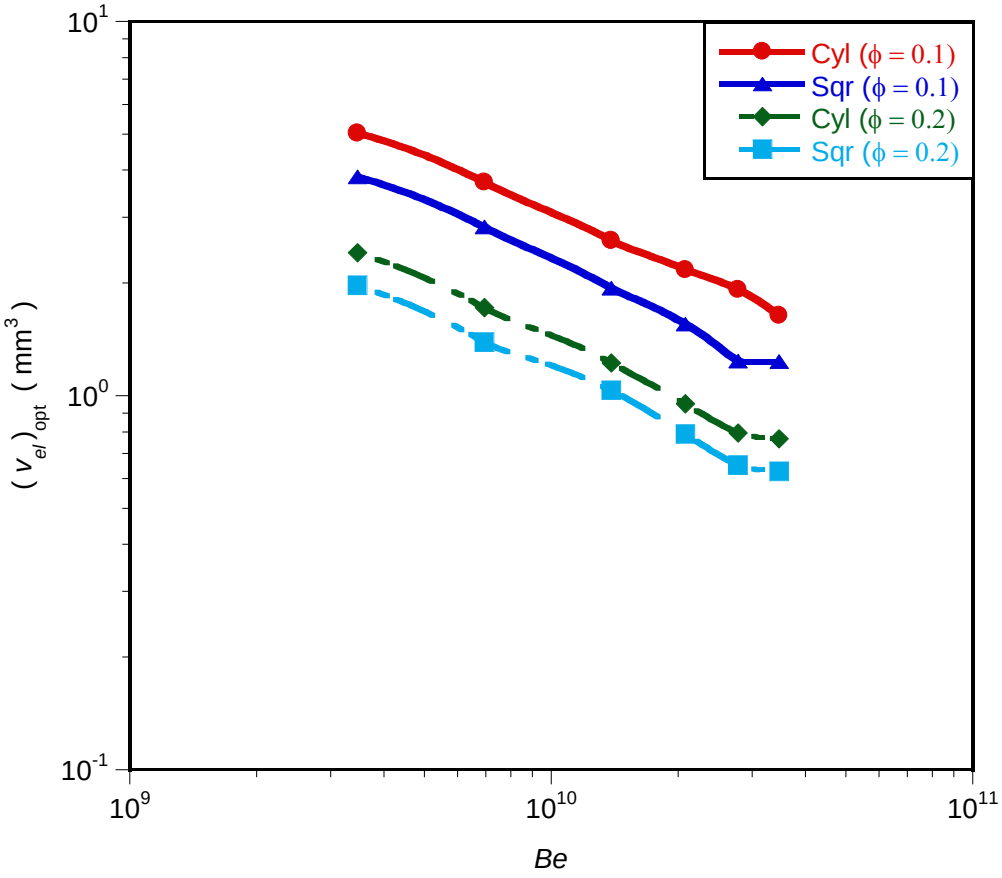

Figure 6. 19 : Effect of dimensionless pressure difference on the dimensionless elemental volume

According to Figure 6.20 the total number of channels (channel arrangement) is a function of pressure difference and porosity increases. The global N_{opt} increases as the pressure difference and porosity increase. N_{opt} lies in the region of $10 \le N_{opt} \le 100$. It is also observed a unique optimal number of channels for every

driving force (*Be*) is required for each configuration so as to achieve effective cooling.

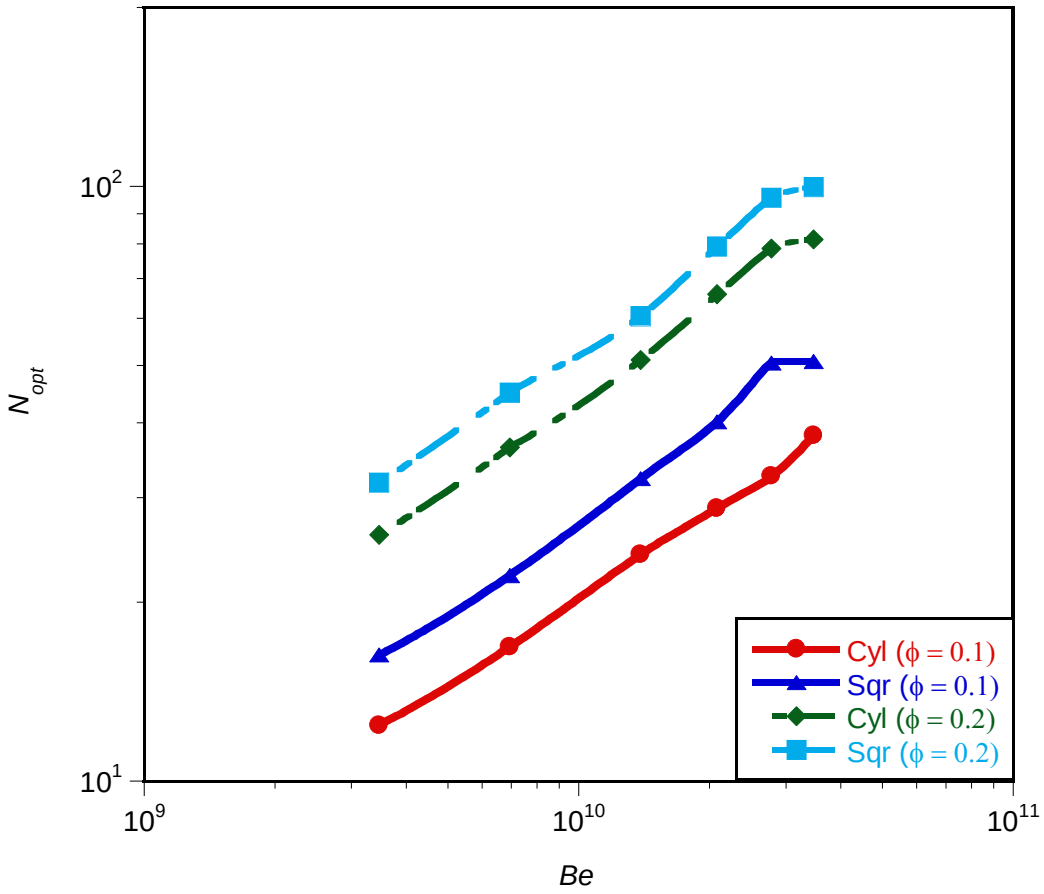

Figure 6. 20 : Effect of dimensionless pressure difference on optimised total number of channels

6.2.10. Comparing the theoretical method and numerical optimisation

6.2.10.1. Effect of dimensionless pressure difference on the minimised dimensionless global thermal resistance

Figure 6.21 shows the minimised dimensionless global thermal resistance as a function of dimensionless pressure difference at optimised design variables for the two configurations. The analytical results of Equations (5.35) and (5.36) validate the numerical solutions. The two optimised solutions have similar trends. Also, the analytical and numerical results show that in the two optimised configurations, the minimised global thermal resistance decreases as the dimensionless pressure difference increases. Although the analytical results are lower than numerical results, the theoretical and numerical values agree within a factor of 1.8 for the worst case. These results are also in agreement with past research work [17, 19, 93].

Equations (6.26) and (6.27) are the correlations for minimised dimensionless thermal resistance and the dimensionless pressure difference for cylindrical and square channels configurations respectively. These are obtained when the geometry is optimised at $\phi = 0.2$ in order to achieve cooling.

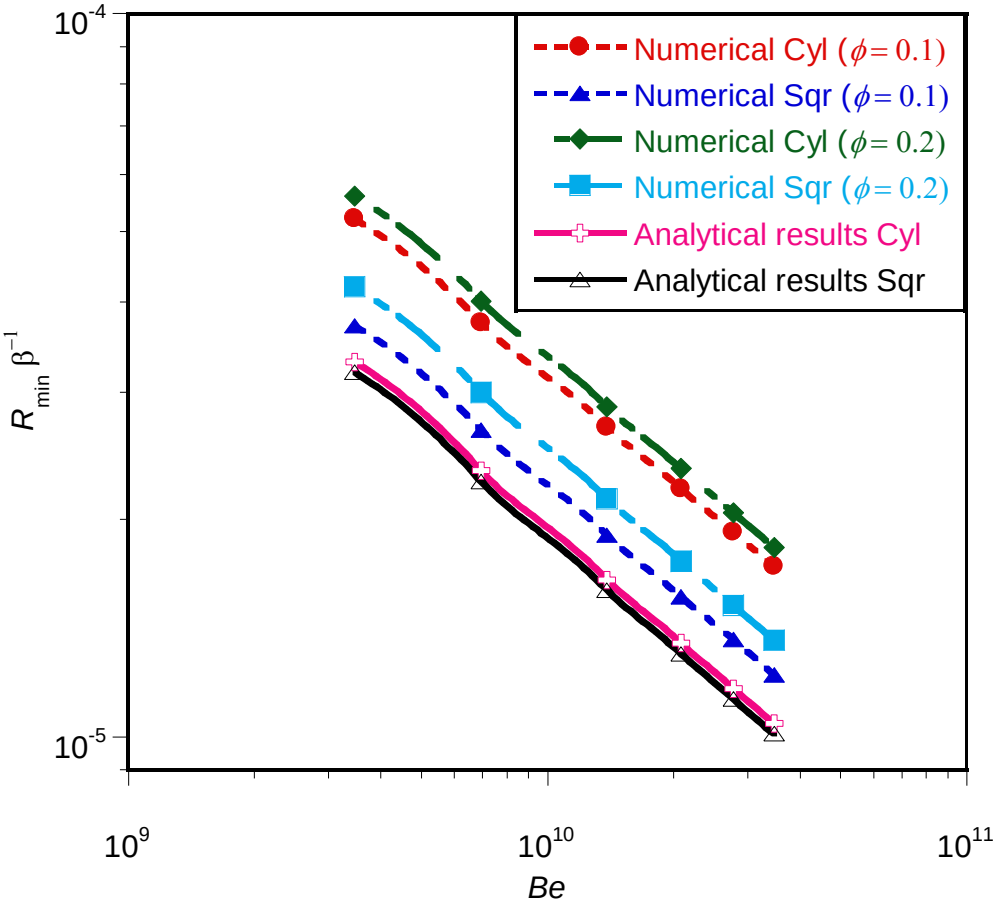

Figure 6. 21 : Correlation of numerical and analytical solutions for the minimised global thermal resistance

$$R_{\min,\,Cyl} = 9.64 Be^{-0.49} \quad , \qquad R^2 = 0.999 \tag{6.26}$$

$$R_{\min,\,Sqr} = 7.68 Be^{-0.49} \quad , \qquad R^2 = 0.999 \tag{6.27}$$

where R^2 is the coefficient of correlation. The correlation given in Equations (6.26) and (6.27) correlate within the error of less than 1% to the CFD results produced.

6.2.10.2. Effect of applied dimensionless pressure difference on optimised design variables

Figures 6.22 and 6.23 show the effect of the dimensionless pressure difference on the optimised hydraulic diameter and channel spacing respectively. The curves show that design variables decrease as applied dimensionless pressure difference and porosity increase.

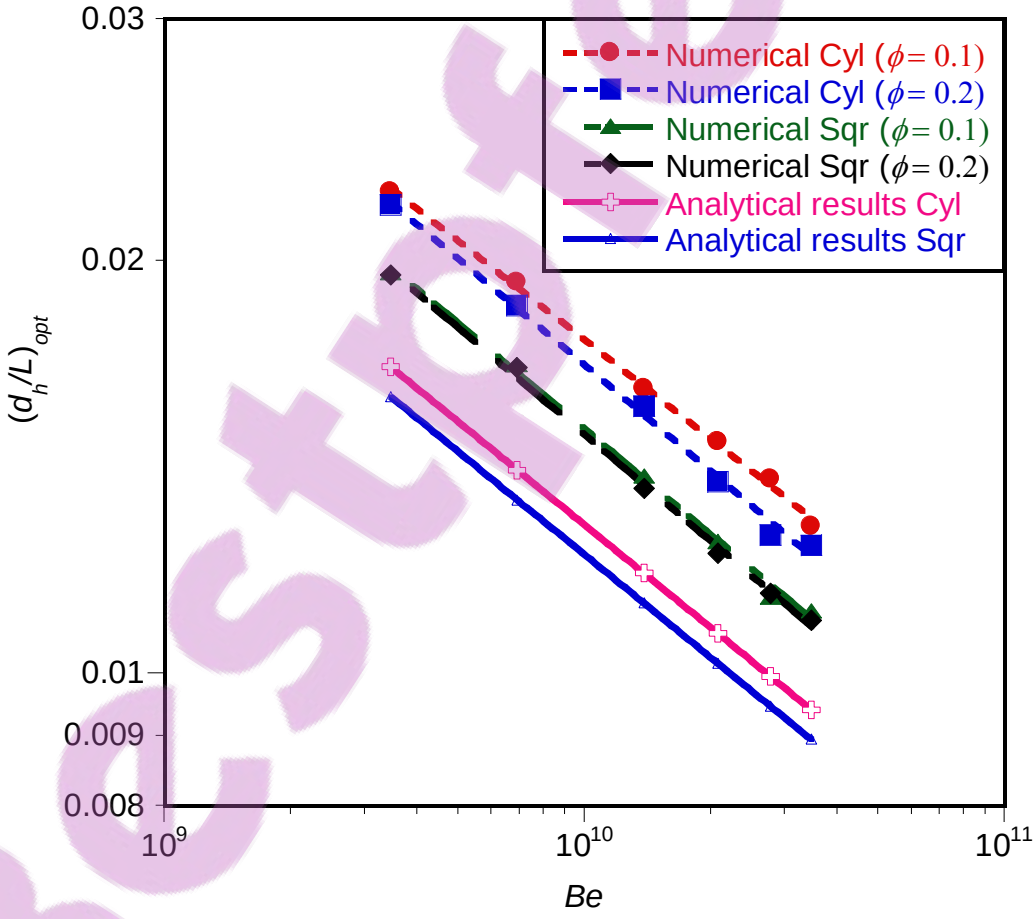

Figure 6. 22 : Correlation between numerical and analytical solutions for the optimised hydraulic diameter

Furthermore, the optimised spacing is directly proportional to the optimised hydraulic diameter. This is also due to the fact that the elemental volume is not fixed, but allowed to morph for a fixed porosity. The graphs also show that, for each configuration, unique optimal design geometries exist for each applied dimensionless pressure number.

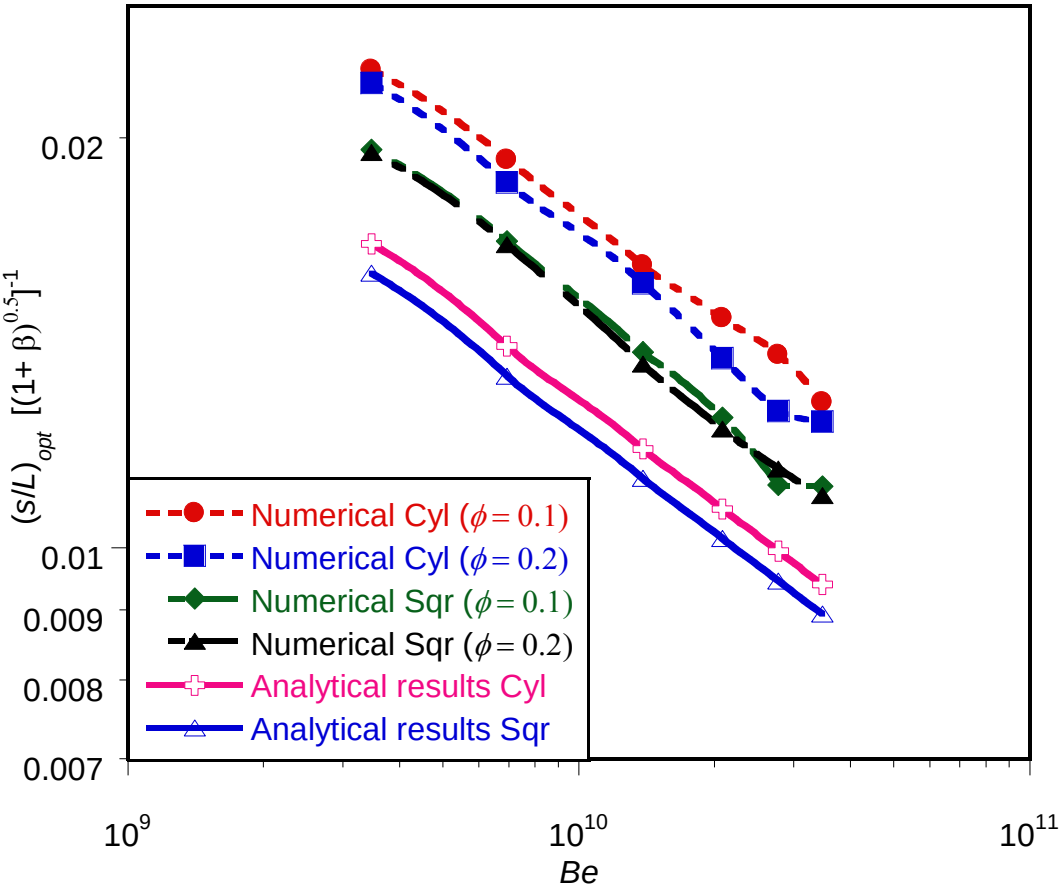

Figure 6. 23 : Correlation beteen numerical and analytical solutions for the optimised spacing

6.2.11. Optimal temperature contours

Figures 6.24(a) and 6.24(b) show the temperature contours of the elemental structure for circular and square configurations, respectively, While Figures 6.24(c) and 6.24(d) show the temperature contours of the inner wall of the cooling channel with cooling fluid for circular and square configurations, respectively. The blue region indicates the region of low temperature and the red region indicates high temperature. The arrow indicates the direction of flow.

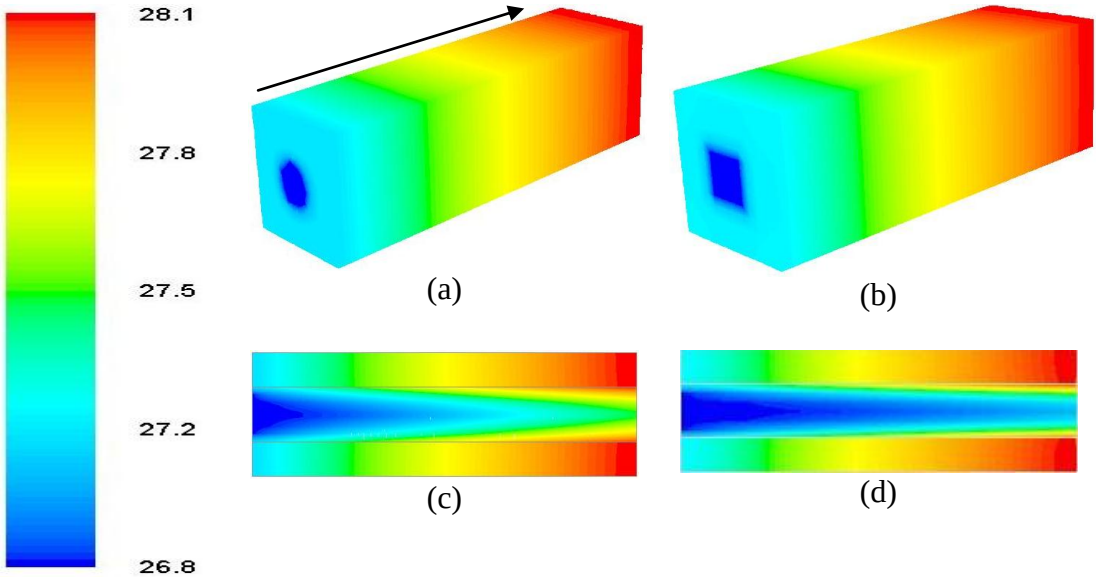

Figure 6. 24 : Temperature distributions on the cooling fluid and inner wall, and unit structure

6.3. CASE STUDY 2: TRIANGULAR COOLING CHANNEL EMBEDDED IN A HIGH-CONDUCTING SOLID

The second case study examines the three-dimensional numerical analysis of thermal resistance in a heat-generated volume. Two types of cross-section channel geometries were used. The first involved equilateral triangles with three equal legs in length and all three internal angles of 60^0. The second was isosceles right triangles with two legs of equal length and internal angles of 90^0, 45^0 and 45^0. Both the equilateral triangle and isosceles right triangle are special case of triangles that can easily and uniformly be packed and arranged to form a larger constructs body, thus minimising the global thermal resistance. A computational elemental volume cell will also be modelled because of the symmetrical heat distribution. The DYNAMIC-Q optimisation algorithm is used to search optimal peak temperatures, hence thermal resistance, by varying the geometric parameters subject to different constraints. The numerical optimisation results obtained that were compared with their analytical solutions in Chapter 5

6.3.1. Computational model

The schematic Figure 5.1(c) in Chapter 5 represents the physical configuration of isosceles right and equilateral triangular cooling channels. The model follows the same principle as that of circular and square configurations in Section 6.2.1.

6.3.1.1. Design variables for isosceles right triangular cooling channels

In Figure 6.25(a), an elemental volume, v_{el}, constraint is considered to be composed of an elemental isosceles right triangular cooling channel of hydraulic diameter, d_h, and the surrounding solid of thickness $s_1$and s_2 at the horizontal and vertical regions respectively. These variables are defined as follows

$$w = h \tag{6.28}$$

$$v_{el} = w^2 L \tag{6.29}$$

$$w = d_h + s \tag{6.30}$$

$$h_c = \frac{w_c}{2} \tag{6.31}$$

$$b = \frac{\sqrt{2}}{2} w_c \tag{6.32}$$

$$d_h = \frac{w_c^{\,2}}{w_c + \sqrt{2} w_c} \tag{6.33}$$

$$v_c = \frac{w_c^{\,2}}{4} L \tag{6.34}$$

However, the void fraction or porosity of the unit structure can be defined as

$$\phi = \frac{v_c}{v_{el}} = \frac{1}{4}\left(\frac{w_c}{w}\right)^2 \tag{6.35}$$

6.3.1.2. Design variables for equilateral triangular cooling channels

Again, in Figure 6.25(b), an elemental volume, v_{el}, constraint is considered to be composed of an elemental equilateral triangular cooling channel of hydraulic diameter, d_h, and the surrounding solid of thickness $s_1$and s_2 at the horizontal and vertical regions respectively. These variables are defined as follows

$$w = h \tag{6.36}$$

$$v_{el} = w^2 L \tag{6.37}$$

$$w = d_h + s \tag{6.38}$$

$$h_c = \frac{\sqrt{3}}{2} w_c \tag{6.39}$$

$$d_h = \frac{1}{\sqrt{3}} w_c \tag{6.40}$$

$$v_c = \frac{\sqrt{3}}{4} w_c^{\,2} L \tag{6.41}$$

However, the void fraction or porosity of the unit structure can be defined as

$$\phi = \frac{v_c}{v_{el}} = \frac{\sqrt{3}}{4} \left(\frac{w_c}{w} \right)^2 \tag{6.42}$$

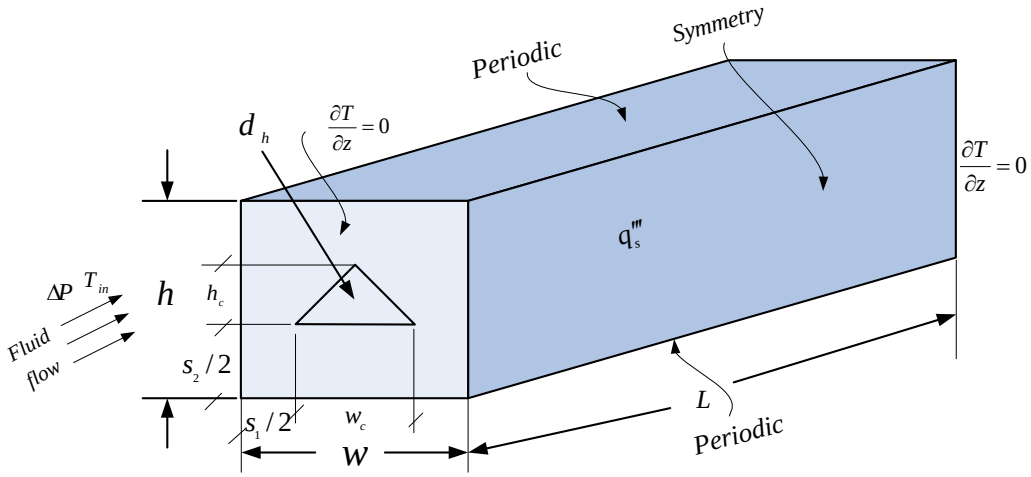

(a)

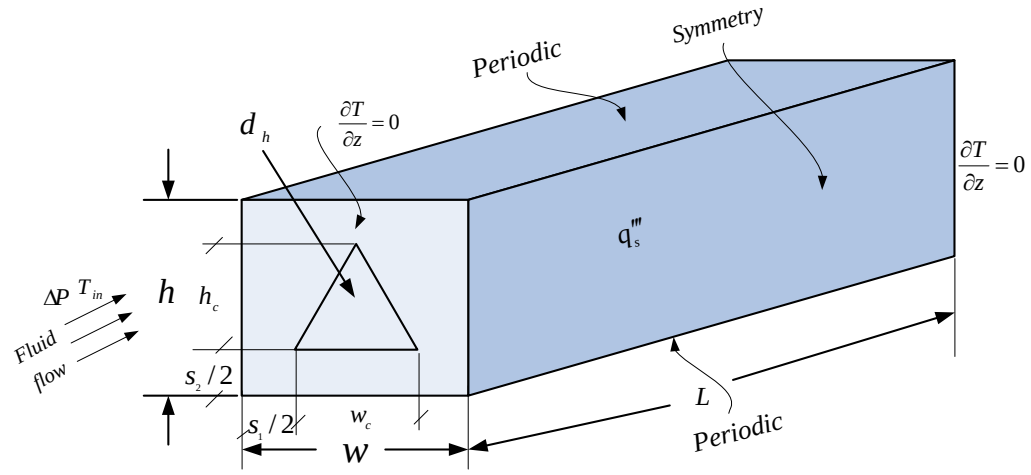

(b)

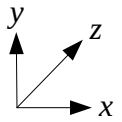

Figure 6. 25 : The boundary conditions of the three-dimensional computational domain for (a) isosceles right triangular cooling channels and (b) equilateral triangular cooling channels

Therefore, the total number of channels in the structure arrangement for the two triangular configurations can be defined as:

$$N = \frac{HW}{hw} = \frac{HW}{(h_c + s_2)(w_c + s_1)} \tag{6.43}$$

The temperature distribution in the model was determined by solving the equation for the conservation of mass, momentum and energy numerically. The discretised three-dimensional computational domain representing the two triangular configurations is shown in Figure 6.26. The cooling fluid was water; it is assumed to be in single-phase, steady, and a Newtonian fluid with constant thermo-physical properties, and was forced through the cooling channels by a specified pressure difference, ΔP across the axial length of the structure.

Also, other assumptions imposed on the triangular configurations are, the solid structure top and bottom boundaries of the domain correspond to periodic boundary conditions, the left and right side of the solid surfaces were taken as symmetry boundary conditions. All the outside walls were taken as plane of symmetry of the solid structure and were modelled as adiabatic as shown in Figure 6.25.

The objective function here is the minimum global thermal resistance which has been expressed in a dimensionless form in equation (6.13) and it is a function of the optimised design variables and the peak temperature. that is:

$$R_{\min} = f\left(AR_{c_{opt}},\ d_{h_{opt}},\ s_{1_{opt}},\ s_{2_{opt}},\ v_{el_{opt}},\ T_{\max_{\min}}\right) \tag{6.44}$$

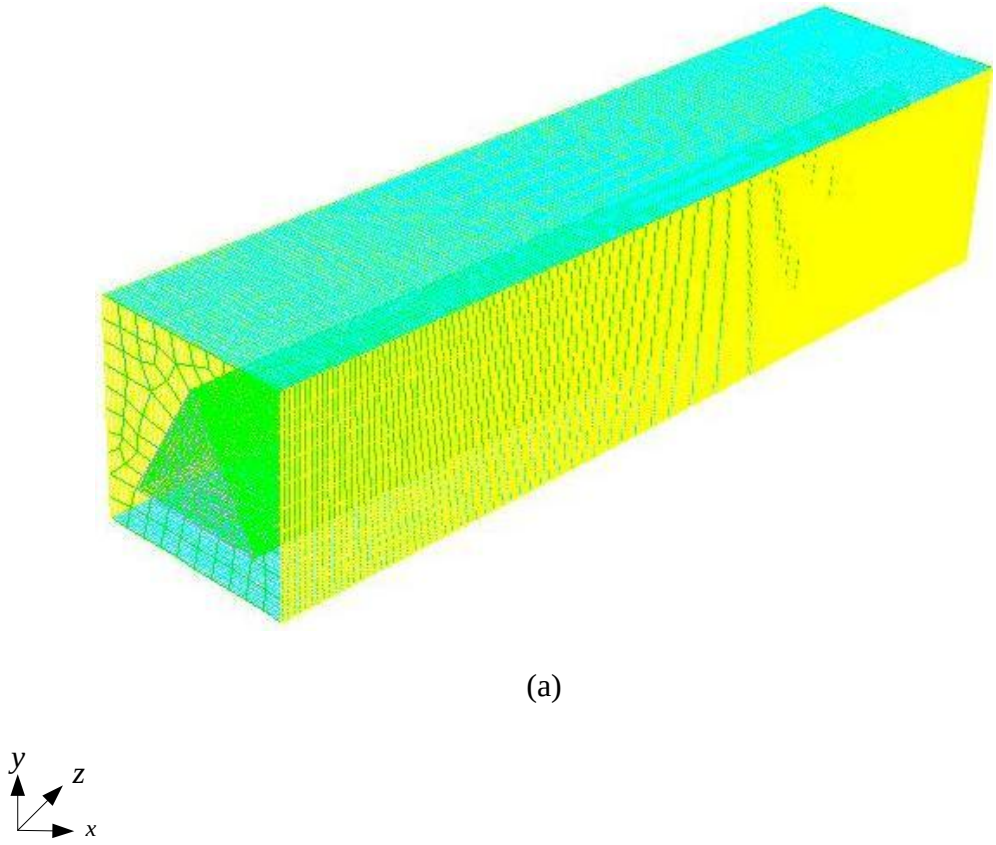

(a)

Figure 6. 26 : The discretised 3-D computational domain for triangular cooling channel

6.3.2. Numerical procedure

The procedure for numerical simulation used here is the same with little modification to that of circular and square configurations discussed in Section 6.2.2. It began by fixing the length of the channel, applied pressure difference, porosity, internal heat generation and material properties. We kept varying the values of elemental volume and hydraulic diameter or base length of the channel in order to identify the best (optimal) geometries that minimised the peak temperature.

The numerical solutions of the continuity, momentum and energy equations (Equations (3.1) to (3.8) of Chapter 3) along with the boundary conditions (Equations (6.6) to (6.12)) were obtained over the discretised domain shown in Figure 6.21 for the two triangular configurations. A three-dimensional finite volume commercial package FLUENT™ [199] was used, coupled with the geometry and mesh generation package GAMBIT [201] and MATLAB [219]. The GAMBIT [201] journal files for the isosceles right and equilateral triangular configurations are supplied in Appendixes B.3 and B.4 respectively. FLUENT [199] journal file in Appendix C is applicable to the simulations with little modification.

6.3.3. Grid analysis and code validation

To ensure accurate results, several grid independence tests were conducted until a mesh size with negligible changes in peak temperature was obtained. Tables 6.1 and 6.2 show the grid independence test for isosceles right triangular and equilateral triangular configurations with $v_{el} = 0.4\ \text{mm}^3$ $\phi = 0.2$, $L = 10\ \text{mm}$ for $\Delta P = 50\ kPa$. Also, computational cells densities of 32 526, 59 000 and 76 728 were used for the grid independence test for an isosceles right triangular configuration. It was observed that almost identical results were predicted when 59 000 and 76 728 cells were used. Therefore, any increase in the cell density beyond 59 000 had a negligible effect on the numerical result.

Again, computational cells densities of 33 360 63 500 and 77 284 were used for the grid independence test for the equilateral triangular configuration. It was observed that almost identical results were predicted when 63 500 and 77 284 cells were used. A further increase in the cell density beyond 63 500 would have a negligible effect on the numerical result.The convergence criterion for the overall thermal resistance as the quantity monitored is given in Equation (6.15).

Table 6. 1 : Grid independence study for the isosceles right triangular configuration with $v_{el} = 0.4\ \text{mm}^3$ $\phi = 0.2$ **and** $\Delta P = 50\ kPa$

Number of nodes	Number of cells	$T_{\max}$	$\gamma = \frac{\left\|(T_{\max})_i - (T_{\max})_{i-1}\right\|}{\left\|(T_{\max})_i\right\|}$
45 950	32 526	27.89944	-
79 120	59 000	27.94366	0.001582
101 332	76 728	27.96155	0.00064
150 190	118 750	27.99271	0.001113

Table 6. 2 : Grid independence study for the equilateral triangular configuration with $v_{el} = 0.4\ \text{mm}^3$ $\phi = 0.2$ **and** $\Delta P = 50\ kPa$

Number of nodes	Number of cells	$T_{\max}$	$\gamma = \frac{\left\|(T_{\max})_i - (T_{\max})_{i-1}\right\|}{\left\|(T_{\max})_i\right\|}$
28 034	1 9 314	27.81091	-
46 786	33 360	27.8580	0.00169
83 629	63 500	27.90048	0.001523
101 889	77 284	27.91846	0.000644

6.3.4. Numerical results

In this section, we present results for the case when the elemental volume was in the range of $0.025\ \text{mm}^3 \le v_{el} \le 5\ \text{mm}^3$ and the porosities ranged between $\phi = 0.2$ with a fixed length of L = 10 mm and fixed applied dimensionless pressure differences of $\Delta P = 50$ kPa. The internal heat generation within the solid was taken to be fixed at 100 kW/m^3.

Figures 6.27 and 6.28 show the existence of an optimal hydraulic diameter and optimal elemental volume of the structure that minimised the peak temperature at any point in the channel for the two types of triangular configurations studied. The abbreviation (E-T) is used for equilateral triangle and (I-T) is used for isosceles right triangle. Figure 6.27 shows the peak temperature as a function of the channel dimensionless hydraulic diameter for prescribed pressure difference. It shows that there exists an optimal channel hydraulic diameter, which lies in the range $0.005 \le d_h/L \le 0.02$ and minimises the peak temperature. Also, the elemental volume of the structure has a strong effect on the peak temperature as shown in Figure 6.28. The minimum peak temperature is achieved when the optimal elemental volume of the structure minimises the peak temperature and this lies in the range of $0.2\ \text{mm}^3 \le v_{el} \le 2.5\ \text{mm}^3$. Any further increase or decrease in the design variable beyond the optimal values indicates that the working fluid is not properly engaged in the cooling process. This is detrimental to the global performance of the system. The results also, show

that the optimal arrangement of the elemental volume for the entire structure at this fixed pressure difference should be very small in order to achieve better cooling.

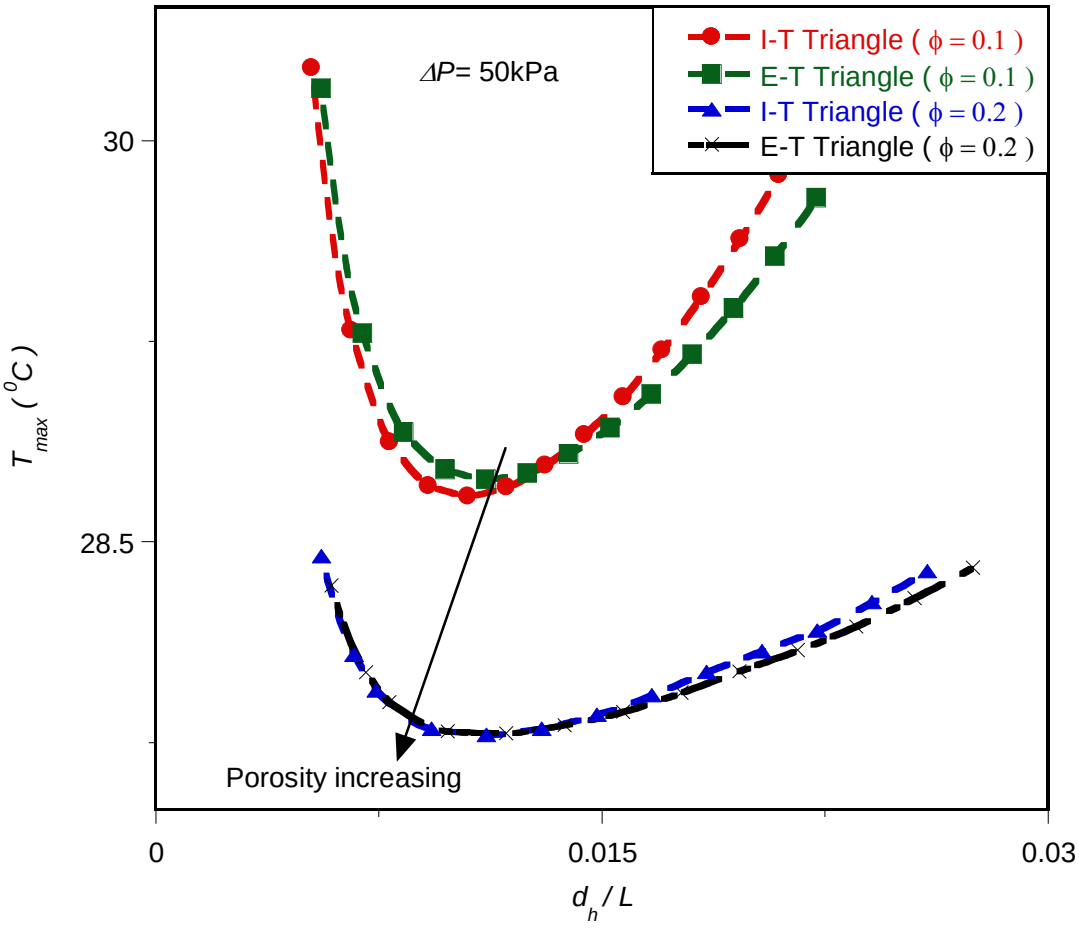

Figure 6. 27 : Effect of the optimised hydraulic diameter d_h on the peak temperature

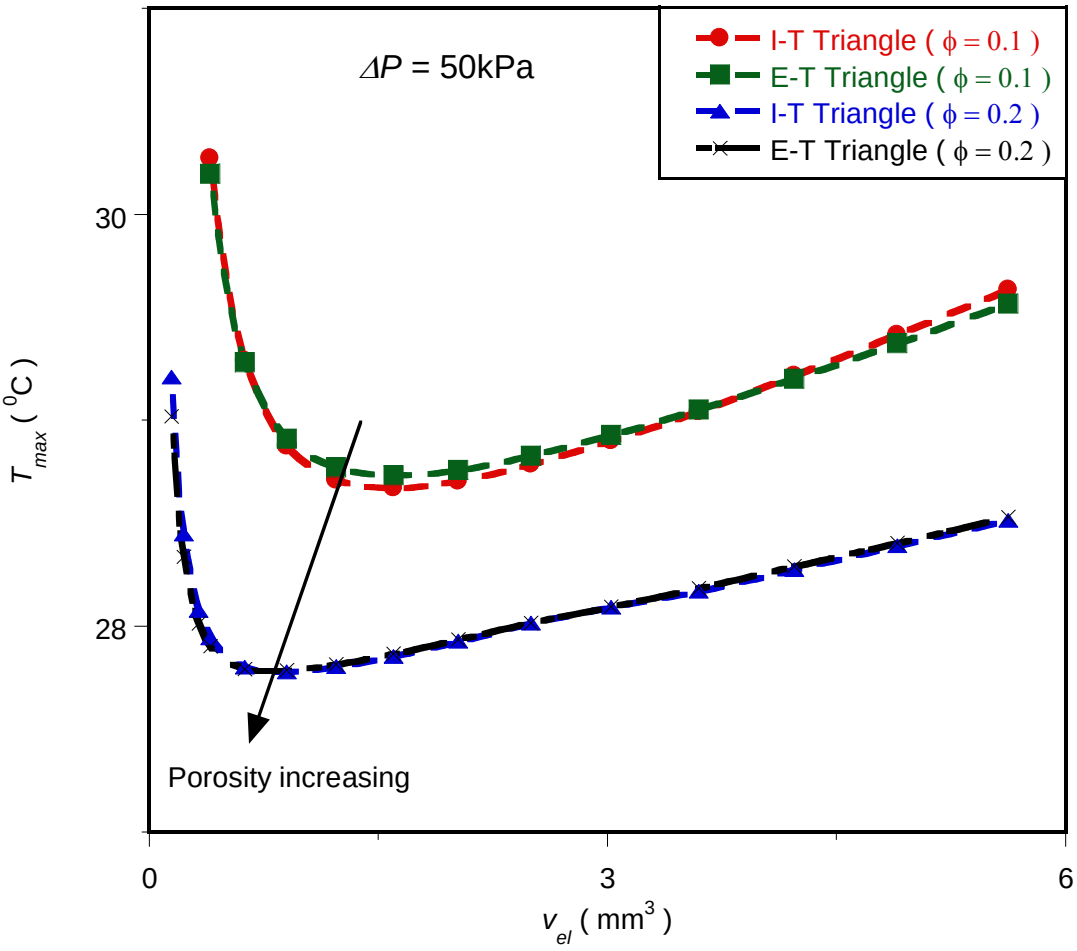

Figure 6. 28 : Effect of optimised elemental volume, v_{el} on the peak temperature

6.3.5. Mathematical formulation of the optimisation problem

In this section, we also introduce an DYNAMIC-Q algorithm that will search and identify the optimal design variables at which the system will perform at an optimum. the objective function is the minimisation of global thermal resistance.

6.3.5.1. Optimisation problem and design variable constraints

The optimisation technique described in Section 6.2.5 was applied to the triangular models described in Section 6.3.1.

The constraint ranges for the two triangular configurations are

$$0.1 \leq \phi \leq 0.2 \tag{6.45}$$

$$0.025\text{mm}^3 \leq v_{el} \leq 5\text{mm}^3 \tag{6.46}$$

$$\text{h}_c = \text{w}_c \tag{6.46}$$

$$0 \leq \text{w}_c \leq w \tag{6.48}$$

$$0 \leq d_h \leq w \tag{6.49}$$

And

$$0 \leq s_1 \leq w \tag{6.50}$$

$$0 \leq s_2 \leq w \tag{6.51}$$

The optimisation process was repeated for pressure differences across the axial length ranging from 5 kPa to 50 kPa within the design constraint ranges given in Equations (6.45) to (6.51). This was done in order to search for and identify the channel layout that minimises the peak temperature $T_{\max}$ so that the minimum thermal resistance between the fixed volume and the cooling fluid is obtained as the desired objectives function

6.3.6. Mathematical statement of the optimisation problem

The variables chosen for the mathematical statement are:

$$x_1 = w_c \tag{6.52}$$

$$x_2 = w \tag{6.53}$$

Substituting Equations (6.52) and (6.53) for Equations (6.45) to (6.51) results in the objective and constraints functions given in Equations (6.54) to (6.56) and in Equations (6.57) to (6.59) for isosceles right and equilateral triangular configurations respectively. The inequality functions g_1(x) and g_2(x) are derived from the porosity constraint of Equations (6.35) and (6.42) for isosceles right and equilateral configurations respectively.

Therefore, the mathematical statement of the optimisation problem for an isosceles right triangular configuration can then be written as:

$$f(x) = T_{\max} \tag{6.54}$$

$$g_1(x) = 0.4x_2^{\,2} - x_1^{\,2} \le 0 \tag{6.55}$$

$$g_2(x) = x_1^{\,2} - 0.8x_2^{\,2} \le 0 \tag{6.56}$$

Also the mathematical statement of the optimisation problem for an equilateral triangular configuration can be written as

$$f(x) = T_{\max} \tag{6.57}$$

$$g_1(x) = \frac{0.4}{\sqrt{3}} x_2^{\,2} - x_1^{\,2} \leq 0 \tag{6.58}$$

$$g_2(x) = x_1^{\,2} - \frac{0.8}{\sqrt{3}} x_2^{\,2} \leq 0 \tag{6.59}$$

6.3.7. Sensitivity analysis of the selection of forward differencing step size

Figure 6.29 shows a graph of the peak temperature as a function of the structure width of isosceles right triangular cooling channels, with a similar sensitivity analysis procedure for cylindrical cooling channel with step sizes of 10^{-6} and 10^{-4}. Although, different values of the step size of structure width as design variable considered are 10^{-6}, 10^{-5}, 10^{-4} and 10^{-3}. Figures 6.30 shows a graph of the peak temperature as a function of channel hydraulic diameter with a candidate step size of 10^{-4}.

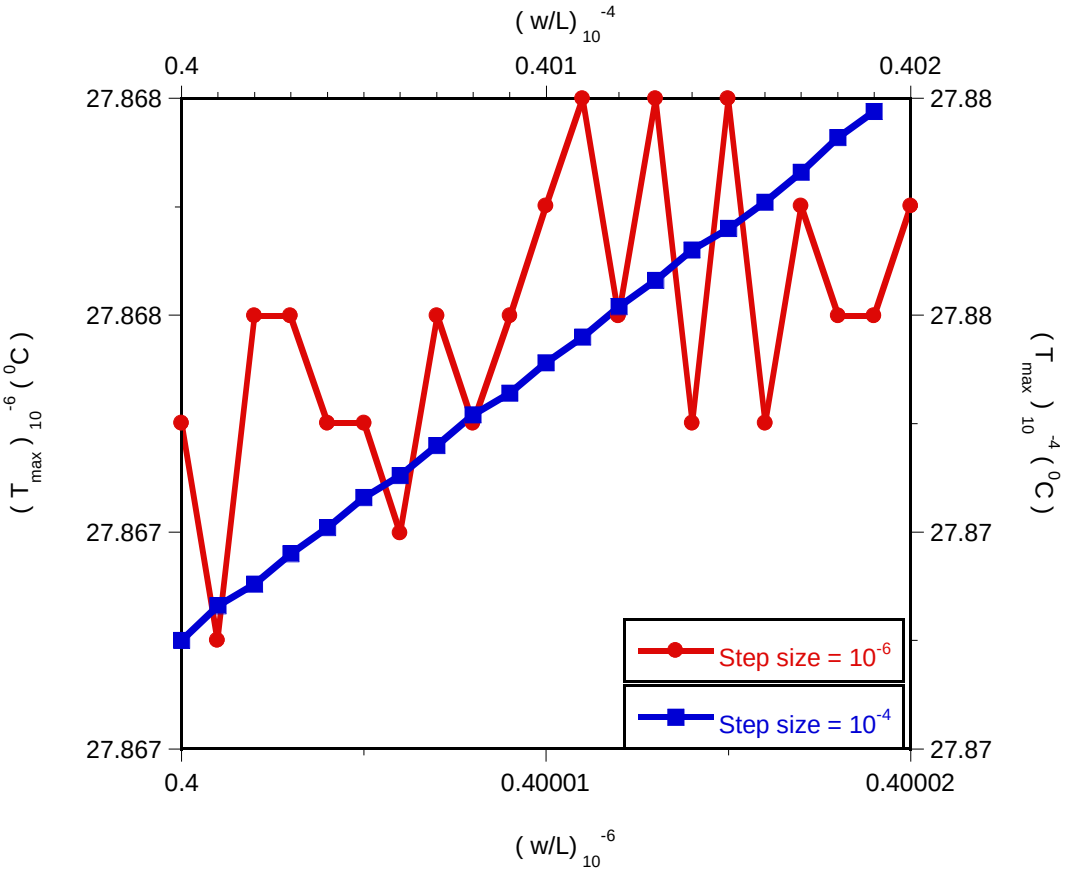

Figure 6. 29 : Plotting temperature for different structure width values with step sizes of 10^{-6} and 10^{-4}

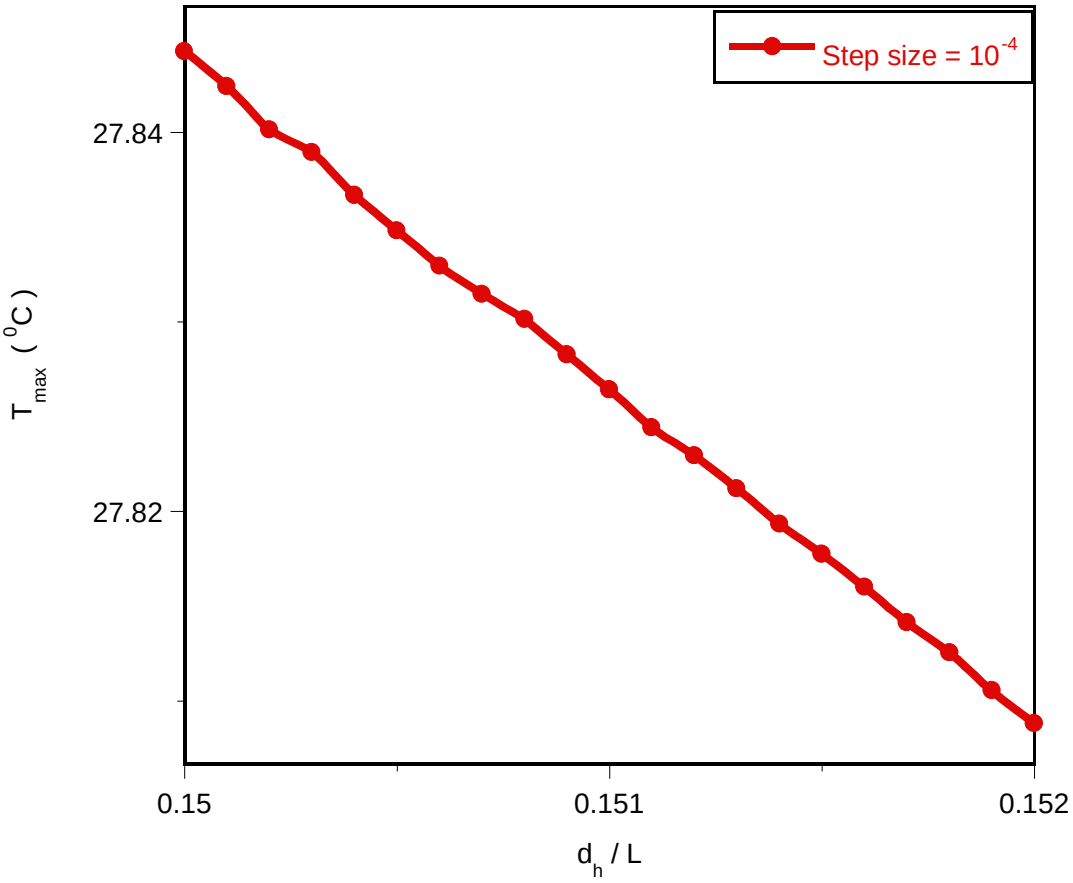

Figure 6. 30 : Plotting temperature for different hydraulic diameter values with a step size of 10^{-4}

6.3.8. Optimisation results

6.3.8.1. Effect of applied pressure difference on optimised geometry and minimised thermal resistance

Figure 6.31 shows the effect of the minimised thermal resistance as a function of applied dimensionless pressure difference. Minimised thermal resistance decreases as

the applied dimensionless pressure difference across the axial length and porosities increase. This trend is in agreement with previous work [94].

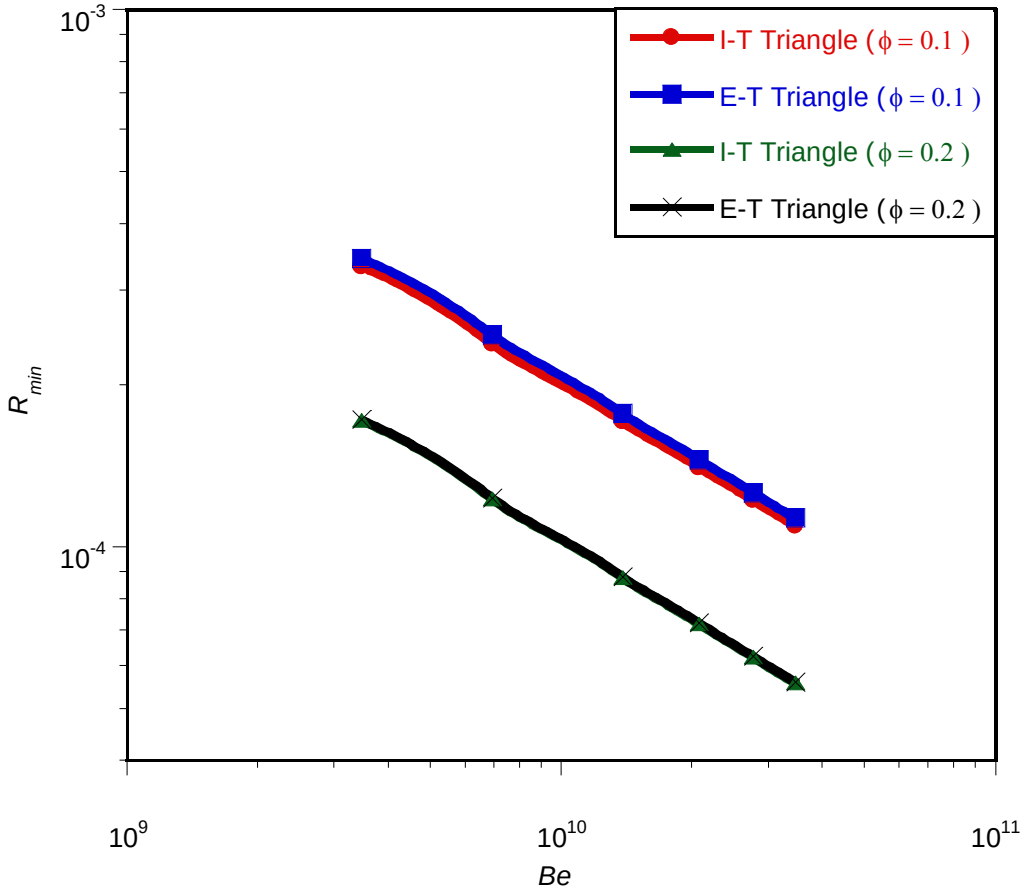

Figure 6. 31 : Effect of dimensionless pressure difference on the minimised global thermal resistance

Also, Figures 6.32 and 6.33 show the optimal behaviours of the geometry with respect to the applied dimensionless pressure difference number (or Bejan number) at different porosity for the two triangular configurations. Figure 6.32 shows that the optimal hydraulic diameter decreases as the dimensionless pressure differences increase. There also exists a unique optimal geometry for each of the applied

dimensionless pressure differences for the configurations. Figure 6.33 shows that the optimal channel spacing ratio (s_1/s_2) remains unchanged regardless of the dimensionless pressure difference number. This constant value could be described as allowable spacing due to manufacturing constraints. It implies that the closer the channels are to one another, the better the effective cooling ability of the global system.

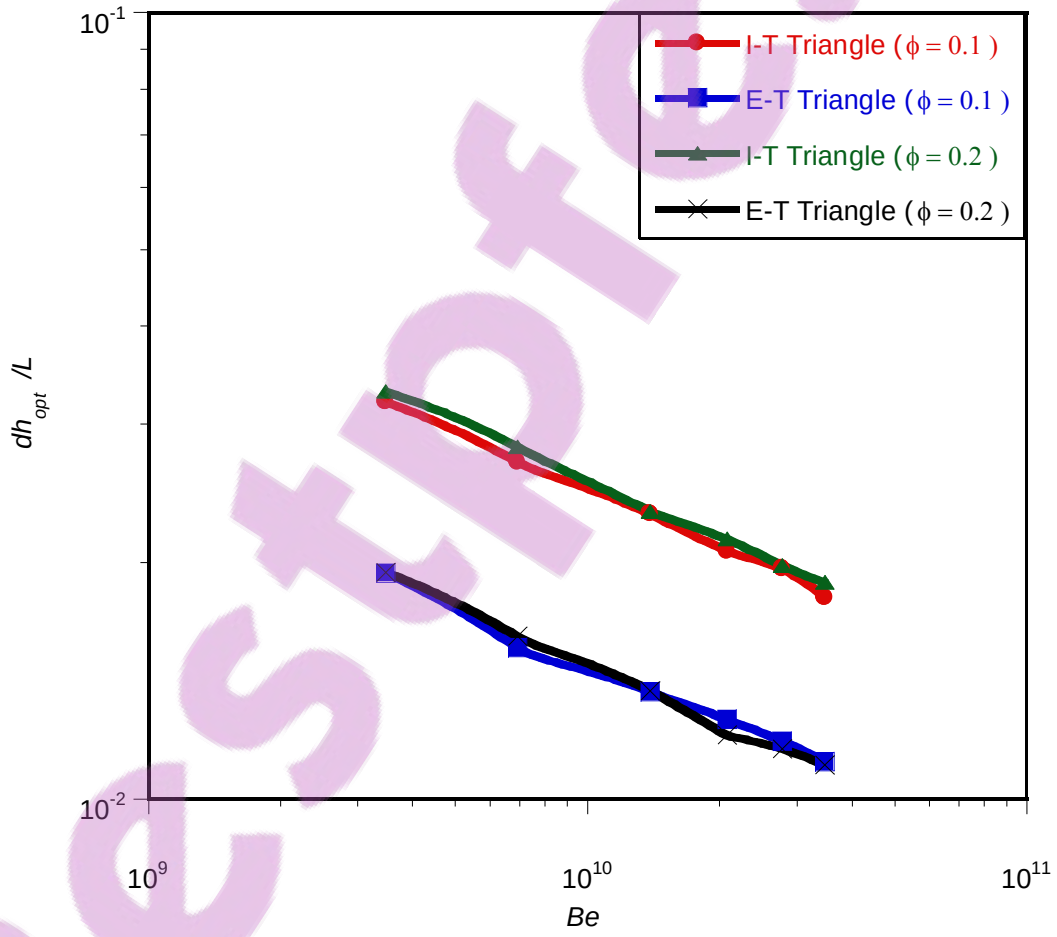

Figure 6. 32 : Effect of dimensionless pressure difference on the optimised hydraulic diameter

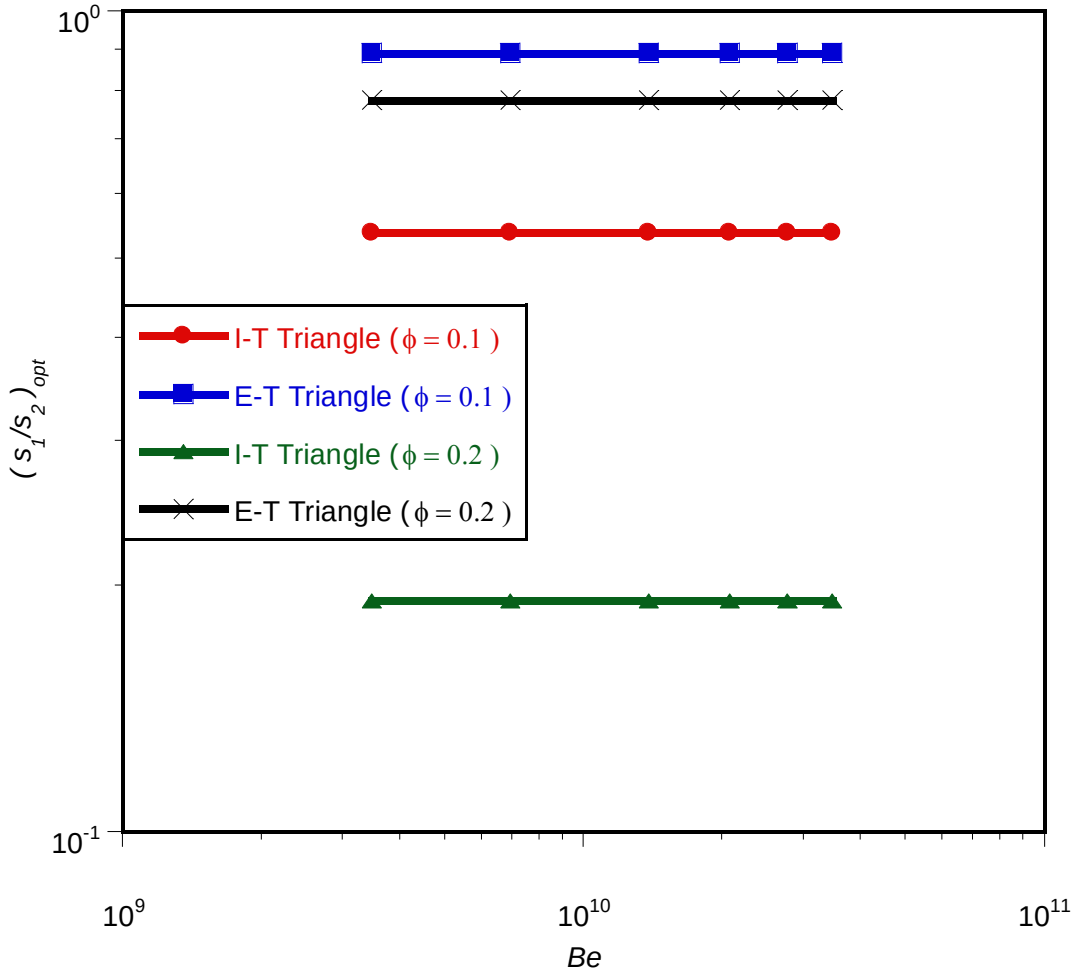

Figure 6. 33 : Effect of dimensionless pressure difference on the optimised channel spacing ratio

6.3.9. Comparison of the theoretical method and numerical optimisation

6.3.9.1. Effect of dimensionless pressure difference on the minimised dimensionless global thermal resistance

The analytical results of Equations (5.37) and (5.38) were used to validate the numerical solutions. The numerical and approximate solutions, based on scale analysis at optimal geometry dimensions, are in good agreement and the solutions follows similar trends as shown in Figure 6.34. Although the analytical results are lower than numerical results, the theoretical and numerical values agree within a factor of 1.5 for the worst case. However, these deviations are attributed to simplifying assumptions made in the formulation of the theoretical solution. These results are also in agreement with past research work [17, 93].

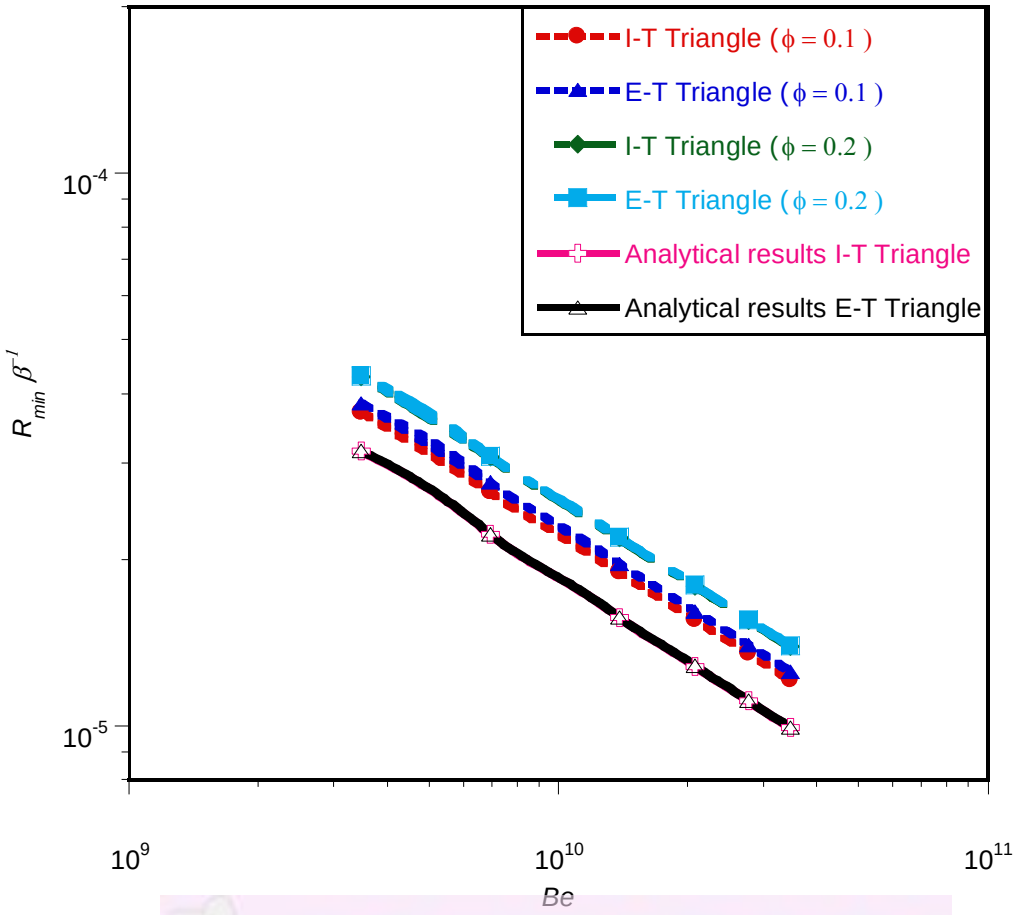

Figure 6. 34 : Correlation between the numerical and analytical solutions for the minimised global thermal resistance

Equations (6.60) and (6.61) are the correlations for minimised dimensionless thermal resistance and the dimensionless pressure difference for isosceles right and equilateral triangular channels. These correlations are obtained when the cooling geometry is optimised in order to achieve cooling for $\phi = 0.2$, where

$$R_{\min,\,\mathrm{Tri\,(I\text{-}T)}} = 7.62Be^{-0.49}, \qquad R^2 = 0.999 \tag{6.60}$$

$$R_{\min,\,\mathrm{Tri\,(E\text{-}T)}} = 7.66Be^{-0.49}, \qquad R^2 = 0.999 \tag{6.61}$$

where R^2 is the coefficient of correlation. The correlation given in Equations (6.60) and (6.61) correlate within the error of less than 0.01 to the CFD results produced.

6.3.9.2. Effect of applied dimensionless pressure difference on optimised design variables

Figure 6.35 shows the effect of the applied dimensionless pressure difference on the optimised dimensionless hydraulic diameter for the two triangular configurations. The curves show that the optimised dimensionless hydraulic diameter decreases as the applied dimensionless pressure difference increases for different porosities. This shows that unique optimal design geometry exists for each applied dimensionless pressure difference and porosity for all the configurations.

The numerical and approximate solutions at optimal geometry dimensions are in good agreement and the solutions follow similar trends as shown in Figures 6.35. However, the deviations are attributed to simplifying assumptions made in the formulation of the theoretical solution.

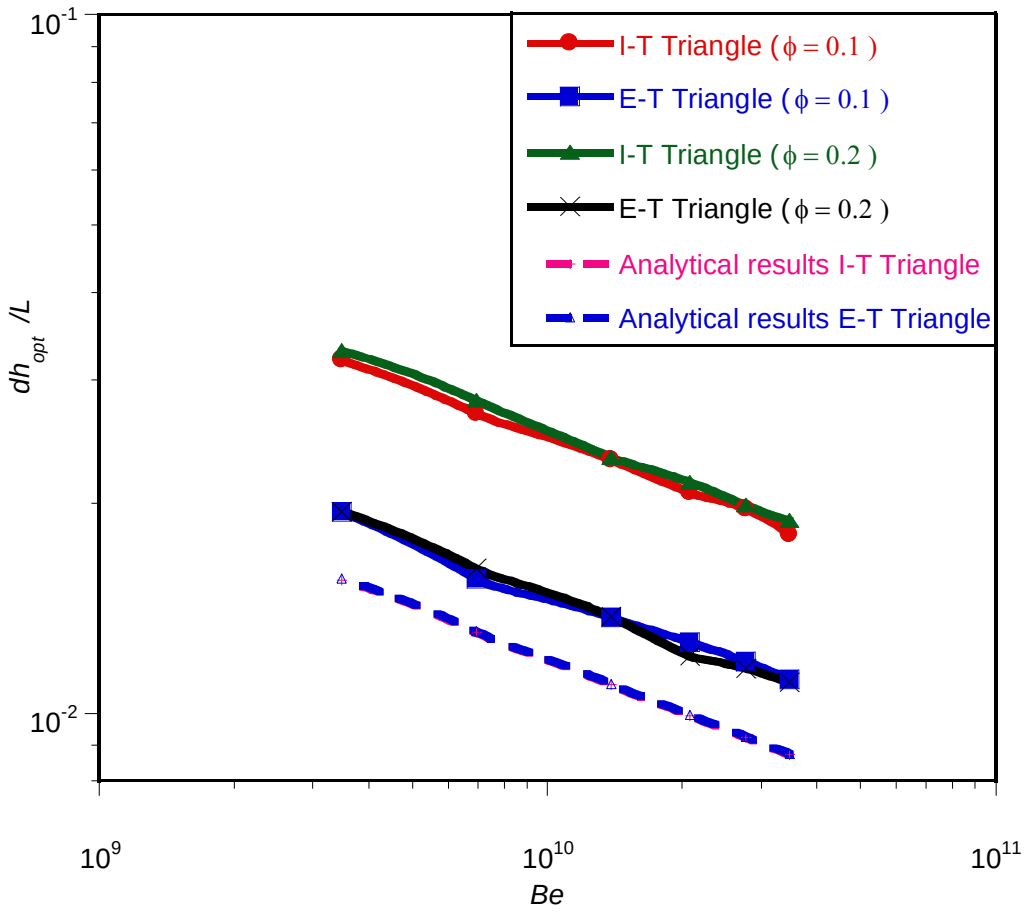

Figure 6. 35 : Correlation between the numerical and analytical solutions for the optimised hydraulic diameter

6.3.10. Optimal temperature contours

Figures 6.36(a) and 6.36(b) show the temperature contours of the elemental structure and the inner wall of the cooling channel with cooling fluid for equilateral triangular configurations, respectively. The blue region indicates the region of low temperature and the red region indicates that of high temperature. The arrow indicates the direction of flow.

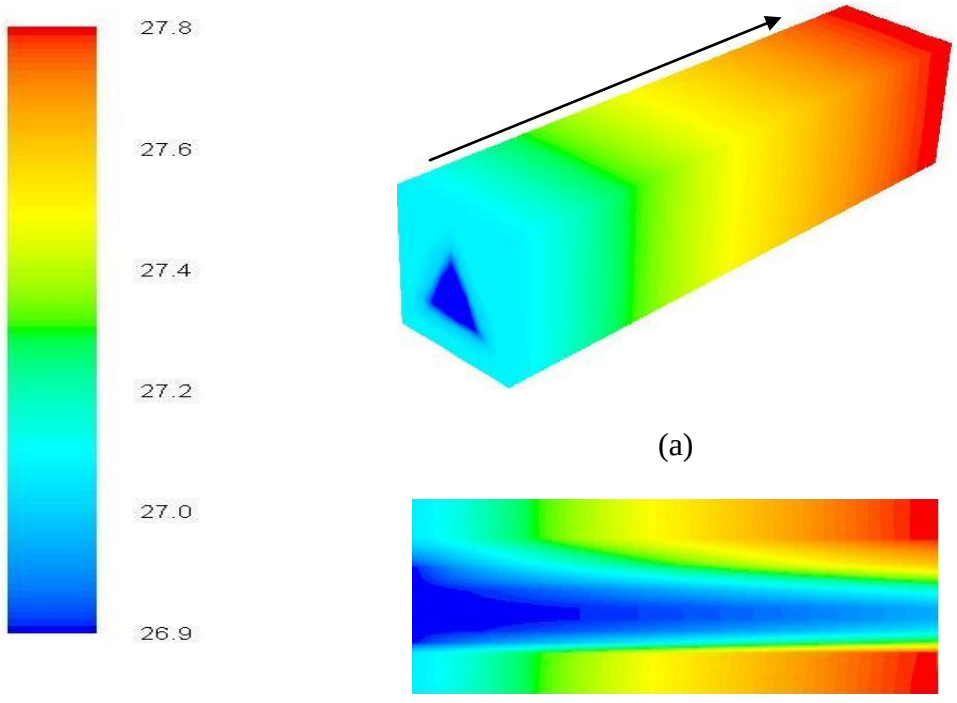

Figure 6. 36 : Temperature distributions on the cooling fluid and inner wall, as well as unit structure

6.4. CASE STUDY 3: RECTANGULAR COOLING CHANNEL EMBEDDED IN A HIGH-CONDUCTING SOLID

This present case study examines the three-dimensional numerical thermal resistance analysis in a heat-generated volume with rectangular cooling channels. The schematic physical configuration is shown in Figure 5.1(d). A computational elemental volume cell will also be modelled because of the symmetrical heat distribution as shown in Figure 6.37. The DYNAMIC-Q optimisation algorithm is used to search the optimal peak temperature (hence thermal resistance) by varying the geometric parameters subject to various constraints. The numerical optimisation results obtained will then be compared with it analytical solution in the preceding chapter.

6.4.1. Computational model

6.4.1.1. Design variables for isosceles rectangular cooling channels

In Figure 6.37, an elemental volume constraint is considered to be composed of an elemental cooling channel of width w_c , height h_c , and the surrounding solid of thickness $s_1$and s_2 which is defined as

$$v_{el} = whL \tag{6.62}$$

$$w = w_c + s_1 \tag{6.63}$$

$$h = h_c + s_2 \tag{6.64}$$

The volume of the elemental rectangular channel is:

$$v_c = w_c h_c L \tag{6.65}$$

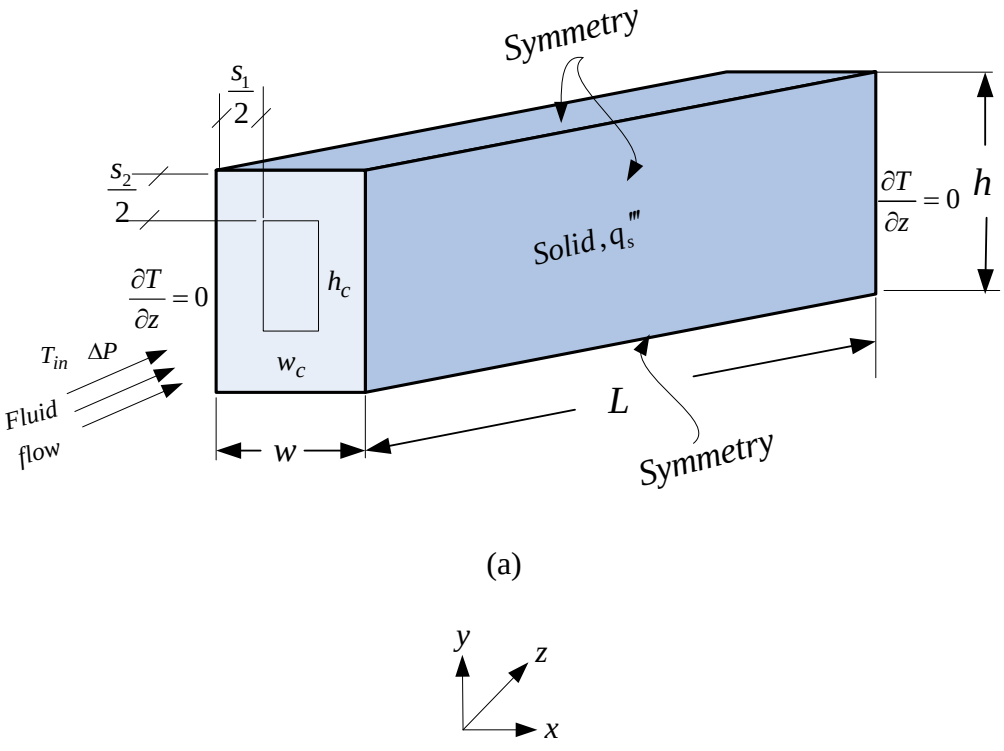

Figure 6. 37 : The boundary conditions of the three-dimensional computational domain of the cooling channel

Hence the number of channels in the structure arrangement can be defined as

$$N = \frac{HW}{hw} = \frac{HW}{(h_c + s_2)(w_c + s_1)} \tag{6.66}$$

However, porosity or void fraction of the unit structure is defined as

$$\phi = \frac{v_c}{v_{el}} = \frac{h_c w_c}{hw} \tag{6.67}$$

Aspect ratio of the unit structure is defined as

$$AR_s = \frac{h}{w} \tag{6.68}$$

Aspect ratio of the elemental channel is defined as

$$AR_c = \frac{h_c}{w_c} \tag{6.69}$$

The temperature distribution in the model was determined by solving the equation for the conservation of mass, momentum and energy numerically. The discretised three-dimensional computational domain of the rectangular configuration is shown in Figure 6.38. The cooling fluid was again water, as it is assumed to be in single-phase, steady, and a Newtonian fluid with constant thermo-physical properties. It was forced through the cooling channels by a specified pressure difference ΔP across the axial length of the structure.

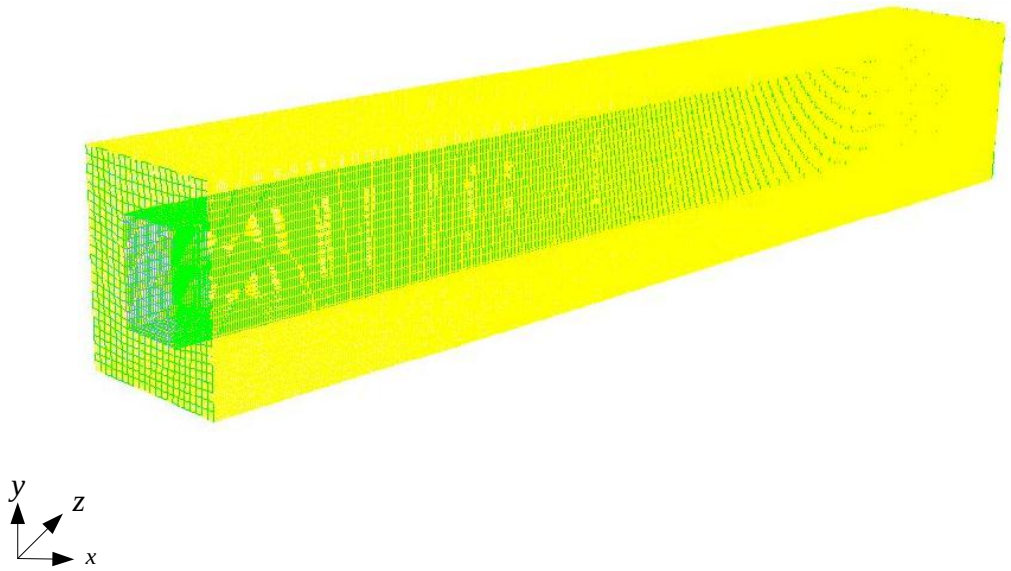

Figure 6. 38 : The discretised 3-D computational rectangualr cooling channels domain

Other assumptions imposed on the rectangular configuration model include, the solid structure top while the bottom right and left sides of the solid surfaces of the domain were taken as symmetry boundary conditions. All the outside walls were taken as plane of symmetry of the solid structure and were modelled as adiabatic as shown in Figure 6.37.

The objective function here is the minimum global thermal resistance as expressed in a dimensionless form in Equation (6.13)

and it is a function of the optimised design variables and the peak temperature,

$$R_{\min} = f\left(AR, d_h, s_1, s_2, \phi, \left(T_{\max}\right)_{\min}\right) \tag{6.70}$$

6.4.2. Numerical procedure

The procedure for numerical simulation used here is the similar (with little modification) to that of circular and square configurations discussed in Section 6.2.2. The simulation work began by fixing the length of the channel, applied pressure difference, porosity, internal heat generation, material properties and the elemental volume of the structure. We kept varying the values of the aspect ratio and the hydraulic diameter of the channel so as to identify the best (optimal) internal configuration that minimised the peak temperature.

The numerical solution of the of continuity, momentum and energy equations (Equations (3.1) to (3.8) of Chapter 3), along with the boundary conditions the two triangular configurations (Equations (6.58) to (6.66)), was obtained over the discretised domain shown in Figure 6.38. A three-dimensional finite volume commercial package FLUENT™ [199] was used, coupled with the geometry and mesh generation package GAMBIT [24] using MATLAB [219]. The GAMBIT [201] journal files for the rectangular configurations are supplied in Appendix B.5. The FLUENT [199] journal file in Appendix C is applicable to the simulations for which little modification is required in respect of the simulation boundary conditions.

6.4.3. Grid analysis and code validation

To ensure accurate results, several grid independence tests were conducted until a mesh size with negligible changes in peak temperature was obtained. Table 6.3 shows the grid independence test for a rectangular configuration for v_{el} = 1.8 mm^3 , w=150 μm, h = 1200 μm, $\emptyset$ = 0.2, AR_C = 8, a fixed length of L = 10 mm and fixed applied pressure differences of ΔP=50 kPa. Also, computational cell densities of 57 720, 101 250 and 125 100 were used for the grid independence test. It was observed that almost identical results were predicted when 101 250 and 125 100 cells were used. This implies that a further increase in the cell density beyond 101 250 had a negligible effect on the numerical result. The convergence criterion for the overall thermal resistance as the quantity monitored is given as in Equation (6.19).

Table 6. 3 : Grid independence study for rectangular configuration for w=150 μm, h = 1200 μm, ϕ = 0.2, AR_C = 8 and $\Delta P = 50\ kPa$

Number of nodes	Number of cells	T_{max}	$\gamma = \frac{\left\|(T_{max})_i - (T_{max})_{i-1}\right\|}{\left\|(T_{max})_i\right\|}$
45 379	30 000	27.65323	-
81 938	57 720	27.65759	0.000158
136 780	101 250	27.71466	0.002059
168 362	125 100	27.71188	0.0001

6.4.4. Numerical results

In this section, we attempt to show that there was an optimal geometry that minimised the peak temperature. The results were presented for the case where vel = 1.8 $mm^{3,}$

w=150 μm, $\varnothing$ = 0.2, h = 1200 μm, a fixed length of L = 10 mm and fixed applied pressure differences of ΔP=50 kPa.

Figures 6.39 and 6.40 show the existence of an optimum aspect ratio and optimum hydraulic diameter of the cooling channel in which the peak temperature is minimised at any point in the channel. Figures 6.39 shows that peak temperature strongly depends on aspect ratio. The peak temperature decreases as the aspect ratio increases. However, at very higher AR, the peak temperature increases. Figure 6.40 is the graph that shows peak temperature as a function of the channel hydraulic diameter. It shows the existence of an optimum hydraulic diameter of the cooling channel where the peak temperature is minimised at any point in the channel. The channel hydraulic diameter has a significant effect on the peak temperature and the overall thermal resistance. It shows that there exists an optimal channel hydraulic diameter that lies in the range $0.005 \leq d_h /L \leq 0.015$ and that minimises the peak temperature. Hence, peak temperature decreases as d_h /L decreases and a minimum value is reached beyond which the peak temperature begins to increase.

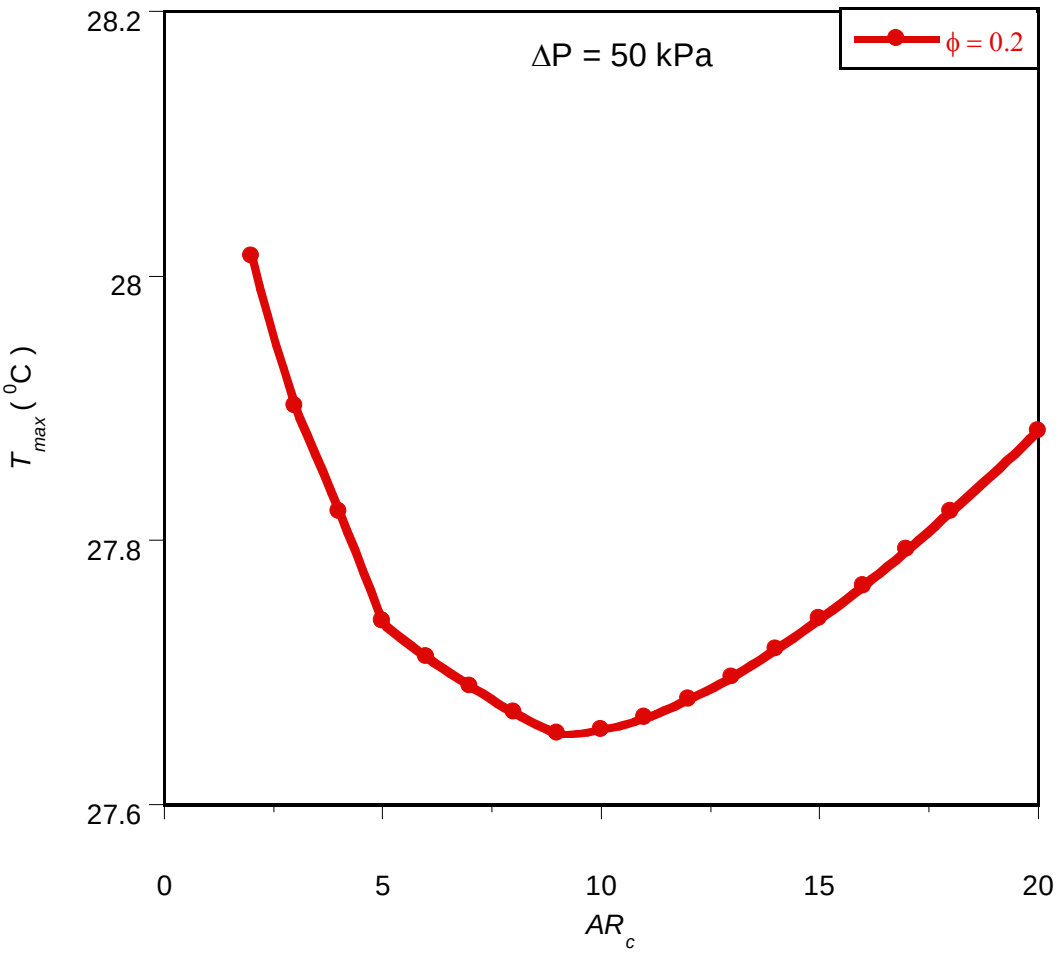

Figure 6. 39 : Effect of the optimised dimensionless channel aspect ratio AR_c on the peak temperature

Therefore, the global thermal resistance decreases as the hydraulic diameter increases. Also, the global thermal resistance decreases as the hydraulic diameter decreases. Any hydraulic diameter values above or below the optimal ranges, will cause the working fluid to be not properly engaged in the cooling process. This process is detrimental to the global performance of the system.

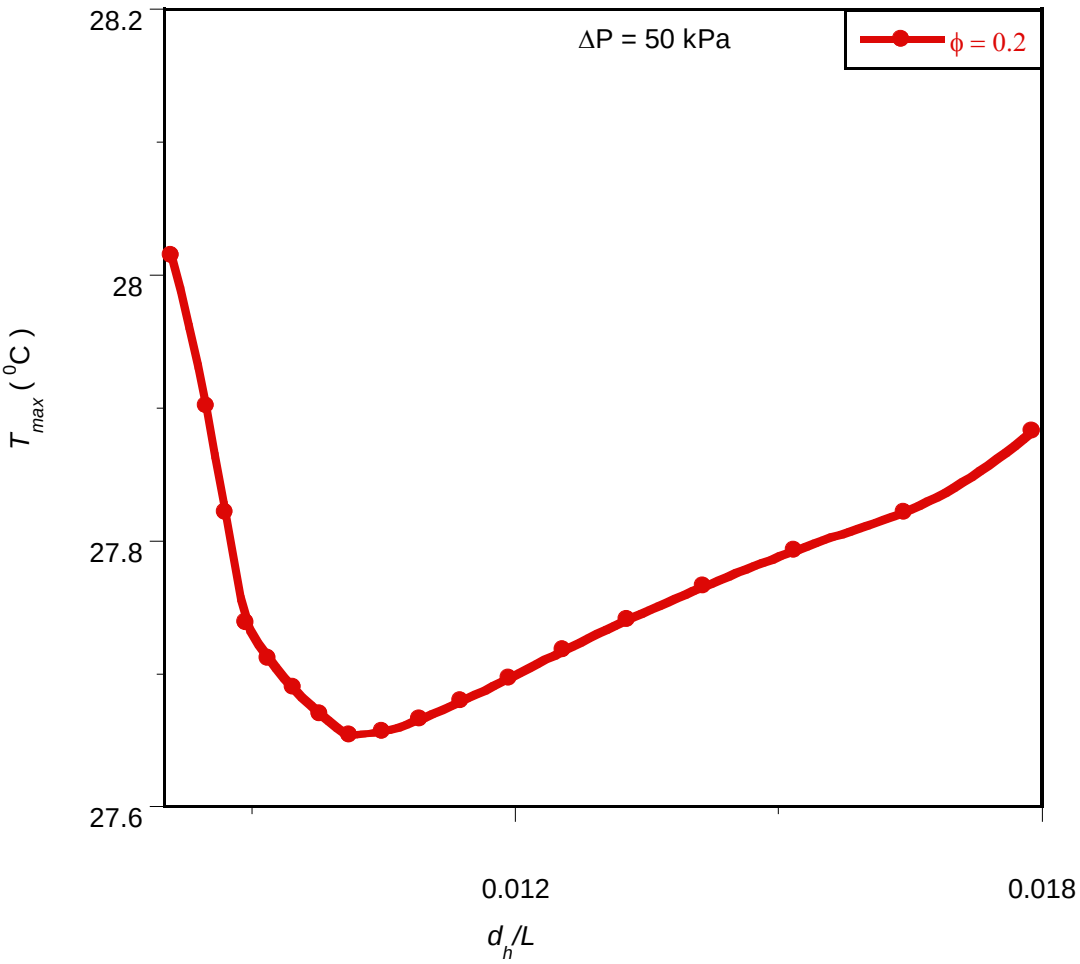

Figure 6. 40 : Effect of the optimised hydraulic diameter d_h , on the peak temperature

6.4.5. Mathematical formulation of the optimisation problem

We again introduce a mathematical optimisation algorithm that will search and identify the optimal design variables at which the system will perform at an optimum. the objective function is the minimisation of global thermal resistance.

6.4.5.1. Optimisation problem and design variable constraints

The optimisation technique described in Section 6.2.5 was applied to the rectangular model described in section 6.4.1.

The constraint ranges for the rectangular configuration optimisation are as follows:

$$0.1 \leq \phi \leq 0.2 \tag{6.71}$$

$$1 \leq AR_s \leq 20 \tag{6.72}$$

$$1 \leq AR_c \leq 20 \tag{6.73}$$

$$v_{el} = 1.8\ mm^3 \tag{6.74}$$

$$0 \leq w \leq L \tag{6.75}$$

$$0 \leq w_c \leq w \tag{6.76}$$

$$0 \leq h_c \leq h \tag{6.77}$$

$$0 \leq s_1 \leq w \tag{6.78}$$

$$0 \leq s_2 \leq h \tag{6.79}$$

The optimisation process was repeated for pressure differences across the axial length, ranging from 5 *kPa* to 50 *kPa* within the design constraint ranges given in Equations (6.71) to (6.79). This is done in order to search for and identify of the channel layout that minimises the peak temperature, T_{max} so that the minimum thermal resistance

between the fixed volume and the cooling fluid is obtained as the desired objectives function.

6.4.6. Mathematical statement of the optimisation problem

The variables chosen for the mathematical statement are:

$$x_1 = w \tag{6.80}$$

$$x_2 = h \tag{6.81}$$

$$x_3 = w_c \tag{6.82}$$

$$x_4 = h_c \tag{6.83}$$

Substituting Equations (6.80) to (6.83) for Equations (6.71) to (6.79), results in the objective and constraints functions given in Equations (6.84) to (6.92). The inequality functions g_1(x) and g_2(x) are derived from the porosity constraint of Equation (6.67).

The mathematical statement of the optimisation problem for rectangular configuration can then be written as:

$$f(x) = T_{\max} \tag{6.84}$$

$$g_1(x) = 0.0018 - x_3 x_4 \leq 0 \tag{6.85}$$

$$g_2(x) = 0.0036 - x_3 x_4 \leq 0 \tag{6.86}$$

$$g_3(x) = -x_1 - x_2 \leq 0 \tag{6.87}$$

$$g_4(x) = -x_2 - 20x_1 \leq 0 \tag{6.88}$$

$$g_5(x) = -x_3 - x_4 \leq 0 \tag{6.89}$$

$$g_6(x) = -x_4 - 20x_3 \leq 0 \tag{6.90}$$

$$g_7(x) = -x_3 - x_1 \leq 0 \tag{6.91}$$

$$g_8(x) = -x_4 - x_2 \leq 0 \tag{6.92}$$

6.4.7. Sensitivity analysis of selecting the forward differencing step size

Figure 6.41 shows the graph of peak temperature as a function of the height of rectangular cooling channels with a similar sensitivity analysis procedure for cylindrical cooling channel with step sizes of 10^{-6} and 10^{-4}. Although, different values of the step size of height of rectangular cooling channel as design variable were considered such as 10^{-6}, 10^{-5}, 10^{-4} and 10^{-3}. A Figures 6.42 shows graph of peak temperature as a function of channel width, with a candidate step size of 10^{-4}.

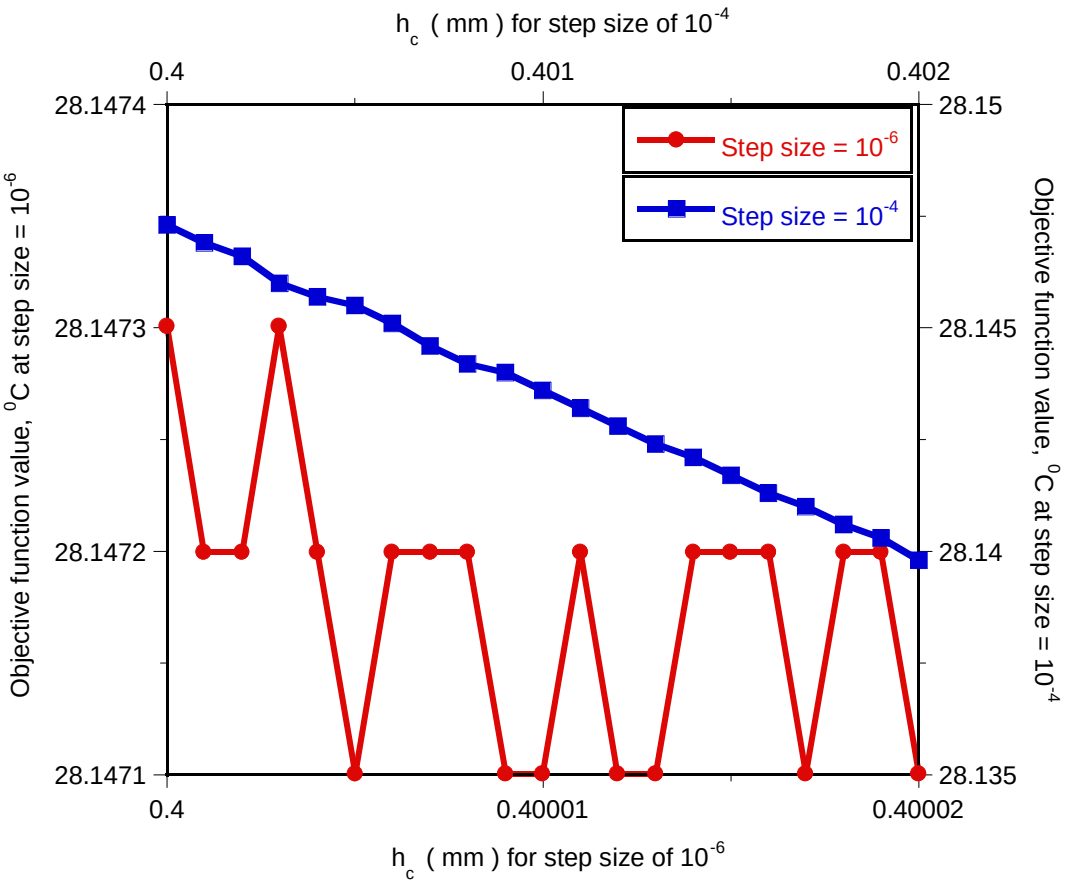

Figure 6. 41 : Plotting temperature for different channel height values with step sizes of 10^{-6} and 10^{-4}

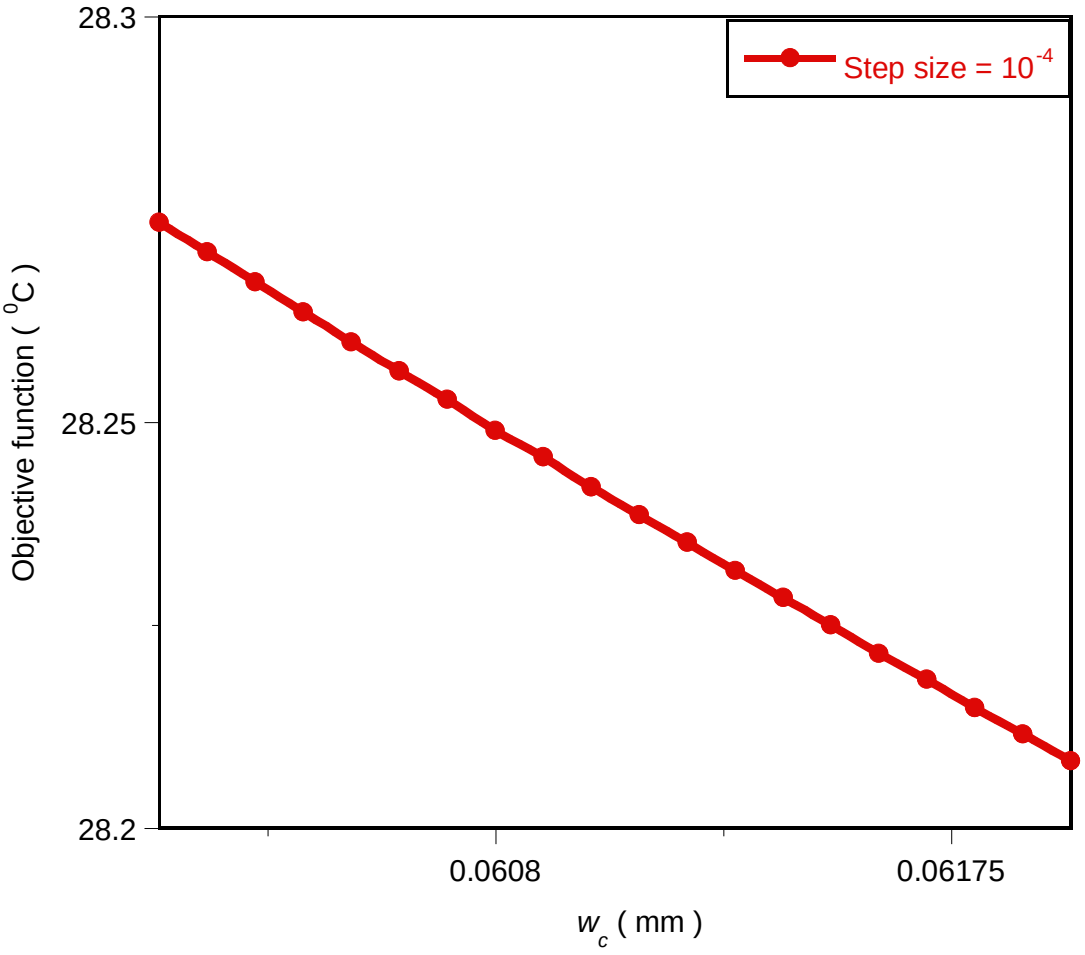

Figure 6. 42: Plotting temperature for different channels width values with a step size of 10^{-4}

6.4.8. Optimisation results

6.4.8.1. Effect of applied pressure difference on optimised geometry and minimised thermal resistance

Figure 6.43 shows the minimised dimensionless global thermal resistance as a function of dimensionless pressure difference at optimised design variables for the configuration. The results show that the dimensionless minimised global thermal resistance decreases as the dimensionless pressure difference increases. This trend is in agreement with previous work [94].

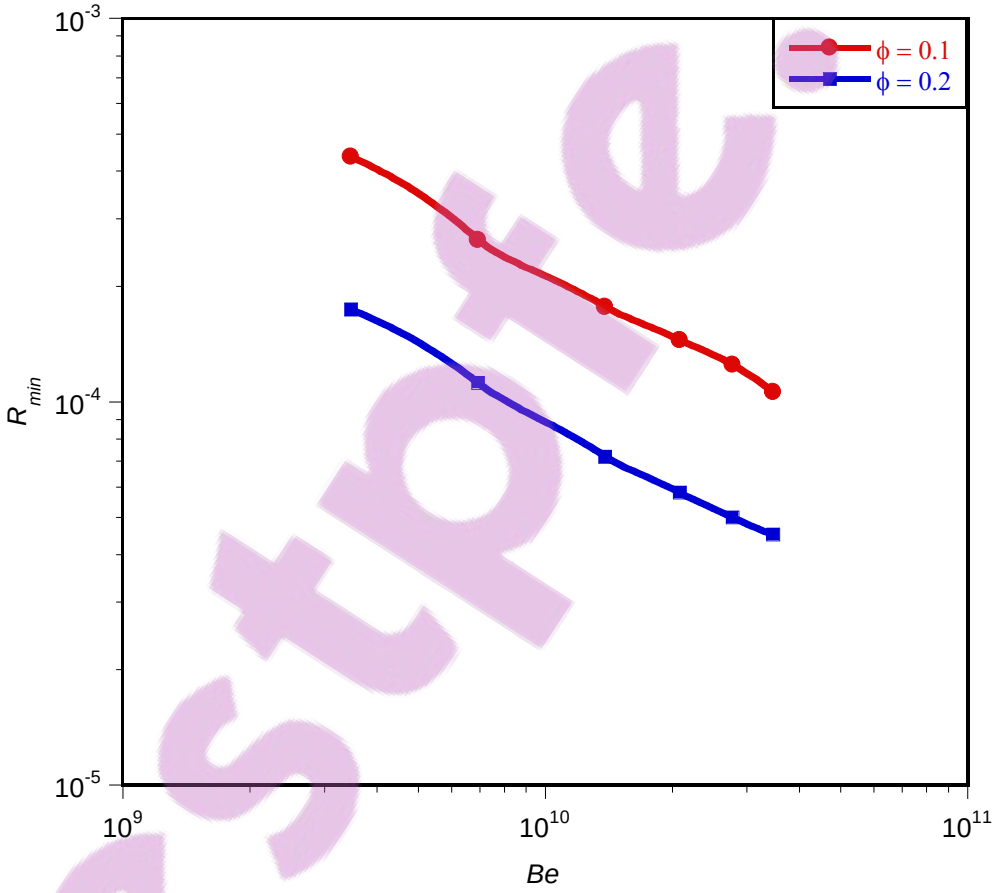

Figure 6. 43 : Effect of dimensionless pressure difference on the minimised dimensionless global thermal resistance

Figures 6.44 to 6.46 show the optimal behaviours of the geometry with respect to applied pressure difference (or Bejan number). It is shown that unique optimal design

geometries exist for each applied dimensionless pressure difference. Figure 6.44 shows that the optimised channel aspect ratio increases as the applied dimensionless pressure difference and porosity increase. Also, in Figures 6.43 and 6.45, it is clearly observed that the global dimensionless thermal resistance decreases as the channel aspect ratio increase. However, it is recognised that the optimal design scheme could lead to a design that could be impractical at very high channel aspect ratios, due to the channel being too thin to be manufactured.

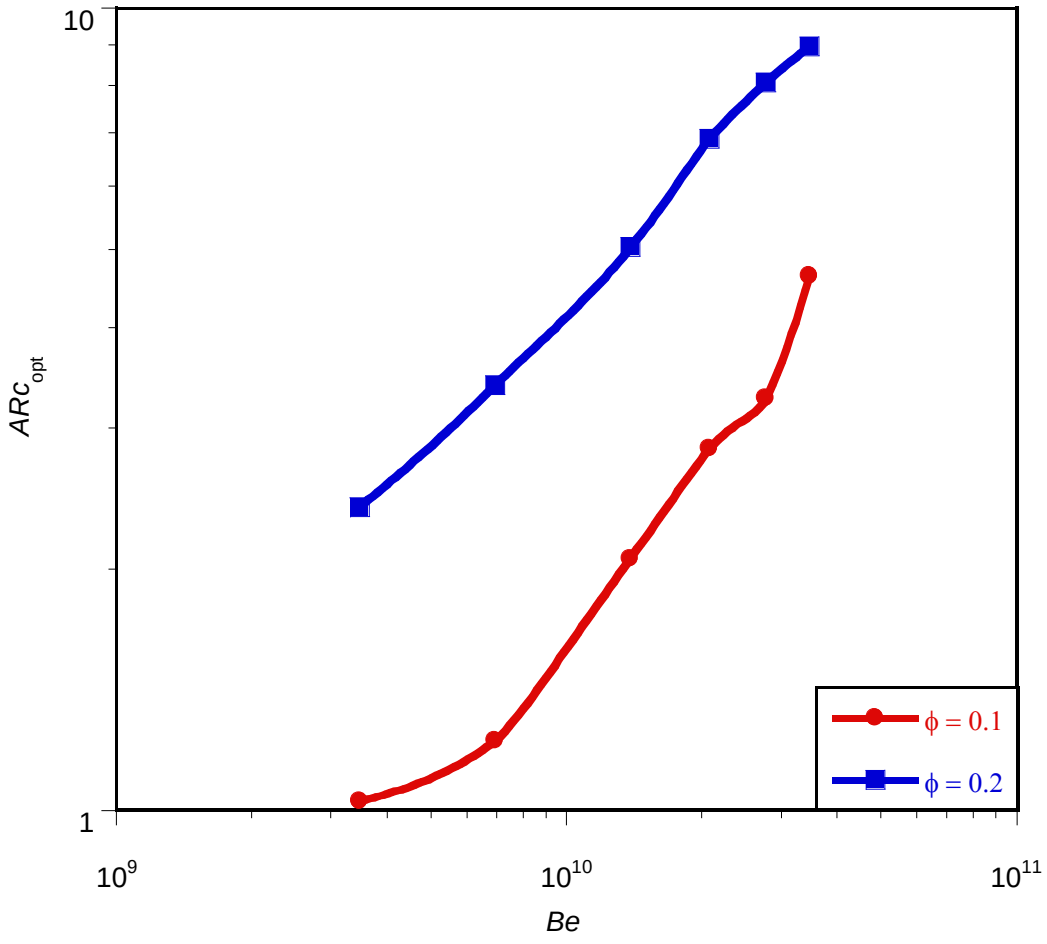

Figure 6. 44 : Effects of dimensionless pressure difference on the optimised aspect ratio

Figures 6.45 and 6.46 show the effect of the dimensionless pressure difference on the optimised dimensionless design variable. Figure 6.45 shows that the optimal hydraulic diameter decreases as the pressure differences increase. Also, Figure 6.46 shows that the optimal channels spacing $(s_1/s_2)_{opt}$ increases as the dimensionless pressure difference increases. We can say that there exists a unique optimal geometry for each of the applied pressure differences. The trend is in agreement with previous work. The trends of these results are also in agreement with previous work [94].

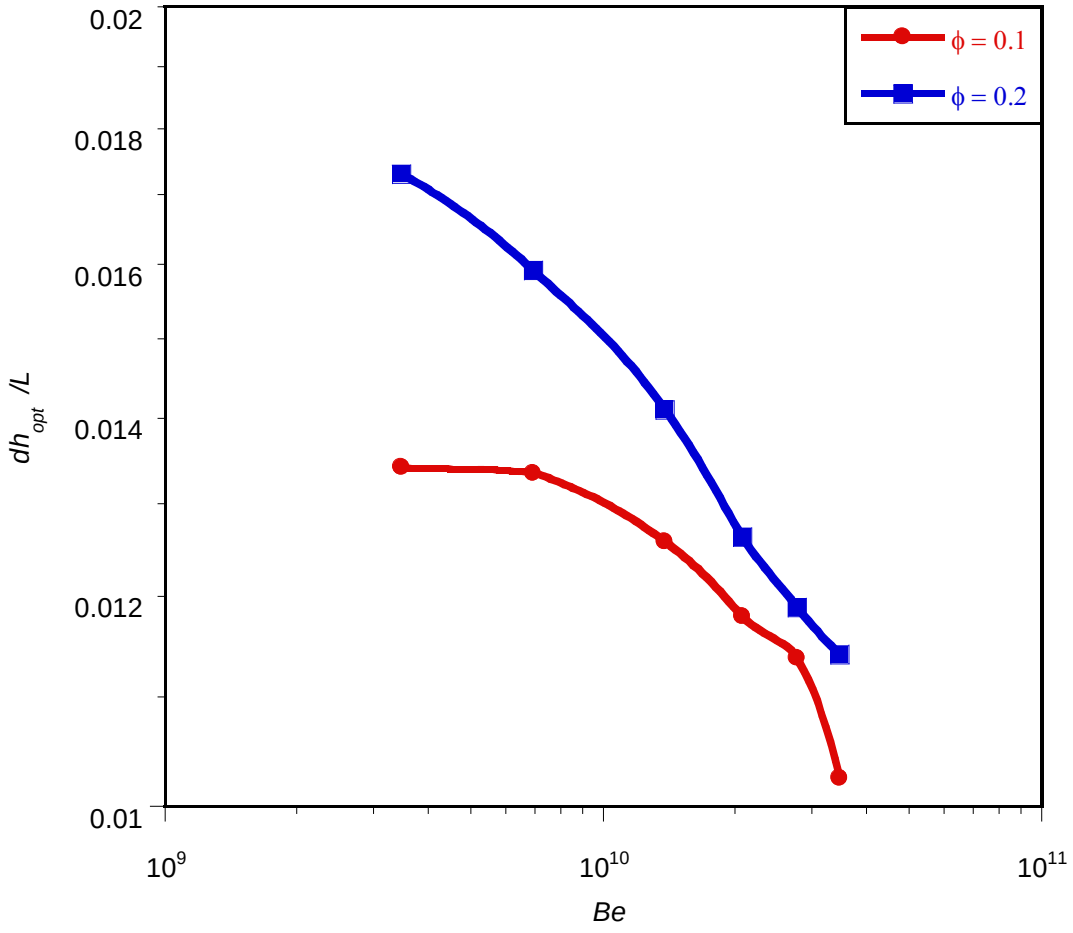

Figure 6. 45 : Effect of dimensionless pressure difference on the optimised hydraulic diameter

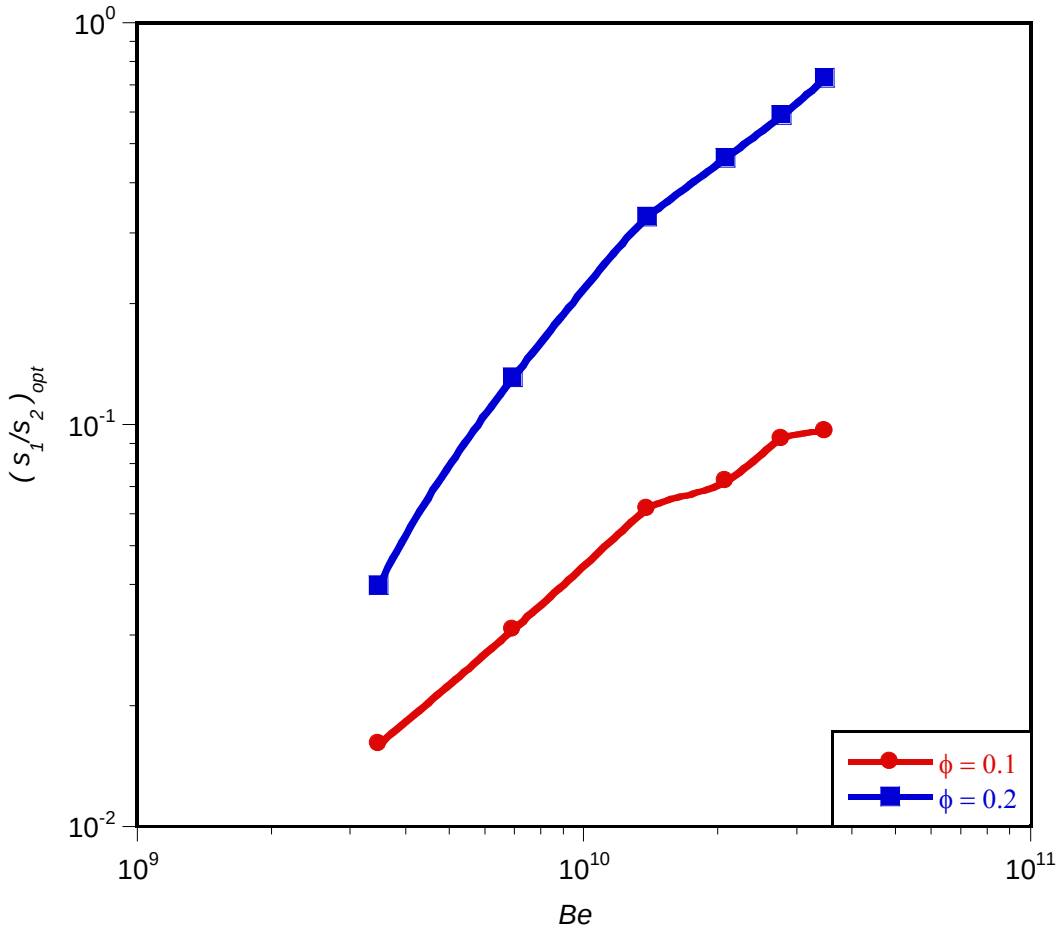

Figure 6. 46 : Effect of dimensionless pressure difference on the optimised channel spacing ratio

6.4.9. Comparison of the theoretical method and numerical optimisation

6.4.9.1. Effect of the applied dimensionless pressure difference on the minimised dimensionless global thermal resistance

The analytical results of Equation (5.39) were used to validate the numerical solutions. The numerical and approximate solutions, based on scale analysis at

optimal geometry dimensions, are in good agreement and the solutions follow similar trends as shown in Figure 6.47. Although the analytical results are lower than the numerical results, the theoretical and numerical values agree within a factor of 1.5 for the worst case. However, these deviations are attributed to simplifying assumptions made in the formulation of the theoretical solution. These results are also in agreement with past research work [94].

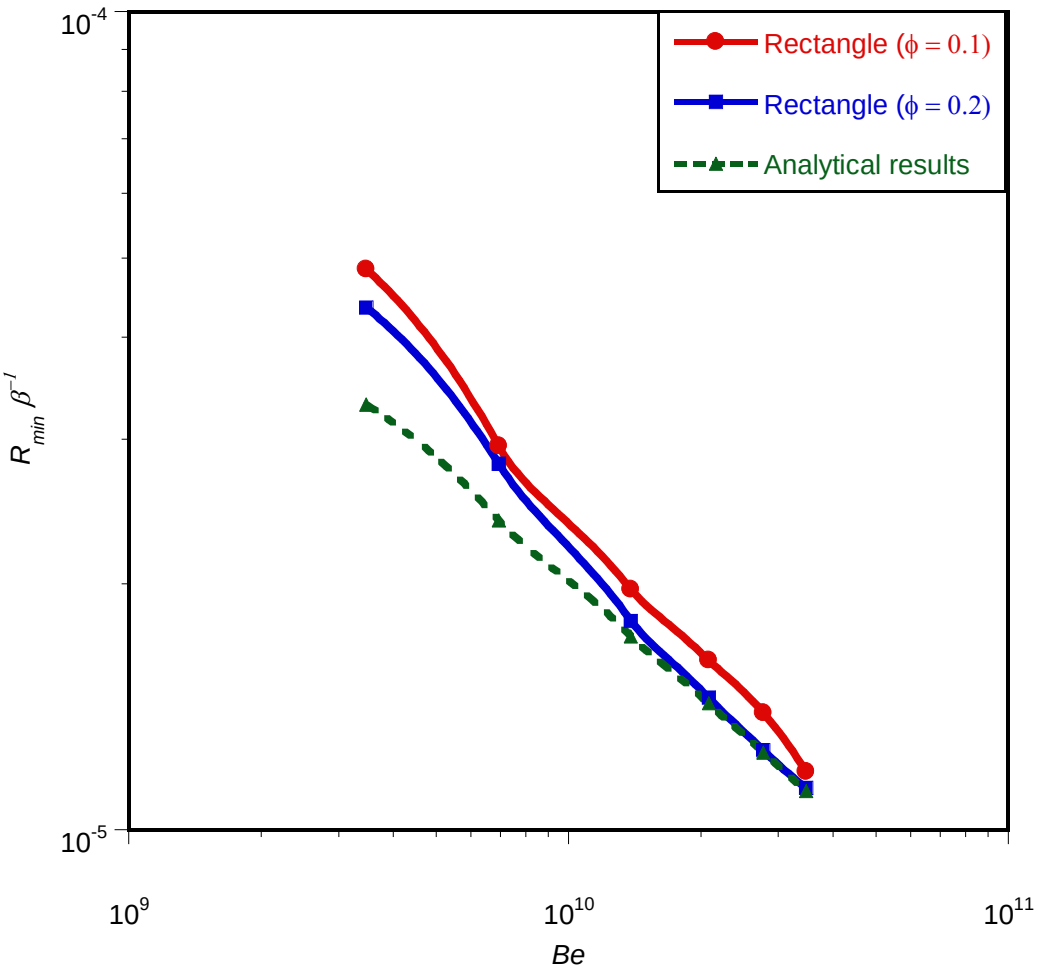

Figure 6. 47 : Correlation of the numerical and analytical solutions for the minimised global thermal resistance

Equation (6.93) presents the correlations for minimised dimensionless thermal resistance and the dimensionless pressure difference that is obtained when the cooling geometry is optimised to achieve cooling.

$$R_{\min} = \alpha Be^{-\beta} \tag{6.93}$$

where α and β are constant that depend on porosity and scale effects. For porosity of 0.2, α and β are 62.07 and 0.59 respectively within the error of less than 0.01.

6.4.9.2. Effect of dimensionless pressure difference on optimised design variables

Figure 6.48 shows the effect of the dimensionless pressure difference on the optimised dimensionless hydraulic diameter for the two triangular configurations. The curves show that the optimised dimensionless hydraulic diameter decreases as the applied dimensionless pressure difference increases for different porosities. This shows that, for all the configurations, unique optimal design geometry exists for each applied dimensionless pressure difference and porosity .

The numerical and approximate solutions at optimal geometry dimensions are in good agreement and the solutions follow similar trends as shown in Figures 6.48. However, the deviations are attributed to simplifying assumptions made in the formulation of the theoretical solution.

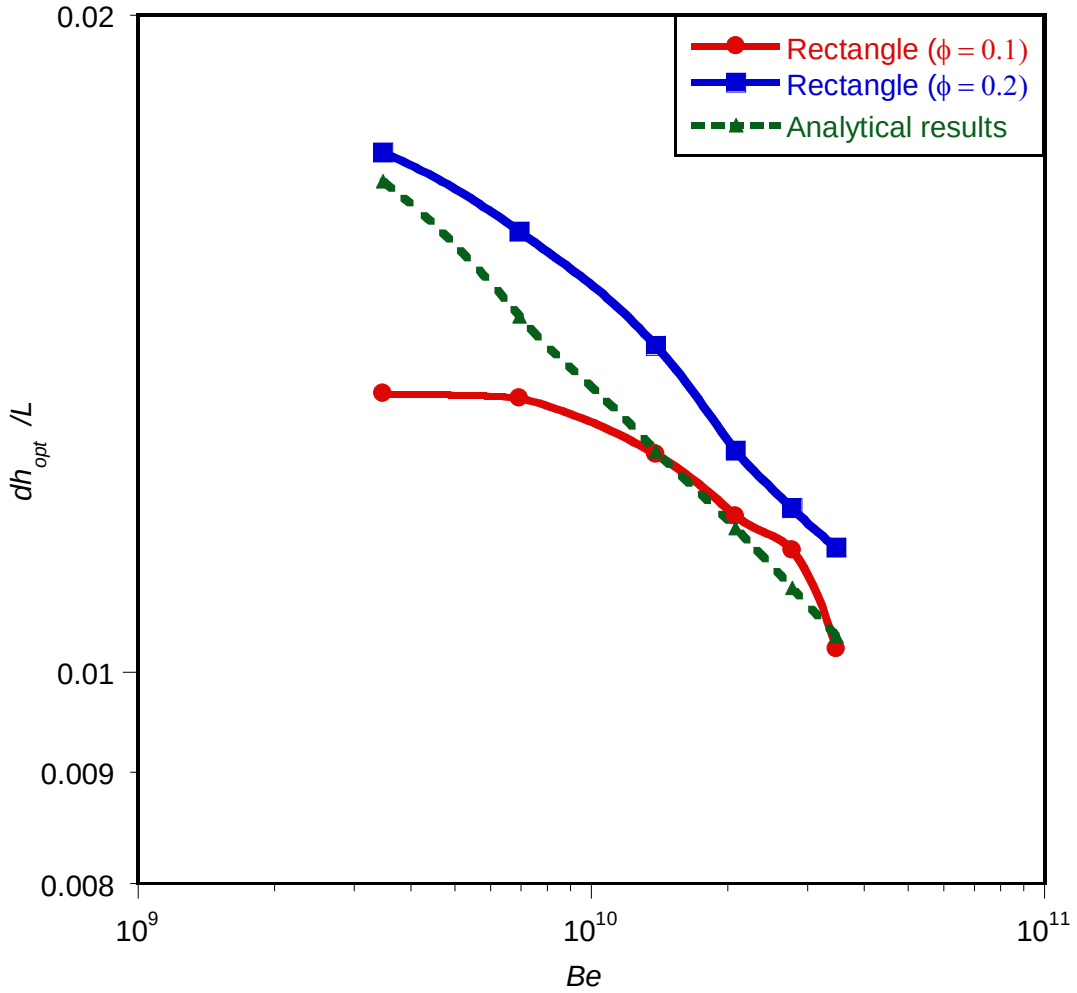

Figure 6. 48 : Correlation of numerical and analytical solutions for the optimised hydraulic diameter

6.4.9.3. Optimisation problem and design variable constraints

Figures 6.49(a) and 6.49(b) shows the temperature contours of the elemental structure and the inner wall of the cooling channel with cooling fluid for rectangular configuration respectively. The blue region indicates the region of low temperature

and the red region indicates that of high temperature. The arrow indicates the direction of flow.

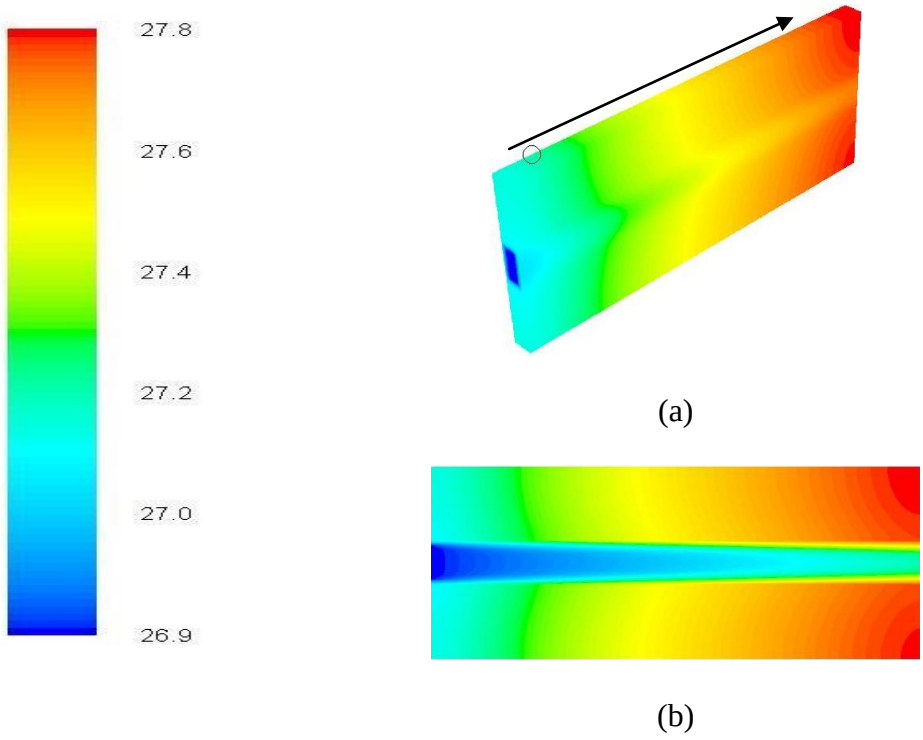

Figure 6. 49 : Temperature distribution on (a) the unit structure and (b) the cooling fluid and inner wall

6.4.10. Comparison and Summarised trends of all the case studies

In the preceding sections, the thermal performances of cooling channels with different cross-sectional shapes were determined by numerically optimising their geometrical parameters. The shapes of the cooling channels studied were, circular, square, isosceles right triangular, equilateral triangular and rectangular. In this section, we summarise trends by comparing all the optimisation cases studied.

Figure 6.50 shows the minimised thermal resistance of all the cooling channels studied as a function of applied dimensionless pressure difference number under uniform heat-generation thermal boundary conditions. As shown in Figure 6.48, all cases of channel shapes studied show a similar increasing trend in their thermal performances with an increase in dimensionless pressure difference number. The optimised numerical solutions show a linear decrease in the minimised global thermal resistance with increasing applied dimensionless pressure difference number.

From these results, it was also observed that the thermal performance of the cylindrical channel was poorer than that of any of the other four configurations.

The isosceles triangular configuration gave the best thermal performance followed by the equilateral triangular configuration. Next in the rank was the rectangular shape and followed by the square channel. This is due to the fact that triangular configurations have high shear stress corners. These findings are all in agreement with analytical solutions provided in Chapter 5.

However, it was clearly observed that the cooling effect was best achieved at a higher aspect ratio of rectangular channels. The optimal design scheme could well lead to a design that would be impractical at very high channel aspect ratios, due to the channel being too thin to be manufactured. Details of the results can be seen in Table 6.4 and 6.5.

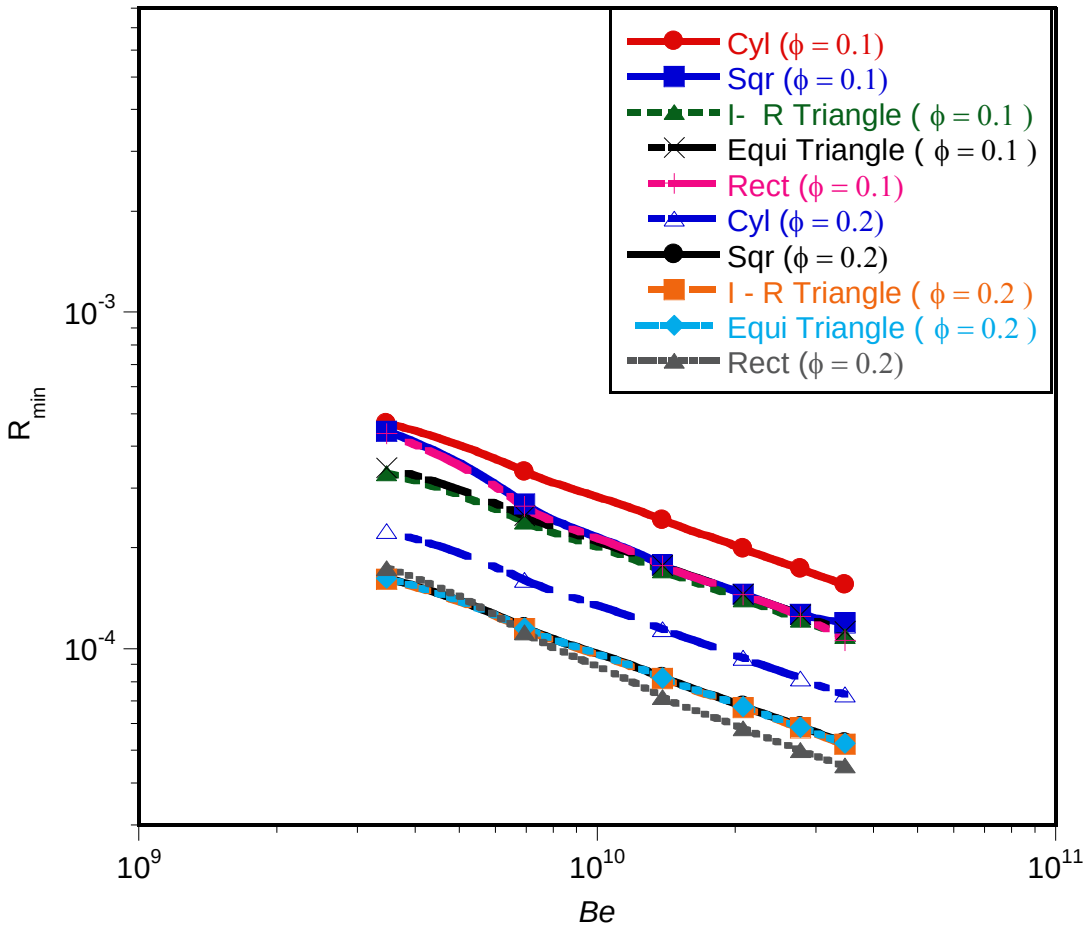

Figure 6. 50 : Comparison of the thermal performance of the cooling channels shapes studied

Table 2: Minimised global thermal resistance, R_{min} at $\phi = 0.1$ for all the cases shapes studied

	R_{min}	R_{min}	R_{min}	R_{min}	R_{min}
	Cylinder	Square	Isosceles	Equilateral	Rectangle
3.47E+09	0.0004685	0.0003333	0.0003327	0.0003449	0.00043600
6.94E+09	0.0003365	0.0002391	0.0002387	0.0002484	0.00026500
1.39E+10	0.0002414	0.0001712	0.0001709	0.0001771	0.00017700
2.08E+10	0.0001986	0.0001406	0.0001403	0.0001453	0.00014500
2.77E+10	0.0001728	0.0001228	0.0001220	0.0001262	0.00012500
3.47E+10	0.0001552	0.0001097	0.0001093	0.0001130	0.00010600

Table 1: Minimised global thermal resistance, R_{min} at $\phi = 0.2$ for all the cases shapes studied

Be	R_{min}	R_{min}	R_{min}	R_{min}	R_{min}
	Cylinder	Square	Isosceles	Equilateral	Rectangle
3.47E+09	0.0002241	0.0001624	0.0001611	0.0001620	0.00017400
6.94E+09	0.0001603	0.0001156	0.0001147	0.0001153	0.00011200
1.39E+10	0.0001146	0.0000823	0.0000816	0.0000821	7.2000e-05
2.08E+10	0.0000940	0.0000675	0.0000670	0.0000674	5.8000e-05
2.77E+10	0.0000817	0.0000587	0.0000582	0.0000585	5.0000e-05
3.47E+10	0.0000732	0.0000526	0.0000521	0.0000524	4.5000e-05

6.5. CONCLUSION

This chapter demonstrates a numerical optimisation methodology of conjugate heat transfer in cooling channels of different cross-sectional shapes with the help of a multidimensional and robust gradient-based optimisation algorithm. Global optimal solutions are obtained using Dynamic-Q, which does not require an explicit line search.

The shapes of the cooling channels studied were, circular, square, isosceles right triangular, equilateral triangular and rectangular. These cooling channels of different shapes penetrated and embedded in a highly conductive solid material were optimised. The overall objective of all these cases was to minimise the peak wall temperature of the conductive solid structure in order to achieve lowered thermal resistances. Under a fixed volume and other material constraints, relationships were developed between various optimal geometric parameters and the dimensionless pressure difference.

The temperature distribution of the different cooling channels shapes was analysed. Sensitivity analysis was performed to make sure CFD noise did not affect the optimal solutions. This highlights the importance of correct formulation and design set-up for effective and accurate optimisations.

It can be concluded that for all the geometrical shapes studied, the design variables had significant effect on the thermal performance of heat-generating devices. The optimisation reveals that there exist a trade-off between the global thermal resistance and the applied dimensionless pressure difference number (pumping power) in order to optimise the heat-generating devices and the channel configurations. The optimum design variables are sensitive to the applied dimensionless pressure difference number (*Be*) within the design space and show an alternating behaviour with change of the applied dimensionless pressure difference number. This shows the existence of unique optimal design variables (geometries) for a given applied dimensionless pressure number for each configuration studied. Therefore, thermal designers can pick an optimal solution according to the applied dimensionless pressure difference number (*Be*) available to drive the fluid or thermal resistance required.

The various case designs emphasised the fact that for cooling channels design, material cost and applied pressure difference considerations are vital elements in achieving optimal designs.

It is also observed that although the thermal performance of the cylindrical channel was poorer than that of any other channels, it was a more viable option and more often used in industry due to the ease of manufacturability and packaging.

The numerical results obtained are in good agreement with results obtained in the approximate solutions based on scale analysis at optimal geometry dimensions in Chapter 5. The approximate dimensionless global thermal resistance predicts the trend obtained in the numerical results. The use of the optimisation algorithm coupled to the CFD package render the numerical results more robust with respect to the selection of optimal structures' internal configurations of the flow channels and dimensionless pressure difference.

7

CHAPTER 7: MATHEMATICAL OPTIMISATION OF LAMINAR-FORCED CONVECTION HEAT TRANSFER THROUGH A VASCULARISED SOLID WITH COOLING CHANNELS[5]

7.1. INTRODUCTION

This section develops numerically and analytically the geometric optimisation of parallel cooling channels in forced convection for a vascularised material with the localised self-cooling property subjected to a heat flux on one side. This is done in such a way that the peak temperature was minimised at every point in the solid body. The self-cooling ability of vascularised material to bathe volumetrically at every point of a solid body gave rise to the name 'smart material'.

Constructal theory ideally helps in the vascularisation of the smart material structure by morphing the flow architecture configuration to provide easier and greater access of flow through it.

This work is follows on that of Kim *et al.* [128], who theoretically and numerically analysed vascularised materials with heating from one side and coolant forced from

[5] This research section is published in part: O.T. Olakoyejo, T. Bello-Ochende and J.P Meyer, "Mathematical optimisation of laminar-forced convection heat transfer through a vascularised solid with square channels", *International Journal of Heat and Mass Transfer*, Vol. 55, 2012, pp. 2402-2411.

the other side. They did the analysis for parallel plates and cylindrical channel configurations in an attempt to find the channel configurations that minimised the non-uniform temperature distribution of a vascularised solid body. The work in this section focuses on the mathematical optimisation of laminar-forced convection heat transfer through a vascularised solid with square channels. It examines the optimisation of a fixed and finite global volume of solid material with an array of square cooling channels. A uniform heat flux applied from one side and the cooling fluid was forced through the channels from the opposite direction with a specified pressure difference. The structure had three degrees of freedom as design variables: the elemental volume, the channel's hydraulic diameter and channel-to-channel spacing. The objective was to build a smaller construct to form part of a larger construct body with a self-cooling function, which would lead to the minimisation of the global thermal resistance or, inversely, the maximisation of the heat transfer rate density (the total heat transfer rate per unit volume). This would be achieved by designing the body in a vascularised manner and by forcing a coolant to the heated spot in a fast and efficient way so as to significantly reduce the peak temperature at any point inside the volume that needs cooling.

We started the optimisation process by carrying out numerical solutions under a fixed global volume of solid material, but the elemental volume was allowed to morph. A gradient-based optimisation algorithm (DYNAMIC-Q) (see Chapter 4), coupled with the numerical CFD and mesh generation packages, was used to determine the optimal

geometry that gave the lowest thermal resistance. This optimiser adequately handled the numerical objective function obtained from numerical simulations of the fluid flow and heat transfer.

We later developed an analytical solution based on the application of the intersection of asymptotes method and scale analysis to prove the existence of an optimal geometry that would minimise the peak temperature and global thermal resistance of this vascularised material.

The numerical results obtained were in agreement with a theoretical formulation for this vascularised solution using scale analysis and the intersection of asymptotes method. The effect of material properties on the minimum thermal resistance and optimised internal configuration was also studied.

7.2. COMPUTATIONAL MODEL

The schematic diagram of the physical configuration is shown in Figure 7.1. The system consists of a solid body of fixed global volume *V*, which is heated with uniform heat flux q'' on the left side. The body is cooled by forcing a single-phase cooling fluid (water) from the right side through the parallel cooling channels.

The flow is driven along the length L of the square channel ($w_c = h_c$) with a fixed pressure difference ΔP in a transverse and counter-direction to the heat flux. An elemental volume (see Figure 7.2) consisting of a cooling channel and the surrounding solid was used for analysis because it was assume that heat distribution would occur symmetrically on the left side of the structure. The heat transfer in the elemental volume is a conjugate problem, which combines heat conduction in the solid and the convection in the working fluid.

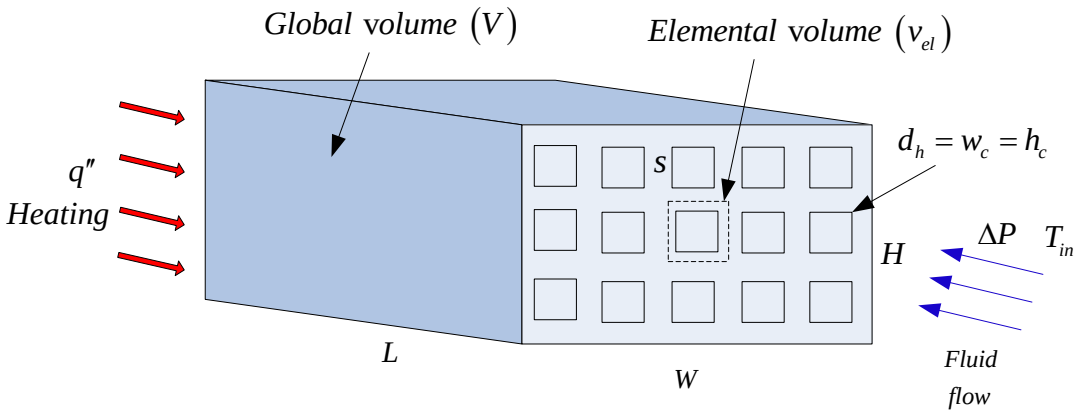

Figure 7. 1 : Three-dimensional parallel square channels across a slab with heat flux from one side and forced flow from the opposite side

7.2.1. Numerical procedure

Figure 7.2 shows that an elemental volume v_{el} constraint is considered to be composed of an elemental cooling channel of hydraulic diameter d_h ($d_h = w_c = h_c$). The surrounding solid of thickness s (the spacing between channels) is defined as

$$w = h \tag{7.1}$$

The elemental volume is

$$v_{el} = w^2 L \tag{7.2}$$

and the width of an elemental volume is

$$w = d_h + s \tag{7.3}$$

Therefore, the number of channels in the structure arrangement can be defined as:

$$N = \frac{HW}{(d_h + s)^2} \tag{7.4}$$

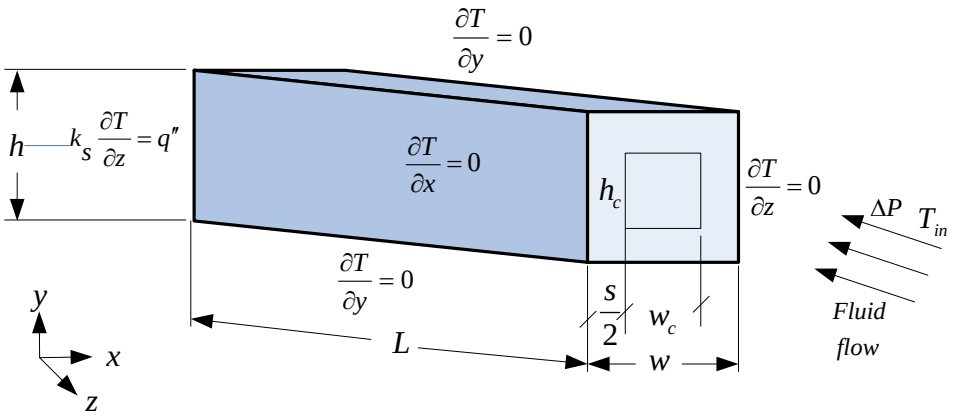

Figure 7. 2 : The boundary conditions of the three-dimensional computational domain of the elemental volume

and the void fraction or porosity of the unit structure can be defined as

$$\phi = \frac{v_c}{v_{el}} = \left(\frac{d_h}{w}\right)^2 \tag{7.5}$$

The fundamental problem under consideration is the numerical optimisation of the channel hydraulic diameter, d_h, and the channel spacing, s, which corresponds to the minimum resistance of a fixed volume for a specified pressure drop. The optimisation is evaluated from the analysis of the extreme limits of $0 \le d_h \le \infty$ and the extreme limits of $0 \le s \le \infty$. The optimal values of the design variables within the prescribed interval of the extreme limits exhibit the minimum thermal resistance.

The temperature distribution in the elemental volume was determined by solving the equation for the conservation of mass and momentum Equations (Equations (3.1) to (3.7) of Chapter 3) numerically. A section of the discretised three-dimensional computational domain of the elemental volume is shown in Figure 7.3. The cooling fluid was water, which was forced through the cooling channels by a specified pressure difference ΔP across the axial length of the structure. The working fluid is water and is assumed to be in single phase, steady and Newtonian with constant properties.

The energy equation for the solid part of the elemental volume can be written as

$$k_s \nabla^2 T = 0 \tag{7.6}$$

The continuity of the heat flux at the interface between the solid and the liquid is given as:

$$k_s \left.\frac{\partial T}{\partial n}\right|_w = k_f \left.\frac{\partial T}{\partial n}\right|_w \tag{7.7}$$

A no-slip boundary condition is specified for the fluid at the wall of the channel,

$$\vec{u} = 0 \tag{7.8}$$

At the inlet ($z = L$),

$$u_x = u_y = 0 \tag{7.9}$$

$$T = T_{in} \tag{7.10}$$

$$P = \frac{Be\alpha\mu}{L^2} + P_{out} \tag{7.11}$$

where, the Bejan number [182, 183], *Be*, is the dimensionless pressure difference and given as:

$$Be = \frac{\Delta P L^2}{\mu\alpha_f} \tag{7.12}$$

and

$$\alpha_f = \frac{k_f}{\rho_f C_{Pf}} \tag{7.13}$$

At the outlet (z = 0), the pressure is prescribed as zero normal stress

$$P_{out} = 1\ atm \tag{7.14}$$

At the left side of the wall, the thermal boundary condition that is imposed is assumed to be:

$$q'' = k_s \frac{\partial T}{\partial z} \tag{7.15}$$

while at the solid boundaries, the remaining outside walls and the plane of symmetry are modelled as adiabatic as shown in Figure 7.2

$$\nabla T = 0 \tag{7.16}$$

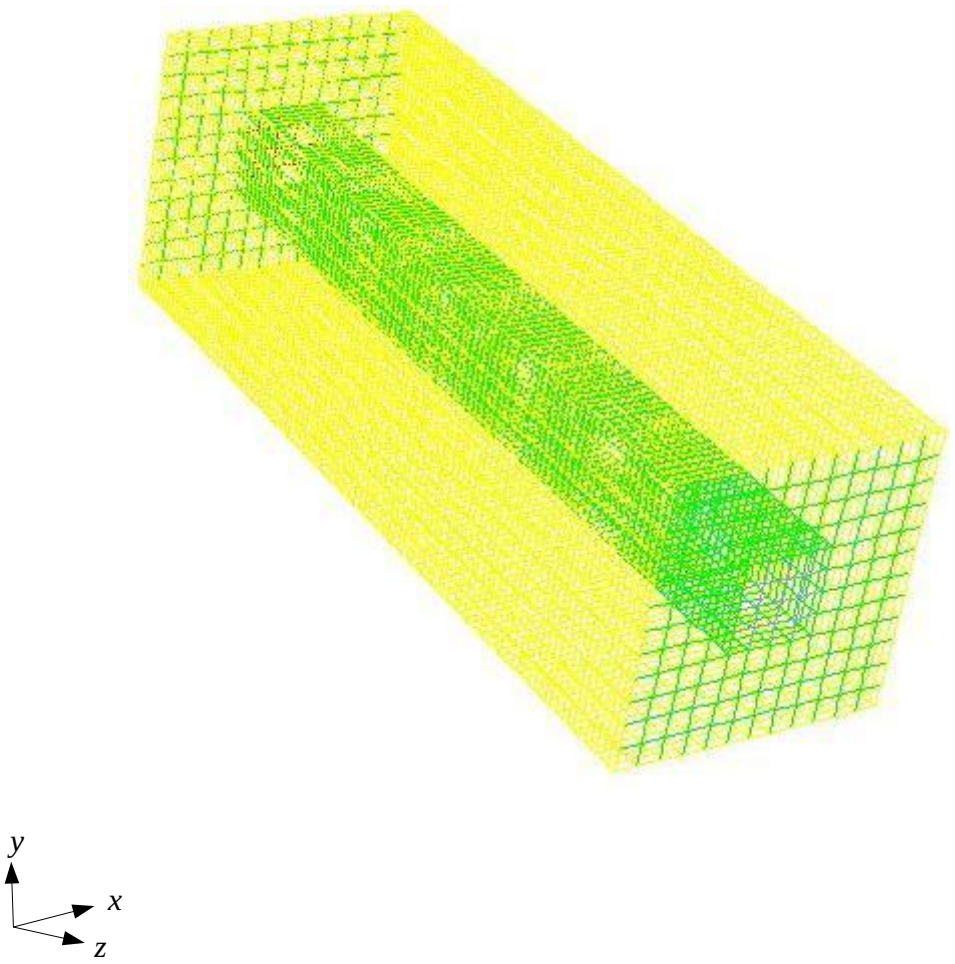

Figure 7. 3 : A section of the discretised 3-D computational domain of the elemental solid-fluid volume considered for the simulation

The measure of performance is the minimum global thermal resistance, which could be expressed in a dimensionless form as:

$$R_{\min} = \frac{k_f \left(T_{\max} - T_{in}\right)_{\min}}{q'' L} \tag{7.17}$$

and it is a function of the optimised design variables and the peak temperature.

$$R_{\min} = f\left(d_{h_{opt}},\, v_{el_{opt}},\, T_{\max_{\min}}\right) \tag{7.18}$$

$R_{\min}$ is the minimised thermal resistance for the optimised design variables. The inverse of $R_{\min}$ is the optimised overall global thermal conductance.

The effect of material properties is later taken into consideration by the ratio of the thermal conductivities

$$k_r = \frac{k_s}{k_f} \tag{7.19}$$

7.3. NUMERICAL PROCEDURE

The simulation work began by fixing the length of the channel, prescribed pressure difference, porosity, heat flux and material properties. We used varying values of the hydraulic diameter of the channel to identify the best (optimal) internal configuration that minimised the peak temperature. The numerical solution of the continuity, momentum and energy equations (Equations (3.1) to (3.7)) along with the boundary conditions (Equations (7.6) to (7.15)) was obtained by using a three-dimensional commercial package Fluent™ [199] which employs a finite volume method. The

details of the method are m explained by Patankar [203]. Fluent™ [199], was coupled with the geometry and mesh generation package Gambit [201] using MATLAB [219] to allow the automation and running of the simulation process. After the simulation had converged, an output file was obtained containing all the necessary simulation data and results for the post-processing and analysis. The computational domain was discretised using hexahedral/wedge elements. A second-order upwind scheme was used to discretise the combined convection and diffusion terms in the momentum and energy equations. The SIMPLE algorithm was subsequently employed to solve the coupled pressure-velocity fields of the transport equations. The solution is assumed to have converged when the normalised residuals of the mass and momentum equations fall below 10^{-6} while the residual convergence of energy equation was set to less than 10^{-10}. The number of grid cells used for the simulations varied for different elemental volume and porosities. However, grid independence tests for several mesh refinements were carried out to ensure the accuracy of the numerical results. The convergence criterion for the overall thermal resistance as the quantity monitored was

$$\gamma = \frac{\left|\left(T_{\max}\right)_i - \left(T_{\max}\right)_{i-1}\right|}{\left|\left(T_{\max}\right)_i\right|} \leq 0.001 \tag{7.20}$$

where i is the mesh iteration index. The mesh was more refined as i increased. The $i-1$ mesh was selected as a converged mesh when the criterion (7.20) was satisfied.

7.4. GRID ANALYSIS AND CODE VALIDATION

To ensure accurate results, several grid independence test were conducted until a mesh size with negligible changes in peak temperature was obtained.

Table 7.1 shows the grid independence test performed for the case where d_h = 400 µm and $\phi = 0.2$ for Be = 10^8. Computational cell densities of 3 675, 5952, 11 200 and 20 160 were used for the grid independence test. Almost identical results were predicted when 5 952 and 11 200 cells were used. Therefore, a further increase in the cell density beyond 11 200 would have a negligible effect on the results.

Table 7. 1: **Grid independence study with** $d_h = 400\mu$m **and** $\phi = 0.2$ **for** $Be = 10^8$

Number of nodes	Number of cells	$T_{\max}$	$\gamma = \dfrac{\left\|(T_{\max})_i - (T_{\max})_{i-1}\right\|}{\left\|(T_{\max})_i\right\|}$
5 456	3 675	33.09371	-
8 718	5 952	32.79123	0.009194
15 005	11 200	32.772	0.000587
26 609	20 160	32.67453	0.002983

The validation of the numerical simulation was carried out by comparing the present simulation with that of Kim *et al* [128] for a cylindrical configuration as shown in Figure 7.4 for the case where $\phi = 0.1$ and k_r = 10. The curves were found to be similar in trend and the solutions were in good agreement with a deviation of less than 7%.

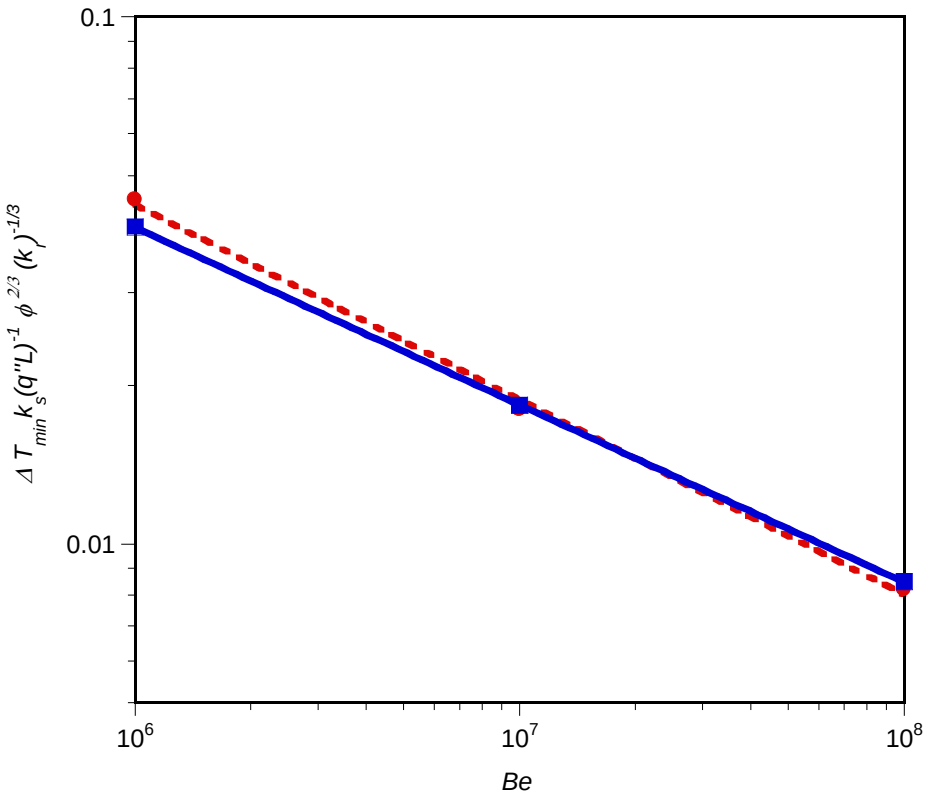

Figure 7. 4 : Comparison of the results of the present numerical study with those of Kim *et al.* [128] for $\phi = 0.1$ and $k_r = 10$

7.5. NUMERICAL RESULTS

In this section, we present results for the case when the channel hydraulic diameter (or channel width/height) was in the range of 0.1 mm to 1.5 mm and the porosities ranged between $0.1 \leq \phi \leq 0.3$, while a fixed length of L = 10 mm and fixed applied dimensionless pressure differences of $Be = 10^8$. The thermal conductivity of the solid structure (stainless steel) was 16.27 W/m.K; and the heat flux supplied at the left wall was 100 kW/m^2. The thermo-physical properties of water [202] used in this study

were based on water at 300 K and the inlet water temperature was fixed at this temperature.

Figures 7.5 and 7.6 show the existence of an optimum hydraulic diameter and elemental volume size in which the peak temperature is minimised at any point in the channel for the square configuration studied. According to Figure 7.5 the peak temperature is a function of the channel hydraulic diameter. It shows that there exists an optimal channel hydraulic diameter, which lies in the range $0.01 \leq d_h/L \leq 0.05$ minimising the peak temperature. Also, the elemental volume of the structure has a strong effect on the peak temperature as shown in Figure 7.6. The minimum peak temperature is achieved when the optimal elemental volume is in the range $0.05\ \text{mm}^3 \leq v_{el} \leq 8\ \text{mm}^3$. This indicates that the global peak temperature decreases as the design variables (hydraulic diameter and elemental volume) increase, or the global peak temperature decreases as the design variables decrease until it gets to the optimal design values. Therefore, any increase or decrease in the design variable beyond the optimal values indicates that the working fluid is not properly engaged in the cooling process, which is detrimental to the global performance of the system. The results show that the optimal arrangement of the elemental volume for the entire structure at this fixed pressure difference should be very small in order to achieve a better cooling. Figures 7.5 and 7.6 also show that porosity has a significant effect on the peak temperature. The best cooling occurs at the highest porosity. Thus, as the porosity increases, the peak temperature decreases.

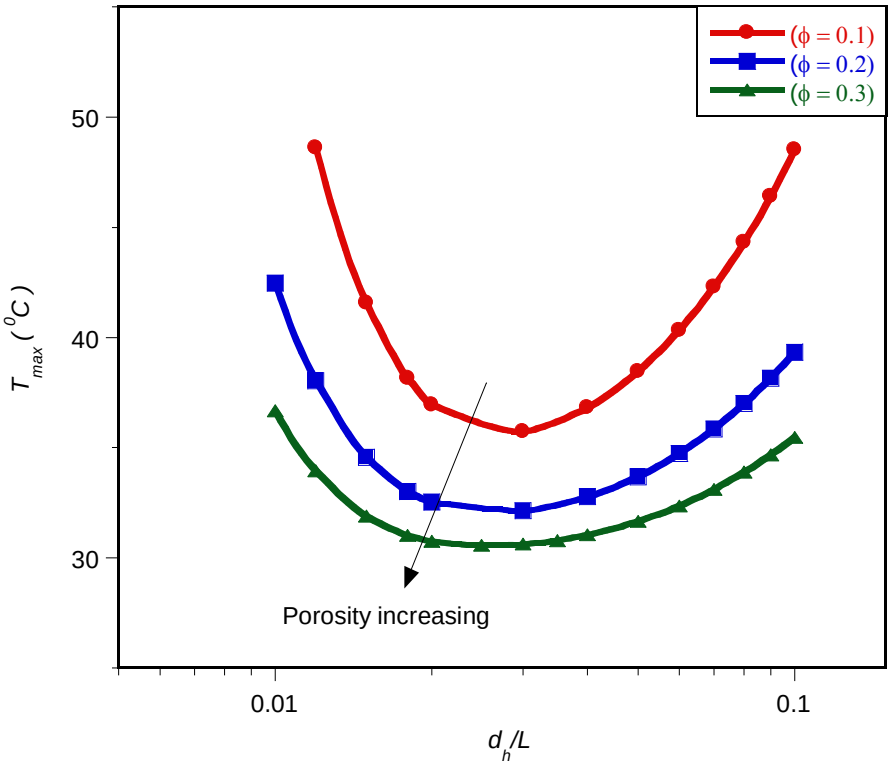

Figure 7. 5 : Effect of the optimised dimensionless hydraulic diameter d_h on the peak temperature at *Be* = 10^8

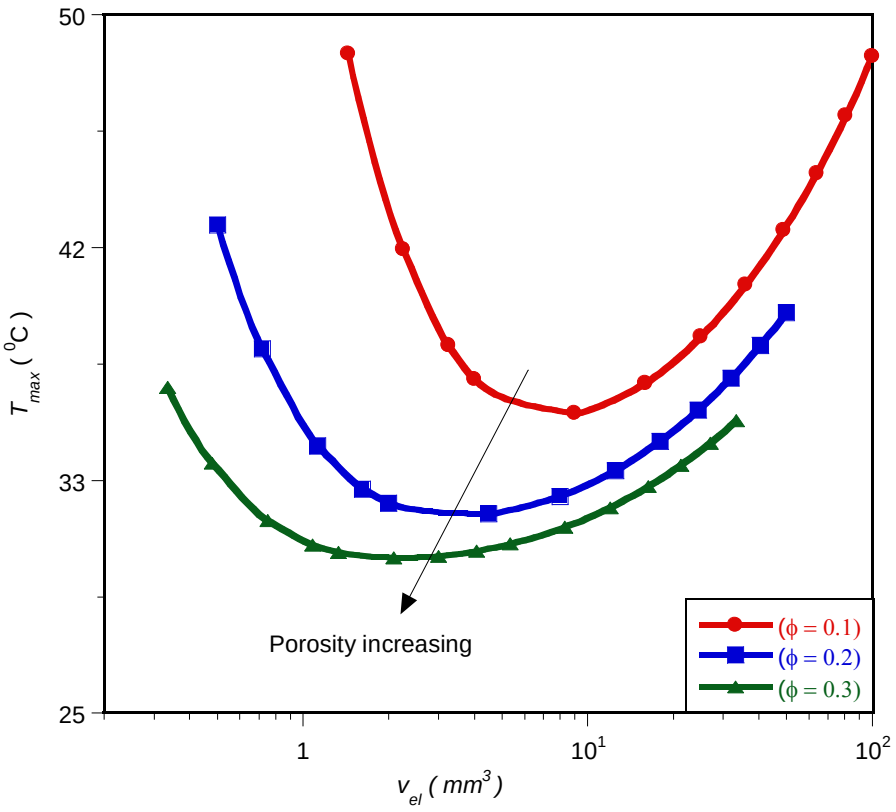

Figure 7. 6 : Effect of the optimised elemental volume on the peak temperature at Be = 10^8

7.6. MATHEMATICAL FORMULATION OF THE OPTIMISATION PROBLEM

In this section, we introduce an optimisation algorithm that will search and identify the design variables at which the system will perform at an optimum. A numerical algorithm, Dynamic-Q [208], was employed and incorporated into the finite volume solver and grid (geometry and mesh) generation package by using MATLAB code for greater efficiency and better accuracy in determining the optimal performance.

7.6.1. Optimisation problem and design variable constraints

The optimisation technique described above was applied to the models described in Section 7.2. The constraint ranges for the optimisation are:

$$0.1 \leq \phi \leq 0.3 \tag{7.21}$$

$$0 \leq w \leq L \tag{7.22}$$

$$0 \leq d_h \leq w \tag{7.23}$$

$$0 \leq s \leq w \tag{7.24}$$

The design and optimisation technique involves the search for and identification of the best channel layout that minimises the peak temperature, $T_{\max}$, so that the minimum thermal resistance between the fixed volume and the cooling fluid is obtained as the desired objectives function. The hydraulic diameter, channel spacing and elemental volume of the square configuration were considered as design variables. A number of numerical optimisations and calculations were carried out within the design constraint ranges given in Equations (7.21) to (7.24). The results are presented in the next section to show the optimal behaviour of the entire system. The optimisation process was repeated for applied dimensionless pressure differences *Be* from 10^5 to 10^9.

7.6.2. Mathematical statement of the optimisation problem

The variables chosen for the mathematical statement are

$$x_1 = d_h \tag{7.25}$$

$$x_2 = w \tag{7.26}$$

Substituting Equations (7.25) to (7.26) for Equations (7.21) to (7.24) results in the objective and constraints functions given in Equations (7.27) to (7.29). The inequality functions g_1(x) and g_2(x) are derived from the porosity constraint of Equation (6.5). The mathematical statement of the optimisation problem is then written as:

$$f(x) = T_{\max} \tag{7.27}$$

$$g_1(x) = 0.1x_2^{\,2} - x_1^{\,2} \le 0 \tag{7.28}$$

$$g_2(x) = x_1^{\,2} - 0.2x_2^{\,2} \le 0 \tag{7.29}$$

7.6.3. Parameterisation of geometry and automation of the optimisation process

Since a large number of CFD simulations were performed, the geometry and mesh generation are parameterised in similar way as those described in Chapter 6. This allowed GAMBIT [201] scripts to be automatically generated. The optimisation problem was done automatically by coupling together the computational fluid dynamics package- FLUENT[199] and the geometry and mesh generation package GAMBIT [201] with the mathematical optimisation algorithm by using MATLAB [219] to allow the automation, mesh generation and running of the simulation process.

The values in the parametric GAMBIT file were changed through MATLAB code, and then the procedure was re-run to generate a new set of geometric modelling and mesh generations for post-processing. This cycle continued until convergence occurred with the step size and function value convergence tolerances set at 10^{-4} and 10^{-8} respectively. Figure 6.10 provides a flow chart of the automated optimisation process. The peak temperature was found and equated to the objective function.

Appendix B.6 shows the parametric GAMBIT file for geometry of the vascularised square cooling channels of Figure 7.1. Appendices A and C show the optimisation algorithm file and the FLUENT journal file respectively for the running of the simulation.

7.6.4. Sensitivity analysis of the selection of forward differencing step size

As discussed in Chapter 4. 6, the fact that noise exists in any simulation made it essentially to carefully choose a step size Δx to be used in the differencing scheme. This step size had to totally minimise the noise and gives an accurate representation of the global gradient of the function. A sensitivity analysis was performed by selecting different values of the step size of design variables that gave a smooth objective function and could later be used as candidate step size. This candidate step size was then verified by running the optimisation program with various starting guesses and

checking for any discrepancies in the final solution. Figure 7.7 shows a graph of peak temperature as a function of cooling channel width with step sizes of 10^{-6} and 10^{-4}. Although, different values of the step size of cooling channel width as design variable considered are 10^{-6}, 10^{-5}, 10^{-4} and 10^{-3}

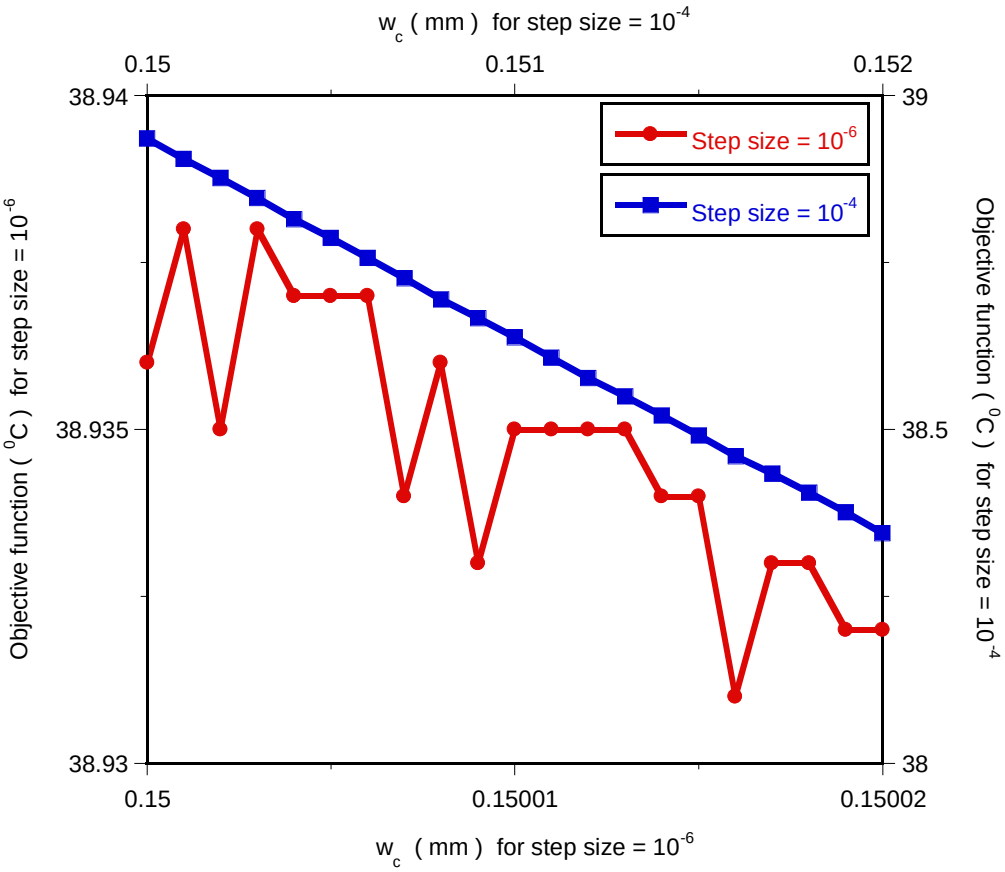

Figure 7. 7 : Plotting peak temperatures for different channel width values with step sizes of 10^{-6} and 10^{-4}

A step size of 10^{-4} gave a smooth continuous function of maximum peak temperature and it indeed proved to be an ideal forward differencing scheme step size for other design variables.

Figure 7.8 shows a graph of peak temperature as a function of channel spacing with the chosen candidate step size of 10^{-4}.

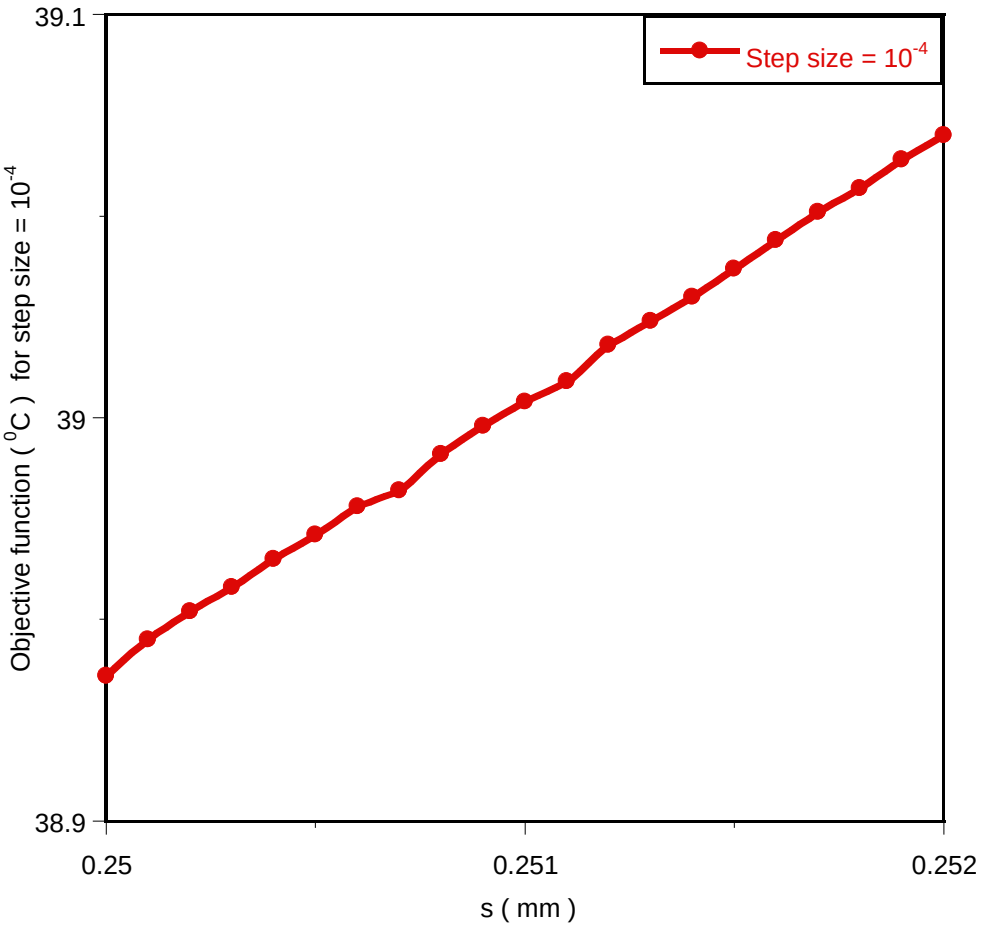

Figure 7. 8 : Plotting peak temperatures for different channels-spacing values with a step size of 10^{-4}

7.7. OPTIMISATION RESULTS

7.7.1. Effect of pressure difference on optimised geometry and minimised thermal resistance

Figure 7.9 shows the effect of the minimised thermal resistance as a function of applied dimensionless pressure difference. Minimised thermal resistance decreases as the applied dimensionless pressure difference and porosity increase. Figure 7.10 shows that the optimal hydraulic diameter decreases as the pressure differences increase and there exists a unique optimal geometry for each of the applied pressure differences. The trend is in agreement with previous work [94].

7.7.2. Effect of material properties on optimised geometry and minimised thermal resistance

The effect of material properties on the minimum thermal resistance and optimised internal configuration was also studied. This was best investigated by numerically simulating conjugate heat transfer in an elemental volume for different values of thermal conductivity ratio. The numerical simulations follow the same procedure that was discussed earlier to show the existence of an optimal geometry.

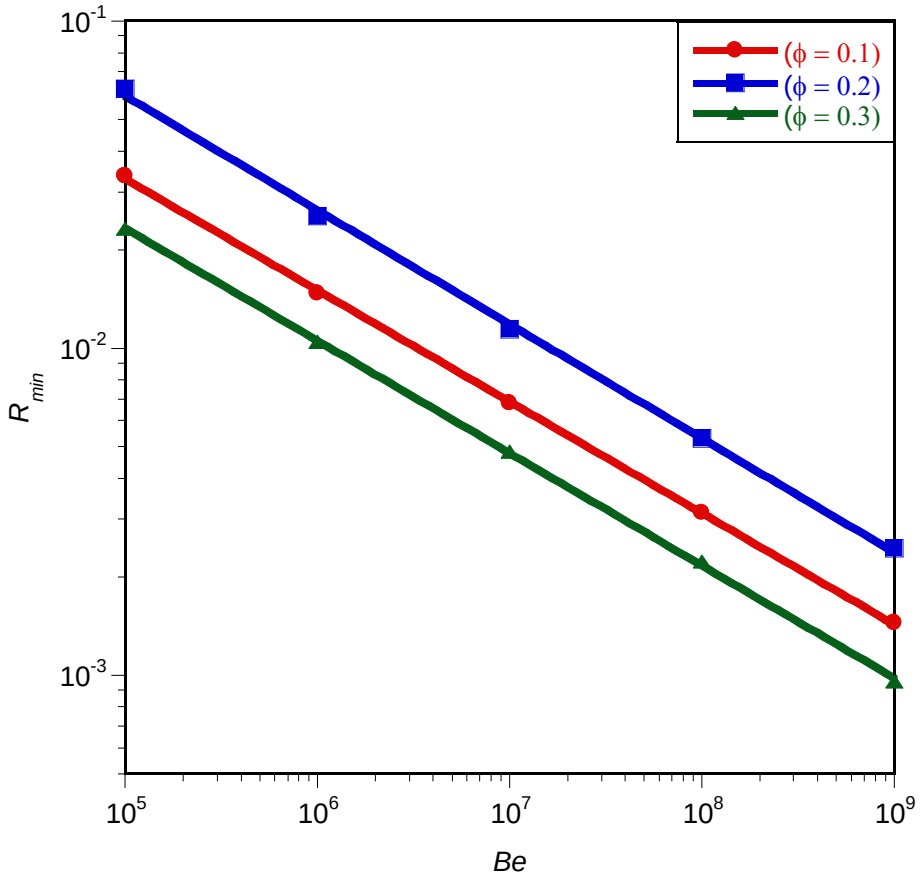

Figure 7. 9 : Effect of dimensionless pressure difference on the dimensionless global thermal resistance

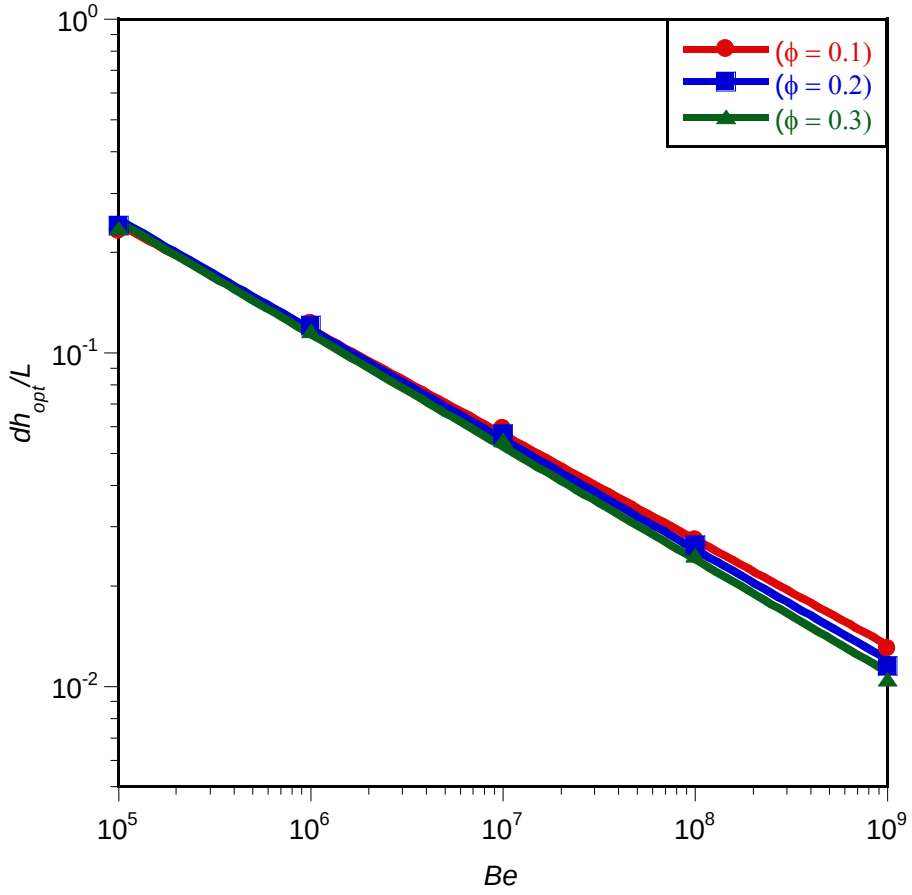

Figure 7. 10 : Effect of dimensionless pressure difference on the optimised hydraulic diameter

We started the simulation by fixing $\phi = 0.2$, $Be = 10^8$ and $k_r = 10$ as well as and $k_r = 100$. We then varied the hydraulic diameter and the elemental volume until we got the minimum peak temperature. Figure 7.11 shows that an optimal geometry exists at different thermal conductivity ratios and that minimum peak temperatures are achieved when k_r is high.

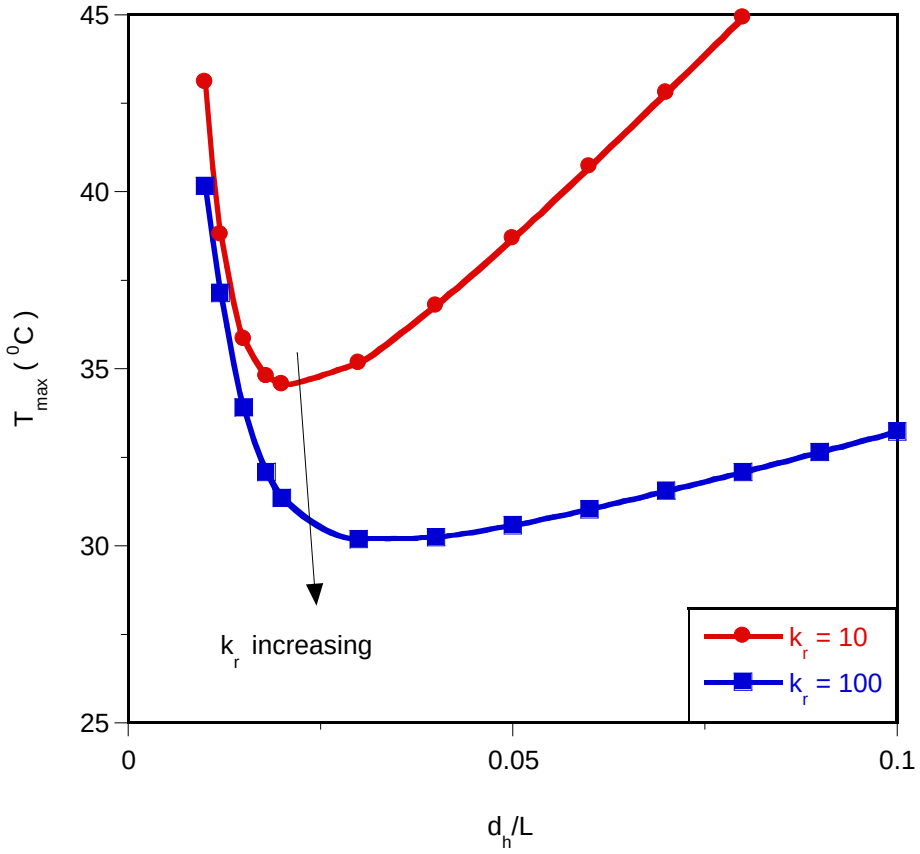

Figure 7. 11 : Effect of a thermal conductivity ratio, k_r , on the peak temperature at a Bejan number of 10^8 and porosity of 0.2

We later performed an optimisation process to determine the best geometry that would render the lowest thermal resistance temperature by using the optimisation algorithm. We fixed $\phi = 0.2$ and $Be = 10^8$ for all the design constraint ranges and for different values of thermal conductivity ratios ranging from $k_r = 1$ to $k_r = 10^4$. Figures 7.12 and 7.13 show the effect of the thermal conductivity ratio on the minimised global thermal resistance and the optimised hydraulic diameter at fixed $\phi = 0.2$ and $Be = 10^8$. The minimised thermal resistance decreases as the thermal conductivity ratio

increases. This shows that material properties have a strong effect on the thermal resistance. Materials with a high thermal conductivity property reduce the thermal resistance. Figure 7.13 shows that the thermal conductivity ratio has a significant influence on the optimised hydraulic diameter. As the thermal conductivity ratio increases, the optimal hydraulic diameter increases. However, at higher thermal conductivity ratios (say $k_r \geq 4\ 000$), the thermal conductivity has a negligible effect on the minimised thermal resistance and optimised hydraulic diameter.

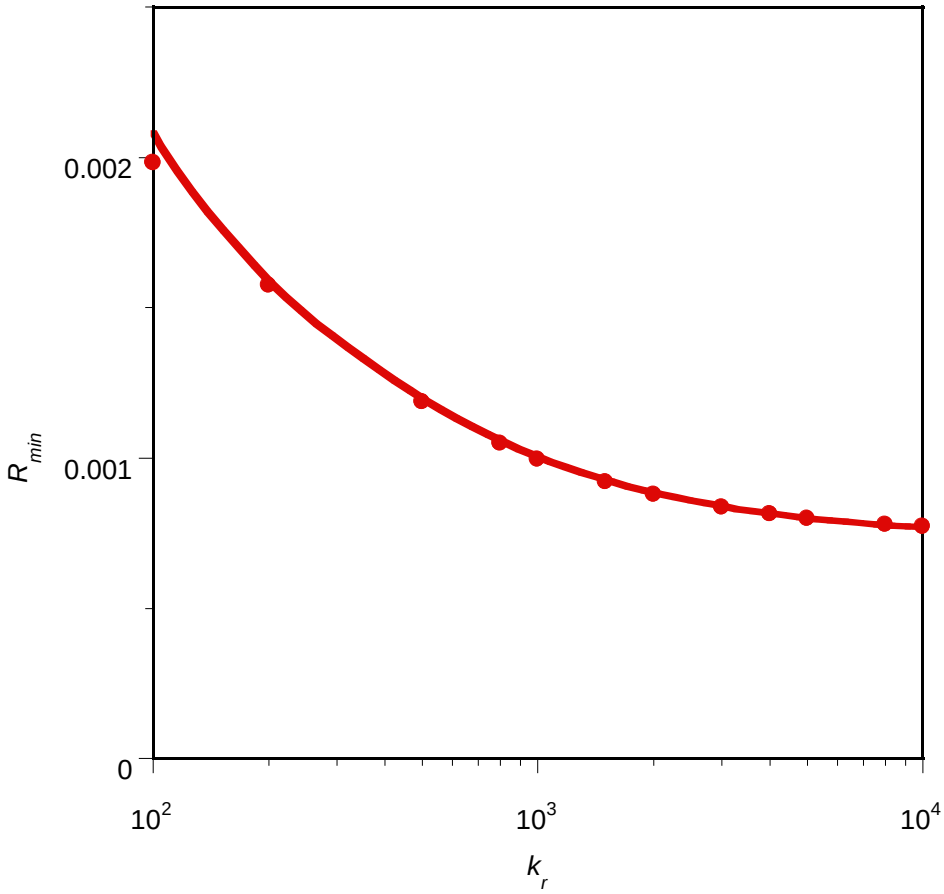

Figure 7. 12 : Effect of a thermal conductivity ratio, k_r on the minimised dimensionless global thermal resistance at Be = 10^8 and porosity of 0.2

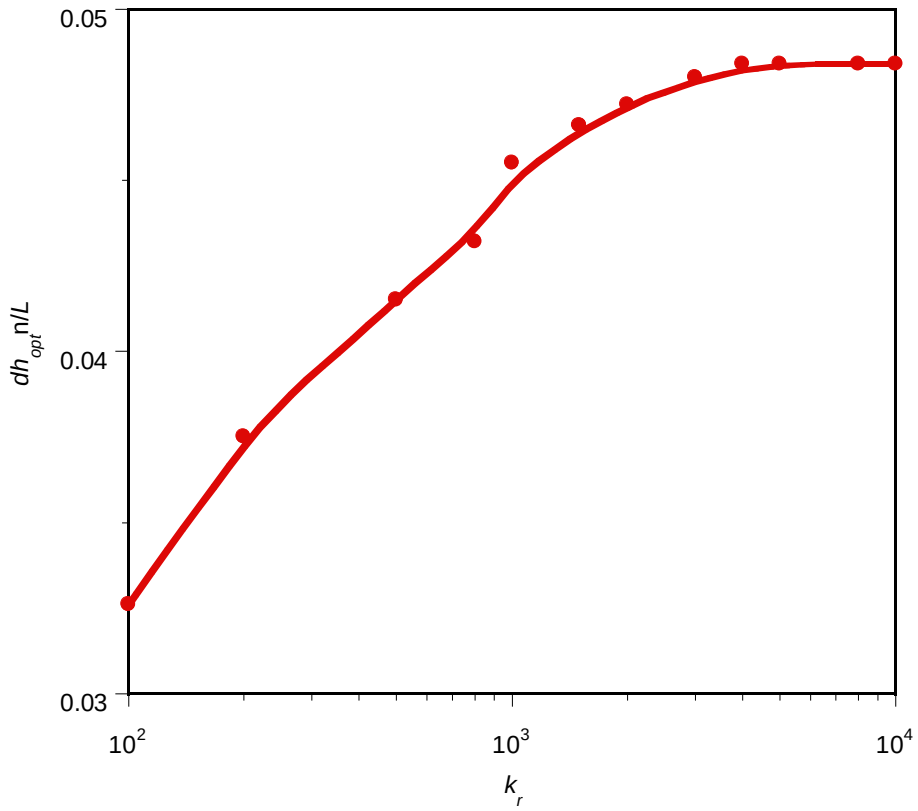

Figure 7. 13 : Effect of thermal conductivity ratio k_r on the optimised hydraudric diameter at Be = 10^8 and porosity of 0.2

For applied dimensionless pressure differences ranging from Be = 10^5 to 10^9 and ϕ = 0.1 to 0.2 we repeated the optimisation process for all the design constraint ranges from k_r = 1 to 100 so as to determine the global behaviour of the whole system. Figures 7.14 to 7.16 show the effect of the applied dimensionless pressure difference on the minimum thermal resistance and the internal geometry for different values of thermal conductivity ratio and porosity. Figure 7.14 shows that the minimised thermal resistance decreases as the applied dimensionless pressure difference, thermal conductivity ratio and porosity increase. Also, Figures 7.15 and 7.16 show that there

are unique design variables for each applied dimensionless pressure difference, thermal conductivity ratio and porosity.

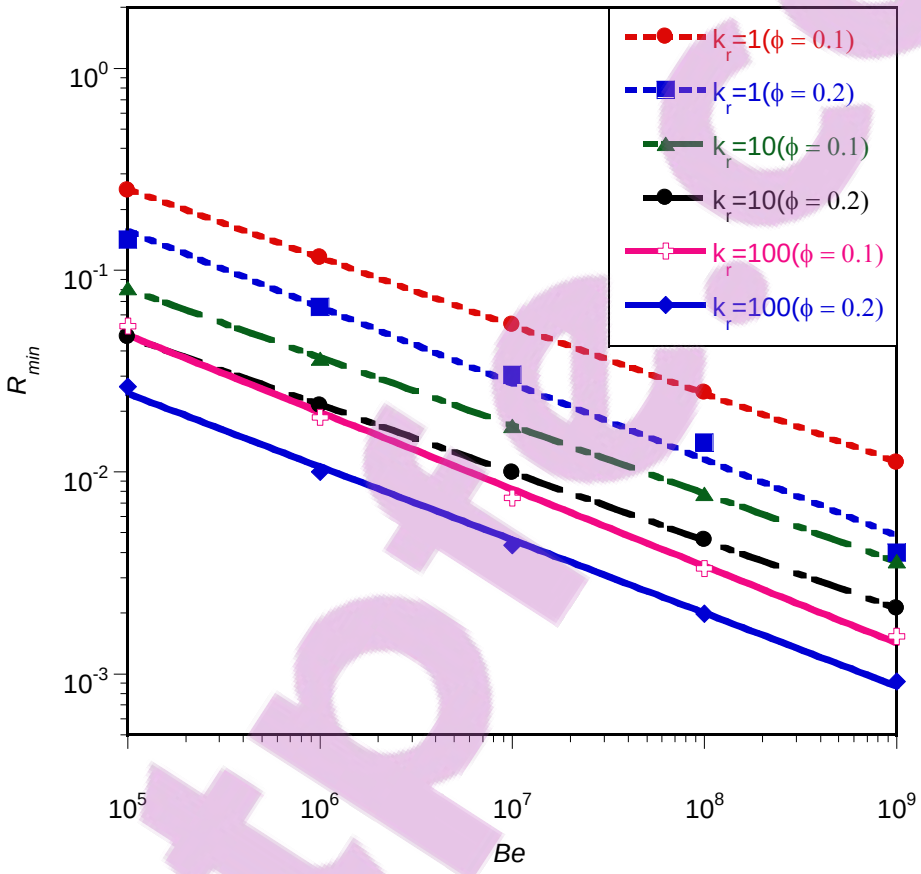

Figure 7. 14 : Effect of thermal conductivity ratio k_r , porosity, and dimensionless pressure difference on the minimised dimensionless global thermal resistance

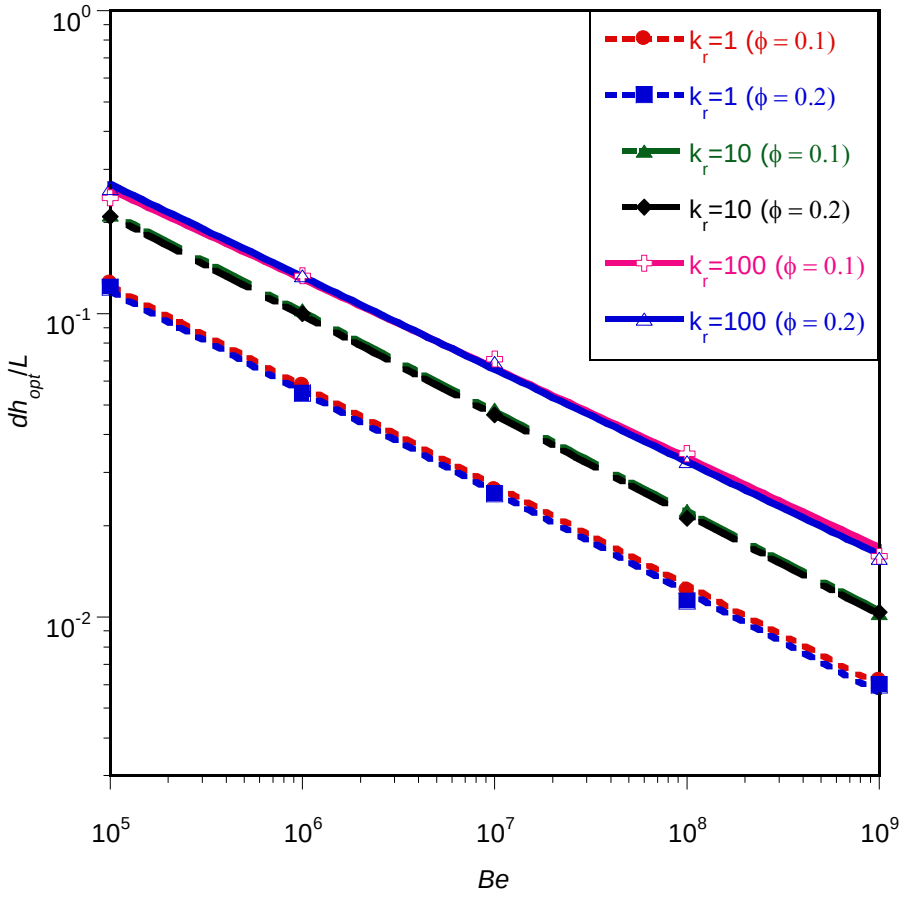

Figure 7. 15 : Effect of thermal conductivity ratio k_r, porosity, and dimensionless pressure difference on the optimised hydraulic diameter

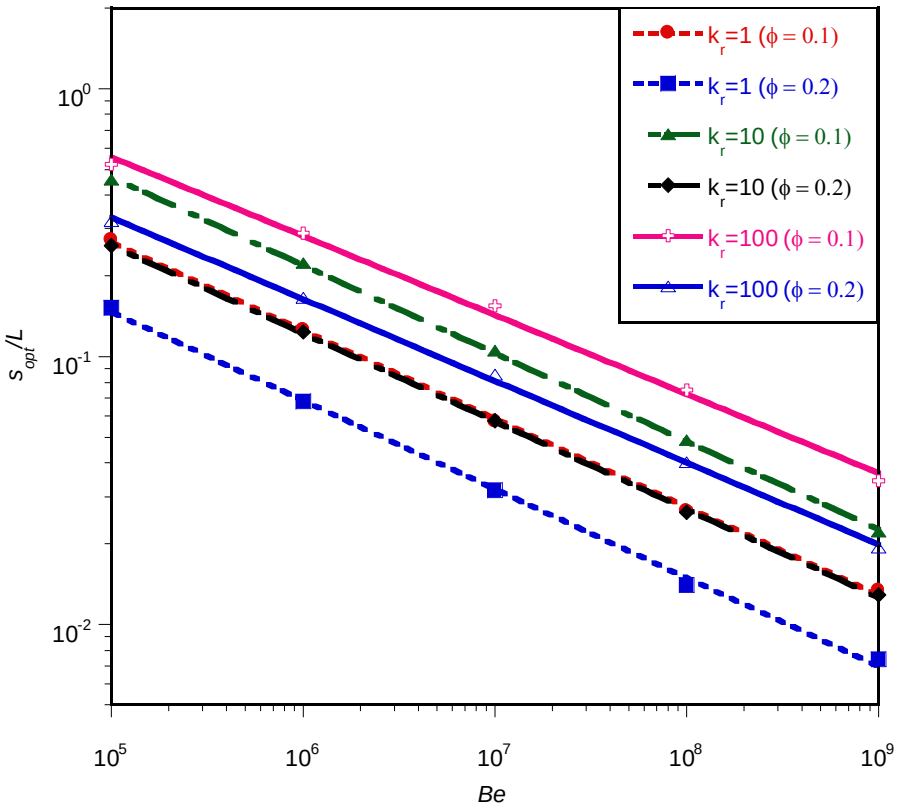

Figure 7.16 : Effect of thermal conductivity ratio k_r, porosity, and dimensionless pressure difference on the optimised channel-spacing

Figures 7.17(a) and 7.17(b) show the temperature contours of the elemental volume and of the inner wall of the cooling channel with cooling fluid, respectively. The blue region indicates the region of low temperature and the red region indicates that of high temperature. The arrow indicates the direction of flow.

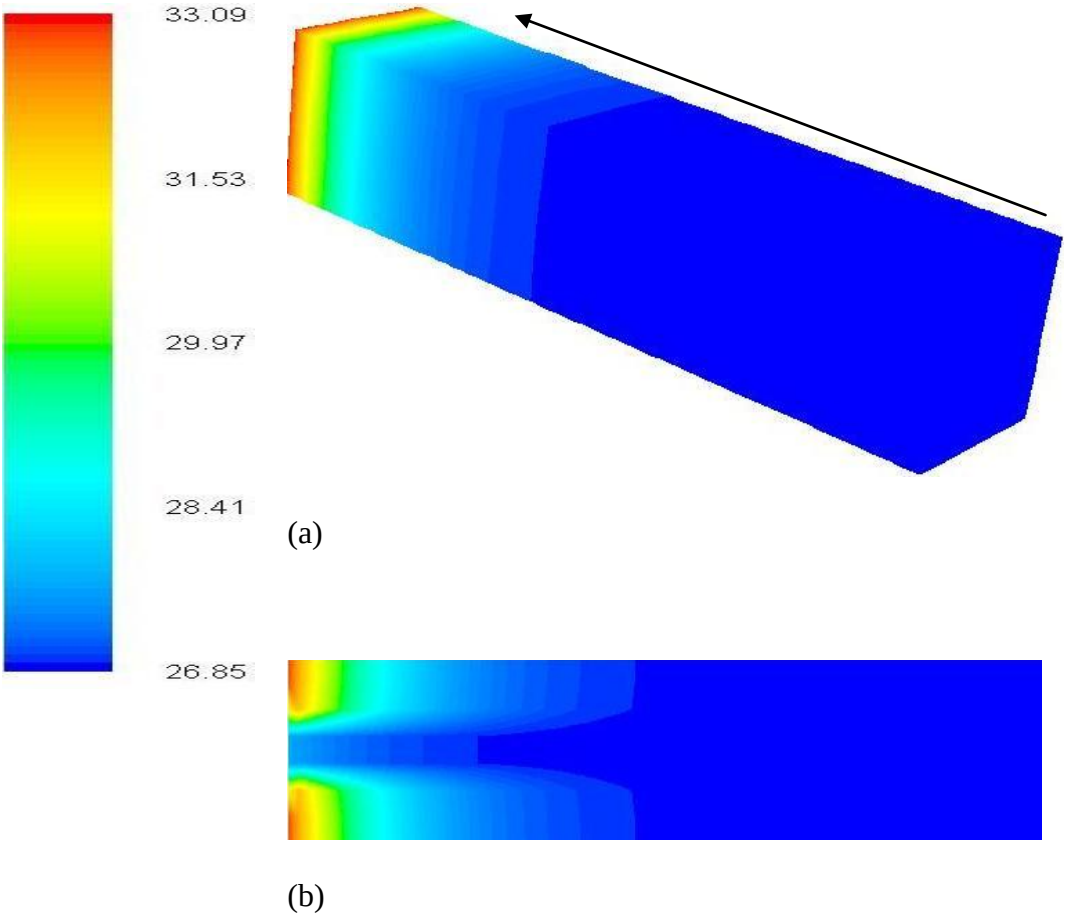

Figure 7. 17: Temperature distributions on (a) the elemental volume and (b) the cooling fluid and the inner wall

7.8. METHOD OF INTERSECTION OF ASYMPTOTES

This section investigated further the numerical solution of the optimisation of flow and heat transfer with the analytical solution. The theoretical analysis for the vascularised configurations followed the application of the intersection of asymptotes method and scale analysis [94, 130, and 218] to prove the existence of an optimal geometry that minimised the peak temperature and global thermal resistance. The

method of intersection of asymptotes outlined by Kim *et al.* [130] was used to determine the optimal geometric shape. The objective was to provide the relationship between the global objective function in terms of global thermal resistance, *R*, and the varying hydraulic diameter d_h in the two extremes at $d_h \to 0$ and $d_h \to \infty$. The optimal geometry value $d_{h_{opt}}$ that corresponds to, $R_{\min}$, is located approximately where the two asymptotes intercept.

The following assumptions were made throughout the analysis: inlet temperature and the pressure difference, ΔP, driving the pump are fixed with a uniform flow distribution in all the channels, laminar flow, constant cross-sectional area of the channels, negligible inlet and exit plenum losses and negligible axial conduction. An elemental volume is treated because of the symmetry of the heat distribution.

7.8.1. Extreme limit 1: small channel

Figure 7.18 shows the extreme limit when the channels characteristic dimension is very small and very slender, that is $d_h \to 0$. and $d_h \square L$, the length layer is treated as a fluid saturated porous medium with Darcy flow. The flow is fully developed along the length, L. In this extreme limit, the fluid in the channel quickly becomes fully developed flow and the working fluid is overworked.

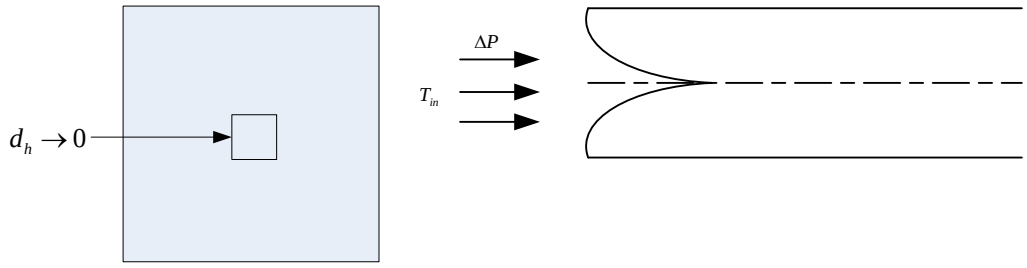

Figure 7. 18 : The extreme limit of the channel's characteristic dimension is very small and very slender, that is $d_h \to 0$ and $d_h \square L$,

The average velocity $\bar{u}$ in a uniform volume points in the z direction given as:

$$\bar{u} = \frac{K}{\mu}\frac{\Delta P}{L} \tag{7.30}$$

where, K is the permeability that is associated with Poiseuille flow through d_h – thin fissures is define [218] as

$$K = \frac{d_h{}^2}{g} \tag{7.31}$$

where g is the porosity function defined [130, 218] as

$$g = \frac{32}{\phi} \tag{7.32}$$

The temperature distribution across the length of the body is obtained by the energy equation

$$\frac{dT}{dz} = -\frac{\alpha}{u}\frac{\partial^2 T}{\partial z^2} \tag{7.33}$$

This is subject to the flowing boundary conditions

$$q'' = -k_{eff}\frac{dT}{dz} \qquad \text{at z} = 0 \tag{7.34}$$

$$T \to T_{\text{in}} \quad \text{as} \quad \text{z} \to \infty \tag{7.35}$$

Where, α is the thermal diffusivity of the saturated porous medium and is defined as:

$$\alpha = \frac{k_{eff}}{\rho C_P} \tag{7.36}$$

and k_{eff} is the effective thermal conductivity of the saturated porous medium with the filling fluid in its pores. The fluid-filled spaces are parallel to the direction of heat flow, therefore k_{eff} is defined as:

$$k_{eff} = \phi k_f + (1-\phi)k_s \tag{7.37}$$

The temperature distribution across the length of the body is obtained solving differential Equation (7.33) with the boundary conditions of Equations (7.34) – (7.35). The solution is

$$T - T_{in} = \frac{\alpha}{uk_{eff}} q'' e^{-ux/\alpha} \tag{7.38}$$

Equation (7.38) shows the effect of the propagation of heat flux q'' in the porous structure to the depth of z of the order α/u. That is the boundary condition (7.35) holds when the penetration dept is smaller than the length of the structure. That is

$$\alpha/u < L \tag{7.39}$$

From Equation (7.38), we find the maximum peak temperature difference $T_{\max} - T_{\text{in}}$, which occur at $z = 0$ surfaces, therefore,

$$T_{\max} - T_{\text{in}} = \frac{\alpha}{uk_{eff}} q'' \tag{7.40}$$

Combining Equations (7.30) to (7.32), as well as Equations (7.36) and (7.40) together, we, have

$$R = \frac{k_f \left(T_{\max} - T_{\text{in}}\right)}{q'' L} \cong \frac{32}{\phi} \left(\frac{d_h}{L} \right)^{-2} Be^{-1} \tag{7.41}$$

where *Be* is the dimensionless pressure number [218] and is defined as:

$$Be = \frac{\Delta P L^2}{\mu \alpha_f} \tag{7.42}$$

and

$$\alpha_f = \frac{k_f}{\rho_f C_{Pf}} \tag{7.43}$$

From Equation (7.41), it can be concluded that in the small diameter extreme, R increases as $d_h \to 0$.

7.8.2. Extreme Limit 2: Large Channel

In this extreme limit, the channels characteristic dimension is sufficiently large in such a way that the working fluid is not properly utilised and working fluid outside the boundary layers becomes useless and the body is not properly cooled in the downstream. (See Figure (7.19)).

The thermal resistance between the heat flux surface and the channel surface is due to conduction in a square chunk of the solid of dimension w/4. All the other assumptions are still maintained.

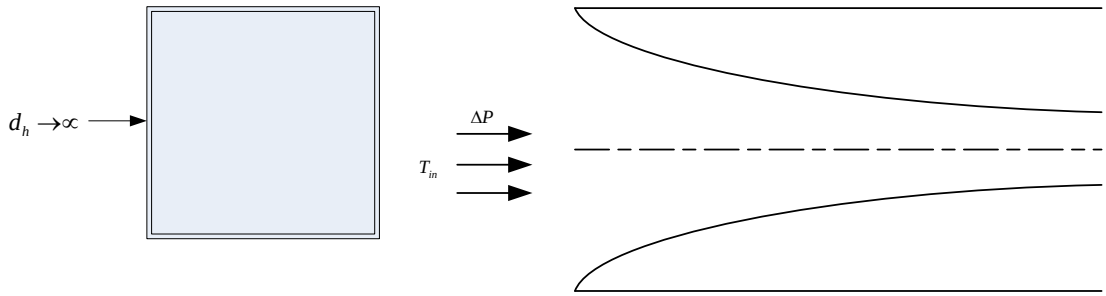

Figure 7. 19 : The extreme limit of the channel's characteristic dimension is sufficiently large, that is $d_h \to \infty$

The energy equation for describing the steady state conduction in the domain is:

$$\nabla T = 0, \tag{7.44}$$

This requires

$$\nabla T / L_z^{\,2} \;\square\; \nabla T / \left(w/4\right)^2, \tag{7.45}$$

or expects that the path of conduction of heat in the *z* direction should be of the same length scale as the path in the *x* or *y* direction.

$$L_z \;\square\; \frac{w}{4}, \tag{7.46}$$

The conservation of heat current through the elemental volume $L_z \times w/2 \times w/2,$

$$q'' \frac{w}{4} \;\square\; k_s \frac{w}{4} \frac{\Delta T_z}{L_z} \;\square\; k_s L_z \frac{\Delta T_x}{w/4}, \tag{7.47}$$

where, $\Delta T = T - T_{\text{in}}$ is temperature difference.

Therefore the overall temperature scale becomes

$$\Delta T \sim \Delta T_z + \Delta T_x + \Delta T_y \sim \frac{q''}{k_s}\left(L_z + \frac{w^2}{16L_z} + \frac{w^2}{16L_z}\right), \tag{7.48}$$

combine Equations (7.46) and (7.48) together to get

$$\left(T_{\max} - T_{\text{in}}\right) \cong 0.75\frac{q''}{k_s}w, \tag{7.49}$$

substitute Equations (7.5) and (7.49) to get

$$\left(T_{\max} - T_{\text{in}}\right) \cong 0.75\frac{q''}{k_s}\frac{d_h}{\phi^{1/2}}, \tag{7.50}$$

The dimensionless global thermal resistance is defined in terms of dimensionless pressure difference as:

$$R = \frac{k_f\left(T_{\max} - T_{\text{in}}\right)}{q''L} \cong 0.75k_r^{-1}\phi^{-1/2}\frac{d_h}{L}, \tag{7.51}$$

From Equation (7.51), it can be concluded that in the large diameter extreme R increases as $d_h \to \infty$.

7.8.3. Optimal Tube Diameter and Spacing

The optimal behaviour of asymptotes can be seen in Figure 7.20 where the fluid is fully utilised. The geometric optimisation in terms of channel hydraulic diameter

could be achieved by combining Equations (7.41) and (7.51) by using the intersection of asymptotes method as shown in Figure. 7.21.

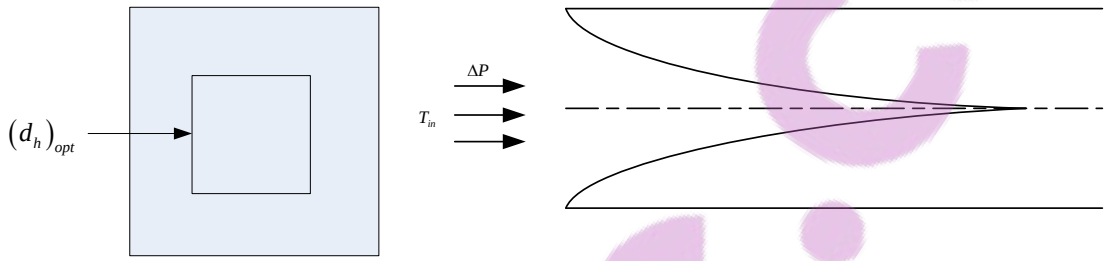

Figure 7. 20 : The optimal limit of the channel's characteristic dimension

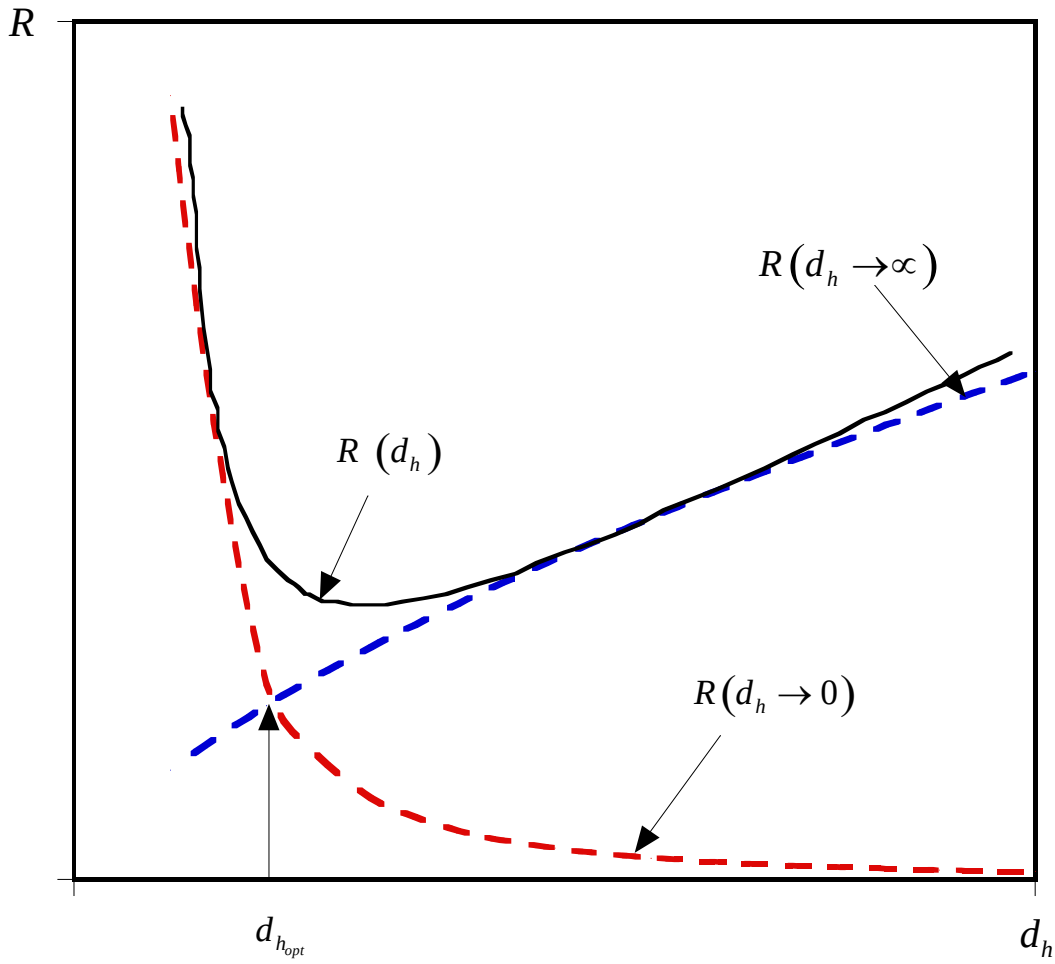

Figure 7. 21 : Intersection of asymptotes Method: Global thermal resistance

The optimal dimension can be generally approximated for the two configurations as the hydraulic diameter where the two extreme curves intersect. The intersection result is

$$\frac{d_{h_{opt}}}{L} \approx 3.494\phi^{-1/6}k_r^{1/3}Be^{-1/3} \tag{7.52}$$

where $d_{h_{opt}}$ is the optimal hydraulic diameter of the cooling channel.

The optimal spacing s_{opt} between channels follows from Equations (7.3), (7.5) and (7.52), namely

$$\frac{s_{opt}}{L} \approx 3.494\phi^{-1/6}k_r^{1/3}Be^{-1/3}\left(\phi^{-1/2}-1\right) \tag{7.53}$$

Equations (7.52) and (7.53) show that in the two extremes, the hydraulic diameter and channel spacing decrease as the pressure difference increases for fixed porosity.

The minimum dimensionless global thermal resistance can be obtained for an elemental volume for the configuration that corresponds to the optimal geometries by substituting Equation (7.52) into Equation (7.41) as follows:

$$R_{\min} = \frac{k_f\left(T_{\max}-T_{\text{in}}\right)_{\min}}{q''L} \cong 2.62\left(k_r\phi\right)^{-2/3}Be^{-1/3}, \tag{7.54}$$

Equation (7.54) shows that the minimised global thermal resistance decreases monotonically as Be increases for a fixed porosity.

The optimisation results of Equations (7.52) and (7.54) agreed within a factor of order of one with the corresponding results obtained by Kim *et al*. [130].

7.9. CORRELATIONS OF THE THEORETICAL METHOD AND NUMERICAL OPTIMISATION

The analytical results of Equations (7.52) to (7.54) were used to validate the numerical solutions. The numerical and approximate solutions based on scale analysis at optimal geometry dimensions are in good agreement and the solutions have similar trends as shown in Figures 7.22 to 7.24.

Figure 7.22 shows the minimised dimensionless global thermal resistance group as a function of the dimensionless pressure difference at optimised design variables for the configuration. The analytical and numerical results show that the minimised global thermal resistance group decreases as the dimensionless pressure difference increases. Figures 7.23 and 7.24 show the effect of the dimensionless pressure difference on the optimised dimensionless design variable groups. The curves show that the optimised design variables decrease as the applied dimensionless pressure difference and porosity increase. This shows that a unique optimal design geometry exists for each applied dimensionless pressure difference, thermal conductivity ratio and porosity.

Furthermore, the optimised channel spacing is directly proportional to the optimised hydraulic diameter. This is due to the fact that the elemental volume is not fixed, but allowed to morph for a fixed porosity. In all cases (objective function and design

variables), the theoretical and numerical values agree within a factor of the order one for the worst case. These results are also in agreement with past research work [130].

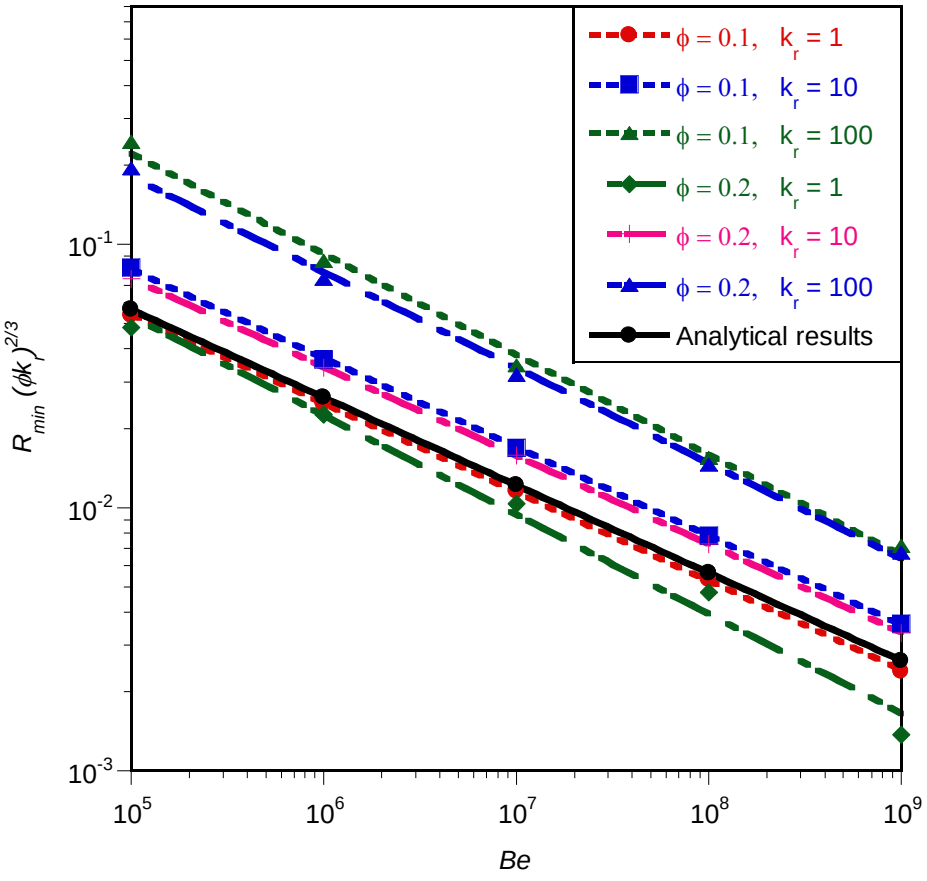

Figure 7. 22 : Correlation of the numerical and analytical solutions for the minimised global thermal resistance

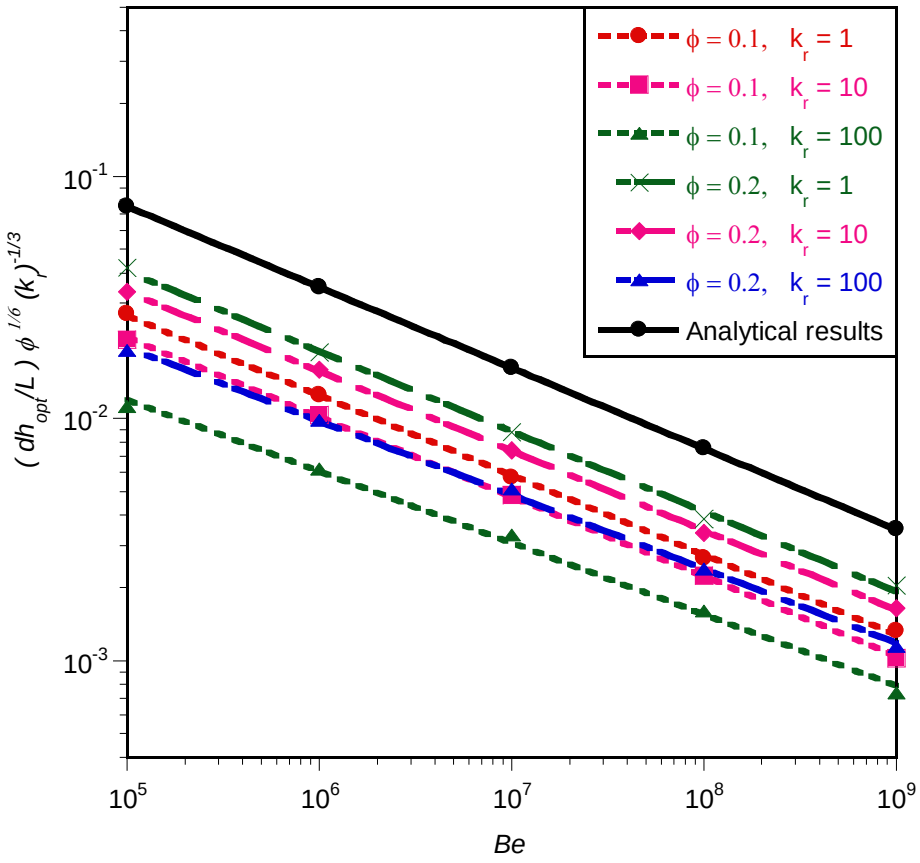

Figure 7. 23 : Correlation of the numerical and analytical solutions for the optimised hydraulic diameter

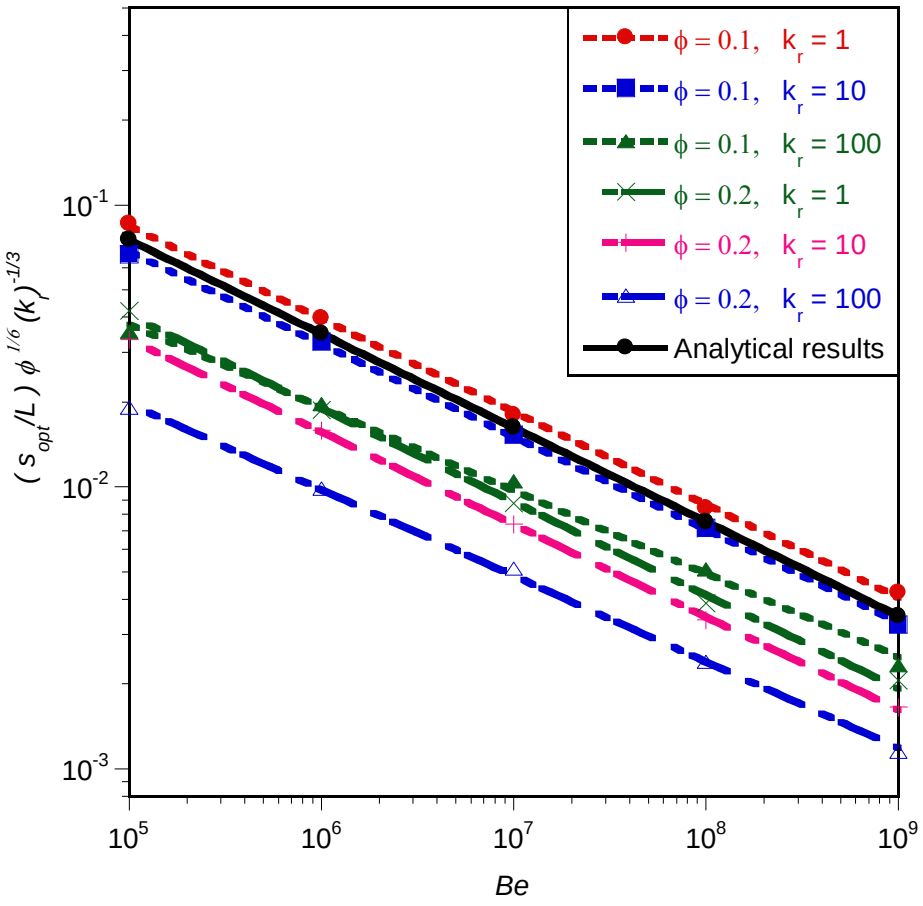

Figure 7. 24 : Correlation of numerical and analytical solutions for the optimised channel spacing

7.10. CONCLUSION

This chapter studied the numerical and analytical optimisation of geometric structures for square cooling channels of vascularised material with a localised self-cooling property, subject to a heat flux on one side in such a way that the peak temperature is minimised at every point in the solid body. The numerical results obtained agree well with results obtained in the approximate solutions based on scale analysis at optimal geometry dimensions. The approximate dimensionless global thermal resistance predicts the trend obtained in the numerical results. This shows that there are unique optimal design variables (geometries) for a given applied dimensionless pressure number for fixed porosity. The use of the optimisation algorithm coupled with the CFD package, rendered the numerical results more robust with respect to the selection of optimal structure geometries, internal configurations of the flow channels and dimensionless pressure difference.

The results also show that material property has a significant influence on the performance of the cooling channel. Therefore, when designing the cooling structure of vascularised material, the internal and external geometries of the structure, material properties and pump power requirements are very important parameters to be considered in achieving efficient and optimal designs for the best performance.

8

CHAPTER 8: CONSTRUCTAL FLOW ORIENTATION IN CONJUGATE COOLING CHANNELS WITH INTERNAL HEAT GENERATION[6]

8.1. INTRODUCTION

This chapter presents the development of a three-dimensional flow architecture of conjugate cooling channels in forced convection - with internal heat generation within the solid - for an array of circular cooling channels with different flow orientation. Three flow orientations were studied: firstly an array of channels with parallel flow; secondly, array of channels in which the flow in every second row is in an opposite direction to its neighbours, and thirdly, an array of channels in which every row is in counter flow relative to each other. The geometric configurations were determined in such a way that the peak temperature was minimised, subject to the constraint of fixed the global volume of solid material. The degrees of freedom of the design were the hydraulic diameter of the channel and channel-to-channel spacing. A gradient-based optimisation algorithm was applied to search for the best optimal geometric

[6] This research section is published in part: T. Bello-Ochende, O.T. Olakoyejo, and J.P Meyer; "Constructal flow orientation in conjugate cooling channels with internal heat generation", *International Journal of Heat and Mass Transfer*, Vol. 57, pp. 241 - 249, 2013

configurations that would improve thermal performance by minimising thermal resistance for a wide range of dimensionless pressure differences. The effect of porosities, applied pressure difference, flow orientation and heat generation rate on the optimal hydraulic diameter and channel-to-channel spacing is reported. The results show that the effects of dimensionless pressure drop on minimum thermal resistance were consistent with those obtained in the open literature.

8.2. COMPUTATIONAL MODEL

Figure 8.1 shows the three flow orientations studied. The system consists of a solid body of fixed global volume *V*, which experiences uniform volumetric heat generation q_s'''. The body is cooled by forcing a single-phase cooling fluid (water) from the left side through the parallel cooling channels. The flow is driven along the length *L* of the circular channel with a fixed pressure difference ΔP. An elemental volume shown in Figure 8.2 consisting of four (4) cooling channels and the surrounding solid was accounted for by making use of symmetry and periodic boundary conditions. The heat transfer in the elemental volume is a conjugate problem, which combines heat conduction in the solid and the convection in the flowing fluid.

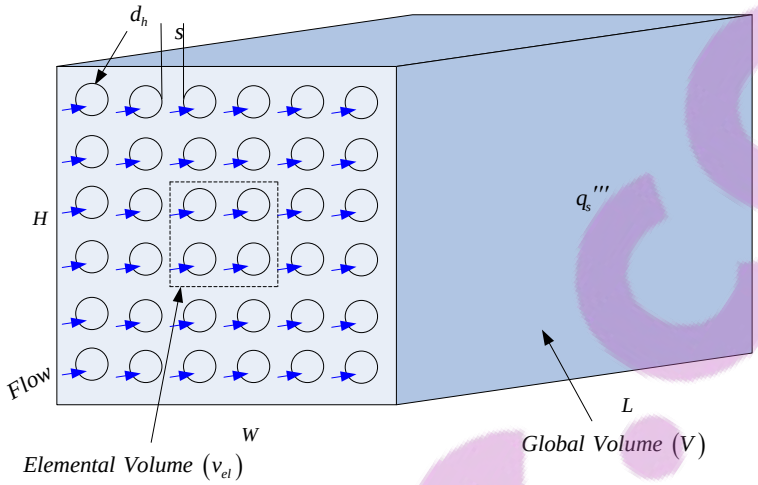

(a)

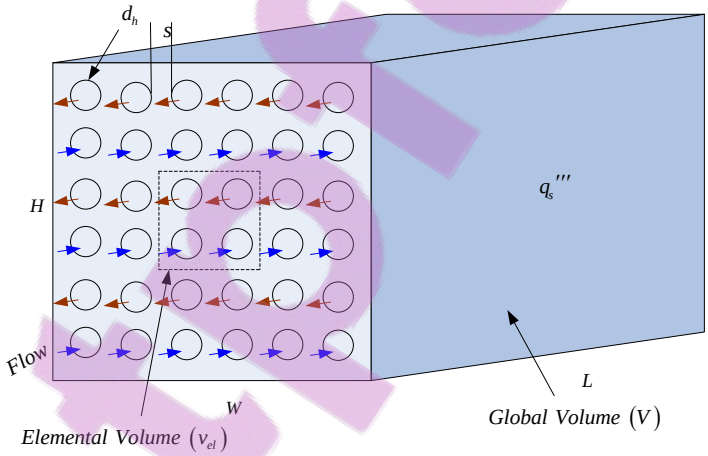

(b)

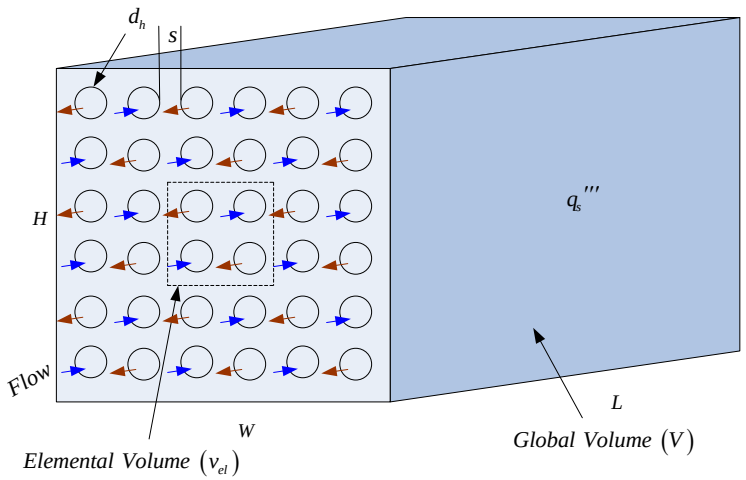

(c)

Figure 8. 1 : Three-dimensional parallel circular of (a) PF-1, (b) CF-2 and (c) CF-3 orientations

8.2.1. Design variables

In Figure 8.2, an elemental volume constraint v_{el} is composed of four circular cooling channels of equal hydraulic diameter d_h. The surrounding solid of thickness s (equal spacing between all channels) means that

$$w = h \tag{8.1}$$

The elemental volume is:

$$v_{el} = w^2 L \tag{8.2}$$

and the volume of a channel is

$$v_c = \frac{\pi}{4} d_h^{\,2} L \tag{8.3}$$

For a fixed length of the channel, the cross-sectional area of the structure is

$$A_s = HW \tag{8.4}$$

which means that the number of channels in the structure arrangement is

$$N = \frac{HW}{hw} \tag{8.5}$$

The void fraction (or porosity) of the elemental structure is defined as

$$\phi = 4\frac{v_c}{v_{el}} \tag{8.6}$$

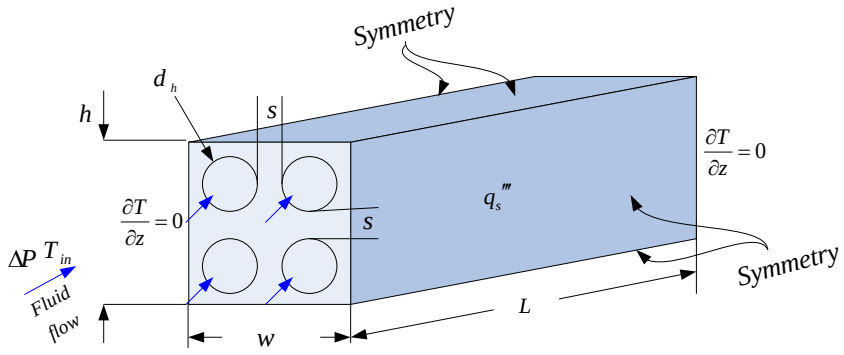

(a)

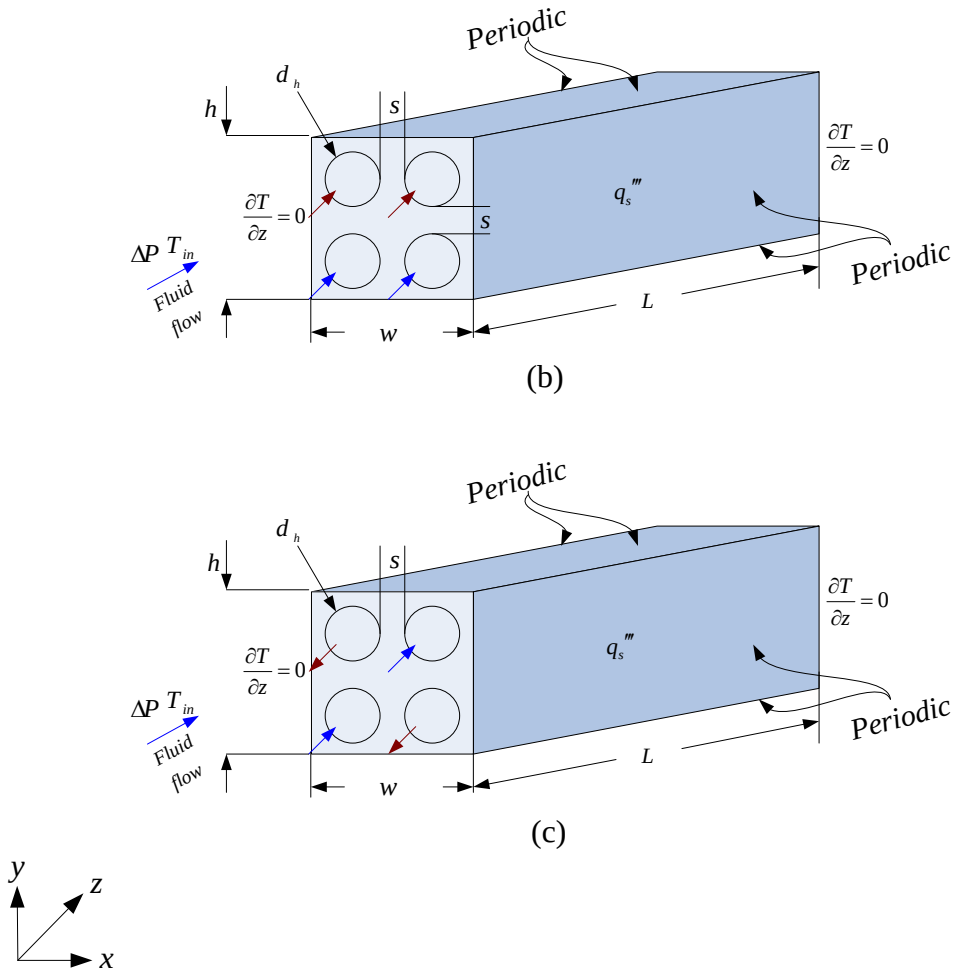

Figure 8. 2 : The boundary conditions of the three-dimensional computational domain of the elemental volume of (a) PF-1, (b) CF-2 and (c) CF-3 orientations

The objective is to find the channel hydraulic diameter d_h and the channel spacing s which offer minimum resistance to heat and flow. The analysis also focuses on the extreme limits of $0 \le d_h \le \infty$ and the extreme limits of $0 \le s \le \infty$.

The cooling fluid was water, which was forced through the cooling channels by a specified pressure difference ΔP across the flow length of the structure. The working

fluid was assumed to be in single phase, steady and Newtonian with constant properties.

Other assumptions imposed on the configuration models were the following: For the PF-1 configuration, the top, bottom, left and right boundaries of the domain corresponded to symmetry boundary conditions. For CF-2 and CF-3, the top, bottom, left and right side of the solid surfaces had spatially periodic thermal boundary conditions. The remaining outside walls and the plane of symmetry were modelled as adiabatic.

The measure of performance was the global thermal resistance, which is expressed in a dimensionless form in Equation (6.13) and it is a function of the optimised design variables, the peak temperature and flow orientations. Thus:

$$R_{\min} = f\left(d_{h_{opt}},\ s_{opt},\ v_{el_{opt}},\ T_{\max_{\min}},\quad \textit{flow orientation}\right) \tag{8.7}$$

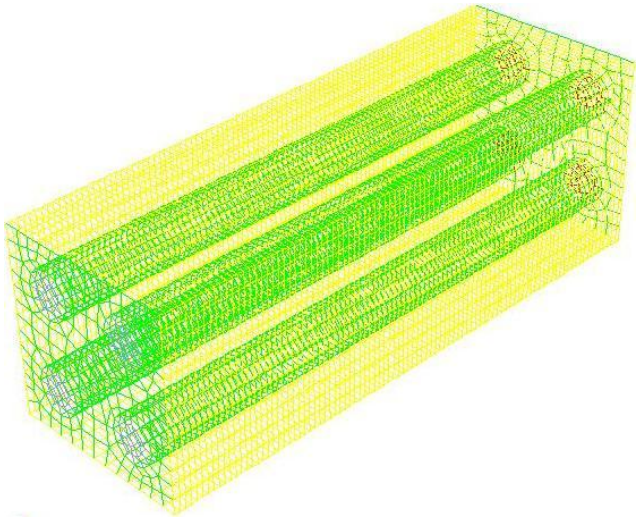

(a)

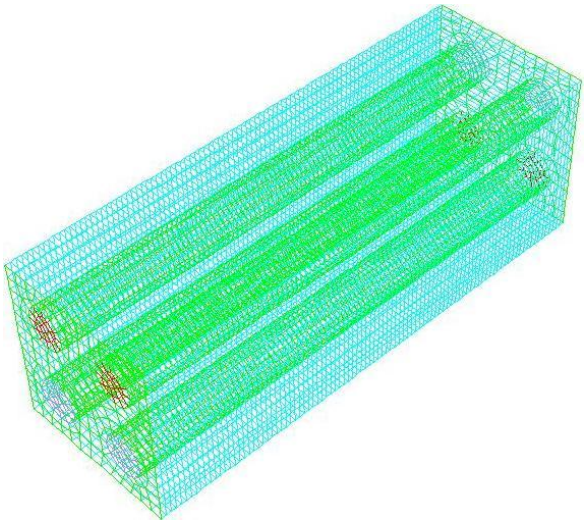

(b)

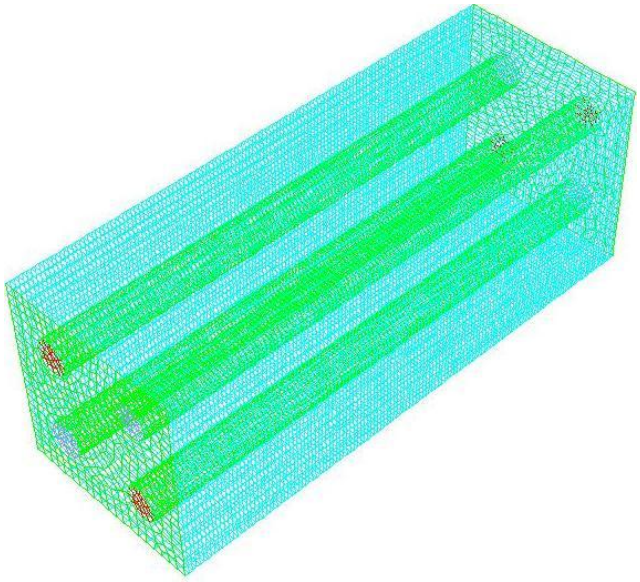

(c)

Figure 8. 3 : The discretised 3-D computational domains of (a) PF-1, (b) CF-2 and (c) CF-3 orientations

8.3. NUMERICAL PROCEDURE

The simulation work began by fixing the channel length, pressure difference, porosity, and heat generation rate, and varying the geometry and flow orientation to identify the configuration that decreased the peak temperature. The numerical solutions of temperature distribution in the elemental volume of each flow orientation configuration were obtained by solving the continuity, momentum and energy equations (Equations (3.1) to (3.8) of Chapter 3) along with the boundary conditions (Equations (8.1) to (8.6)) by using a three-dimensional commercial package Fluent™

[199], which employs a finite volume method. The details of the method are explained by Patankar [203]. Fluent™ was coupled with the geometry and mesh generation package Gambit [201] using MATLAB [219] to allow the automation and running of the simulation process. The computational domain was discretised using hexahedral/wedge elements. A second-order upwind scheme was used to discretise the combined convection and diffusion terms in the momentum and energy equations. The SIMPLE algorithm was then employed to solve the coupled pressure-velocity fields of the transport equations. The solution is assumed to have converged when the normalised residuals of the mass and momentum equations fall below 10^{-6} while the residual convergence of the energy equation was set to less than 10^{-10}. After the simulation had converged, an output file was obtained containing all the necessary simulation data and results for the post-processing and analysis.

The GAMBIT [201] journal files for the three flow orientation configurations are provided in Appendices B.7 to B.9 respectively. FLUENT [199] journal file in Appendix C is applicable to the simulations and need little modification.

8.4. GRID ANALYSIS AND CODE VALIDATION

To ensure accurate results, several grid independence tests were conducted until a mesh size with negligible changes in peak temperature was obtained. The number of grid cells used for the simulations varied for different elemental volume and

porosities. However, grid independence tests for several mesh refinements were carried out to ensure the accuracy of the numerical results. The convergence criterion for the overall thermal resistance as the quantity monitored is given as in Equation (6.15).

Tables 8.1 to 8.3 show the grid independence test for the PF-1, CF-2 and CF-3 configurations respectively with $v_{el} = 2.5\ \text{mm}^3$, $\phi = 0.2$ and $\Delta P = 50\ kPa$. The number of cells were 20 400, 36 186, 61 410 and 162 400 for the PF-1 orientation configuration. It is observed that almost identical results were predicted when 61 410 and 162 400 cells were used. Therefore, a further increase in the cell density beyond 61 410 has a negligible effect on the numerical result. The number of cells were 39 960, 43 000, 61 410 and 162 400 for both the CF-2 and CF-3 configurations.

Table 8. 1 : Grid independence study for the PF-1 configuration with $v_{el} = 2.5\ \text{mm}^3$, $\phi = 0.2$ and $\Delta P = 50\ kPa$

Number of nodes	Number of cells	$T_{\max}$	$\gamma = \dfrac{\left\|(T_{\max})_i - (T_{\max})_{i-1}\right\|}{\left\|(T_{\max})_i\right\|}$
31 091	20 400	27.77	-
50 318	36 186	27.754	0.000577
81 644	61 410	27.764	0.000216
204 783	162 400	27.764	0.000144

Table 8. 2 : Grid independence study for the CF-2 configuration with v_{el} = 2.5 mm^3 , ϕ = 0.2 **and** $\Delta P = 50\ kPa$

Number of nodes	Number of cells	$T_{\max}$	$\gamma = \frac{\left\|(T_{\max})_i - (T_{\max})_{i-1}\right\|}{\left\|(T_{\max})_i\right\|}$
54 109	39 960	27.671	-
59 909	43 000	27.670	0.00000325
81 644	61 410	27.693	0.000827
204 783	162 400	27.709	0.000577

Table 8. 3 : Grid independence study for the CF-3 configuration with v_{el} = 2.5 mm^3 ϕ = 0.2 **and** $\Delta P = 50\ kPa$

Number of nodes	Number of cells	$T_{\max}$	$\gamma = \frac{\left\|(T_{\max})_i - (T_{\max})_{i-1}\right\|}{\left\|(T_{\max})_i\right\|}$
54 109	39 960	27.671	-
59 909	43 000	27.672	0.00000361
81 644	61 410	27.694	0.000794
204 783	162 400	27.710	0.000577

It was worthy to note that almost identical convergence performance emerged when 61 410 and 162 400 cells were used. Therefore, a further increase in the cell density beyond 61 410 had a negligible effect on the numerical result.

8.5. NUMERICAL RESULTS

The elemental volume of the structure varied in the range of 0.125 mm^3 to 20 mm^3, and the porosity range was between $0.1 \leq \phi \leq 0.3$. The length was fixed at L = 10 mm, and the applied pressure difference was specified as $\Delta P = 50\ kPa$. The thermal conductivity of the solid structure (silicon) was 148 W/m.K, and the internal heat generation within the solid was taken to be fixed as 100 W/cm^3. The thermo-physical properties of water [202] used in this study was for water at 300 K and the inlet water temperature was fixed at this temperature.

Figures 8.4 and 8.5 show the existence of an optimum hydraulic diameter and elemental volume size in which the peak temperature is minimised at any point in the channel for the square configuration studied. Figure 8.4 shows the peak temperature as a function of the dimensionless channel hydraulic diameter. It also confirms existence of an optimal channel hydraulic diameter that lies in the range $0.005 \leq d_h/L \leq 0.025$ and minimises the peak temperature.

The elemental volume of the structure has a strong effect on the peak temperature as shown in Figure 8.5. The minimum peak temperature is achieved when the elemental volume is in the range $0.5\ mm^3 \leq v_{el} \leq 8\ mm^3$. This indicates that the global peak temperature decreases as the design variables (hydraulic diameter and elemental volume) increase or the global peak temperature decreases as the design variables decrease until it gets to the optimal design values. Therefore, any increase or decrease

in the design variable beyond the optimal values indicates that the working fluid is not properly engaged in the cooling process, which is detrimental to the global performance of the system.

The results show that the optimal arrangement of the elemental volume for the entire structure at this fixed pressure difference should be very small in order to achieve a better cooling. The results also show that the flow orientation has a strong influence on the convective heat transfer as the peak temperature is lower in the two counter-flow arrangements compared to their parallel-flow counterpart. What's more, the two counter-flow arrangements show almost the same performance. However, the peak temperature of the CF-2 orientation is slightly lower (if $d_h/L < 0.01$) than that of the CF-3 orientation.

According to Figures 8.4 and 8.5, porosity has a significant effect on the peak temperature. The best cooling occurs at the highest porosity. Thus, as the porosity increases, the peak temperature decreases. Furthermore, when the porosity increases the flow direction has almost no impact on the results. This means that this research finds its application in low porosity designs.

.

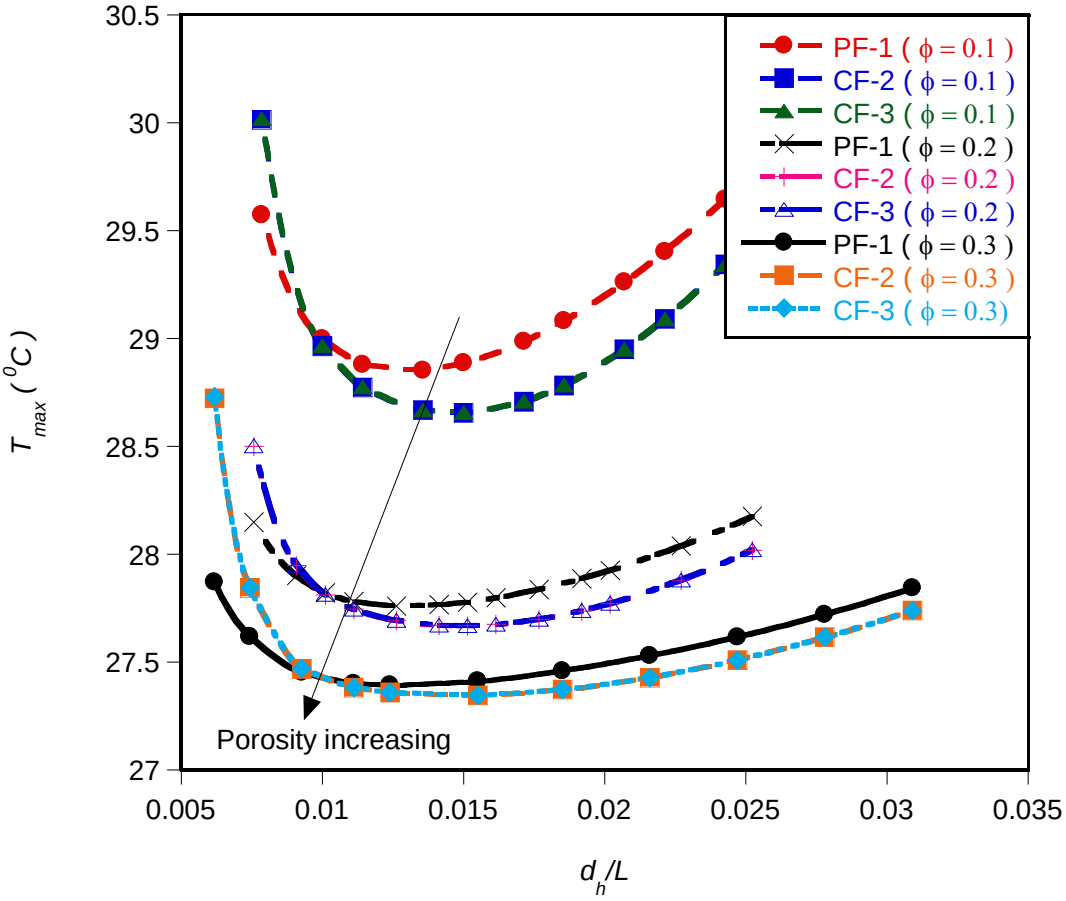

Figure 8. 4 : Effect of the optimised dimensionless hydraulic diameter d_h on the peak temperature at ΔP = 50 *kPa*

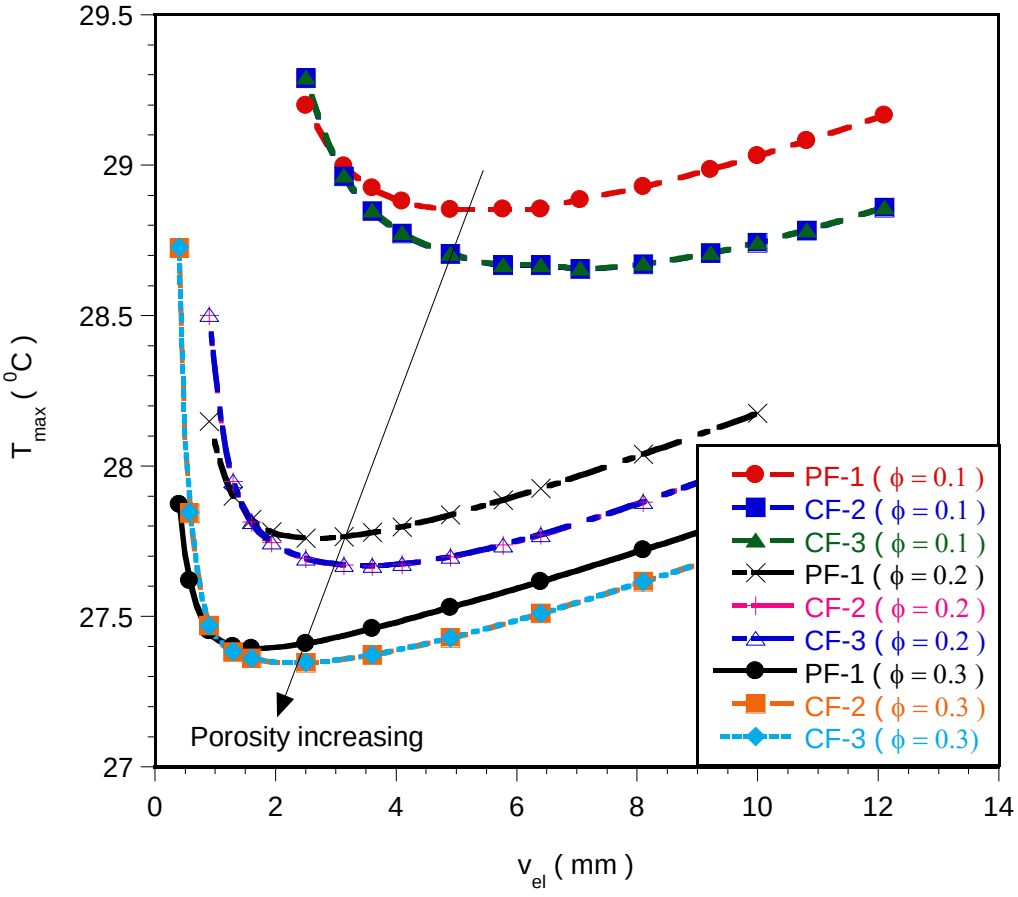

Figure 8. 5 : Effect of the optimised elemental volume on the peak temperature at ΔP = 50 *kPa*

8.6. MATHEMATICAL FORMULATION OF THE OPTIMISATION PROBLEM

In this section, we introduce an optimisation algorithm, Dynamic-Q [208], that will search and identify the design variables at which the system will perform at an optimum.

8.6.1. Optimisation problem and design variable constraints

The optimisation technique described in Chapter 4 was applied to the models described in Section 8.2. The constraint ranges for the optimisation of the three flow orientation configurations are

$$0.125\ \text{mm}^3 \leq v_{el} \leq 20\ \text{mm}^3 \tag{8.8}$$

$$0.1 \leq \phi \leq 0.3 \tag{8.9}$$

$$0 \leq w \leq L \tag{8.10}$$

$$0 \leq d_h \leq w \tag{8.11}$$

$$0 \leq s \leq w \tag{8.12}$$

The optimisation process was repeated for pressure differences across the axial length ranging from 5 *kPa* to 50 *kPa* within the design constraint ranges given in Equations (6.45) to (6.51). This was done in order to search for and identify the channel layout that minimises the peak temperature, $T_{\max}$, such that the minimum thermal resistance between the fixed volume and the cooling fluid is obtained as the desired objectives function.

8.6.2. Mathematical statement of the optimisation problem

The variables chosen for the mathematical statement are

$$x_1 = d_h \tag{8.13}$$

$$x_2 = w \tag{8.14}$$

Substituting Equations (8.13) and (8.14) for Equations (8.8) to (8.12), results in the objective and constraints functions given in Equations (8.15) to (8.17). The inequality functions g_1(x) and g_2(x) are derived from the porosity constraint of Equation (8.6). The mathematical statement of the optimisation problem is then written as

$$f(x) = T_{\max} \tag{8.15}$$

$$g_1(x) = 0.05\pi x_2^{\,2} - x_1^{\,2} \leq 0 \tag{8.16}$$

$$g_2(x) = x_1^{\,2} - 0.3\pi x_2^{\,2} \leq 0 \tag{8.17}$$

8.6.3. Sensitivity analysis of the selection of forward differencing step size

As discussed in Chapter 4. 6, noise exists in any simulation. It is therefore essential to carefully choose a step size Δx to be used in the differencing scheme carefully so that it minimises the noise and gives an accurate representation of the global gradient of the function. A sensitivity analysis was performed by selecting different values of step size for design variables. These values gave a smooth objective function that would later be used as candidate step size. This candidate step size was then verified by running the optimisation program with various starting guesses and checking for any discrepancies in the final solution. Figure 8.6 shows a graph of peak temperature as a function of cooling channel hydraulic diameter with step sizes of 10^{-6} and 10^{-3}. Although, different values of the step size of hydraulic diameter of the cooling

channels as design variable considered are 10^{-6}, 10^{-5}, 10^{-4} and 10^{-3}. A step size of 10^{-3} gave a smooth continuous function of maximum peak temperature and it indeed proved to be an ideal forward-differencing scheme step size for other design variables.

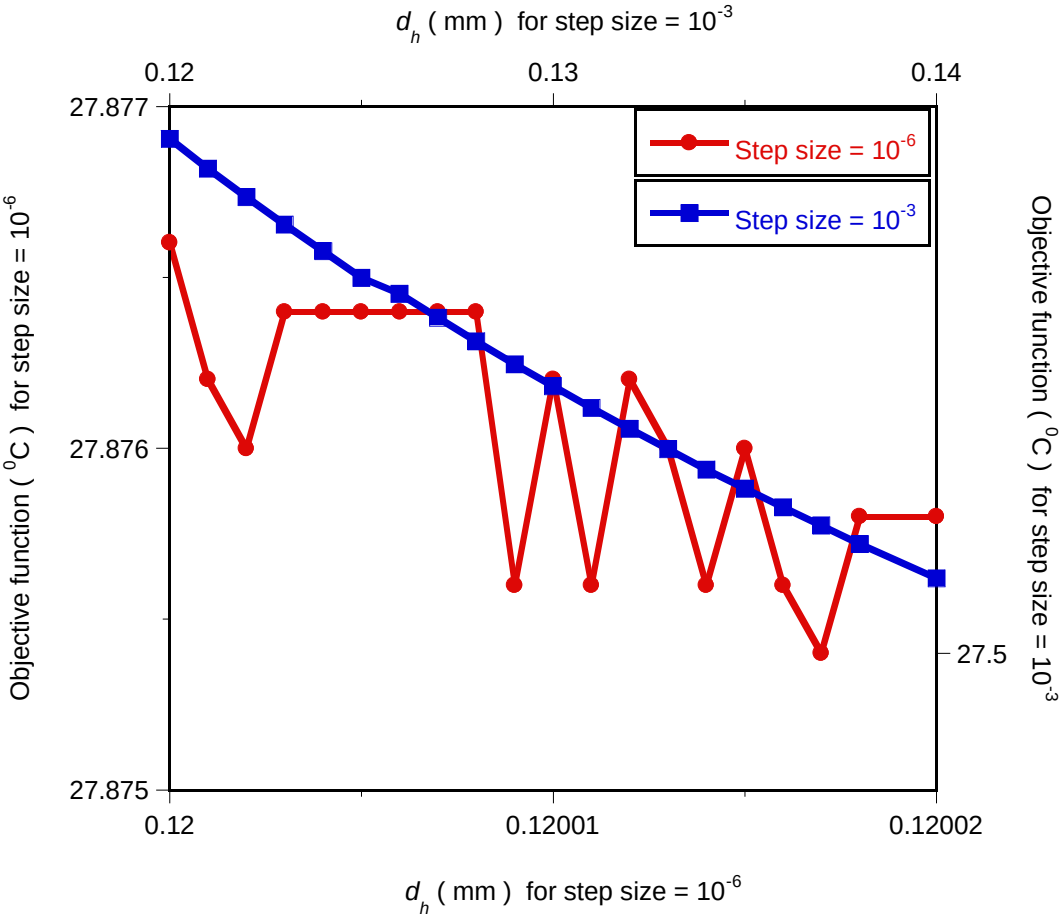

Figure 8. 6 : Plotting peak temperature for different channel width values with step sizes of 10^{-6} and 10^{-3}

Figure 8.7 shows graph of peak temperature as a function of channel-spacing with the chosen candidate step size of 10^{-3}.

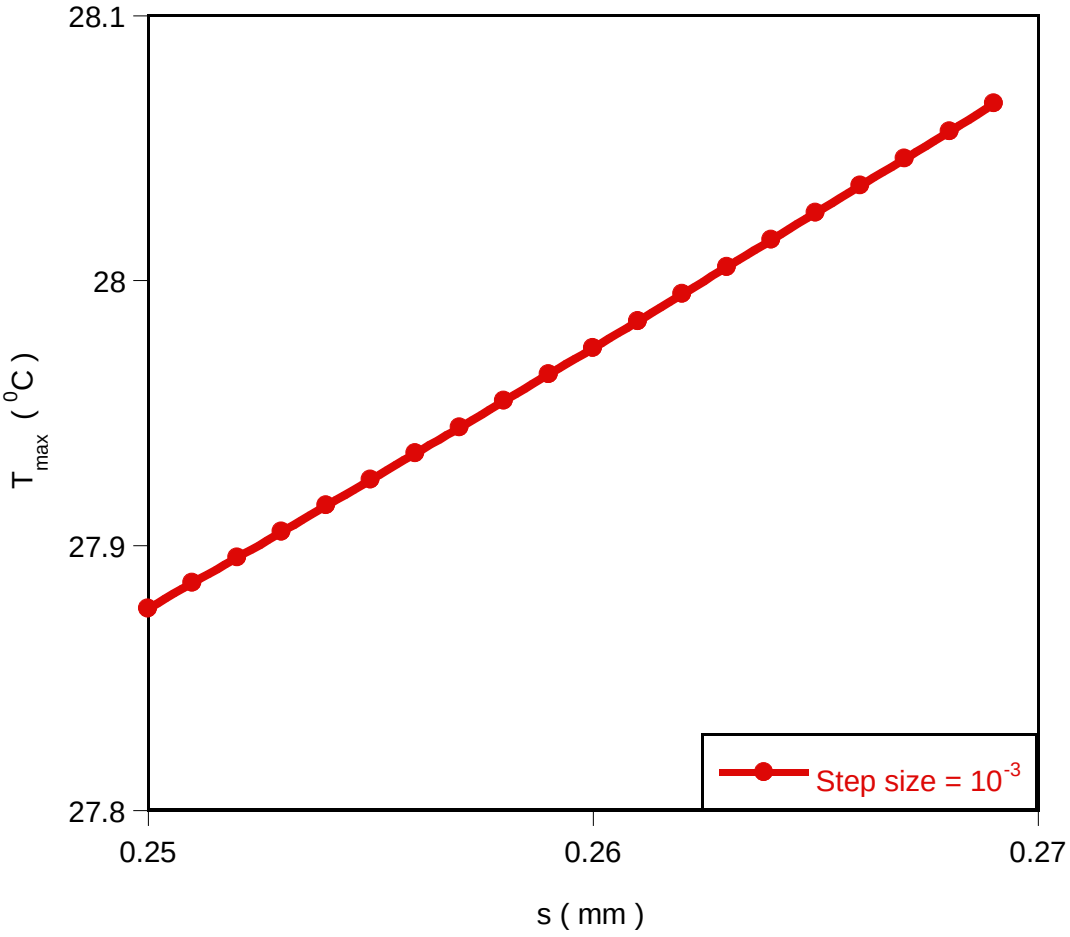

Figure 8. 7: Plotting peak temperature for different channels-spacing values with a step size of 10^{-3}

8.7. OPTIMISATION RESULTS

8.7.1. Effect of the applied pressure difference on optimised geometry and minimised thermal resistance

Figure 8.8 shows the effect of the minimised thermal resistance as a function of applied dimensionless pressure difference for the three flow orientations. The minimised thermal resistance decreases as the applied dimensionless pressure difference and porosity increase. The results also show that the flow orientation has a strong influence on the convective heat transfer. For a specified applied dimensionless pressure difference and porosity, the CF-2 and CF-3 orientations have better performances than the PF1 orientation by 9% for all ranges of porosities and Bejan number used. This is significant enough over a long period of using the CF-2 and CF-3. The CF-2 and CF-3 orientations have almost the same performance. However, the performance of the CF-2 orientation is better than the performance of the CF-3 orientation. Details of the results can be seen in Table 8.4.

Table 8. 4 : Minimised global thermal resistance R_{min} of the three configurations, $R_{\min} \times 10^3$.

	$\phi = 0.1$			$\phi = 0.2$			$\phi = 0.3$		
Be	PF-1	CF-2	CF-3	PF-1	CF-2	CF-3	PF-1	CF-2	CF-3
3.47×10^{9}	0.36	0.33	0.33	0.17	0.15	0.15	0.1	0.092	0.092
6.94×10^{9}	0.26	0.24	0.24	0.12	0.11	0.11	0.071	0.066	0.066
1.39×10^{10}	0.19	0.17	0.17	0.086	0.077	0.077	0.051	0.047	0.047
2.08×10^{10}	0.15	0.14	0.14	0.07	0.063	0.063	0.042	0.038	0.038
2.77×10^{10}	0.13	0.12	0.12	0.061	0.055	0.055	0.036	0.033	0.033
3.47×10^{10}	0.12	0.11	0.11	0.055	0.049	0.049	0.033	0.03	0.03

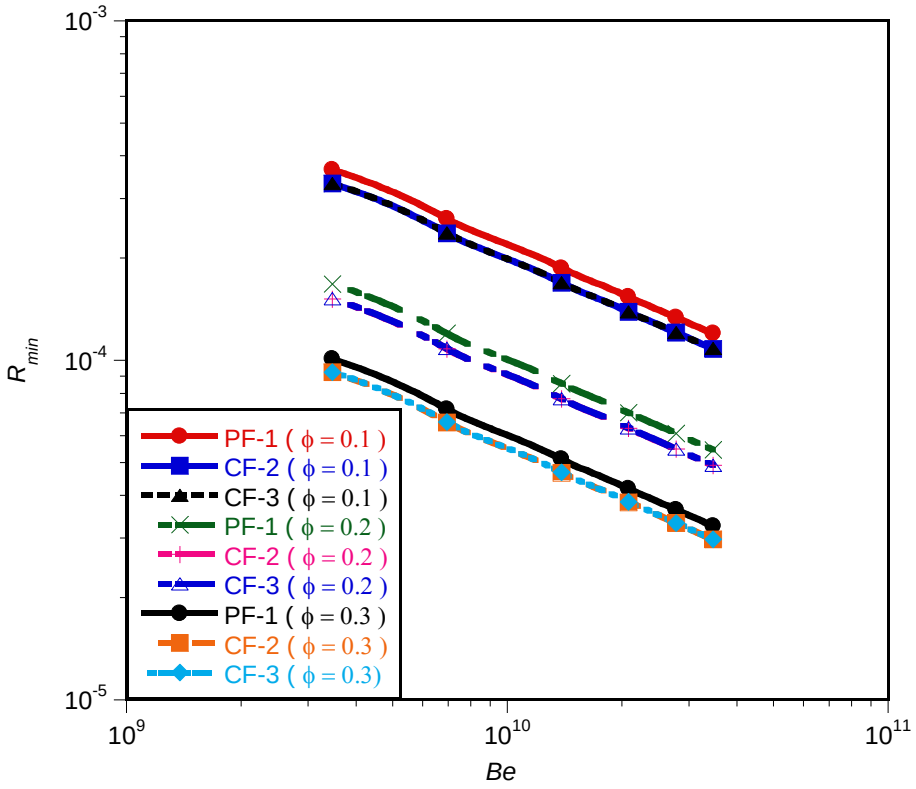

Figure 8. 8 : Effect of dimensionless pressure difference on the minimiseddimensionless global thermal resistance

Figures 8.9 and 8.10 show the behaviour of the geometry with respect to the applied dimensionless pressure difference at different porosities for the three configurations. The optimal hydraulic diameter $d_{h_{opt}}$ decreases as the dimensionless pressure difference increases. There exists an optimal geometry for each of the applied dimensionless pressure differences for the three configurations. According to Figure 8.10, the optimal channel spacing s_{opt} is sensitive to the performance of the system. It

decreases as the dimensionless pressure differences increase and there is a unique optimal spacing for each of the applied dimensionless pressure differences for the configurations. The optimised spacing S_{opt} is directly proportional to the optimised hydraulic diameter $d_{h_{opt}}$. This is also due to the fact that the elemental volume is not fixed, but allowed to morph for a fixed porosity. These results are also in agreement with past research work [94].

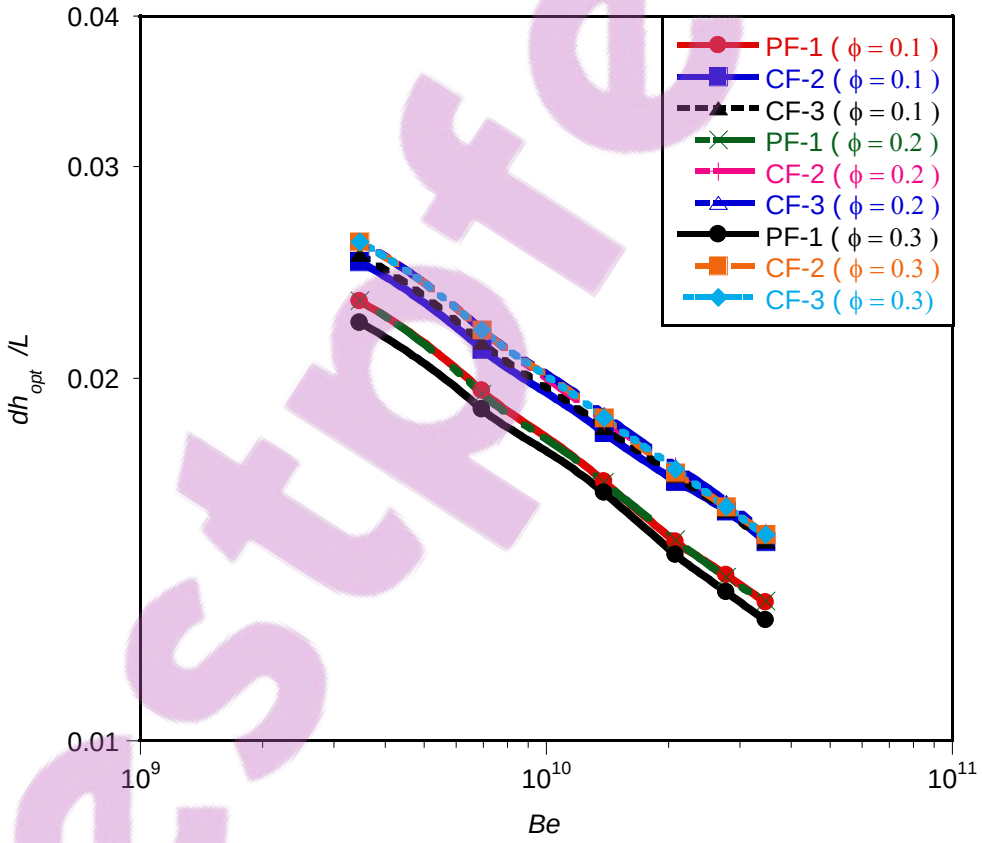

Figure 8. 9 : Effect of dimensionless pressure difference on the optimised hydraulic diameter

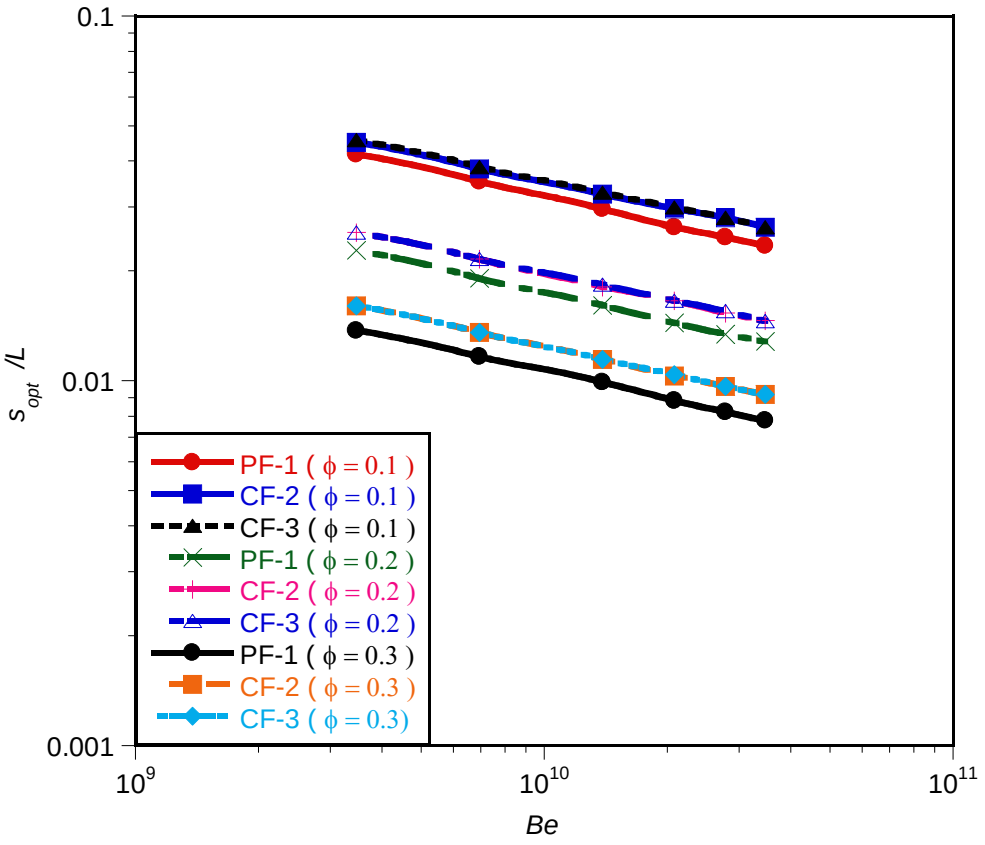

Figure 8. 10 : Effect of dimensionless pressure difference on the optimised channel spacing

8.8. CONCLUSION

This chapter documented the numerical search for geometric structures of conjugate cooling channels in forced convection where internal heat was generated within the solid for an array of parallel cylindrical cooling channels with three flow orientations, PF-1, CF-2 and CF-3.

The configurations were developed in such a way that the peak temperature was minimised subject to the constraint of fixed global volume. The results show that the resulting geometry is a function of the dimensionless pressure difference number. The minimised dimensionless thermal resistance was found to be sensitive to flow orientations. For specified applied dimensionless pressure difference and porosity, the CF-2 and CF-3 orientations perform better than the PF-1 orientation by 9% for all ranges of porosities and Bejan number used. This is significant enough over a long period of using the CF-2 and CF-3. The CF-2 and CF-3 orientations performed almost the same.

The use of the optimisation algorithm coupled with a CFD package made the numerical results robust with respect to the selection of optima geometries, flow orientations of the flow channels and dimensionless pressure difference. Therefore, when designing the cooling structure of heat exchange equipment, the internal and external geometries of the structure, flow orientation and the pump power requirements are very important parameters to be considered in achieving efficient performance.

9

CHAPTER 9: CONCLUSIONS AND RECOMMENDATIONS

9.1. INTRODUCTION

The new trend in modern heat transfer for thermal performance is shape and geometric optimisation. This research was devoted to a study of geometric optimisation of conjugate heat transfer in cooling channels with different cross-sectional shapes, based on constructal theory and design. The objective of the study was to geometrically optimise the cooling structure in such a way that the global thermal resistance or peak temperature between the volume and the cooling fluid would be minimised in heat-generating devices. The configurations of the cooling channels studied were circular, square, isosceles right triangular, equilateral triangular and rectangular.

The research was carried out by performing and developing analytical and numerical analyses of heat transfer for the optimisation of the cooling structure. The analytical solution was based on the asymptotes of intersection method and scale analysis. The numerical simulations, which were guided by the analytical solution, presented a comprehensive explanation of the global thermal behaviour of the problem. To this purpose, computational fluid dynamic software (FLUENT) and mathematical

optimisation algorithms (DYNAMIC – Q) were combined to search for the optimal design variables that would minimise the thermal resistance. The detailed procedures of the theoretical and numerical analyses, as well as the mathematical optimisation algorithms used in this thesis were discussed.

By using the intersection of asymptotes method, the analytical solution provided the existence of an optimal geometry of the external structures and internal architectures of parallel channels of different cross-sectional shapes for cooling volumes that generate heat uniformly. This geometry minimised the global thermal resistance. The numerical modelling section is devoted to a discussion of a set of non-linear partial differential equations governing the transport of mass and heat. The numerical scheme that was implemented in solving the flow and heat transfer was also examined.

The DYNAMIC-Q, which builds on the LFOPC algorithm, presents a multi-dimensional, accurate, reliable and robust penalty method for solving practical constrained engineering design problems and helps to design optimal systems. Numerical noise during simulation and its effect on the gradient-based optimisation algorithms and global performance were also discussed and an efficient way of dealing with the associated problems was suggested.

The analytical and numerical methodology developed in Chapters 3, 4 and 5 were applied to different design cases of cooling channels shapes in heat-generating devices in Chapter 6. The analytical results of Chapter 5 were used to validate the

numerical solutions of Chapter 6. It was found that the numerical and approximate solutions based on scale analysis at optimal geometry dimensions are in good agreement and that the solutions have similar trends. Although the analytical results were lower than the numerical results the theoretical and numerical values agreed within a factor of 1.5 for the worst case. These deviations can be attributed to simplifying assumptions made in the formulation of the theoretical solution.

9.2. CONCLUSIONS

The minimised thermal resistance of all the cooling channels studied is a function of the dimensionless pressure difference number under uniform heat-generation thermal boundary conditions. The minimised thermal resistance decreased monotonically as the applied dimensionless pressure and porosity increased. Also, the optimal geometry is a function of the applied dimensionless pressure number for different configurations. It was shown that a unique optimal geometric configuration exists for a given applied dimensionless pressure difference across a channel which would result in a minimised thermal resistance.

When comparing the shape configurations in Chapter 6, we found that the thermal performance of the circular channel configuration was poorer than any of the other four configurations. An isosceles triangular configuration gave the best thermal performance, followed by the equilateral triangular configuration, the rectangular

shape and square channel. These findings were all in agreement with the analytical solutions provided in Chapter 5.

However, it was clearly observed that cooling was best achieved at a higher aspect ratio of rectangular channels. It was recognised that the optimal design scheme at the higher value of aspect ratio in cross-section for an array of rectangular cooling channels could result in a weaker structure design and increase the difficulty of manufacturing could in fact become impractical due to the channel being too thin.

In Chapter 7, an analytical and numerical CFD package coupled with the optimisation algorithm were used to investigate the geometric optimisation of square cooling channels. These were made of vascularised material with a localised self-cooling property and were subjected to a heat flux on one side in such a way that the peak temperature was minimised at every point in the solid body. The numerical results obtained were in good agreement with the results obtained in the approximate solutions based on a scale analysis at optimal geometry dimensions. The approximate dimensionless global thermal resistance predicted the trend obtained in the numerical results. This showed that there are unique optimal design variables (geometries) for a given applied dimensionless pressure number for fixed porosity.

The material property has a significant influence on the performance of the cooling channel. Therefore, when designing the cooling structure of vascularised material, the internal and external geometries of the structure, material properties and pump power

requirements are very important parameters to be considered in achieving efficient and optimal designs for the best performance.

Chapter 8 documented the numerical search for geometric structures of conjugate cooling channels in forced convection with internal heat generation within the solid for an array of parallel cylindrical cooling channels with three flow orientations, PF-1, CF-2 and CF-3.

The configurations were so developed that the peak temperature was minimised subject to the constraint of fixed global volume. The results show that the resulting geometry is a function of the dimensionless pressure difference number. The minimised dimensionless thermal resistance is sensitive to flow orientations. For specified applied dimensionless pressure difference and porosity, the CF-2 and CF-3 orientations performed better than the PF-1 orientation. The CF-2 and CF-3 orientations performed almost the same.

Therefore, when designing the cooling structure of heat-generating devices or heat exchange equipment, the internal and external geometries of the structure, flow orientation material properties and pump power requirements are very important parameters to be considered in achieving optimal performance.

The use of the optimisation algorithm coupled with the CFD package rendered the numerical results to be more robust with respect to the selection of optima structure

geometries, internal configurations of the flow channels, material properties and pump power requirements.

9.3. RECOMMENDATIONS

The optimisation methodology was applied to the in-line configuration of a cooling channels array. The optimisation can be extended to cooling channels arrays of a staggered configuration. This will enable a comparative study on the minimised thermal resistance analysis and thermal performance capabilities of both configurations. Also, future research may consider the optimisation of additional micro-channels placed in the interstitial regions of an array of cooling channels of different cross-sectional shapes for multi-scale design.

Another interesting extension of this work would be to add one degree of freedom in the system by allowing the tube to have a different diameter while keeping the porosity constant.

Again, future work may investigate the effect of pin fins of any shape transversely arranged along the flow channel of the configurations on the temperature distribution and dimensionless pressure difference characteristics with the global objective of minimising thermal resistance and improving thermal performance.

Furthermore, a study on the effect of temperature-dependent thermo-physical properties of fluid on the minimised thermal resistance is recommended. This is because the thermo-physical properties of some working fluids, such as viscosity, density and thermal conductivity, are sensitive to temperature changes due to relatively large variation of working fluid properties at high heat flux and low Reynolds number (*Re*).

This current research should be extended to the non-Newtonian fluids used in many industries such as the petrochemical, biochemical, pharmaceutical and food industries. This could provide a more comprehensive understanding of the analysis for practical purposes.

REFERENCES

[1] A. Bejan, *Advanced Engineering Thermodynamics*, 2nd ed., Wiley, New York, 1997.

[2] A. Bejan, *Shape and Structure from Engineering to Nature*, Cambridge University Press, Cambridge, UK, 2000.

[3] A. Bejan and E. Sciubba, The optimal spacing of parallel plates cooled by forced convection, *International Journal of Heat and Mass Transfer*, Vol. 35, No. 12, pp. 3259-3264, 1992.

[4] S. Mereu, E. Sciubba and A. Bejan, The optimal cooliing of a stack of heat generating boards with fixed pressure drop, flow rate and pumping power, *International Journal of Heat and Mass Transfer*, Vol. 36, pp.3677–3686, 1993.

[5] A. Bejan, A.J Fowler and G. Stanecu, The optimal spacing of between horizontal cylinders in a fixed volume cooled by Natural Convection, *International Journal of Heat and Mass Transfer*, Vol. 38, pp.2047–2055, 1995.

[6] G. Ledezema and A. Bejan, Optimal geometric arrangement of staggered vertical plates in natural convection, *International Journal of Heat and Mass Transfer*, Vol. 119, pp.700–708, 1997.

[7] A.J Fowler, G.A. Ledezema and A. Bejan, Optimal geometric arrangement of staggered plates in forced convection, *International Journal of Heat and Mass Transfer*, Vol. 40, pp.1795–1805, 1997.

[8] G. Stanecu, A.J. Fowler and A. Bejan, The optimal spacing of cylinders in a free-stream cross-flow forced convection, *International Journal of Heat and Mass Transfer*, Vol. 39, pp. 311–317, 1996.

[9] A. Bejan, The optimal spacing for cylinders in cross-flow forced convection, *International Journal of Heat and Mass Transfer*, Vol. 117, pp.767–770, 1995.

[10] G. Ledezema A.M. Morega and A. Bejan, Optimal spacing between pin fins with impinging flow, *Journal of Heat and Mass Transfer*, Vol. 118, pp.570–577, 1996.

[11] A. Bejan, Constructal-theory network of conducting paths for cooling a heat generating volume, *International Journal of Heat and Mass Transfer*, Vol. 40, pp. 799–816, 1997.

[12] A. Bejan and S. Lorente, *Design with Constructal Theory*, Wiley, Hoboken, 2008.

[13] L. Ghodoossi, Conceptual study on Constructal theory, *Energy. Conversion. Management*, Vol.45, pp. 1379–1395, 2004.

[14] S. Lee, Optimum design and selection of heat sinks, *IEEE Transactions on Components, Packaging and Manufacturing Technology – Part A*, Vol. 18, No. 4, pp. 812 – 817, 1995.

[15] H-S Kou, J-J Lee, and C-W Chen, Optimum thermal performance of microchannel heat sink by adjusting channel width and height, *International Communications in Heat and Mass Transfer* Vol. pp. 577–582, 2008.

[16] R. W. Knight, J. S. Goodling, and D. J. Hall, Optimal thermal design of Forced convection heat sinks - Analytical, *Journal of Electron Packaging* Vol. 113, pp. 313 – 321, 1991.

[17] Y.S. Muzychka, Constructal design of forced convection cooled microchannel heat sinks and heat exchangers, *International Journal of Heat and Mass Transfer*, Vol. 48, pp. 3119–3127, 2005.

[18] Y.S. Muzychka, Constructal multi-scale design of compact micro-tube heat sinks and heat exchangers, *International Journal of Thermal Science*. Vol. 46, pp. 245–252, 2007.

[19] T. Bello-Ochende, L. Liebenberg, J.P. Meyer, A.G. Malan and A. Bejan, Consrtuctal conjugate heat transfer in three-dimensional cooling channels, *International Journal of Heat and Mass Transfer*, Vol. 14, pp. 279 – 293, 2007.

[20] K.K. Ambatipidi and M.M. Rahman, Analysis of conjugate heat transfer in mircochannel heat sinks, *Numerical Heat Transfer, Part A: Applications*, Vol. 37, No. 7, pp. 711 – 731, 2000.

[21] L.G. Page, T. Bello-Ochende, and J.P. Meyer, Maximum heat transfer density rate enhancement from cylinders rotating in natural convection, *International Communications in Heat and Mass Transfer*, Vol. 38, pp. 1354–1359, 2011.

[22] B. Xu, K.T. Ooti, N.T. Wong and W.K. Choi, Experimental investigation of flow friction for liquid flow in micro-channels, *International Communications in Heat and Mass Transfer*, Vol. 27, No. 8, pp. 1165 – 1176, 200.

[23] X.F. Peng and G.P. Peterson, Convective heat transfer and flow friction for water flow in micro-channel structures, *International Journal of Heat and Mass Transfer*, Vol. 39, pp. 2599 – 2608, 1996.

[24] P. Lee, S.V. Garimella and D. Liu, Investigation of heat transfer in rectangular microchannels, *International Journal of Heat and Mass Transfer*, Vol. 48, pp. 1688-1704, 2005.

[25] T.M. Harms, M.J. Kazmierczak, and F.M. Gerner, Developing convective heat transfer in deep rectangular microchannels, *International Journal of Heat and Fluid Flow*, Vol. 20, pp. 149 – 157, 1999.

[26] J. Judy, D. Maynes, and B.W. Webb, Characterization of frictional pressure drop for liquid flows through microchannels, *International Journal of Heat and Mass Transfer*, Vol. 45, pp. 3477 – 3489, 2002.

[27] G. L. Morini, Single-phase convective heat transfer in microchannels: a review of experimental results, *International Journal of Thermal Sciences*, Vol. 43, pp. 631– 651, 2004.

[28] B.A. Jubran, M.A. Hamdan and R.M. Abdullah, Enhanced heat transfer, missing pin, and optimisation for cylindrical pin fin arrays, *ASME Journal of Heat Transfer*, Vol. 115, pp. 576 – 583, 1993.

[29] M. Tahat, Z.H. Kodah, B.A. Jarrah and S.D. Probert, Heat transfers from pin-fin arrays experiencing forced convection, *Applied Energy*, Vol. 67, pp. 419 – 442, 2000.

[30] G.A. Ledezma, A. Bejan, and M. R. Errera, Constructal Tree Networks for Heat Transfer, *Journal of Applied Physics*, Vol. 82, No. 1, 1997, pp. 89 – 100.

[31] A. Bejan, G. Tsatsaronis and M. Moran, *Thermal design and optimisation*, New York: John Wiley. 1996.

[32] J.C. Ordonez and A. Bejan, Entropy generation minimization in parallel- plate counterflow heat exchangers. *International Journal of Energy Research*, Vol. 24, pp. 843 – 864, 2000.

[33] A. Bejan, S. Lorente and J. Lee, Unifying constructal theory of tree roots, canopies and forests, *Journal of Theoretical. Biology*, Vol. 254, pp. 529–540, 2008.

[34] T. Bello-Ochende and A. Bejan, Fitting the duct to the ‘‘body” of the convective flow, *International Journal of Heat and Mass Transfer*, Vol. 46, pp. 1693–1701, 2006.

[35] H. Wang, W. Dai and A. Bejan, Optimal temperature distribution in a 3D triple-layered skin structure embedded with artery and vein vasculature and induced by electromagnetic radiation, *International Journal of Heat and Mass Transfer*, Vol. 50, pp. 1843 – 1854, 2007.

[36] A. Bejan, V. Badescu and A. De Vos, Constructal theory of economics structure generation in space and time, *Energy Conversion Management*. Vol. 41, pp. 1429 –1451, 2000.

[37] A. Bejan, V. Badescu, and A. De Vos, Constructal theory of economics, *Applied Energy*. Vol. 67, pp. 37 – 60, 2000.

[38] A. Bejan, Optimal internal structure of volumes cooled by single phase forced and natural convection, *Journal of Electronic Packaging*, Vol. 125, 200–207, 2003.

[39] A. Bejan, Constructal theory of pattern formation. *Hydrology and Earth System Science*, Vol. 11, pp. 753- 768, 2007.

[40] A. Bejan, Why university rankings do not change: education as a natural hierarchical flow architecture. *International Journal of Design and Nature and Ecodynamics*, Vol. 2, pp. 319–27, 2007.

[41] A. Bejan, Two hierarchies in science: the free flow of ideas and the academy, *International Journal of Design and Nature and Ecodynamics*, Vol. 4, pp. 386–94, 2009.

[42] G. Weinerth, The constructal analysis of warfare. *International Journal of Design and Nature and Ecodynamics*, Vol. 5, pp. 268–76, 2010.

[43] A. Bejan, and J.H. Marden, Unifying constructal theory for scale effects in running, swimming and flying. *Journal of Experimental Biology*, Vol. 209, pp. 238–48, 2008.

[44] J. D Charles, and A. Bejan, The evolution of speed, size and shape in modern athletics, *Journal of Experimental Biology* Vol. 2012, pp. 2419 – 25, 2009.

[45] A. Bejan, E.C. Jones and J.D Charles. The evolution of speed in athletics: why the fastest runners are black and swimmers white, *International Journal of Design and Nature and Ecodynamics*, Vol. 5, pp. 199–211, 2010.

[46] A. H. Reis, A.F Miguel and M. Aydin. Constructal theory of flow architecture of the lungs. *Journal of Medical Physics*, Vol. 31, pp. 1135–40, 2004.

[47] A.F Miguel, Constructal pattern formation in stony corals, bacterial colonies and plant roots under different hydrodynamics conditions, *Theoretical Biology*, Vol. 242, pp. 954–61, 2006.

[48] A. Nakayama, F. Kuwahara and W. Liu, A macroscopic model for counter-current bioheat transfer in a circulatory system. *Journal of Porous Medium*, Vol. 12, pp. 289–300, 2009.

[49] S. Quéré, Constructal theory of plate tectonics, *International Journal of Design and Nature and Ecodynamics*, Vol. 5 pp. 242–53, 2010.

[50] A.H Reis, C. Gama, Sand size versus beachface slope – an explanation based on the constructal law. *Geomorphology*, Vol. 114, pp. 276–83, 2010.

[51] J.P., Meyer, Constructal law in technology, thermofluid and energy systems, and in design education, *Physics of Life Reviews*, Vol. 8, pp. 247 – 248, 2011.

[52] A. Bejan and S. Lorente, The constructal law and the evolution of design in nature, *Physics of Life Reviews*, Vol. 8, pp. 209 – 240, 2011.

[53] T. Basak, The law of life: the bridge between physics and biology, *Physics of Life Reviews*, Vol. 8, pp. 249 – 252, 2011.

[54] A.F. Miguel, The physics principle of generation of flow configuration, *Physics of Life Reviews*, Vol. 8, pp. 243 – 244, 2011.

[55] L. A. O. Rocha, Constructal law: from law of physics to applications and conferences, *Physics of Life Reviews*, Vol. 8, pp. 245–246, 2011.

[56] G. Lorenzini and C. Biserni, The constructal law: from design in nature to social dynamics and wealth as physics, *Physics of Life Reviews*, Vol. 8, pp. 259–260, 2011.

[57] J.O. Tuhtan, Go with the flow: connecting energy demand, hydropower, and fish with constructal theory, *Physics of Life Reviews*, Vol. 8, pp. 253–254, 2011.

[58] L. Wang, Universality of design and its evolution, *Physics of Life Reviews*, Vol. 8, pp. 257-258, 2011.

[59] Y. Ventikos, The importance of the constructal framework in understanding and eventually replicating structure in tissue, *Physics of Life Reviews*, Vol. 8, pp. 241–242, 2011.

[60] Y. S. Kim, Design with Constructal Theory: Steam Generators, Turbines and Heat Exchangers, PhD thesis, Duke University, USA, 2010.

[61] S. Kim, Constructal vascular composites for cooling and heating, PhD thesis, Duke University USA, 2008.

[62] A. K. Pramanick, Natural Philosophy of Thermodynamic Optimization, PhD thesis Duke University Indian Institute of Technology Kharagpur, 2007.

[63] R. S. Kulkarni, Infusion of Robustness into the Product Platform Constructal Theory Method, MSc thesis, Georgia Institute of Technology, 2005.

[64] E. Cetkin, The Natural Emergence of Vascular Design with Turbulent Flow, MSc, thesis, Duke University, USA, 2010.

[65] L.A.O. Rocha, E. Lorenzini and C. Biserni, Geometric optimization of shapes on the basis of Bejan's Constructal theory, *International Communications in Heat and Mass Transfer*, Vol 32, pp. 1281–1288, 2005.

[66] T. Bello-Ochende, J. P. Meyer and A. Bejan, Constructal multi-scale pin fins, *International Journal of Heat and Mass Transfer*, Vol. 53, pp. 2773–2779, 2010.

[67] T. Bello-Ochende, J.P. Meyer and O.I. Ogunronbi, Constructal multiscale cylinders rotating in cross-flow, *International Journal of Heat and Mass Transfer*, Vol. 54, pp.2568–2577, 2011.

[68] A. Bejan and Y. Fautrelle, Constructal multi-scale structure for maximal heat transfer density, *Acta Mechanica*, Vol. 163, pp. 39–49, 2003.

[69] A. Bejan , L.A.O. Rocha and S. Lorente, Thermodynamic optimization of geometry: T- and Y-shaped constructs of fluid streams , *International Journal of Thermal Sciences*, Vol. 39, pp. 949–960, 2000.

[70] A. Bejan, and N. Dan, Two constructal routes to minimal heat flow resistance via greater internal complexity, *Journal of Heat Transfer*, Vol. 121, pp. 6 – 14, 1999.

[71] L.A.O. Rocha, S. Lorente, and A. Bejan, Constructal design for cooling a disc-shaped area by conduction, *International Journal of Heat and Mass Transfer*, Vol. 45, pp. 1642 – 1652, 2003.

[72] A.H., Reis, Constructal Theory – Complex flow structures in engineering and in Nature III Conferência Nacional em Mecânica de Fluidos, Termodinâmica e Energia (MEFTE - BRAGANÇA 09), pp. 1– 17, 2009.

[73] A. H. Reis, Constructal Theory: From Engineering to Physics, and How Flow Systems Develop Shape and Structure, *Applied Mechanics Reviews*, Vol. 59, pp. 269–282, 2006.

[74] Y. Fan, and L. Luo, Recent Applications of Advances in Microchannel Heat Exchangers and Multi-Scale Design Optimisation, *Heat Transfer Engineering*, Vol. 29, pp. 461–474, 2008.

[75] H. H. Bau, optimisation of conduits' shape in micro heat exchangers, *International Journal of Heat and Mass Transfer*, Vol. 43, pp. 2717–2723, 1998.

[76] A. Yilmaz, O. Buyukalaca and T. Yilmaz, Optimum shape and dimensions of ducts for convective heat transfer in laminar flow at constant wall temperature, *International Journal of Heat and Mass Transfer*, Vol. 43, pp. 767–775, 2000.

[77] W Yang, T. Furukawa and S. Torii, Optimal package of stacks of convection – Cooled printed circuit boards using entropy generation minimization method, *International Journal of Heat and Mass Transfer* Vol. 51, pp. 4038 – 4046, 2008.

[78] A. Bejan, and Y. Fautrelle, Constructal multi-scale structure for maximal heat transfer density, *Acta Mechanical.* Vol. 163, pp. 39–49, 2003.

[79] R. W. Knight, J. S. Goodling, and D. J. Hall, Optimal thermal design of Forced convection heat sinks - Analytical, *Journal of Electronic Packaging*, Vol. 113, pp. 313 – 321, 1991.

[80] R. W. Knight, D. J. Hall, J. S. Goodling, and R. C. Jaeger, Heat sink optimization with application to microchannels, *IEEE Transaction on Component, Hybrids, Manufacturing. Technology.* Vol. 15, pp. 832–842, 1992.

[81] R. W. Knight, J. S. Goodling, and B. E. Gross "Optimal thermal design of air cooled forced convection finned heat sinks – e*xperimental verification, – Intersociety Conference on Thermal Phenomena*, 1992.

[82] D.C. Knupp, C.P. Naveira-Cotta and R.M. Cotta, Theoretical analysis of conjugated heat transfer with a single domain formulation and integral transforms, *International Communications in Heat and Mass Transfer*, Vol. 39, pp. 355–362, 2012.

[83] S.H. Kim and N.K. Anand, Laminar developing flow and heat transfer between a series of parallel plates with surface mounted discrete heat sources, *International Journal of Heat and Mass Transfer*, Vol. 37, pp. 2231–2244, 1994.

[84] J.H. Ryu, D.H. Choi, and S.J. Kim, Numerical optimization of the thermal performance of a microchannel heat sinks, *International Journal of Heat and Mass Transfer*, Vol. 45, pp. 2823 – 2827, 2002.

[85] A. G. Fedorov and Viskanta, Three-dimensional conjugate heat transfer in the microchannel heat sink for electronic packaging, *International Journal of Heat and Mass Transfer*, Vol.43, pp. 399 – 415, 2000.

[86] W. Qu, and I. Mudawar, Analysis of three-dimensional heat transfer in micro-channel heat sinks, *International Journal of Heat and Mass Transfer*, Vol. 45, pp. 3973 – 3985, 2002.

[87] R.K. Shah and A.L. London, *Laminar Flow Forced Convection in Ducts: a source Book for Compact Heat Exchanger Analytical Data, Supplement. 1*, Academic Press, New York, 1978.

[88] K. Kawano, K. Minakami, H. Iwasaki and M. Ishizuka, Microchannel Heat Exchanger For Cooling Electrical Equipment, *Application of Heat Transfer In*

Equipment, Systems And Education, ASME HTD-361-3/PID- 3, pp. 173–180, 1998.

[89] K.K. Ambatipudi, and M.M. Rahman, Analysis of conjugate heat transfer in microchannel heat sinks, *Numerical Heat Transfer* Part A Vol. 37, pp. 711–731, 2000.

[90] C. Chen, Forced convection heat transfer in microchannel heat sinks, *International Journal of Heat and Mass Transfer,* Vol. 50, pp. 2182–2189, 2007.

[91] A.K. da Silva, S. Lorente and A. Bejan, Optimal distribution of discrete heat sources on a plate with laminar forced convection, *International Journal of Heat and Mass Transfer,* Vol. 47, pp. 2139–2148, 2004.

[92] A.K. da Silva, S. Lorente and A. Bejan, Optimal distribution of discrete heat sources on a wall with natural convection, *International Journal of Heat and Mass Transfer*, Vol. 47 pp. 203–214, 2004.

[93] T. Bello-Ochende and A. Bejan, Maximum heat transfer density: Plates with multiple lengths in forced convection *International Journal Thermal Sciences* Vol. 43, pp. 1181–1186, 2004.

[94] T. Bello-Ochende, L. Liebenberg and J.P. Meyer, Constructal cooling Channels for micro-channel heat sinks, *International Journal of Heat and Mass Transfer*, Vol. 50, pp. 4141 – 4150, 2007.

[95] T. Bello-Ochende, L. Liebenberg and J. P. Meyer, Constructal Design: Geometric optimization of micro-channel heat sinks, *South African Journal of Science*, Vol. 103, 12, pp. 483 – 489, 2007.

[96] T. Bello-Ochende, L. Liebenberg, A. G. Malan, A. Bejan and J. P. Meyer, Optimization of conjugate heat transfer in three-dimensional cooling channels, *Journal of Enhanced Heat Transfer*, Vol. 14, pp. 279 – 293, 2007.

[97] T. Bello-Ochende T and J. P. Meyer, Constructal cooling channels: application to heat transfer in micro-channel heat sinks, *International Journal of Emerging Multidisciplinary Fluid Sciences*, Vol. 1, pp. 61 – 83, 2009.

[98] T. Bello-Ochende, J. P. Meyer and A. Bejan, Constructal ducts with wrinkled entrances, *International Journal of Heat Mass Transfer*, Vol. 52, pp. 3628 – 3633, 2009.

[99] T. Bello-Ochende, J. P. Meyer and F. U. Ighalo, Combined numerical and constructal theory for the design of micro-channel heat sinks, *Journal of Numerical Heat Transfer, Part A*: Applications, Vol. 58 pp. 882 – 899, 2010.

[100] T. Bello-Ochende and A. Bejan, Optimal spacing for mixed convection, *Journal of Heat Transfer*, Vol. 126, pp. 956 – 962, 2004.

[101] T. Bello-Ochende, A. Bejan, Constructal multi-scale cylinder in cross flow, International *Journal of Heat and Mass Transfer*, Vol. 48, pp. 1373 – 1383, 2005.

[102] T. Bello-Ochende, and A. Bejan, Constructal multi-scale cylinders with natural convention, *International Journal of Heat and Mass Transfer*, Vol. 48, pp. 4300 – 4306, 2005.

[103] T. Bello-Ochende, J. P. Meyer and J. Dirker, Three-dimensional Multi-Scale Plate Assembly for Maximum heat Transfer Rate Density, *International Journal of Heat Mass Transfer*, Vol. 53, pp. 586 – 593, 2010.

[104] M.R. Rajkumar, G. Venugopal and S. A. Lal, Numerical study of natural convection from a heat-generating element using a locally divergence free FEM and comparison with experiment, *International Communications in Heat and Mass Transfer* Vol. 39, pp. 530–536, 2012.

[105] H.A. Mohammed, P. Gunnasegaran and N.H. Shuaib, Influence of channel shape on the thermal and hydraulic performance of microchannel heat sink, *International Communications in Heat and Mass Transfer*, Vol. 38 pp. 474 – 480, 2011.

[106] L.A.O. Rocha, E. Lorenzini, C. Biserni and Y. Cho, Constructal design of a cavity cooled by convection, *International Journal of Design and Nature and Ecodynamics*, Vol. 5, pp. 212–220, 2010.

[107] C. Biserni, L.A.O. Rocha G. Stanescu and E. Lorenzini, Constructal H-shaped cavities according to Bejan's theory *International Journal of Heat and Mass Transfer*, Vol. 50, 2132–2138, 2007.

[108] C. Biserni, L.A.O. Rocha and A. Bejan, Inverted fins: geometric optimization of the intrusion into a conducting wall, *International Journal of Heat and Mass Transfer*, Vol. 47, pp. 2577–2586, 2004.

[109] G. Lorenzini, and L.A.O. Rocha, Geometric optimization of T-Y-shaped cavity according to constructal design, *International Journal of Heat Mass Transfer*, Vol. 52 pp. 4683–8, 2009.

[110] G. Lorenzini, C. Biserni, and L.A.O. Rocha, Geometric optimization of isothermal cavities according to Bejan's theory. *International Journal of Heat Mass Transfer*, Vol. 54 pp. 3868–73, 2011.

[111] G. Lorenzini, and L.A.O. Rocha, Constructal design of Y-shaped assembly of fins. *International Journal of Heat Mass Transfer*, Vol. 49, pp. 4552–7, 2006.

[112] G. Lorenzini, and L.A.O. Rocha, Constructal design of T-Y assembly of fins for an optimized heat removal, *International Journal of Heat Mass Transfer*, Vol. 52, pp. 458–63, 2008.

[113] G. Lorenzini, R.L. Corrêa, E.D. Dos Santos and L.A.O. Rocha, Constructal design of complex assembly of fins, *ASME Journal of Heat Transfer*, Vol. 133, pp. 071801-1 – 071801-10, 2011.

[114] M. R. Salimpour, M. Sharifhasan, and E. Shirani, Constructal optimization of the geometry of an array of micro-channels, *International Communication of Heat and Mass Transfer*, Vol. 38, pp. 93–99, 2011.

[115] R.S. Matos, J.V.C. Vargas and A. Bejan, Three-dimensional optimization of staggered finned circular and elliptic tubes in forced convection, *International Journal of Heat and Mass Transfer*, Vol. 44, pp. 3953–3961, 2000.

[116] R.S. Matos , T.A. Laursen, J.V.C. Vargas and A. Bejan, Three-dimensional optimization of staggered finned circular and elliptic tubes in forced convection, *International Journal of Thermal Sciences* Vol. 43, pp. 477–487, 2004.

[117] J.C. Ordonez, Integrative energy-systems design: system structure from thermodynamic optimization, PhD thesis, Duke University, USA, 2003.

[118] J. Dirker and J.P. Meyer, Cooling layers in rectangular heat-generating electronic regions for two boundary condition types: A comparison with a

traditional approach, *South African Journal of Science* Vol. 103, pp. 474 – 482, 2007.

[119] A.H. Reis, A.F. Miguel and A. Bejan, Constructal Theory of Particle Agglomeration of Design of Air-cleaning Devices, *Journal of Physics D: Applied Physics*, Vol. 39, pp. 3086–3096, 2006.

[120] J.V.C. Vargas, J.C. Ordonez and A. Bejan Constructal flow structure for a PEM fuel cell, *International Journal of Heat and Mass Transfer*, Vol. 47, pp. 4177–4193, 2004.

[121] J. C. Ordonez, S. Chen, J. V. C. Vargas, F. G. Dias, J. E. F. C. Gardolinski and D. Vlassov, Constructal flow structure for a single SOFC, *International Journal of Energy Research*, Vol. 31, pp. 1337–1357, 2007.

[122] H., Wen , J.C., Ordonez and J.V.C, Vargas, Single solid oxide fuel cell modeling and optimization, *Journal of Power Source*, Vol. 196, pp. 7519–7532, 2011.

[123] S. O. Obayopo, T. Bello-Ochende and J.P. Meyer, Three-dimensional optimisation of a fuel gas channel of a proton exchange membrane fuel cell for maximum current density, *international journal of energy research*, 2011 doi: 10.1002/er.1935.

[124] S. O. Obayopo, T. Bello-Ochende and J.P. Meyer, Modelling and optimization of reactant gas transport in a PEM fuel cell with a transverse pin fin insert in channel flow, *International journal of hydrogen energy* Vol. 37, pp. 10286–10298, 2012.

[125] S.R. White, N.R. Sottos, J. Moore, P. Geubelle, M. Kessler, E. Brown, S. Suresh and S. Viswanathan, Autonomic Healing of Polymer Composites, *Nature*, Vol. 409, pp. 794–797, 2001.

[126] A. Bejan, S. Lorente and K.-M. Wang, Network of Channels for Self-healing Composite Materials, *Journal of Applied Physics*, Vol. 100, pp. 033528–033528-6, 2006.

[127] K.-M. Wang, S. Lorente and A. Bejan, Vascularised Networks with Two Optimised Channels Sizes, *Journal of Physics D: Applied Physics*, Vol. 39, pp. 3086–3096, 2006.

[128] S.W. Kim, S. Lorente and A. Bejan, Vascularised Materials: Tree-shaped flow architectures matched canopy to canopy, *Journal of Applied Physics*, Vol. 100, pp. 063525–063525-8, 2006.

[129] S. Lorente and A. Bejan, Heterogeneous porous media as multiscale structures for maximum flow access, *Journal of Applied Physics*, Vol. 100, pp. 114909–114909-8, 2006.

[130] S.W. Kim, S. Lorente, and A. Bejan, 'Vascularised materials with heating from one side and coolant forced from the other side', *International Journal of Heat and Mass Transfer*, Vol. 50, pp. 3498–3506, 2007.

[131] K-H. Cho, J. Lee, H.S. Ahn, A. Bejan and M.H. Kim, Fluid Flow and Heat Transfer in Vascularised Cooling Plates, *International Journal of Heat and Mass Transfer*, Vol. 53, pp. 3607–3614, 2010.

[132] S. Lorente, and A. Bejan, Svelteness, freedom to morph, and constructal multi-scale flow structures, *International Journal of Thermal Sciences*, Vol. 44, pp. 1123–1130, 2005.

[133] K-M. Wang, S. Lorente and A. Bejan, Vascularisation with grids of channels: multiple scales, loops and body shapes, *Journal of Physics D, Applied Physics*, Vol. 40, pp. 4740–4749, 2007.

[134] S. Kim, S. Lorente and A. Bejan, Dendritic vascularisation for countering intense heating from the side, *International Journal of Heat and Mass Transfer* Vol. 5, pp. 5877–5886, 2008.

[135] S. Kim, S. Lorente, A. Bejan, W. Miller and J. Morse, The emergence of vascular design in three dimensions , *Journal of Applied Physics* Vol. 103, pp. 123511-1 123511-8, 2008.

[136] K-M. Wang, S. Lorente and A. Bejan, Vascular materials cooled with grids and radial channels, *International Journal of Heat and Mass Transfer*, Vol. 52, pp. 1230–1239, 2009.

[137] E. Cetkin, S. Lorente, and A. Bejan, Natural constructal emergence of vascular design with turbulent flow, *Journal of Applied Physics*, Vol. 107, pp. 114901-1–114901-9, 2010.

[138] A. V. Azad and M. Amidpour, Economic Optimization of Shell and Tube Heat Exchanger based on Constructal Theory, *Energy*, Vol. 36 pp. 1087 – 1096, 2011.

[139] A. Beyene, and J. Peffley, Constructal Theory, Adaptive Motion, and Their Theoretical Application to Low-speed Turbine Design, Journal of Energy Engineering -ASCE, Vol. 135, pp. 112 – 118, 2009.

[140] Y. Kim, S. Lorente, and A. Bejan, Constructal Multi-tube Configuration for Natural and Forced convection in cross-flow *International Journal of Heat Mass Transfer*, Vol. 53, pp. 5121 – 5128, 2010.

[141] Y. Kim, S. Lorente, and A. Bejan, Steam Generator structure: continuous model and constructal design, *International Journal of Energy Research*, Vol. 35, pp. 336 – 345, 2011.

[142] A.Y. Alharbi, D.V. Pence and R.N. Cullion, Fluid flow through microscale fractallike branching channel networks, *Journal of Fluids Engineering*, Vol. 125, 1051–1057, 2003.

[143] A.H. Reis, A.F. Miguel and M. Aydin, Constructal theory of flow architecture of lungs, *Journal of Medical Physics*. Vol. 31, pp. 1135–1140, 2004.

[144] C. Amador, A. Gavriilidis, P. Angeli, Flow distribution in different microreactor scale-out geometries and the effect of manufacturing tolerances and channel blockage. *Chemical Engineering Journal*, Vol. pp. 101, 379–90, 2004.

[145] Y. Azoumah, N. Mazet and P. Neveu, Constructal network for heat and mass transfer in a solid–gas reactive porous medium, *International Journal of Heat Mass Transfer*, Vol. 47, pp. 2961–2970, 2004.

[146] D. Tondeur and L. Luo, Design and scaling laws of ramified fluid distributors by the constructal approach, *Chemical Engineering Science*. Vol. 59, pp. 1799–1813, 2004.

[147] L. Luo and D. Tondeur, Multiscale optimization of flow distribution by Constructal approach, *China Particuology*, Vol. 3, pp. 329–336, 2005.

[148] A. Bhakta and S. Bandyopadhyay, Constructal optimization of top contact metallization of a photovoltaic solar cell. *International Journal of Thermodynamics*, Vol. 8, pp. 175–81, 2005.

[149] Y. Chen and P. Cheng, An experimental investigation on the thermal efficiency of fractal tree-like microchannel nets, *International Communications in Heat and Mass Transfer*, Vol. 32, pp. 931–938, 2005.

[150] A.H. Reis and A.F. Miguel, Constructal theory and flow architectures in living systems, *Journal of Thermal Science*, Vol. 10, 57–64, 2006.

[151] A.-H. Wang, X.-G. Liang and J.-X. Ren, Constructal enhancement of heat conduction with phase change, *International Journal of Thermophysics*, Vol. 27, pp. 126–138, 2006.

[152] A.H. Reis, Constructal theory: from engineering to physics, and how flow systems develop shape and structure, *Applied Mechanical Review*, Vol. 59, pp. 269–282, 2006.

[153] A.H. Reis, Constructal view of scaling laws of river basins, *Geomorphology* Vol. 78, pp. 201–206, 2006.

[154] A.F. Miguel, Constructal pattern formation in stony corals, bacterial colonies and plant roots under different hydrodynamics conditions, *Journal of Theoretical Biology*. Vol. 242, pp. 954–961, 2006.

[155] X.-Q. Wang, A.S. Mujumdar and C. Yap, Numerical analysis of blockage and optimization of heat transfer performance of fractal-like microchannel nets, *Journal of Electronic Packaging*. Vol. 128, pp. 38–45, 2006.

[156] W. Wechsatol, J.C. Ordonez and S. Kosaraju, Constructal dendritic geometry and the existence of asymmetric bifurcations, *Journal of Applied Physics*. Vol. 100 pp. 113514, 2006.

[157] S. Lorente, Constructal view of electrokinetic transfer through porous media, *Journal of Physics, D Applied. Physic*. Vol. 40, 2941–2947, 2007.

[158] S. Zhou, L. Chen and F. Sun, Optimization of constructal volume-point conduction with variable cross section conducting path, *Energy Conversion and Management*. Vol. 48, pp. 106–111, 2007.

[159] W. Wu, L. Chen and F. Sun, On the "area to point" flow problem based on constructal theory, *Energy Conversion and Management*. Vol. 48, pp. 101–105, 2007.

[160] Y. Azoumah, P. Neveu and N. Mazet, Optimal design of thermochemical reactors based on constructal approach, *AICHE Journal*. Vol. 53, pp. 1257–1266, 2007.

[161] S. Zhou, L. Chen and F. Sun, Constructal entropy generation minimization for heat and mass transfer in a solid–gas reactor based on triangular element, *Journal of Physics. D Applied. Physics*, Vol. 40, pp. 3545–3550, 2007.

[162] W. Wu, L. Chen and F. Sun, Heat-conduction optimization based on Constructal theory, *Applied Energy*, Vol. 84, pp. 39–47, 2007.

[163] V.A.P. Raja, T. Basak and S.K. Das, Thermal performance of a multi-block heat exchanger designed on the basis of Bejan's constructal theory, *International Journal of Heat Mass Transfer*, Vol. 51, pp. 3582–3594, 2008.

[164] P. Xu, B. Yu, S. Qiu and J. Cai, An analysis of the radial flow in the heterogeneous porous media based on fractal and constructal tree networks, *Physica A: Statistical Mechanics and its Applications*, pp. 6471–6483, 2008.

[165] A. Beyene and J. Peffley, Constructal theory, adaptive motion, and their theoretical application to low-speed turbine design, *Journal of Energy Engineering*. Vol. 135, 112–118, 2009.

[166] M.J. Carone, C.B. Williams, J.K. Allen and F. Mistree, An application of constructal theory in the multi-objective design of product platforms, *ASME 2003 Design Engineering Technical Conferences and Computer and Information in Engineering Conference Chicago, Illinois USA, September 2-6*, 2003.

[167] C. Bai and L. Wang, Constructal design of particle volume fraction in nanofluids. *Journal of Heat Transfer*, Vol. 131, pp. 112402-1 - 112402-7, 2009.

[168] F. Wu, L. Chen, X. Kan, A. Shu, K. Wu, Z. Yang. Constructal design of stack filled with parallel plates in standing-wave thermo-acoustic cooler, *Cryogenics* Vol. 49, pp. 107–11, 2009.

[169] C. Bai, and L. Wang, Constructal structure of nanofluids. *Journal of Applied Physics*, Vol. 108, pp. 074317, 2010.

[170] J. Fan, and L. Wang, Constructal design of nanofluids. *International Journal of Heat and Mass Transfer*, Vol. 53, pp. 4238–47, 2010.

[171] S.B. Zhou, L.G Chen and F.R. Sun, Constructal optimization for a solid–gas reactor based on triangular element, *Science China-technological Sciences*, Vol. 51, pp. 1554–62, 2008.

[172] Z. Fan, X. Zhou, L. Luo and W. Yuan. Experimental investigation of the flow distribution of a 2-dimensional constructal distributor, *Experimental Thermal Fluid Science*, Vol. 33, 77–83, 2008.

[173] D. Tondeur, Y. Fan and L Luo, Constructal optimization of arborescent structures with flow singularities, *Chemical Engineering Science*, Vol. 64, pp. 3968–82, 2009.

[174] J. Yue, R. Boichot, L Luo, Y. Gonthier, G. Chen and Q. Yuan, Flow distribution and mass transfer in a parallel microchannel contactor integrated with constructal distributors, *AIChE Journal*, Vol. 56, pp. 298–317, 2010.

[175] J-F Cornet, Calculation of optimal design and ideal productivities of volumetrically lightened photobioreactors using the constructal approach, *Chemical Engineering Science*, Vol. 65, pp. 985–98, 2010

[176] M. Mehrgoo and M. Amidpour, Constructal design of humidification – dehumidification desalination unit architecture, *Desalination*, Vol. 271, pp. 62–71, 2010.

[177] S. Tescari, N. Mazet and P. Neveu, Constructal method to optimize solar thermochemical reactor design, *Solar Energy*, Vol. 84 pp. 1555–66, 2010.

[178] F. Mathieu-Potvin and L. Gosselin, Optimal conduction pathways for cooling a heat generating body: A comparison exercise, *International Journal of Heat Mass Transfer*, Vol. 50, pp. 2996 – 3006, 2007.

[179] Y. Azoumah, P. Neveu and N. Mazet, Constructal design combined with entropy generation minimization for solid-gas reactors, *International Journal of Thermal Science*, Vol. 45, pp. 716–728, 2006.

[180] Y.S. Kim, S. Lorente and A. Bejan, Constructal Steam Generator architecture, *International Journal of Heat Mass Transfer*, Vol. 52, pp. 2362 – 2369, 2009.

[181] Y.S. Kim, S. Lorente and A. Bejan, Distribution of size in steam turbine power plants, *International Journal of Energy Research*, Vol. 33, pp. 989-998, 2011.

[182] S. Bhattacharjee and W.L. Grosshandler, The formation of wall jet near a high temperature wall under microgravity environment, *ASME HTD*, Vol. 96, pp. 711–716, 1998.

[183] S. Petrescu, Comments on the optimal spacing of parallel plates cooled by forced convection, *International Journal of Heat Mass Transfer*, Vol. 37, 1283, 1994.

[184] A. Bejan and S. Lorente, Thermodynamic optimisation of flow geometry in mechanical and civil engineering, J*ournal of non-equilibrum thermodynamic*, Vol. 26, pp. 305 – 354, 2001.

[185] A.H. Ries, Constructal Theory: From Engineering to Physics, and How Flow Systems Develop Shape and Structure, *Applied Mechanics Reviews*, Transactions of the ASME, 2006, Vol. 59, pp. 269–282.

[186] W-P. Ma, S-C. Tzeng and W-J. Jwo, Flow resistance and forced convective heat transfer effects for various flow orientations in a packed channel, *International Communications in Heat and Mass Transfer*, Vol. 33, pp. 319–326, 2006.

[187] X-Q Wang, A. S. Mujumdar and C. Yap, Effect of orientation for phase change material (PCM)-based heat sinks for transient thermal management of electric components, *International Communications in Heat and Mass Transfer*, Vol. 34, pp. 801–808, 2007.

[188] R-T. Huang, W-J. Sheu and C-C. Wang, Orientation effect on natural convective performance of square pin fin heat sinks, *International Journal of Heat and Mass Transfer*, Vol. 51, pp. 2368–2376, 2008.

[189] H. Zhang, I. Mudawar and M. M. Hasan, Experimental and theoretical study of orientation effects on flow boiling CHF, *International Journal of Heat and Mass Transfer*, Vol. 45, pp. 4463–4477, 2002.

[190] P. Dutta, S. Dutta, Effect of baffle size, perforation, and orientation on internal heat transfer enhancement, *International Journal of Heat and Mass Transfer*, Vol. 41, pp. 3005 – 3013, 1998.

[191] A. Tandiroglu, Effect of flow geometry parameters on transient heat transfer for turbulent flow in a circular tube with baffle inserts, *International Journal of Heat and Mass Transfer*, Vol. 49, pp. 1559–1567, 2006.

[192] J.A. Snyman, *Practical mathematical optimisation: an introduction to basic optimisation theory and classical and new gradient-based algorithms*, Springer, New York, 2005.

[193] W.G. Le Roux, Maximum net power output from an intergrated design of a small-scale open and direct solar thermal brayton cycle, M.Eng dissertation, Department of Mechanical and Aeronautical Engineering, University of Pretoria, 2011.

[194] O.A.A. Abdelaziz, Development of multi-scale, Multi-physics, analysis capability and its application to novel heat Exchanger design and Optimization , PhD Thesis, Department of Mechanical Engineering, University of Maryland, College Park, 2009.

[195] A. J. Pacheco-Vega, Simulation of compact heat exchangers using global regression and soft computing, PhD Thesis, Department of Aerospace and Mechanical Engineering, University of Notre Dame, Indiana, 2002.

[196] K. Foli, T. Okabe, M. Olhofer, Y. Jin and B. Sendhoff, Optimization of micro heat exchanger: CFD, analytical approach and multi-objective evolutionary algorithms, *International Journal of Heat and Mass Transfer*, Vol. 49, pp. 1090 – 1099, 2006.

[197] A. Husain and K-Y. Kim, Multiobjective optimisation of a microchannel Heat Sink Using Evolutionary Algorithm, *Journal of Heat Transfer*, Vol. 130, pp. 114505-1-3, 2008.

[198] S. Baodong, W. Lifeng, L. Jianyun and C. Heming, Multi-objective optimization design of a micro-channel heat sink using adaptive genetic algorithm *International Journal of Numerical Methods for Heat and Fluid Flow*, Vol. 21, pp. 353 – 364, 2011.

[199] Fluent Inc., *Fluent Version 6 Manuals*, Centerra Resource Park, 10 Cavendish Court, Lebanon, New Hampshire, USA, 2001 (www.fluent.com).

[200] H.K. Versteeg and W. Malalasekra, *An introduction to computational fluid dynamics: the finite volume method*, 2nd ed., Prentice Hall, England, 2007.

[201] Fluent Inc., *Gambit Version 6 Manuals*, Centerra Resource Park, 10 Cavendish Court, Lebanon, New Hampshire, USA, 2001 (www.fluent.com).

[202] F.M. White, *Viscous Fluid Flow,* 2nd Edition, McGraw-Hill International Editions, Singapore, 1991.

[203] S.V. Patankar, *Numerical Heat Transfer and Fluid flow*, Hemisphere, New York. 1980.

[204] J.A. Snyman, A new dynamic method for unconstrained minimization, *Applied. Mathematical Modelling*, Vol. 6, pp. 449 – 462, 1982.

[205] J.A. Snyman, An improved version of the original leap-frog dynamic method for unconstrained minimization: LFOP1(b), *Applied. Mathematical Modelling*, Vol. 7, pp. 216 – 218, 1983.

[206] J.A. Snyman, N. Stander, and W.J. Roux, A dynamic penalty function method for the solution of structural optimisation problems, *Applied. Mathematical Modelling*, Vol. 18, pp. 453 – 460, 1994.

[207] J.A. Snyman, The LFOPC Leap-frog algorithm for constrained optimisation, *Computer and Mathematics with Applications*, Vol. 40, pp. 1085 – 1096, 2000.

[208] J.A. Snyman, A.M. and Hay, The DYNAMIC-Q optimisation method: an alternative to SQP?, *Computer and Mathematics with Applications*, Vol. 44, pp. 1589–1598, 2002.

[209] J.A. Snyman, and N. Stander, A New successive approximation method for optimum structure design, *AIAA Journal* , Vol. 32, pp. 1310 – 1315, 1994

[210] J.A. Snyman, and N. Stander, Feaseable descent cone methods for inequality constrained optimisation method in engineering, *international journal for numerical engineering*, Vol. 38, pp. 119 – 135, 1995.

[211] D.J. de Kock, Optimal tundish methodology in a continuous casting process, PhD Thesis, Department of Mechanical and Aeronautical Engineering, University of Pretoria, 2005.

[212] D.J. de Kock, Industrial applications of computational flow optimisation. M.Eng dissertation, Department of Mechanical and Aeronautical Engineering, University of Pretoria, 1999.

[213] O.S. Motsamai, Optimisation techniques for combustion designs, PhD Thesis, Department of Mechanical and Aeronautical Engineering, University of Pretoria, 2005.

[214] R.M. Morris , J.A. Snyman and J.P. Meyer, Jets in cross flow mixing analysis using computational fluid dynamics and mathematical optimisation, *Journal Of Propulsion and Power*, Vol. 23, no 14, pp. 1589 – 1598, 2002.

[215] F.U Ighalo, Optimisation of microchannels and micropin-fin heat sinks with computational fluid dynamics in combination with a mathematical optimisation algorithm. M.Eng dissertation, Department of Mechanical and Aeronautical Engineering, University of Pretoria, 2010.

[216] R.C. Chu, Thermal management roadmap cooling electronic products from hand held device to supercomputers Proceedings of MIT Rohsenow Symposium Cambridge, MA, 2002.

[217] SEMATECH The National Technology Roadmap For Semiconductors: Technology Needs, SEMATECH, Austin TX, 1997.

[218] A. Bejan, *Convection Heat Transfer*, third ed., Wiley, Hoboken, 2004.

[219] The MathWorks, Inc., MATLAB & Simulink Release Notes for R2008a, Apple Hill Drive, Natick, MA, 2008 (www.mathworks.com).

A

APPENDIX A: DYNAMIC-Q OPTIMISATION ALGORITHM

A.1 DYNQ.M

```
function [X,F]=dynq(x0,varargin);
tic
%
%          DYNAMIC-Q ALGORITHM FOR CONSTRAINED OPTIMISATION
%               GENERAL MATHEMATICAL PROGRAMMING CODE
%               ------------------------------------
%
% This code is based on the Dynamic-Q method of Snyman documented
% in the paper "THE DYNAMIC-Q OPTIMISATION METHOD: AN ALTERNATIVE
% TO SQP?" by J.A. Snyman and A.M. Hay. Technical Report, Dept Mech.
% Eng., UP.
%
%                 MATLAB implementation by A.M. HAY
%         Multidisciplinary Design Optimisation Group (MDOG)
%  Department of Mechanical Engineering, University of Pretoria
%                       August 2002
%
%                    UPDATED : 23 August 2002
%
%                       BRIEF DESCRIPTION
%                       -----------------
%


%  Dynamic-Q solves inequality and equality constrained optimisation
%  problems of the form:
%
%                    minimise F(X)   ,  X={X(1),X(2),...,X(N)}
%    such that
%                     Cp(X) <= 0        p=1,2,...,NP
%    and
%                     Hq(X) =  0        q=1,2,...,NQ
%    with lower bounds
%        CLi(X) = V_LOWER(i)-X(NLV(i)) <= 0   i=1,2,...,NL
%    and upper bounds
%        CUj(X) = X(NUV(j))-V_UPPER(j) <= 0   j=1,2,...,NU
%
% This is a completely general code - the objective function and the
% constraints may be linear or non-linear. The code therefore solves
% LP, QP and NLP problems.
%
%                       -----------------
%
% User specified functions:
%
% The objective function F and constraint functions C and H must be
```

```
% specified by the user in function FCH. Expressions for the
respective
% gradient vectors must be specified in function GRADFCH.
%
% {The user may compute gradients by finite differences if necessary
%  - see example code in GradFCH}
%
% Side constraints should not be included as inequality constraints
% in the above subroutines, but passed to the dynq function as
% input arguments LO and UP. (Described below)
%
% In addition to FCH and GRADFCH the following functions are called
% by DYNQ and should not be altered:
%       DQLFOPC,DQFUN,DQCONIN,DQCONEQ,DQGRADF,DQGRADC,DQGRADH
%
% In addition the script HISTPLOT.m plots various optimisation
% histories. To suppress automatic plotting set PRNCONST=0 below.
%
%                       -----------------
%
%   synopsis:
%
%           [X,F] = dynq(x0,lo,up,dml,xtol,ftol,clim,np,nq,kloop);
%
%   outputs:
%       X  = optimal solution (1xN)
%       F  = optimal function value
%
%   inputs:
%       x0 = starting point (1xN)
%       lo = NLx2 matrix associated with lower limits on the
variables
%               containing variable index NLV(i) in the first column
and
%               associated value V_LOWER of that limit in the second
column
%               (optional, otherwise assumed no lower side
constraints)
%       up = NUx2 matrix associated with lower limits on the
variables
%               containing variable index NUV(i) in the first column
and
%               associated value V_UPPER of that limit in the second
column
%               (optional, otherwise assumed no upper side
constraints)
%      dml = the move limit which should be approximately the same
order
%               of magnitude as the "radius of the region of
interest"
%               = sqrt(n)*max-variable-range (optional, default =1)
%     xtol = convergence tolerance on the step size (optional,
default =1e-5)
%     ftol = convergence tolerance on the function value (optional,
default =1e-8)
```

```
%     clim = tolerance for determining whether constraints are
violated

%               (optional, default =ftol*1e2)
%       np = number of inequality constraints (optional)
%       nq = number of equality constraints (optional)
%               Note: Both np and nq are optional and determined
automatically
%               if not specified, but at the cost of an extra
function evalution.
%    kloop = maximum number of iterations (optional, default = 100)
%
%     NOTE: use [] to activate default inputs, for example
%
%  [X,F]=dynq(x0,[],[],2); uses dml=2 but default values for all
other inputs.
%
%       See FCH and GRADFCH for an example problem.
%
%   ---- This program is for educational purposes only ----


%*****PLOT OPTIMISATION HISTORIES AT END OF
PROGRAM?******************
%           YES: 1        OR            NO: 0
%
PRNCONST=1;
%*****************************************************************
**

clc;

N=length(x0);   % Determine number of variables
X=x0;

[dum,D]=size(varargin);
vars=cell(1,9);
vars(1:D)=varargin;

LO=vars{1};
UP=vars{2};
DML=vars{3};
XTOL=vars{4};
FTOL=vars{5};
CLIM=vars{6};
NP=vars{7};
NQ=vars{8};
KLOOPMAX=vars{9};

% default values
[NL,dum]=size(LO);
if NL>0
    NLV=LO(:,1)';
    V_LOWER=LO(:,2)';
else
    NLV=[];
```

```
    V_LOWER=[];
end
[NU,dum]=size(UP);

if NU>0
    NUV=UP(:,1)';
    V_UPPER=UP(:,2)';
else
    NUV=[];
    V_UPPER=[];
end
if isempty(DML)
    DML=1; end
if isempty(XTOL)
    XTOL=1e-5; end
if isempty(FTOL)
    FTOL=1e-8; end
if isempty(CLIM)
    CLIM=FTOL*1e2; end
if isempty(NP)|isempty(NQ)
    [F,C,H]=fch(X);
    NP=length(C);
    if isempty(C)
        NP=0;
    end
    NQ=length(H);
    if isempty(H)
        NQ=0;
    end
end
if isempty(KLOOPMAX)
    KLOOPMAX=100; end

%#########################################################################
##C
%************************************************************************
**C
%     MAIN PROGRAM FOLLOWS: Do not alter!!!!
%************************************************************************
**C
%#########################################################################
##C

%*****OPEN OUPUT
FILES************************************************C
%
fidA=fopen('Approx.out','wt+');
fidD=fopen('DynamicQ.out','wt+');
fidH=fopen('History.out','wt+');
%
%*****SPECIFY INITIAL APPROXIMATION
CURVATURES************************C
%
ACURV=0.D0;
BCURV=zeros(1,NP);
if NP==0
    BCURV=[];
```

```
end
CCURV=zeros(1,NQ);
if NQ==0
    CCURV=[];

end
%
%
%
%*****INITIALIZE
OUTPUT***********************************************C
FEASIBLE=0;

fprintf(fidA,' DYNAMICQ OUTPUT FILE \n');
fprintf(fidA,' -------------------- \n');
fprintf(fidA,' Number of variables [N]= %i \n',N);
fprintf(fidA,' Number of inequality constraints [NP]= %i \n',NP);
fprintf(fidA,' Number of equality constraints [NQ]= %i \n',NQ);
fprintf(fidA,' Move limit= %12.8e \n',DML);

fprintf(1,'\n DYNAMICQ OPTIMISATION ALGORITHM \n');
fprintf(1,' ------------------------------ \n');
% (MAXX=Maximum number of X-values to be displayed on screen)
MAXX=4;
if N<=MAXX
    fprintf(1,' Iter Function value  ? XNORM      RFD        ');
    fprintf(1,'X(%i)       ',1:N);
    fprintf(1,'\n ----------------------------------------');
    for I=1:N
        fprintf(1,'------------',1:N);
    end
    fprintf(1,'\n');
else
    fprintf(1,' Iter Function value  ? XNORM      RFD ');
    fprintf(1,'\n ----------------------------------------\n');
end

fprintf(fidD,' DYNAMICQ OPTIMISATION ALGORITHM\n');
fprintf(fidD,' ------------------------------\n');
fprintf(fidD,' Iter Function value       ? XNORM      RFD        ');
fprintf(fidD,'X(%i)           ',1:N);
fprintf(fidD,'\n');

fprintf(fidD,' ------------------------------------------------');
for i=1:N
    fprintf(fidD,'---------------');
end
fprintf(fidD,'\n');

% Initialize outer loop counter
KLOOP=0;

% Arbitrary large values to prevent premature termination
F_LOW=1.D6;
RFD=1.D6;
RELXNORM=1.D6;
```

```
C_A=zeros(1,NP+NL+NU+1);

%*****START OF OUTER OPTIMISATION
LOOP*******************************C

while KLOOP<=KLOOPMAX

%*****APPROXIMATE
FUNCTIONS*****************************************C

% Determine function values
    [F,C,H]=fch(X);

% Calculate relative step size
    if KLOOP>0
        DELXNORM=sqrt((X_H(KLOOP,:)-X)*(X_H(KLOOP,:)-X)');
        XNORM=sqrt(X*X');
        RELXNORM=DELXNORM/(1+XNORM);
    end

% Determine lowest feasible function value so far
    if KLOOP>0
    FEASIBLE=1;
        check=find(C<CLIM);
        if isempty(check)&NP>0;
            FEASIBLE=0;
        end
        check=find(abs(H)<CLIM);
        if isempty(check)&NQ>0;
            FEASIBLE=0;
        end
        for I=1:NL
            if C_A(I+NP)>CLIM
                FEASIBLE=0;
            end
        end
        for I=1:NU
            if C_A(I+NP+NL)>CLIM
                FEASIBLE=0;
            end
        end
    end

% Calculate relative function difference
    if F_LOW~=1.D6&FEASIBLE==1
        RFD=abs(F-F_LOW)/(1+abs(F));
    end

    if FEASIBLE==1&F<F_LOW
        F_LOW=F;
    end

% Store function values
    X_H(KLOOP+1,:)=X;   % Need to adjust from Fortran version since
```

```
    F_H(KLOOP+1)=F;     % Matlab does not accept 0 as a matrix index
    if NP>0
        C_H(KLOOP+1,1:NP)=C;
    end
    if NL>0
        C_H(KLOOP+1,NP+1:NP+NL)=C_A(NP+1:NP+NL);

    end
    if NU>0
        C_H(KLOOP+1,NP+NL+1:NP+NL+NU)=C_A(NP+NL+1:NP+NL+NU);
    end
    C_H(KLOOP+1,NP+NL+NU+1)=C_A(NP+NL+NU+1);
    if NQ>0
        H_H(KLOOP+1,:)=H;
    end

% Determine gradients
    [GF,GC,GH]=gradfch(X);

% Calculate curvatures
    if KLOOP>0
        DELX=X_H(KLOOP,:)-X_H(KLOOP+1,:);
        DELXNORM=DELX*DELX';

% Calculate curvature ACURV
        DP=GF*DELX';
        ACURV=2.*(F_H(KLOOP)-F_H(KLOOP+1)-GF*DELX')/DELXNORM;

        for J=1:NP
            DP=GC(J,:)*DELX';
% Calculate corresponding curvature BCURV(J)
            BCURV(J)=2.*(C_H(KLOOP,J)-C_H(KLOOP+1,J)-
GC(J,:)*DELX')/DELXNORM;
        end

        for J=1:NQ
            DP=GH(J,:)*DELX';
% Calculate corresponding curvature CCURV(J)
            CCURV(J)=2.*(H_H(KLOOP,J)-H_H(KLOOP+1,J)-
GH(J,:)*DELX')/DELXNORM;
        end
    end

%*****RECORD PARAMETERS FOR THE
ITERATION*****************************C

% Write approximation constants to Approx.out
    fprintf(fidA,' Iteration %i \n',KLOOP);
    fprintf(fidA,' --------------\n');
    fprintf(fidA,' X=\n');
    for I=1:N
        fprintf(fidA,' %12.8f ',X(I));
    end
    fprintf(fidA,'\n F= %15.8e\n',F);
    for I=1:NP
        fprintf(fidA,' C(%i)=%15.8e',I,C(I));
```

```
    end
    for I=1:NQ
         fprintf(fidA,' H(%i)=%15.8e',I,H(I));
    end

    fprintf(fidA,' Acurv=%15.8e',ACURV);
    for I=1:NP

     fprintf(fidA,' Bcurv(%i)=%15.8e',I,BCURV(I));
    end
    for I=1:NQ
        fprintf(fidA,' Ccurv(%i)=%15.8e',I,CCURV(I));
    end

% Write solution to file
    if KLOOP==0
        fprintf(fidD,' %4i %+19.12e %i
',KLOOP,F,FEASIBLE);
    else
        if RFD~=1.D6
            fprintf(fidD,' %4i %+19.12e %i %9.3e
%9.3e',KLOOP,F,FEASIBLE,RELXNORM,RFD);
        else
            fprintf(fidD,' %4i %+19.12e %i %9.3e
',KLOOP,F,FEASIBLE,RELXNORM);
        end
    end
    fprintf(fidD,' %+13.6e',X);
    fprintf(fidD,'\n');

% Write solution to screen
    if KLOOP==0
        if N<=MAXX
            fprintf(1,' %4i %+14.7e %i
',KLOOP,F,FEASIBLE);
            fprintf(1,' %+9.2e',X);
            fprintf(1,'\n');
        else
            fprintf(1,' %4i %+14.7e %i\n',KLOOP,F,FEASIBLE);
        end
     else
        if N<=MAXX
            if RFD~=1.D6&FEASIBLE==1
                fprintf(1,' %4i %+14.7e %i %9.3e
%9.3e',KLOOP,F,FEASIBLE,RELXNORM,RFD);
            else
                fprintf(1,' %4i %+14.7e %i %9.3e
',KLOOP,F,FEASIBLE,RELXNORM);
            end
            fprintf(1,' %+9.2e',X);
            fprintf(1,'\n');
        else
            if RFD~=1.D6&FEASIBLE==1
                fprintf(1,' %4i %+14.7e %i %9.3e
%9.3e\n',KLOOP,F,FEASIBLE,RELXNORM,RFD);
            else
```

```
                fprintf(1,' %4i %+14.7e %i
%9.3e\n',KLOOP,F,FEASIBLE,RELXNORM);
            end
        end
    end

% Exit do loop here on final iteration
    if KLOOP==KLOOPMAX|RFD<FTOL|RELXNORM<XTOL
        if KLOOP==KLOOPMAX

        fprintf(1,' Terminated on max number of steps\n');
            fprintf(fidD,' Terminated on max number of steps\n');
        end
        if RFD<FTOL
            fprintf(1,' Terminated on function value\n');
            fprintf(fidD,' Terminated on function value\n');
        end
        if RELXNORM<XTOL
            fprintf(1,' Terminated on step size\n');
            fprintf(fidD,' Terminated on step size\n');
        end
        fprintf(1,'\n');
        fprintf(fidD,'\n');
        break;
    end

%*****SOLVE THE APPROXIMATED
SUBPROBLEM*******************************C

[X,F_A,C_A,H_A]=dqlfopc(X,NP,NQ,F,C,H,GF,GC,GH,ACURV,BCURV,CCURV,DML.
..
    ,NL,NU,NLV,NUV,V_LOWER,V_UPPER,XTOL,KLOOP);

% Record solution to approximated problem

    fprintf(fidA,'Solution of approximated problem:\n');
    fprintf(fidA,'X=\n');
    for I=1:N
        fprintf(fidA,' %12.8f\n',X(I));
    end
    fprintf(fidA,' F_A=%15.8e\n',F_A);
    for I=1:NP+NL+NU+1
        fprintf(fidA,'C_A(%i)=%15.8e\n',I,C_A(I));
    end
    for I=1:NQ
        fprintf(fidA,'H_A(%i)=%15.8e\n',I,H_A(I));
    end

% Increment outer loop counter
    KLOOP=KLOOP+1;
end

% Write final constraint values to file

if NP>0
    fprintf(fidD,' Final inequality constraint function values:\n');
```

```
    for I=1:NP
        fprintf(fidD,'  C(%i)=%15.8e\n',I,C(I));
    end
end
if NQ>0
    fprintf(fidD,' Final equality constraint function values:\n');
    for I=1:NQ
        fprintf(fidD,'  H(%i)=%15.8e\n',I,H(I));
    end
end

if NL>0
    fprintf(fidD,' Final side (lower) constraint function
values:\n');
    for I=1:NL
        fprintf(fidD,'  C(X(%i))=%15.8e\n',NLV(I),C_A(NP+I));
    end
end
if NU>0
    fprintf(fidD,' Final side (upper) constraint function
values:\n');
    for I=1:NU
        fprintf(fidD,'  C(X(%i))=%15.8e\n',NUV(I),C_A(NP+NL+I));
    end
end

% Write final constraint values to screen
fprintf(1,' Constraint values follow:\n\n')
if NP>0
    fprintf(1,' Final inequality constraint function values:\n');
    for I=1:NP
        fprintf(1,'  C(%i)=%15.8e\n',I,C(I));
    end
end
if NQ>0
    fprintf(1,' Final equality constraint function values:\n');
    for I=1:NQ
        fprintf(1,'  H(%i)=%15.8e\n',I,H(I));
    end
end
if NL>0
    fprintf(1,' Final side (lower) constraint function values:\n');
    for I=1:NL
        fprintf(1,'  C(X(%i))=%15.8e\n',NLV(I),C_A(NP+I));
    end
end
if NU>0
    fprintf(1,' Final side (upper) constraint function values:\n');
    for I=1:NU
        fprintf(1,'  C(X(%i))=%15.8e\n',NUV(I),C_A(NP+NL+I));
    end
end

% Write history vectors

fprintf(fidH,' %3i%3i%3i%3i%3i%3i\n', KLOOP,N,NP,NL,NU,NQ);
for I=1:KLOOP+1
```

```
    fprintf(fidH,' %3i %15.8e',I-1,F_H(I));
    for J=1:N
        fprintf(fidH,' %15.8e',X_H(I,J));
    end
    fprintf(fidH,'\n');
end
if NP>0
    for I=1:KLOOP+1
        fprintf(fidH,' %3i',I-1);
        for J=1:NP
            fprintf(fidH,' %15.8e',C_H(I,J));

      end
        fprintf(fidH,'\n');
    end
end
if NL>0
    for I=1:KLOOP+1
        fprintf(fidH,' %3i',I-1);
        for J=NP+1:NP+NL
            fprintf(fidH,' %15.8e',C_H(I,J));
        end
        fprintf(fidH,'\n');
    end
end
if NU>0
    for I=1:KLOOP+1
        fprintf(fidH,' %3i',I-1);
        for J=NP+NL+1:NP+NL+NU
            fprintf(fidH,' %15.8e',C_H(I,J));
        end
        fprintf(fidH,'\n');
    end
end
if NQ>0
    for I=1:KLOOP+1
        fprintf(fidH,' %3i',I-1);
        for J=1:NQ
            fprintf(fidH,' %15.8e',H_H(I,J));
        end
        fprintf(fidH,'\n');
    end
end

fclose(fidD);
fclose(fidH);
fclose(fidA);

if PRNCONST
    histplot;
%    disp('Press a key to continue');
%    pause;
%    close all;
end
toc
```

A.2 FCH.M

```
function [F,C,H]=fch(X);
% Objective and constraint function evaluation for DYNAMIC-Q
%           (USER SPECIFIED)
%
%   synopsis:
%
%       [F,C,H]=fch(X);
%
%   outputs:
%       F  = objective function value
%       C  = vector of inequality constraint functions (1xNP)
%       H  = vector of equality constraint functions (1xNQ)
%
%   inputs:
%       X = design vector (1xN)
%
%                       -----------------
%
% The application of the code is illustrated here for the very simple
% but general example problem (Hock 71):
%
%      minimise  F(X) = X(1)*X(4)*(X(1)+X(2)+X(3))+X(3)
% such that
%                 C(X) = 25-X(1)*X(2)*X(3)*X(4) <= 0
%      and
%                 H(X) = X(1)^2+X(2)^2+X(3)^2+X(4)^2-40 = 0
%
%     and side constraints
%
%                 1 <= X(I) <= 5 , I=1,2,3,4
%
%   Starting point is (1,5,5,1)
%
%   Solution of this problem is accomplished by:
%       (with FCH and GRADFCH unaltered)
%
%       x0=[1,5,5,1] % Specify starting point
%       lo=[1:4;1,1,1,1]' % Specify lower limits
%       up=[1:4;5,5,5,5]' % Specify upper limits
%       [X,F]=dynq(x0,lo,up); % Solve using Dynamic-Q
%
%   NOTE: This function should return C=[]; H=[]; if these are
%         not defined.
%
%   See also DYNQ and GRADFCH
%

%%My programme in FCH

%-----------------------------------------------------------------

% x1 is the hydraulic diameter  of the elemental channel
```

```
% x2 is the height or width  of the elemental volume

%x = [ 0.00005*0.8^0.5    0.00005]


fid = fopen('designvariable.jou','w');

for i=1:2

fprintf(fid,'$x%g = %g\n',i,X(i));

end

  fclose(fid);

%-----------------------------------------------------------------------
-----

!cd C:\FLUENT PRACTICE 3\CYLINDER\CYLINDER DYNQ

!designlink.bat

!Gabitlink.bat

!Fluentlink.bat

fid = fopen('CylinderTemp.dat', 'r');

CylinderTemp = textscan(fid, '%f %f %f %f %f ', 20000, 'headerlines',
1);


Tmax = max(CylinderTemp{:,5})-273.15;


fclose(fid);

F = Tmax';

%w = X(1) + 2*X(2) ;

POROSITY = (X(1)/X(2))^2.;

%POROSITY = (X(1)/(X(1)+2*X(2)))^2;

   X  ,      POROSITY,     F
%-------------------------------------------------------

%Inequality Constraints
```

```
%using dh and h FOR C
%------------------------------------------------------

 % porosity
%------------------------------------------------------

%C(1)= 0.2 - (X(1)/X(2))^2;


%C(2)= (X(1)./X(2)).^2 - 0.8;

%%%%%%%%%%%%%%%%%%%%%%%%%%%%%%%%%%%%%%%%%%%%%%%%%%%%%%%%%%%%%%%%%%%%%
%%%%%%

%C(1)= 0.05.*X(2)^2 - X(1)^2;

%C(2)= X(1)^2 - 0.1.*X(2)^2;

C(1)= 0.05.*X(2)^2 - X(1)^2;

C(2)= X(1)^2 - 0.2.*X(2)^2;

%%%%%%%%%%%%%%%%%%%%%%%%%%%%%%%%%%%%%%%%%%%%%%%%%%%%%%%%%%%%%%%%%%%%%
%%%%%

%C = [];

%H(1)=X(1)^2 - 0.2.*X(2)^2;

%H(1)=X(1)^2 - 0.1.*X(2)^2;

% h > d  value
%------------------------------------------------------

%C(3)= X(1) - X(2);

%------------------------------------------------------

%Equality Constraints
%H(1)=(X(1)*X(2)/0.01)-1;

% To eliminate error messages
% Do not delete

if ~exist('C')
    C=[];
end
if ~exist('H')
    H=[];
end
```

```
%-------------------------------------------------------------------
-----
```

A.3 GRADFCH.M

```
function [GF,GC,GH]=gradfch(X);
% Objective and constraint function GRADIENT evaluation for DYNAMIC-Q
%           (USER SPECIFIED)
%
%   synopsis:
%
%       [GF,GC,GH]=gradfch(X);
%
%   outputs: Partial derivatives wrt variables X(I) of
%      GF  = objective function (1xN)
%      GC  = inequality constraint functions (NPxN)
%      GH  = equality constraint functions (NQxN)
%
%   inputs:
%       X = design vector (1xN)
%
%     COMPUTE THE GRADIENT VECTORS OF THE OBJECTIVE FUNCTION F,
%     INEQUALITY CONSTRAINTS C, AND EQUALITY CONSTRAINTS H
%     W.R.T. THE VARIABLES X(I):
%              GF(I),I=1,N
%              GC(J,I), J=1,NP I=1,N
%              GH(J,I), J=1,NQ I=1,N
%
%   NOTE: This function should return GC=[]; GH=[]; if these are
%         not defined.
%
%   See also DYNQ, FCH
%

% Determine gradients by finite difference
FDFLAG=1;

if FDFLAG
    DELTX=1.D-4;    % Finite difference interval
    [F,C,H]=fch(X);
    N=length(X);
    for I=1:N
        DX=X;
        DX(I)=X(I)+DELTX;
        [F_D,C_D,H_D]=fch(DX);
        GF(I)=(F_D-F)/DELTX;
        if ~isempty(C)
              GC(1,1)= - 2.*X(1);


     GC(1,1)= - 2.*X(1);

     GC(1,2)=  0.1.*X(2);
```

```
 GC(2,1)=  2.*X(1);

     GC(2,2)= -0.4.*X(2);


   end

        end
    end
end

% To eliminate error messages
% Do not erase
if ~exist('GC')
    GC=[];
end
if ~exist('GH')
    GH=[];
end
```

A.4 RUNDYNQ

```
%This program initiates DYNQ.M

clear all

clc

tic

dml = 0.005;
xtol = 1e-8;
ftol = 1e-6;
clim = ftol;
np = 2;
nq = [];
kloop = 100;

%-----------------------------------------------------------------------
------

x0 = [0.25     0.4    ]; % Specify starting point 40kbc 1.238774e-001

lo = [1:2; 0.08 , 0.2  ]'; %Specify lower limits   %(Note the use of
the transpose)

up = [1:2; 0.25 , 0.8  ]'; %Specify upper limits %(Note the use of
the transpose)

%  Synopsis: % Solve using Dynamic-Q

[X,F] = dynq(x0,lo,up,dml,xtol,ftol,clim,np,nq,kloop);

toc
```

B

APPENDIX B: GAMBIT JOURNAL FILE FOR GEOMETRY AND MESH GENERATION OF COOLING CHANNELS

B.1 CIRCULAR COOLING CHANNELS JOURNAL FILE

```
/-----------------------------------------------------------------/

/Parameter
/////

/-----------------------------------------------------------------/
/read the dimension of the brick volume 1

/$v = ((( $x )^2* (0.01))^(1/3))

/$w1 = ( $x1 + 2*$x2)/1000

$w1 = $x2/1000


/$w1 = $x/$v

/$w1 = $x

/$w1 = $x/1000

$d1 = $w1

$h1 = 0.01

/-----------------------------------------------------------------/

/read the dimension of the cylinder volume 2

$r1=$x1/2/1000

/$r1=$dh/2/$v

/$r1=$dh

/$r1=$dh/1000

$r3=$r1
```

```
$h1 = 0.01

/-----------------------------------------------------------------/

/read the offset origin of brick volume 1

$offsetx1 = 0.5*$w1
$offsety1 = 0.5*$d1
$offsetz1 =-0.5*$h1

/-----------------------------------------------------------------/
/read the offset origin of cylinder volume 2

$offsetcylh1 = 0
$offsetcylr1 = 0
$offsetcylr3 =-0.5*$h1

/-----------------------------------------------------------------/

/move by offset cylinder volume 2

$movex1 = 0.5*$w1
$movey1 = 0.5*$w1

$movez1 = 0

/-----------------------------------------------------------------/
/mesh brick V1

/$meshv1=0.12*$w1

$meshv1=0.1*$w1

/$meshv1=0.08*$w1

/$meshv1=$mesh1

/-----------------------------------------------------------------/
/mesh cylinder V2

$meshv2=0.1*$x1/1000

/$meshv2=0.1*2*$r1


/$meshv2=0.07*2*$r1

$meshv2=0.1*$dh

/$meshv2=$mesh2

/-----------------------------------------------------------------/

volume create width $w1 depth $d1 height $h1 offset $offsetx1

$offsety1 $offsetz1 brick
```

```
volume create height $h1 radius1 $r1 radius3 $r3 offset $offsetcylh1
$offsetcylr1 $offsetcylr3 zaxis frustum
volume move "volume.2" offset $movex1 $movey1 $movez1
/-----------------------------------------------------------------/
volume subtract "volume.1" volumes "volume.2" keeptool
face connect "face.7" "face.8" "face.9" "face.10" real
/-----------------------------------------------------------------/
volume mesh "volume.1" cooper source "face.1" "face.6" size $meshv1
volume mesh "volume.2" cooper source "face.7" "face.9" size $meshv2
/-----------------------------------------------------------------/
physics create "wall front" btype "WALL" face "face.6"
physics create "wall back" btype "WALL" face "face.1"
physics create "symmetry top" btype "SYMMETRY" face "face.5"
physics create "symmetry bottom" btype "SYMMETRY" face "face.2"
physics create "symmetry left" btype "SYMMETRY" face "face.3"
physics create "symmetry right" btype "SYMMETRY" face "face.4"
physics create "pressure inlet" btype "PRESSURE_INLET" face "face.9"
physics create "pressure outlet" btype "PRESSURE_OUTLET" face
"face.7"
physics create "wall internal" btype "WALL" face "face.8"
physics create "solid" ctype "SOLID" volume "volume.1"
physics create "fluid" ctype "FLUID" volume "volume.2"

/-----------------------------------------------------------------/

save name "C:\\FLUENT PRACTICE 3\\CYLINDER\\CYLINDER
DYNQ\\CylinderDYNQDW.dbs"


export fluent5 \
  "C:\\FLUENT PRACTICE 3\\CYLINDER\\CYLINDER
DYNQ\\CylinderDYNQDW.msh"

save

/-----------------------------------------------------------------/
```

B.2 SQUARE COOLING CHANNELS JOURNAL FILE

```
/-----------------------------------------------------------------/

/Parameter

/-----------------------------------------------------------------/

/read the dimension of the brick volume 1

$w1 = $x2/1000

/$w1 = $x

$d1 = $w1

$h1 = 0.01

/-----------------------------------------------------------------/

/read the dimension of the brick volume 2

$w2=$x1/1000

/$w2=$dh

$d2=$w2

$h1 = 0.01

/-----------------------------------------------------------------/

/read the offset origin of brick volume 1

$offsetx1 = 0.5*$w1

$offsety1 = 0.5*$d1

$offsetz1 =-0.5*$h1

/-----------------------------------------------------------------/

/read the offset origin of brick volume 2

$offsetx2 = 0.5*$w2

$offsety2 = 0.5*$d2

$offsetz2 =-0.5*$h1


/-----------------------------------------------------/

/move by offset brick volume 2

$movex2 = 0.5*($w1-$w2)
```

```
$movey2 = 0.5*($d1-$d2)

$movez2 = 0

/-----------------------------------------------------------------/

/mesh brick V1


$meshv1=0.08*$w1

/$meshv1=0.2*$w1

/$meshv1=$mesh1

/-----------------------------------------------------------------/
/mesh brick V2


/$meshv2=0.07*$w2

$meshv2=0.2*$w2

/$meshv2=$mesh2

/-----------------------------------------------------------------/

volume create width $w1 depth $d1 height $h1 offset $offsetx1

$offsety1 $offsetz1 brick


volume create width $w2 depth $d2 height $h1 offset $offsetx2

$offsety2 $offsetz2 brick

/-----------------------------------------------------------------/

volume move "volume.2" offset $movex2 $movey2 $movez2

volume subtract "volume.1" volumes "volume.2" keeptool

/---------------------------------------------------------/

face connect "face.7" "face.8" "face.9" "face.10" "face.11" "face.12"

\ "face.15" "face.16" "face.17" "face.18" real

/-----------------------------------------------------------------/

volume mesh "volume.1" cooper source "face.1" "face.6" size $meshv1

volume mesh "volume.2" cooper source "face.7" "face.12" size $meshv2
```

```
/-------------------------------------------------------------------/

physics create "wall front" btype "WALL" face "face.6"

physics create "wall back" btype "WALL" face "face.1"

physics create "symmetry top" btype "SYMMETRY" face "face.5"

physics create "symmetry bottom" btype "SYMMETRY" face "face.2"

physics create "symmetry left" btype "SYMMETRY" face "face.3"

physics create "symmetry right" btype "SYMMETRY" face "face.4"

physics create "wall top internal" btype "WALL" face "face.11"

physics create "wall bottom internal" btype "WALL" face "face.8"

physics create "wall left internal" btype "WALL" face "face.9"

physics create "wall right internal" btype "WALL" face "face.10"

physics create "Pressure inlet" btype "PRESSURE_INLET" face "face.12"

physics create "Pressure outlet" btype "PRESSURE_OUTLET" face

"face.7"

physics create "fluid" ctype "FLUID" volume "volume.2"

physics create "solid" ctype "SOLID" volume "volume.1"

/-------------------------------------------------------------------/

save name "C:\\FLUENT PRACTICE 3\\SQUARE\\SQUARE
DYNQ\\SquareDYNQDW.dbs"

export fluent5 "C:\\FLUENT PRACTICE 3\\SQUARE\\SQUARE
DYNQ\\SquareDYNQDW.msh"

save

/-------------------------------------------------------------------/
```

B.3 ISOCELES RIGHT TRIANGULAR COOLING CHANNELS

JOURNAL FILE

```
/-------------------------------------------------------------------/

/Parameter
/////

/read the dimension of the Brick volume 1
```

```
/$w1 = ( $x1 + $x2)


$w1 = $x2/1000

/$w1 = $w

$d1 = $w1

$h1 = 0.01

/-----------------------------------------------------------------/

/read the offset origin of brick volume 1

$offsetx1 = 0.5*$w1
$offsety1 = 0.5*$d1
$offsetz1 = 0.5*$h1

/-----------------------------------------------------------------/

/read the dimension of the Triangle volume 2

/-----------------------------------------------------------------/

/$hT = $hT

/$dh = $dh

$a = $x1/1000

$hT = $a/2

$dh = $a^2/($a + (2)^0.5*$a )

/-----------------------------------------------------------/
vertice or point 1


$vertx1 =  0
$verty1 =  0

$vertz1  = 0

/-----------------------------------------------------------/

vertice or point 2

$vertx2 =  $a
$verty2 =  0
$vertz2  = 0

/-----------------------------------------------------------/
vertice or point 3

$vertx3 =  0.5*$a
```

```
$verty3 =  $hT
$vertz3  = 0

/-----------------------------------------------------------------/

/move by  offset Triangle volume 2

$movex1 = 0.5*($w1-$a)

$movey1 = 0.5*($w1-$hT)

$movez1 = 0

/-----------------------------------------------------------------/

/mesh brick V1

$meshv1=0.09*$w1

/-------------------------------------------------

/mesh Triangle  V2

/$meshv2=0.1*$x1

/$meshv2=0.1*$w1

$meshv2=0.09*$dh

/-----------------------------------------------------------------/
volume create width $w1 depth $d1 height $h1 offset $offsetx1
$offsety1 \
  -$offsetz1 brick

/-----------------------------------------------------------------/

vertex create coordinates $vertx1 $verty1 $vertz1

vertex create coordinates $vertx2 $verty2 $vertz2


vertex create coordinates $vertx3 $verty3 $vertz3

/-----------------------------------------------------------/

edge create straight "vertex.9" "vertex.10"
edge create straight "vertex.10" "vertex.11"
edge create straight "vertex.9" "vertex.11"

/-----------------------------------------------------------------/
face create wireframe "edge.13" "edge.14" "edge.15" real

/-----------------------------------------------------------------/
volume create translate "face.7" vector 0 0 -$h1

/-----------------------------------------------------------------/
```

```
volume move "volume.2" offset $movex1 $movey1 $movez1

/-----------------------------------------------------------------/

volume subtract "volume.1" volumes "volume.2" keeptool

/-----------------------------------------------------------------/

face connect "face.1" "face.2" "face.3" "face.4" "face.5" "face.6"
"face.7" \
  "face.8" "face.9" "face.10" "face.11" "face.12" "face.13" "face.14"
real

/-----------------------------------------------------------------/

face link "face.2" "face.5" edges "edge.5" "edge.12" vertices
"vertex.5" \
  "vertex.7" reverse periodic

/-----------------------------------------------------------------/

volume mesh "volume.1" cooper source "face.1" "face.6" size $meshv1

volume mesh "volume.2" cooper source "face.8" "face.7" size $meshv2

/-----------------------------------------------------------------/

physics create "wall front" btype "WALL" face "face.6"
physics create "wall back" btype "WALL" face "face.1"
physics create "wall internal left" btype "WALL" face "face.10"

physics create "wall internal right" btype "WALL" face "face.11"

physics create "wall internal bottom" btype "WALL" face "face.9"

physics create "symmetry left" btype "SYMMETRY" face "face.3"

physics create "symmetry right" btype "SYMMETRY" face "face.4"

physics create "Periodic BT" btype "PERIODIC" face "face.2" "face.5"

physics create "pressure inlet" btype "PRESSURE_INLET" face "face.7"

physics create "pressure outlet" btype "PRESSURE_OUTLET" face

"face.8"

physics create "solid" ctype "SOLID" volume "volume.1"

physics create "fluid" ctype "FLUID" volume "volume.2"


/-----------------------------------------------------------------/

save name \
```

```
  "C:\\FLUENT PRACTICE 3\\TRIANGLE\\TRIANGLE
DYNQPeriodic45\\TriangleDYNQPeriodic45DW.dbs"

export fluent5 \
  "C:\\FLUENT PRACTICE 3\\TRIANGLE\\TRIANGLE
DYNQPeriodic45\\TriangleDYNQPeriodic45DW.msh"

save

/------------------------------------------------------------------/
```

B.4 EQUILATERAL TRIANGULAR COOLING CHANNELS

JOURNAL FILE

```
/------------------------------------------------------------------/

/Parameter

/read the dimension of the Brick volume 1

/$w1 = ( $x1 + $x2)

 $w1 = $x2/1000

/$w1 = $w

 $d1 = $w1

 $h1 = 0.01

/------------------------------------------------------------------/

/read the offset origin of brick volume 1

$offsetx1 = 0.5*$w1
$offsety1 = 0.5*$d1
$offsetz1 = 0.5*$h1

/------------------------------------------------------------------/

/read the dimension of the Triangle volume 2


/$a = $x1/1000


/$a = $x1/1000

$hT = (3)^0.5/2*$a

$dh = $a/(3)^0.5
```

```
/vertice or point 1


$vertx1 =  0
$verty1 =  0
$vertz1  = 0

/-------------------------------------------------------------/

/vertice or point 2

$vertx2 =  $a
$verty2 =  0
$vertz2  = 0


/-------------------------------------------------------------------/
/vertice or point 3

$vertx3 =  0.5*$a
$verty3 =  $hT
$vertz3  = 0

/-------------------------------------------------------------------/

/move by offset Triangle volume 2

$movex1 = 0.5*($w1-$a)

$movey1 = 0.5*($w1-$hT)

$movez1 = 0

/-------------------------------------------------------------------/

/mesh brick V1

$meshv1=0.09*$w1

/mesh Triangle V2

/$meshv2=0.1*$x1

/$meshv2=0.1*$w1

$meshv2=0.09*$dh

/-------------------------------------------------------------------/

volume create width $w1 depth $d1 height $h1 offset $offsetx1
$offsety1 \
  -$offsetz1 brick

/-------------------------------------------------------------------/

vertex create coordinates $vertx1 $verty1 $vertz1
```

```
vertex create coordinates $vertx2 $verty2 $vertz2

vertex create coordinates $vertx3 $verty3 $vertz3

/-----------------------------------------------------------------/

edge create straight "vertex.9" "vertex.10"
edge create straight "vertex.10" "vertex.11"
edge create straight "vertex.9" "vertex.11"

/-----------------------------------------------------------------/

face create wireframe "edge.13" "edge.14" "edge.15" real

/-----------------------------------------------------------------/

volume create translate "face.7" vector 0 0 -$h1
/-----------------------------------------------------------------/
volume move "volume.2" offset $movex1 $movey1 $movez1

/-----------------------------------------------------------------/

volume subtract "volume.1" volumes "volume.2" keeptool

/-----------------------------------------------------------------/

face connect "face.1" "face.2" "face.3" "face.4" "face.5" "face.6"
"face.7" \
  "face.8" "face.9" "face.10" "face.11" "face.12" "face.13" "face.14"
real

/-----------------------------------------------------------------/

face link "face.2" "face.5" edges "edge.5" "edge.12" vertices
"vertex.5" \
  "vertex.7" reverse periodic

/-----------------------------------------------------------------/

volume mesh "volume.1" cooper source "face.1" "face.6" size $meshv1

volume mesh "volume.2" cooper source "face.8" "face.7" size $meshv2

/-----------------------------------------------------------------/

physics create "wall front" btype "WALL" face "face.6"
physics create "wall back" btype "WALL" face "face.1"

physics create "wall internal left" btype "WALL" face "face.10"

physics create "wall internal right" btype "WALL" face "face.11"


physics create "wall internal bottom" btype "WALL" face "face.9"

physics create "symmetry left" btype "SYMMETRY" face "face.3"
```

```
physics create "symmetry right" btype "SYMMETRY" face "face.4"

physics create "Periodic BT" btype "PERIODIC" face "face.2" "face.5"

physics create "pressure inlet" btype "PRESSURE_INLET" face "face.7"

physics create "pressure outlet" btype "PRESSURE_OUTLET" face

"face.8"

physics create "solid" ctype "SOLID" volume "volume.1"

physics create "fluid" ctype "FLUID" volume "volume.2"


/-----------------------------------------------------------------/

save name \
  "C:\\FLUENT PRACTICE 3\\TRIANGLE\\TRIANGLE
DYNQPeriodic60\\TriangleDYNQPeriodicDW.dbs"


export fluent5 \
  "C:\\FLUENT PRACTICE 3\\TRIANGLE\\TRIANGLE
DYNQPeriodic60\\TriangleDYNQPeriodicDW.msh"

save

/-----------------------------------------------------------------/
```

B.5 RECTANGULAR COOLING CHANNELS JOURNAL FILE

```
/-----------------------------------------------------------------/

/Parameter
/////


/read the dimension of the brick volume 1


/$w1 = $Wex

/$d1 = $Hex

$w1 = $x1/1000

$d1 = $x2/1000

/$w1 = $x1

/$d1 = $x2
```

```
/$DHex = (2*($x1*$x2))/($x1 + $x2)/1000

$h1 = 0.01

/-----------------------------------------------------------------/

/read the dimension of the brick volume 2

/$w2 = $win

/$d2 = $hin

$w2 = $x3/1000

$d2 = $x4/1000

/$w2 = $x3

/$d2 = $x4

/$dhin = (2*($x3*$x4))/($x3 + $x4)/1000

$h1 = 0.01

/-----------------------------------------------------------------/

/read the offset origin of brick volume 1

$offsetx1 = 0.5*$w1

$offsety1 = 0.5*$d1

$offsetz1 =-0.5*$h1

/read the offset origin of brick volume 2

$offsetx2 = 0.5*$w2

$offsety2 = 0.5*$d2

$offsetz2 =-0.5*$h1

/-----------------------------------------------------------/

/move by offset brick volume 2

$movex2 = 0.5*($w1-$w2)

$movey2 = 0.5*($d1-$d2)

$movez2 = 0


/-----------------------------------------------------------------/

/mesh brick V1
```

```
$meshv1=0.09*$DHex

/$meshv1=0.2*($DHex - $dhin)

/$meshv1=0.12*(2*($x1*$x2))/($x1 + $x2)/1000

/$meshv1=0.12*(2*($x1*$x2))/($x1 + $x2)

/$meshv1=0.12*$Hex

/$meshv1=0.12*$Wex


/-----------------------------------------------------------------/

/mesh brick V2

$meshv2=0.09*$dhin

/$meshv2=0.1*(2*($x3*$x4))/($x3 + $x4)/1000

/$meshv2=0.1*(2*($x3*$x4))/($x3 + $x4)

/$meshv2=0.1*$win

/-----------------------------------------------------------------/

volume create width $w1 depth $d1 height $h1 offset $offsetx1

$offsety1 $offsetz1 brick

volume create width $w2 depth $d2 height $h1 offset $offsetx2

$offsety2 $offsetz2 brick

/-----------------------------------------------------------------/

volume move "volume.2" offset $movex2 $movey2 $movez2

volume subtract "volume.1" volumes "volume.2" keeptool

/-----------------------------------------------------------------/

face connect "face.7" "face.8" "face.9" "face.10" "face.11" "face.12"
\
  "face.15" "face.16" "face.17" "face.18" real

/-----------------------------------------------------------------/

volume mesh "volume.1" cooper source "face.1" "face.6" size $meshv1

volume mesh "volume.2" cooper source "face.7" "face.12" size $meshv2

/-----------------------------------------------------------------/

physics create "wall front" btype "WALL" face "face.6"
```

```
physics create "wall back" btype "WALL" face "face.1"

physics create "symmetry top" btype "SYMMETRY" face "face.5"

physics create "symmetry bottom" btype "SYMMETRY" face "face.2"

physics create "symmetry left" btype "SYMMETRY" face "face.3"

physics create "symmetry right" btype "SYMMETRY" face "face.4"

physics create "wall top internal" btype "WALL" face "face.11"

physics create "wall bottom internal" btype "WALL" face "face.8"

physics create "wall left internal" btype "WALL" face "face.9"

physics create "wall right internal" btype "WALL" face "face.10"

physics create "pressure inlet" btype "PRESSURE_INLET" face "face.12"

physics create "pressure outlet" btype "PRESSURE_OUTLET" face

"face.7"

/-----------------------------------------------------------/

physics create "solid" ctype "SOLID" volume "volume.1"

physics create "fluid" ctype "FLUID" volume "volume.2"


/-----------------------------------------------------------/

save name \
  "C:\\FLUENT PRACTICE 3\\RECTANGLE\\RECTANGLE
DYNQ\\RECTANGLEDYNQDW.dbs"


export fluent5 \
  "C:\\FLUENT PRACTICE 3\\RECTANGLE\\RECTANGLE
DYNQ\\RECTANGLEDYNQDW.msh"


save

/-----------------------------------------------------------------/
```

B.6 VASCULARISED SOLID WITH COOLING CHANNELS

JOURNAL FILE

```
/read the dimension of the brick volume 1

/$w1 = $x2/1000 opt

/$w1 = $x2/1000
/$w1 = 0.0004
/$w1 =  $x  BF
/$w1 =  $x
/$w1 =  $x/1000  sensitivity analysis
$w1 =  $x/1000
$d1 = $w1
/$h1 = 0.01
$h1 = 0.01
/read the dimension of the brick volume 2

/$w2=$x1/1000  opt

/$w2=$x1/1000
/$w2=$dh =0.0002

/$w2=$dh BF
/$w2=$dh
/$w2=$dh/1000   sensitivity analysis
$w2=$dh/1000
$d2=$w2
/$h1 = 0.01
```

```
$h1 = 0.01

/-----------------------------------------------------------------------

/read the offset origin of brick volume 1

$offsetx1 = 0.5*$w1
$offsety1 = 0.5*$d1
$offsetz1 =-0.5*$h1

/read the offset origin of brick volume 2

$offsetx2 = 0.5*$w2
$offsety2 = 0.5*$d2
$offsetz2 =-0.5*$h1

/move by  offset brick volume 2

$movex2 = 0.5*($w1-$w2)
$movey2 = 0.5*($d1-$d2)
$movez2 = 0

/-----------------------------------------------------------------------

/mesh brick V1

/$meshv1=0.09*$w1

$meshv1=0.08*$w1

/$meshv1=$mesh1

/mesh brick V2

/$meshv2=0.09*$w2

$meshv2=0.05*$w2

/$meshv2=$mesh2

/-----------------------------------------------------------------------

volume create width $w1 depth $d1 height $h1 offset $offsetx1
$offsety1 $offsetz1 brick


volume create width $w2 depth $d2 height $h1 offset $offsetx2
$offsety2 $offsetz2 brick

volume move "volume.2" offset $movex2 $movey2 $movez2

volume subtract "volume.1" volumes "volume.2" keeptool


face connect "face.7" "face.8" "face.9" "face.10" "face.11" "face.12"
\
  "face.15" "face.16" "face.17" "face.18" real
```

```
/-----------------------------------------------------------------

volume mesh "volume.1" cooper source "face.1" "face.6" size $meshv1

volume mesh "volume.2" cooper source "face.7" "face.12" size $meshv2

/-----------------------------------------------------------------

physics create "wall front" btype "WALL" face "face.6"

physics create "wall back" btype "WALL" face "face.1"

physics create "symmetry top" btype "SYMMETRY" face "face.5"

physics create "symmetry bottom" btype "SYMMETRY" face "face.2"

physics create "symmetry left" btype "SYMMETRY" face "face.3"

physics create "symmetry right" btype "SYMMETRY" face "face.4"

physics create "wall top internal" btype "WALL" face "face.11"

physics create "wall bottom internal" btype "WALL" face "face.8"

physics create "wall left internal" btype "WALL" face "face.9"

physics create "wall right internal" btype "WALL" face "face.10"

physics create "Pressure inlet" btype "PRESSURE_INLET" face "face.12"

physics create "Pressure outlet" btype "PRESSURE_OUTLET" face

"face.7"

physics create "fluid" ctype "FLUID" volume "volume.2"

physics create "solid" ctype "SOLID" volume "volume.1"

/-----------------------------------------------------------------


save name "C:\\FLUENT PRACTICE 3\\SMART MATERIAL\\SQUARE\\SQUARESmart
DYNQ\\SquareSmartDYNQ.dbs"
export fluent5 "C:\\FLUENT PRACTICE 3\\SMART
MATERIAL\\SQUARE\\SQUARESmart DYNQ\\SquareSmartDYNQ.msh"
save

/-----------------------------------------------------------------
```

B.7 PF-1 ORIENTATION COOLING CHANNELS JOURNAL FILE

```
$w1 = $x2/1000

/$w1 = $x
```

```
$d1 = $w1

/read the dimension of the cylinder volume 2

$r1=$x1/2/1000

/$r1=$dh/2

$r3=$r1

$h1 = 0.01

/read the offset origin of brick volume 1

$offsetx1 = 0.5*$w1

$offsety1 = 0.5*$d1

$offsetz1 =-0.5*$h1


/read the offset origin of cylinder volume 2

$offsetcylh1 = 0

$offsetcylr1 = 0

$offsetcylr3 =-0.5*$h1


/move by offset cylinder volume 2


$movex1 = 0.5*$w1
$movey1 = 0.5*$w1

$movez1 = 0

/-------------------------------------------------

$cmovex1 = 0
$cmovey1 = $d1

$cmovez1 = 0


/-----------------------------------------------------------------

$cmovex2 = $w1
$cmovey2 = 0
```

```
$cmovez2 = 0


/-----------------------------------------

/Optimisation   /Optimisation   /Optimisation   /Optimisation
/Optimisation

/-----------------------------------------------------------------

/mesh brick V1


/ Optimisation mesh

/$meshv1=0.15*$x2/1000  po = 0.2   0.3

$meshv1=0.15*$x2/1000

/$meshv1=0.1*$x2/1000  po = 0.1

/$meshv1=0.1*$x2/1000


/Optimisation   /Optimisation   /Optimisation   /Optimisation
/Optimisation
/-----------------------------------------------------------------


/mesh cylinder V2

/$meshv2=0.15*$x1/1000  po = 0.2   0.3

$meshv2=0.15*$x1/1000

/$meshv2=0.1*$x1/1000  po = 0.1

/$meshv2=0.1*$x1/1000

/-----------------------------------------------------------------

/normal  /normal   /normal   /normal   /normal  /normal   /normal
/normal


/$meshv1=0.15*$w1  po = 0.2

/$meshv1=0.15*$w1

/$meshv1=0.1*$w1  po = 0.1

/$meshv1=0.1*$w1

/$meshv1=0.08*$w1

/$meshv1=$mesh1
```

```
/-----------------------------------------------------------------

/normal  /normal   /normal   /normal   /normal  /normal   /normal
/normal
/-----------------------------------------------------------------

/$meshv2=0.1*2*$r1

/$meshv2=0.07*2*$r1

/$meshv2=0.15*$dh  po = 0.2


/$meshv2=0.15*$dh

/$meshv2=0.1*$dh  po = 0.1

/$meshv2=0.1*$dh

/$meshv2=$mesh2

/-----------------------------------------------------------------


volume create width $w1 depth $d1 height $h1 offset $offsetx1

$offsety1 $offsetz1 brick

volume create height $h1 radius1 $r1 radius3 $r3 offset $offsetcylh1

$offsetcylr1 $offsetcylr3 zaxis frustum

/-----------------------------------------------------------------

/volume create width $w1 depth $d1 height $h1 offset $offsetx1

$offsety1 \

 / $offsetz1 brick

/volume create height $h1 radius1 $r1 radius3 $r3 offset $offsetcylh1

$offsetcylr1 \

/  zaxis frustum


/-----------------------------------------------------------------

volume move "volume.2" offset $movex1 $movey1 $movez1


/-----------------------------------------------------------------
```

```
volume cmove "volume.1" "volume.2" multiple 1 offset $cmovex1
$cmovey1 $cmovez1
volume unite volumes "volume.1" "volume.3"
/-----------------------------------------------------------------
volume cmove "volume.1" "volume.2" "volume.4" multiple 1 offset
$cmovex2 $cmovey2 $cmovez2
volume unite volumes "volume.1" "volume.5"
/-----------------------------------------------------------------
volume subtract "volume.1" volumes "volume.2" "volume.4" "volume.6" \
  "volume.7" keeptool
/-----------------------------------------------------------------
face connect "face.1" "face.2" "face.3" "face.6" "face.7" "face.8"
"face.9" \
  "face.14" "face.16" "face.17" "face.18" "face.24" "face.25"
"face.26" \
  "face.27" "face.28" "face.29" "face.30" "face.31" "face.34"
"face.37" \
  "face.40" real
/-----------------------------------------------------------------
volume mesh "volume.1" cooper source "face.1" "face.6" size $meshv1
volume delete "volume.2" onlymesh
/-----------------------------------------------------------------
volume mesh "volume.2" cooper source "face.7" "face.9" size $meshv2
volume mesh "volume.4" cooper source "face.17" "face.18" size $meshv2
volume mesh "volume.6" cooper source "face.26" "face.27" size $meshv2
volume mesh "volume.7" cooper source "face.29" "face.30" size $meshv2
/-----------------------------------------------------------------
physics create "wall front" btype "WALL" face "face.6"
physics create "wall back" btype "WALL" face "face.1"
```

```
physics create "symmetry left" btype "SYMMETRY" face "face.3"
physics create "symmetry right" btype "SYMMETRY" face "face.24"
physics create "symmetry bottom" btype "SYMMETRY" face "face.2"
physics create "symmetry top" btype "SYMMETRY" face "face.14"
physics create "pressure inlet 1" btype "SYMMETRY" face "face.9"
physics create "pressure inlet 2" btype "SYMMETRY" face "face.18"
physics create "pressure inlet 3" btype "SYMMETRY" face "face.27"
physics create "pressure inlet 4" btype "SYMMETRY" face "face.30"
physics modify "pressure inlet 1" btype "PRESSURE_INLET" face
"face.9"
physics modify "pressure inlet 2" btype "PRESSURE_INLET" face
"face.18"
physics modify "pressure inlet 3" btype "PRESSURE_INLET" face
"face.27"
physics modify "pressure inlet 4" btype "PRESSURE_INLET" face
"face.30"
physics create "pressure outlet 1" btype "PRESSURE_OUTLET" face
"face.7"
physics create "pressure outlet 2" btype "PRESSURE_OUTLET" face
"face.17"
physics create "pressure outlet 3" btype "PRESSURE_OUTLET" face
"face.26"
physics create "pressure outlet 4" btype "PRESSURE_OUTLET" face
"face.29"
physics create "wall internal 1" btype "WALL" face "face.8"
physics create "wall internal 2" btype "WALL" face "face.16"
physics create "wall internal 3" btype "WALL" face "face.25"
physics create "wall internal 4" btype "WALL" face "face.28"
```

```
physics create "solid" ctype "SOLID" volume "volume.1"

physics create "fluid 1" ctype "FLUID" volume "volume.2"

physics create "fluid 2" ctype "FLUID" volume "volume.4"

physics create "fluid 3" ctype "FLUID" volume "volume.6"

physics create "fluid 4" ctype "FLUID" volume "volume.7"


/------------------------------------------------------------------

save name \
  "C:\\FLUENT PRACTICE 3\\FLOW
ORIENTATION\\Parallelflow\\parallelflowchannelDYNQDW.dbs"
export fluent5 \
  "C:\\FLUENT PRACTICE 3\\FLOW
ORIENTATION\\Parallelflow\\parallelflowchannelDYNQDW.msh"
save

/------------------------------------------------------------------
```

B.8 CF-2 ORIENTATION COOLING CHANNELS JOURNAL FILE

```
$w1 = $x2/1000

/$w1 = $x

$d1 = $w1

/read the dimension of the cylinder volume 2


$r1=$x1/2/1000

/$r1=$dh/2

$r3=$r1

$h1 = 0.01

/read the offset origin of brick volume 1

$offsetx1 = 0.5*$w1

$offsety1 = 0.5*$d1

$offsetz1 =-0.5*$h1
```

```
/read the offset origin of cylinder volume 2

$offsetcylh1 = 0

$offsetcylr1 = 0

$offsetcylr3 =-0.5*$h1


/move by offset cylinder volume 2


$movex1 = 0.5*$w1

$movey1 = 0.5*$w1

$movez1 = 0


/----------------------------------------------------------------------

$cmovex1 = 0
$cmovey1 = $d1

$cmovez1 = 0
/----------------------------------------------------------------------

$cmovex2 = $w1
$cmovey2 = 0

$cmovez2 = 0

/-------------------------------------------

/mesh brick V1


/optimisation   /optimisation   /optimisation   /optimisation

/optimisation   /optimisation

/$meshv1=0.15*$x2/1000  po = 0.2    0.3

$meshv1=0.15*$x2/1000

/$meshv1=0.1*$x2/1000  po = 0.1

/$meshv1=0.1*$x2/1000

/ normal   /  normal    /  normal    /  normal   /  normal    /
normal    /  normal    /  normal   /  normal

/$meshv1=0.15*$w1  po = 0.2

/$meshv1=0.15*$w1
```

```
/$meshv1=0.1*$w1  po = 0.1

/$meshv1=0.1*$w1

/$meshv1=0.08*$w1

/$meshv1=$mesh1

/mesh cylinder V2

/optimisation   /optimisation  /optimisation   /optimisation
/optimisation

/$meshv2=0.15*$x1/1000  po = 0.2   0.3

$meshv2=0.15*$x1/1000

/$meshv2=0.1*$x1/1000  po = 0.1

/$meshv2=0.1*$x1/1000


/ normal   /  normal    /  normal    /  normal   /  normal    /
normal    /  normal    /  normal   /  normal


/$meshv2=0.1*2*$r1


/$meshv2=0.07*2*$r1

/$meshv2=0.15*$dh  po = 0.2


/$meshv2=0.15*$dh


/$meshv2=0.1*$dh  po = 0.1


/$meshv2=0.1*$dh


/$meshv2=$mesh2

/-----------------------------------------------------------------------

volume create width $w1 depth $d1 height $h1 offset $offsetx1

$offsety1 $offsetz1 brick


volume create height $h1 radius1 $r1 radius3 $r3 offset $offsetcylh1

$offsetcylr1 $offsetcylr3 zaxis frustum
```

```
/-------------------------------------------------------------------

/volume create width $w1 depth $d1 height $h1 offset $offsetx1
$offsety1 \
 / $offsetz1 brick


/volume create height $h1 radius1 $r1 radius3 $r3 offset $offsetcylh1
$offsetcylr1 \
/  zaxis frustum


/-------------------------------------------------------------------

volume move "volume.2" offset $movex1 $movey1 $movez1

/-------------------------------------------------------------------

volume cmove "volume.1" "volume.2" multiple 1 offset $cmovex1
$cmovey1 $cmovez1

volume unite volumes "volume.1" "volume.3"

/-------------------------------------------------------------------

volume cmove "volume.1" "volume.2" "volume.4" multiple 1 offset
$cmovex2 $cmovey2 $cmovez2

volume unite volumes "volume.1" "volume.5"

/-------------------------------------------------------------------

volume subtract "volume.1" volumes "volume.2" "volume.4" "volume.6" \
  "volume.7" keeptool

/-------------------------------------------------------------------
/-------------------------------------------------------------------

face connect "face.7" "face.8" "face.9" "face.16" "face.17" "face.18"
\
  "face.25" "face.26" "face.27" "face.28" "face.29" "face.30"
"face.1" \
  "face.2" "face.3" "face.6" "face.14" "face.24" "face.31" "face.34"
\
  "face.37" "face.40" real

/-------------------------------------------------------------------

face link "face.2" "face.14" edges "edge.5" "edge.16" vertices
"vertex.5" \
  "vertex.13" reverse periodic

/-------------------------------------------------------------------
face link "face.3" "face.24" edges "edge.10" "edge.40" vertices
"vertex.5" \
  "vertex.25" reverse periodic
```

```
/-------------------------------------------------------------------
volume mesh "volume.1" cooper source "face.1" "face.6" size $meshv1
/-------------------------------------------------------------------
volume mesh "volume.2" cooper source "face.7" "face.9" size $meshv2
volume mesh "volume.4" cooper source "face.17" "face.18" size $meshv2
volume mesh "volume.6" cooper source "face.26" "face.27" size $meshv2
volume mesh "volume.7" cooper source "face.29" "face.30" size $meshv2
/-------------------------------------------------------------------
physics create "wall front" btype "WALL" face "face.6"
physics create "wall back" btype "WALL" face "face.1"
physics create "periodic bt" btype "PERIODIC" face "face.2" "face.14"
physics create "periodic lr" btype "PERIODIC" face "face.3" "face.24"
physics create "pressure inlet f1" btype "PRESSURE_INLET" face
"face.9"
physics create "pressure inlet f3" btype "PRESSURE_INLET" face
"face.27"
physics create "pressure inlet b2" btype "PRESSURE_INLET" face
"face.17"
physics create "pressure inlet b4" btype "PRESSURE_INLET" face
"face.29"
physics create "pressure outlet b2" btype "PRESSURE_OUTLET" face
"face.7"
physics create "pressure outlet b3" btype "PRESSURE_OUTLET" face
"face.26"
physics modify "pressure outlet b2" btype label "pressure outlet b1"
face \
  "face.7"
```

```
physics create "pressure outlet f2" btype "PRESSURE_OUTLET" face
"face.18"
physics create "pressure outlet f4" btype "PRESSURE_OUTLET" face
"face.30"
physics create "wall internal 1" btype "WALL" face "face.8"
physics create "wall internal 2" btype "WALL" face "face.16"
physics create "wall internal 3" btype "WALL" face "face.25"
physics create "wall internal 4" btype "WALL" face "face.28"
/-----------------------------------------------------------------
physics create "solid" ctype "SOLID" volume "volume.1"
physics create "fluid 1" ctype "FLUID" volume "volume.2"
physics create "fluid 2" ctype "FLUID" volume "volume.4"
physics create "fluid 3" ctype "FLUID" volume "volume.6"
physics create "fluid 4" ctype "FLUID" volume "volume.7"
/-----------------------------------------------------------------
save name \
  "C:\\FLUENT PRACTICE 3\\FLOW ORIENTATION\\Counterflow
row\\CounterflowrowDYNQDW.dbs"
export fluent5 \
  "C:\\FLUENT PRACTICE 3\\FLOW ORIENTATION\\Counterflow
row\\CounterflowrowDYNQDW.msh"
save
save
/-----------------------------------------------------------------
```

B.9 CF-3 ORIENTATION COOLING CHANNELS JOURNAL FILE

```
$w1 = $x2/1000
/$w1 = $x
$d1 = $w1
/read the dimension of the cylinder volume 2
$r1=$x1/2/1000
/$r1=$dh/2
```

```
$r3=$r1

$h1 = 0.01

/-----------------------------------------------------------------

/read the offset origin of brick volume 1

$offsetx1 = 0.5*$w1

$offsety1 = 0.5*$d1

$offsetz1 =-0.5*$h1

/read the offset origin of cylinder volume 2

$offsetcylh1 = 0

$offsetcylr1 = 0

$offsetcylr3 =-0.5*$h1

/move by offset cylinder volume 2

$movex1 = 0.5*$w1

$movey1 = 0.5*$w1

$movez1 = 0

/-------------------------------------------------

$cmovex1 = 0

$cmovey1 = $d1

$cmovez1 = 0

/-----------------------------------------------------------------

$cmovex2 = $w1

$cmovey2 = 0

$cmovez2 = 0

/-----------------------------------------------------------------

/mesh brick V1

/Optimisation /Optimisation /Optimisation /Optimisation /Optimisation

/Optimisation /Optimisation

/$meshv1=0.15*$x2/1000  po = 0.2   0.3

$meshv1=0.15*$x2/1000
```

```
/$meshv1=0.1*$x2/1000  po = 0.1
/$meshv1=0.1*$x2/1000
/Normal /Normal  /Normal  /Normal  /Normal  /Normal  /Normal  /Normal
/Normal  /Normal  /Normal  /Normal
/$meshv1=0.15*$w1  po = 0.2
/$meshv1=0.15*$w1
/$meshv1=0.1*$w1  po = 0.1
/$meshv1=0.16*$w1
/$meshv1=0.08*$w1
/$meshv1=$mesh1
/mesh cylinder V2
/Optimisation /Optimisation /Optimisation /Optimisation /Optimisation
/Optimisation /Optimisation
/$meshv2=0.15*$x1/1000  po = 0.2   0.3
$meshv2=0.15*$x1/1000
/$meshv2=0.1*$x1/1000  po = 0.1
/$meshv2=0.1*$x1/1000
/Normal /Normal  /Normal  /Normal  /Normal  /Normal  /Normal  /Normal
/Normal  /Normal  /Normal  /Normal
/$meshv2=0.1*2*$r1
/$meshv2=0.07*2*$r1
/$meshv2=0.15*$dh  po = 0.2
/$meshv2=0.15*$dh
/$meshv2=0.15*$dh  po = 0.1
/$meshv2=0.1*$dh
/$meshv2=$mesh2
/-----------------------------------------------------------------
volume  create  width  $w1  depth  $d1  height  $h1  offset  $offsetx1
$offsety1 $offsetz1 brick
```

```
volume create height $h1 radius1 $r1 radius3 $r3 offset $offsetcylh1
$offsetcylr1 $offsetcylr3 zaxis frustum
/-----------------------------------------------------------------
/volume create width $w1 depth $d1 height $h1 offset $offsetx1
$offsety1 \
 / $offsetz1 brick
/volume create height $h1 radius1 $r1 radius3 $r3 offset $offsetcylh1
$offsetcylr1 \
/  zaxis frustum
/-----------------------------------------------------------------
volume move "volume.2" offset $movex1 $movey1 $movez1
/-----------------------------------------------------------------
volume cmove "volume.1" "volume.2" multiple 1 offset $cmovex1
$cmovey1 $cmovez1
volume unite volumes "volume.1" "volume.3"
/-----------------------------------------------------------------
volume cmove "volume.1" "volume.2" "volume.4" multiple 1 offset
$cmovex2 $cmovey2 $cmovez2
volume unite volumes "volume.1" "volume.5"
/-----------------------------------------------------------------
volume subtract "volume.1" volumes "volume.2" "volume.4" "volume.6" \
  "volume.7" keeptool
/-----------------------------------------------------------------
face connect "face.1" "face.2" "face.3" "face.6" "face.7" "face.8"
"face.9" \
  "face.14" "face.16" "face.17" "face.18" "face.24" "face.25"
"face.26" \
  "face.27" "face.28" "face.29" "face.30" "face.31" "face.34"
"face.37" \
```

```
  "face.40" real
/-----------------------------------------------------------------
face link "face.2" "face.14" edges "edge.5" "edge.16" vertices
"vertex.5" \
  "vertex.13" reverse periodic
/-----------------------------------------------------------------
face link "face.3" "face.24" edges "edge.10" "edge.40" vertices
"vertex.5" \
  "vertex.25" reverse periodic
/-----------------------------------------------------------------
volume mesh "volume.1" cooper source "face.1" "face.6" size $meshv1

volume mesh "volume.2" cooper source "face.7" "face.9" size $meshv2
volume mesh "volume.4" cooper source "face.17" "face.18" size $meshv2
volume mesh "volume.6" cooper source "face.26" "face.27" size $meshv2
volume mesh "volume.7" cooper source "face.29" "face.30" size $meshv2
/-----------------------------------------------------------------
physics create "wall front" btype "WALL" face "face.6"
physics create "wall back" btype "WALL" face "face.1"
physics create "periodic lr" btype "PERIODIC" face "face.3" "face.24"
physics create "periodic bt" btype "PERIODIC" face "face.2" "face.14"
physics create "pressure inlet f1" btype "PRESSURE_INLET" face
"face.9"
physics create "pressure inlet b2" btype "PRESSURE_INLET" face
"face.17"
physics create "pressure inlet b3" btype "PRESSURE_INLET" face
"face.26"
physics create "pressure inlet f4" btype "PRESSURE_INLET" face
"face.30"
```

```
physics create "pressure outlet b1" btype "PRESSURE_OUTLET" face
"face.7"
physics create "pressure outlet f2" btype "PRESSURE_OUTLET" face
"face.18"
physics create "pressure outlet f3" btype "PRESSURE_OUTLET" face
"face.27"
physics create "pressure outlet b4" btype "PRESSURE_OUTLET" face
"face.29"
physics create "wall internal 1" btype "WALL" face "face.8"
physics create "wall internal 2" btype "WALL" face "face.16"
physics create "wall internal 3" btype "WALL" face "face.25"
physics create "wall internal 4" btype "WALL" face "face.28"
physics create "solid" ctype "SOLID" volume "volume.1"
physics create "fluid 1" ctype "FLUID" volume "volume.2"
physics create "fluid 2" ctype "FLUID" volume "volume.4"
physics create "fluid 3" ctype "FLUID" volume "volume.6"
physics create "fluid 4" ctype "FLUID" volume "volume.7"
/-----------------------------------------------------------------
save name \
  "C:\\FLUENT      PRACTICE      3\\FLOW      ORIENTATION\\Counterflow
channels\\CounterflowchannelsDYNQDW.dbs"
export fluent5 \
  "C:\\FLUENT      PRACTICE      3\\FLOW      ORIENTATION\\Counterflow
channels\\CounterflowchannelsDYNQDW.msh"
save
/-----------------------------------------------------------------
```

C

APPENDIX C: FLUENT JOURNAL FILEN FOR NUMERICAL SIMULATION OF COOLING CHANNELS

C.1 COOLING CHANNELS FLUENT JOURNAL FILE

```
FLUENT
Version: 3d, dp, pbns, lam (3d, double precision, pressure-based,
laminar)
Release: 13.0.0
Title:

Models
------

   Model                         Settings
   ------------------------------------
   Space                         3D
   Time                          Steady
   Viscous                       Laminar
   Heat Transfer                 Enabled
   Solidification and Melting    Disabled
   Radiation                     None
   Species                       Disabled
   Coupled Dispersed Phase       Disabled
   NOx Pollutants                Disabled
   SOx Pollutants                Disabled
   Soot                          Disabled
   Mercury Pollutants            Disabled



Material Properties
-------------------

   Material: silicon (solid)

      Property                Units    Method     Value(s)
      ------------------------------------------------------
      Density                 kg/m3    constant   2330
      Cp (Specific Heat)      j/kg-k   constant   720
```

```
      Thermal Conductivity   w/m-k    constant   148

   Material: water-liquid (fluid)

      Property                          Units      Method     Value(s)
      ------------------------------------------------------------------
-
      Density                           kg/m3      constant   998.20001
      Cp (Specific Heat)                j/kg-k     constant   4182
      Thermal Conductivity              w/m-k      constant   0.60000002
      Viscosity                         kg/m-s     constant   0.001003
      Molecular Weight                  kg/kgmol   constant   18.0152
      Thermal Expansion Coefficient     1/k        constant   0
      Speed of Sound                    m/s        none       #f

   Material: air (fluid)

      Property                          Units      Method     Value(s)
      ------------------------------------------------------------------
-
      Density                           kg/m3      constant   1.225
      Cp (Specific Heat)                j/kg-k     constant   1006.43
      Thermal Conductivity              w/m-k      constant   0.0242
      Viscosity                         kg/m-s     constant   1.7894e-
05
      Molecular Weight                  kg/kgmol   constant   28.966
      Thermal Expansion Coefficient     1/k        constant   0
      Speed of Sound                    m/s        none       #f

   Material: aluminum (solid)

      Property               Units    Method     Value(s)
      ------------------------------------------------------
      Density                kg/m3    constant   2719
      Cp (Specific Heat)     j/kg-k   constant   871
      Thermal Conductivity   w/m-k    constant   202.4

Cell Zone Conditions
--------------------

   Zones

      name    id   type
      ------------------
      fluid   2    fluid
      solid   3    solid

   Setup Conditions

      fluid

         Condition                                                Value
         ------------------------------------------------------------
-------------------------------------------------------------------
-------------------------------------------------------------------
```

```
------------------------------------------------------------------------
-----------------
         Material Name
water-liquid
         Specify source terms?                                      no
         Source Terms
((mass) (x-momentum) (y-momentum) (z-momentum) (energy))
         Specify fixed values?                                      no
         Local Coordinate System for Fixed Velocities               no
         Fixed Values
((x-velocity (inactive . #f) (constant . 0) (profile  )) (y-velocity
(inactive . #f) (constant . 0) (profile  )) (z-velocity (inactive .
#f) (constant . 0) (profile  )) (temperature (inactive . #f)
(constant . 0) (profile  )))
         Frame Motion?                                              no
         Relative To Cell Zone                                      -1
         Reference Frame Rotation Speed (rad/s)                      0
         Reference Frame X-Velocity Of Zone (m/s)                    0
         Reference Frame Y-Velocity Of Zone (m/s)                    0
         Reference Frame Z-Velocity Of Zone (m/s)                    0
         Reference Frame X-Origin of Rotation-Axis (m)               0
         Reference Frame Y-Origin of Rotation-Axis (m)               0
         Reference Frame Z-Origin of Rotation-Axis (m)               0
         Reference Frame X-Component of Rotation-Axis                0
         Reference Frame Y-Component of Rotation-Axis                0
         Reference Frame Z-Component of Rotation-Axis                1
         Reference Frame User Defined Zone Motion Function        none
         Mesh Motion?                                               no
         Relative To Cell Zone                                      -1
         Moving Mesh Rotation Speed (rad/s)                          0
         Moving Mesh X-Velocity Of Zone (m/s)                        0
         Moving Mesh Y-Velocity Of Zone (m/s)                        0
         Moving Mesh Z-Velocity Of Zone (m/s)                        0
         Moving Mesh X-Origin of Rotation-Axis (m)                   0
         Moving Mesh Y-Origin of Rotation-Axis (m)                   0
         Moving Mesh Z-Origin of Rotation-Axis (m)                   0
         Moving Mesh X-Component of Rotation-Axis                    0
         Moving Mesh Y-Component of Rotation-Axis                    0
         Moving Mesh Z-Component of Rotation-Axis                    1
         Moving Mesh User Defined Zone Motion Function            none
         Deactivated Thread                                         no
         Embedded Subgrid-Scale Model                                0
         Momentum Spatial Discretization                             0
         Cwale                                                   0.325
         Cs                                                        0.1
         Porous zone?                                               no
         Conical porous zone?                                       no
         X-Component of Direction-1 Vector                           1
         Y-Component of Direction-1 Vector                           0
         Z-Component of Direction-1 Vector                           0
         X-Component of Direction-2 Vector                           0
         Y-Component of Direction-2 Vector                           1
         Z-Component of Direction-2 Vector                           0
         X-Component of Cone Axis Vector                             1
         Y-Component of Cone Axis Vector                             0
         Z-Component of Cone Axis Vector                             0
```

```
         X-Coordinate of Point on Cone Axis (m)                    1

         Y-Coordinate of Point on Cone Axis (m)                    0
         Z-Coordinate of Point on Cone Axis (m)                    0
         Half Angle of Cone Relative to its Axis (deg)             0
         Relative Velocity Resistance Formulation?               yes
         Direction-1 Viscous Resistance (1/m2)                     0
         Direction-2 Viscous Resistance (1/m2)                     0
         Direction-3 Viscous Resistance (1/m2)                     0
         Choose alternative formulation for inertial resistance?   no
         Direction-1 Inertial Resistance (1/m)                     0
         Direction-2 Inertial Resistance (1/m)                     0
         Direction-3 Inertial Resistance (1/m)                     0
         C0 Coefficient for Power-Law                              0
         C1 Coefficient for Power-Law                              0
         Porosity                                                  1
         Solid Material Name                                 aluminum

      solid

         Condition                                                 Value
         ------------------------------------------------------------
------------------------------------------------
         Material Name                                          silicon
         Specify source terms?                                  yes
         Source Terms                                           ((energy
((constant . 1e+08) (inactive . #f) (profile  ))))
         Specify fixed values?                                  no
         Fixed Values
((temperature (inactive . #f) (constant . 0) (profile  )))
         Frame Motion?                                          no
         Relative To Cell Zone                                  -1
         Reference Frame Rotation Speed (rad/s)                 0
         Reference Frame X-Velocity Of Zone (m/s)               0
         Reference Frame Y-Velocity Of Zone (m/s)               0
         Reference Frame Z-Velocity Of Zone (m/s)               0
         Reference Frame X-Origin of Rotation-Axis (m)          0
         Reference Frame Y-Origin of Rotation-Axis (m)          0
         Reference Frame Z-Origin of Rotation-Axis (m)          0
         Reference Frame X-Component of Rotation-Axis           0
         Reference Frame Y-Component of Rotation-Axis           0
         Reference Frame Z-Component of Rotation-Axis           1
         Reference Frame User Defined Zone Motion Function      none
         Mesh Motion?                                           no
         Relative To Cell Zone                                  -1
         Moving Mesh Rotation Speed (rad/s)                     0
         Moving Mesh X-Velocity Of Zone (m/s)                   0
         Moving Mesh Y-Velocity Of Zone (m/s)                   0
         Moving Mesh Z-Velocity Of Zone (m/s)                   0
         Moving Mesh X-Origin of Rotation-Axis (m)              0
         Moving Mesh Y-Origin of Rotation-Axis (m)              0
         Moving Mesh Z-Origin of Rotation-Axis (m)              0
         Moving Mesh X-Component of Rotation-Axis               0
         Moving Mesh Y-Component of Rotation-Axis               0
         Moving Mesh Z-Component of Rotation-Axis               1
         Moving Mesh User Defined Zone Motion Function          none
         Deactivated Thread                                     no
```

```
Boundary Conditions

--------------------

   Zones

      name                      id   type
      ----------------------------------------
      wall_internal-shadow      15   wall
      wall_internal             4    wall
      pressure_outlet           5    pressure-outlet
      pressure_inlet            6    pressure-inlet
      symmetry_right            7    symmetry
      symmetry_left             8    symmetry
      symmetry_bottom           9    symmetry
      symmetry_top              10   symmetry
      wall_back                 11   wall
      wall_front                12   wall

   Setup Conditions

      wall_internal-shadow

         Condition                                                  Value
         ----------------------------------------------------------------
         Wall Thickness (m)                                       0
         Heat Generation Rate (w/m3)                              0
         Material Name                                            silicon
         Thermal BC Type                                          3
         Temperature (c)                                          26.85
         Heat Flux (w/m2)                                         0
         Convective Heat Transfer Coefficient (w/m2-k)            0
         Free Stream Temperature (c)                              26.85
         Enable shell conduction?                                 no
         Wall Motion                                              0
         Shear Boundary Condition                                 0
         Define wall motion relative to adjacent cell zone?       yes
         Apply a rotational velocity to this wall?                no
         Velocity Magnitude (m/s)                                 0
         X-Component of Wall Translation                          1
         Y-Component of Wall Translation                          0
         Z-Component of Wall Translation                          0
         Define wall velocity components?                         no
         X-Component of Wall Translation (m/s)                    0
         Y-Component of Wall Translation (m/s)                    0
         Z-Component of Wall Translation (m/s)                    0
         External Emissivity                                      1
         External Radiation Temperature (c)                       26.85
         Rotation Speed (rad/s)                                   0
         X-Position of Rotation-Axis Origin (m)                   0
         Y-Position of Rotation-Axis Origin (m)                   0
         Z-Position of Rotation-Axis Origin (m)                   0
         X-Component of Rotation-Axis Direction                   0
         Y-Component of Rotation-Axis Direction                   0
         Z-Component of Rotation-Axis Direction                   1
         X-component of shear stress (pascal)                     0
```

```
   Y-component of shear stress (pascal)                  0
   Z-component of shear stress (pascal)                  0
   Surface tension gradient (n/m-k)                      0

Specularity Coefficient                                  0

wall_internal

   Condition                                             Value
   ------------------------------------------------------------
   Wall Thickness (m)                                    0
   Heat Generation Rate (w/m3)                           0
   Material Name                                         silicon
   Thermal BC Type                                       3
   Temperature (c)                                       26.85
   Heat Flux (w/m2)                                      0
   Convective Heat Transfer Coefficient (w/m2-k)         0
   Free Stream Temperature (c)                           26.85
   Enable shell conduction?                              no
   Wall Motion                                           0
   Shear Boundary Condition                              0
   Define wall motion relative to adjacent cell zone?    yes
   Apply a rotational velocity to this wall?             no
   Velocity Magnitude (m/s)                              0
   X-Component of Wall Translation                       1
   Y-Component of Wall Translation                       0
   Z-Component of Wall Translation                       0
   Define wall velocity components?                      no
   X-Component of Wall Translation (m/s)                 0
   Y-Component of Wall Translation (m/s)                 0
   Z-Component of Wall Translation (m/s)                 0
   External Emissivity                                   1
   External Radiation Temperature (c)                    26.85
   Rotation Speed (rad/s)                                0
   X-Position of Rotation-Axis Origin (m)                0
   Y-Position of Rotation-Axis Origin (m)                0
   Z-Position of Rotation-Axis Origin (m)                0
   X-Component of Rotation-Axis Direction                0
   Y-Component of Rotation-Axis Direction                0
   Z-Component of Rotation-Axis Direction                1
   X-component of shear stress (pascal)                  0
   Y-component of shear stress (pascal)                  0
   Z-component of shear stress (pascal)                  0
   Surface tension gradient (n/m-k)                      0
   Specularity Coefficient                               0

pressure_outlet

   Condition                                             Value
   ------------------------------------------------------------
   Gauge Pressure (pascal)                               0
   Backflow Total Temperature (c)                        26.85
   Backflow Direction Specification Method               1
   Coordinate System                                     0
   X-Component of Flow Direction                         1
   Y-Component of Flow Direction                         0
   Z-Component of Flow Direction                         0
```

```
   X-Component of Axis Direction                     1
   Y-Component of Axis Direction                     0
   Z-Component of Axis Direction                     0
   X-Coordinate of Axis Origin (m)                   0

   Y-Coordinate of Axis Origin (m)                   0
   Z-Coordinate of Axis Origin (m)                   0
   is zone used in mixing-plane model?               no
   Radial Equilibrium Pressure Distribution          no
   Specify Average Pressure Specification            no
   Specify targeted mass flow rate                   no
   Targeted mass flow (kg/s)                         1
   Upper Limit of Absolute Pressure Value (pascal)   5000000
   Lower Limit of Absolute Pressure Value (pascal)   1

pressure_inlet

   Condition                                         Value
   ------------------------------------------------------
   Reference Frame                                   0
   Gauge Total Pressure (pascal)                     5000
   Supersonic/Initial Gauge Pressure (pascal)        0
   Total Temperature (c)                             26.85
   Direction Specification Method                    1
   Coordinate System                                 0
   X-Component of Flow Direction                     1
   Y-Component of Flow Direction                     0
   Z-Component of Flow Direction                     0
   X-Component of Flow Direction                     1
   Y-Component of Flow Direction                     0
   Z-Velocity (m/s)                                  0
   X-Component of Axis Direction                     1
   Y-Component of Axis Direction                     0
   Z-Component of Axis Direction                     0
   X-Coordinate of Axis Origin (m)                   0
   Y-Coordinate of Axis Origin (m)                   0
   Z-Coordinate of Axis Origin (m)                   0
   is zone used in mixing-plane model?               no

symmetry_right

   Condition   Value
   -----------------

symmetry_left

   Condition   Value
   -----------------

symmetry_bottom

   Condition   Value
   -----------------

symmetry_top

   Condition   Value
```

```
   -----------------

wall_back

   Condition                                                Value

   ---------------------------------------------------------------
   Wall Thickness (m)                                       0
   Heat Generation Rate (w/m3)                              0
   Material Name                                            silicon
   Thermal BC Type                                          1
   Temperature (c)                                          26.85
   Heat Flux (w/m2)                                         0
   Convective Heat Transfer Coefficient (w/m2-k)            0
   Free Stream Temperature (c)                              26.85
   Enable shell conduction?                                 no
   Wall Motion                                              0
   Shear Boundary Condition                                 0
   Define wall motion relative to adjacent cell zone?       yes
   Apply a rotational velocity to this wall?                no
   Velocity Magnitude (m/s)                                 0
   X-Component of Wall Translation                          1
   Y-Component of Wall Translation                          0
   Z-Component of Wall Translation                          0
   Define wall velocity components?                         no
   X-Component of Wall Translation (m/s)                    0
   Y-Component of Wall Translation (m/s)                    0
   Z-Component of Wall Translation (m/s)                    0
   External Emissivity                                      1
   External Radiation Temperature (c)                       26.85
   Rotation Speed (rad/s)                                   0
   X-Position of Rotation-Axis Origin (m)                   0
   Y-Position of Rotation-Axis Origin (m)                   0
   Z-Position of Rotation-Axis Origin (m)                   0
   X-Component of Rotation-Axis Direction                   0
   Y-Component of Rotation-Axis Direction                   0
   Z-Component of Rotation-Axis Direction                   1
   X-component of shear stress (pascal)                     0
   Y-component of shear stress (pascal)                     0
   Z-component of shear stress (pascal)                     0
   Surface tension gradient (n/m-k)                         0
   Specularity Coefficient                                  0

wall_front

   Condition                                                Value
   ---------------------------------------------------------------
   Wall Thickness (m)                                       0
   Heat Generation Rate (w/m3)                              0
   Material Name                                            silicon
   Thermal BC Type                                          1
   Temperature (c)                                          26.85
   Heat Flux (w/m2)                                         0
   Convective Heat Transfer Coefficient (w/m2-k)            0
   Free Stream Temperature (c)                              26.85
   Enable shell conduction?                                 no
   Wall Motion                                              0
```

```
          Shear Boundary Condition                              0
          Define wall motion relative to adjacent cell zone?   yes
          Apply a rotational velocity to this wall?            no
          Velocity Magnitude (m/s)                             0
          X-Component of Wall Translation                      1
          Y-Component of Wall Translation                      0

          Z-Component of Wall Translation                      0
          Define wall velocity components?                     no
          X-Component of Wall Translation (m/s)                0
          Y-Component of Wall Translation (m/s)                0
          Z-Component of Wall Translation (m/s)                0
          External Emissivity                                  1
          External Radiation Temperature (c)                   26.85
          Rotation Speed (rad/s)                               0
          X-Position of Rotation-Axis Origin (m)               0
          Y-Position of Rotation-Axis Origin (m)               0
          Z-Position of Rotation-Axis Origin (m)               0
          X-Component of Rotation-Axis Direction               0
          Y-Component of Rotation-Axis Direction               0
          Z-Component of Rotation-Axis Direction               1
          X-component of shear stress (pascal)                 0
          Y-component of shear stress (pascal)                 0
          Z-component of shear stress (pascal)                 0
          Surface tension gradient (n/m-k)                     0
          Specularity Coefficient                              0

Solver Settings
---------------

   Equations

      Equation   Solved
      -----------------
      Flow       yes
      Energy     yes

   Numerics

      Numeric                            Enabled
      ---------------------------------------
      Absolute Velocity Formulation      yes

   Relaxation

      Variable      Relaxation Factor
      -------------------------------
      Pressure      0.30000001
      Density       1
      Body Forces   1
      Momentum      0.69999999
      Energy        1

   Linear Solver

                    Solver     Termination   Residual Reduction
      Variable      Type       Criterion     Tolerance
```

```
      ------------------------------------------------------
      Pressure     V-Cycle    0.1
      X-Momentum   Flexible   0.1           0.7
      Y-Momentum   Flexible   0.1           0.7
      Z-Momentum   Flexible   0.1           0.7
      Energy       Flexible   0.1           0.7

   Pressure-Velocity Coupling

      Parameter   Value
      ------------------
      Type        SIMPLE

   Discretization Scheme

      Variable   Scheme
      ------------------------------
      Pressure   Second Order
      Momentum   Second Order Upwind
      Energy     Second Order Upwind

   Solution Limits

      Quantity                    Limit
      --------------------------------
      Minimum Absolute Pressure   1
      Maximum Absolute Pressure   5e+10
      Minimum Temperature         1
      Maximum Temperature         5000

;;/-------------------------------------------------------------/;;
```

C.2 COOLING CHANNELS FLUENT BOUNDARY CONDITIONS JOURNAL FILE

```
;;1-------------------------------------------------------------------
------------------------

;;cylinder50kbc

;; Read Mesh and Scale Mesh

file/set-batch-options no yes no

file/start-transcript CylinderDYNQDW_trans.trn

file/read-case CylinderDYNQDW.msh

grid/scale 1 1 1
```

```
;; Read Boundary Conditions

file/read-bc cylinder50kbc

;;file/read-bc CylinderBe=10^3

;; Define Models and Units

define/models/energy yes no no no yes

define/models/viscous/laminar yes

define/units temperature c

;; Monitors

solve/monitors/residual/plot yes

solve/monitors/residual/print yes

solve/monitors/residual/convergence-criteria 1e-6 1e-6 1e-6 1e-6 1e-
10

;; Initialize and Solve

solve/initialize/compute-defaults all-zones

solve/initialize/initialize-flow

solve/iterate 300

;; Post Processing

file/export/ascii CylinderTemp.dat default-interior:001 default-
interior wall_front

wall_back symmetry_top symmetry_bottom symmetry_left symmetry_right

pressure_inlet pressure_outlet wall_internal wall_internal-shadow ()
no temperature ()

no

file/stop-transcript

file/write-case-data CylinderDYNQDW_data.cas.gz


exit

/-----------------------------------------------------
```